WILLIAM & MARY
CHARTERED 1693

Dissertations, Theses, and Masters Projects      Theses, Dissertations, & Master Projects

2006

# UV cure kinetics of dimethacrylate thin and thick samples

Yuemei Zhang
*College of William & Mary - Arts & Sciences*

Follow this and additional works at: https://scholarworks.wm.edu/etd

Part of the Polymer Chemistry Commons

## Recommended Citation

# UV CURE KINETICS OF DIMETHACRYLATE THIN AND THICK SAMPLES

_____

A Dissertation

Presented to

The Faculty of the Department of Applied Science

The College of William and Mary in Virginia

In Partial Fulfillment

Of the Requirements for the Degree of
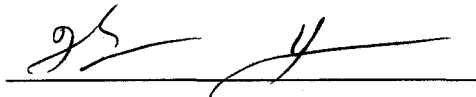
Doctor of Philosophy

_____

by

Yuemei Zhang

2006

**APPROVAL SHEET**

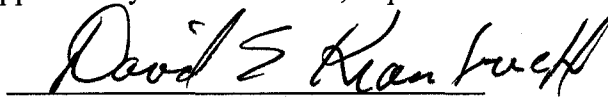This dissertation is submitted in partial fulfillment of

The requirements for the degree of
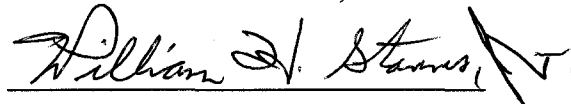
Doctor of Philosophy

_____
Yuemei Zhang
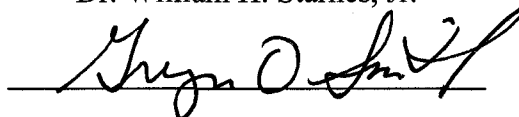
Approved by the Committee, September 2006
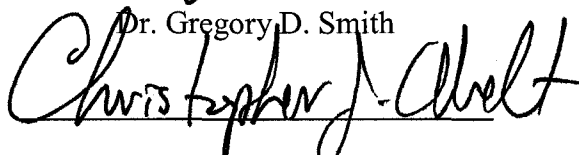
_____
Dr. David Kranbuehl, Chair
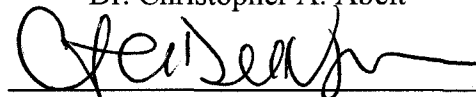
_____
Dr. William H. Starnes, Jr.

_____
Dr. Gregory D. Smith

_____
Dr. Christopher A. Abelt

_____
Dr. Christopher A. Del Negro

ii

# TABLE OF CONTENTS

iii

iv

**CHAPTER 7. DIFFUSION OF OXYGEN AND FREE RADICALS    241
DURING FREE RADICAL POLYMERIZATION**

viii

# ACKNOWLEDGEMENTS

The author would like to give her sincere appreciation to her advisor Dr. David E. Kranbuehl for his invaluable guidance to this research. He also helped improve her English and gave her many valuable suggestions and information for her career. The author is also indebted to Drs. H. Sautereau, G. Seytre, and J. Dupuy of INSA and the University Claude Bernard, Lyon, France for their help and suggestions to the project. The author thanks Drs. William H. Starnes, Jr., Gregory D. Smith, Christopher A. Abelt, and Christopher A. Del Negro for their contributions to this manuscript and careful instruction during this endeavor.

The author wants to acknowledge the exceptional support of the entire Kranbuehl group and the Departments of Applied Science and Chemistry.

In addition, the author is grateful to her parents, husband, and all her friends for their unending support, care, encouragement, and love.

Finally, the author gives her glory and thanks to God. He carried her through the hardest period of her life and research and will lead her forever in the future.

# LIST OF TABLES

x

sample is 4 mm, [PI]=0.2wt%, $\varepsilon_i$=760 l mol$^{-1}$ cm$^{-1}$, $\phi$'=0.5, st=1minute, NL=1.

considering the absorption of monomer, $\varepsilon_i = 760$ 1 mol$^{-1}$ cm$^{-1}$. Two

darker curves in the middle of other curves are the average of all 10

layers.

) model predictions.

the total radical population (○) as a function of conversion. TEGDMA polymerization. Polymerization conditions: light intensity, 5 uw/cm$^2$; initiator concentration, 0.1wt%." Reported by Bowman in Macromolecules (2005)

experimental data

xx

xxiv

0.1kHz

of the sample without toluene.

agent(CT)) under a mask (dark strip width = clear strip width=0.025inch) at the intensity of 32.5 $\mu w/cm^2$, f=0.1kHz, thickness=0.05 mm. **a** is the system without CT and Figure **b** is the system with CT. m represents the measured cure curve under a mask, n represents the calculated curves without considering the diffusion effect.

have 50% dark area and 50% clear area. Incident intensity is 32.5 $\mu w/cm^2$.

# ABSTRACT

UV curing is using UV light as the energy source to induce the polymerization of liquid monomers and oligomers to form a solid polymer. Because UV polymerization is fast and energy-saving and a UV curable system has no VOC (volatile organic compound), this new technology has developed rapidly from thin film applications to thick sample applications. In addition, since the UV cure process can be controlled spatially and temporally, it also has an important application to make gradient materials with locally optimized properties. However, most research on UV cure is based on thin film applications, and the cure kinetics of thick samples are more complex and not well understood.

In this study, we focus on the UV cure kinetics of CD540 (ethoxylated (4) Bisphenol-A dimethacrylate) thin and thick samples (2-8 mm). A photo-bleaching initiator, bis(2,4,6-trimethylbenzoyl)phenylphosphine oxide (Irgacure 819), is used in the system. UV cure kinetics are complex, especially when the sample is thick, since the light intensity is a function of depth and also a function of exposure time. In order to understand the complex cure kinetics of thick samples, we first studied the variation in the transmitted intensity and initiator concentration through the depth in thick samples. Based on the experimental measured transmitted intensity, a Matlab program was written to predict the intensity versus depth and exposure time of a thick sample. Then, the UV cure kinetics of thin samples (0.05 mm) were studied. In this part, we studied the effect of light intensity, initiator concentration, and temperature on the cure kinetics experimentally and theoretically. A model was developed based on a unimolecular termination mechanism in order to predict the cure kinetics at different conditions for thin samples. Combining the Matlab program for calculating the intensity in thick samples and the model for calculating the cure kinetics of thin samples, the cure kinetics through the depth of thick samples were predicted and compared with experimental results measured by frequency dependent dielectric sensing.

The diffusion of free radicals in a UV cure free radical cure system was studied by monitoring the cure in the dark nonirradiated region under a mask. In addition, a free radical thermal cure of an acrylic resin was characterized in order to study oxygen diffusion from the surface layers into deeper layers.

# UV CURE KINETICS OF DIMETHACRYLATE THIN AND THICK SAMPLES

# Chapter 1. Introduction

## 1.1    Definition of UV cure

What is UV cure? To "Cure" means to have a polymer resin set or harden in the coating or ink industries. It's a process in which the phase of the system changes from a flowing liquid state to a solid state. Conventional coatings and inks are made of monomer and low molecular weight polymers dissolved in a solvent. Therefore, curing is often a physical drying process, which happens due to the evaporation of the solvent from the system. However, UV cure is a chemical curing process. It is a technology using ultra-violet light as an energy source to induce the polymerization of a liquid monomer to form solid polymer. (As shown in fig.1.1)
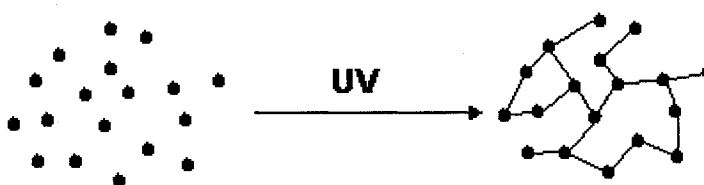
Figure 1.1 Schematic representation of UV curing

## 1.2    History of UV cure and its application

It is well known that photo curing experienced its rapid development from infancy to a mature industry in the past fifty years. However the history of UV polymerization began much earlier than that. Actually, as early as the 1820s, the first photopolymer---

Asphalt known as Judea bitumen, had been invented by a French man, Joseph Nicéphore Niépce, as image material for photography. Hence, Niépce is regarded as the inventor of photography and also the "father" of the microlithography[1]. But the exposure time for the bitumen process is very long and therefore it could not survive. It was replaced by dichromated colloids in 1839 for photomechanical reproduction by Mungo Ponton. In 1852, a patent by Fox Talbot using dichromated gelatin as the resist material for printing plates opened the way for the further development of photomechanical reproduction.

After the 1940s, UV curing entered its golden development period and found many applications, mainly in the coating industry for producing varnishes and inks. Hoyle gave the key dates of the photocuring history in his review[2]. In 1945, Christ first indicated benzoin as the photoinitiator to induce free radical polymerization as described in a duPont patent. This is the basis of the photocuring of clear coatings. Following that, a photocurable coating for the production of plastic printing plates and a coating for wood substrates and several other similar systems was formulated in the US in the following years. It has been reported that the world consumption of UV- curable products increases about 15% every year around 1995.[2] Today, UV curable material is not limited to the coating industry. It has found new applications in other fields, such as encapsulants for microelectronic devices,[3] glass fiber and silica-filled polymer composites,[4] adhesives, stereolithography,[5] and dental restorative materials. In the field of graphic arts, laser-stereolithography, and the coating of optical fibers, it even occupies a dominant position.

## 1.3    Advantages of UV curable system

The reasons for its fast development is UV curing has many advantages compared with thermal curing and physical drying. **First,** UV curable systems usually contain 100% active components and no VOC (volatile organic compound). All of the active components convert to a solid after polymerization. There is no emission of polluting organic vapors to the environment during its application. Hence, UV cure is called "green technology". Mandates issued by the government to limit the volatile organic components in coatings pushed the rapid development of this technology in the coating industry. **Second,** UV curing is very fast. Using a 200 watt mercury arc lamp as an energy source, a dimethacrylate thin film can be cured in a few minutes and the cure rate increases with light intensity and initiator concentration. Fast curing cuts off the producing time and thus increases the producing efficiency.    **Third,** the system can be cured at ambient temperature. It consumes only a small fraction of the energy required for thermal cure. Saving energy is another currently important objective. Ambient temperature cure is also good for some heat sensitive applications and make its application more convenient. **Fourth,** UV curable monomers and oligomers are cheap and versatile which meets the requirements of a variety of applications. **Finally,** the UV cure process can be controlled spatially and temporally. It can be used to make a gradient material for optical applications. The combination of all these advantages make UV curable material unique and its application has expanded quickly to many fields in the past 50 years.

## 1.4 Types of UV curable systems

UV curable systems can be generally divided into two groups according to the polymerization mechanism, free radical polymerization and cationic polymerization. Each system has its own advantages and limitations. First, free radical UV curable systems have many kinds of monomers and oligomers so that the products are versatile. However, the cationic systems have only limited monomers and oligomers, so the product properties are limited. Second, free radical polymerization may stop as soon as the light is eliminated, but the cationic polymerization continues after the radiation source is removed. Another important difference is the free radical systems are subject to oxygen inhibition. This means the cure of free radical system in the air is delayed and the surface of the sample exposed to the air stays wet and can not been cured well due to the high diffusion speed of oxygen from the air. The cationic systems are not affected by oxygen as much so they are good for the application of thin films in the air. However, the cationic systems are poisoned by high humidity. The UV curable systems studied in this dissertation are free radical systems.

## 1.5 Components of UV curable system

A UV curable system is generally composed of 4 parts: initiator, oligomer (prepolymer), monomer and additives.

**Initiator** is the key component in the system even though it's only a small fraction (<5%). Under UV exposure initiators break into reactive free radicals or cations, which initiate further polymerization of oligomer and monomers. A good photo initiator for UV cure should have the following characteristics: 1, suitable extinction coefficient in

the 300-400nm range; 2, significant initiation quantum yield; 3, soluble in the monomer or oligomer; 4, good thermal stability and long pot-life; 5, no yellowing or odor release on cure; 6, post-radiation product is non-toxic. There are essentially two types of initiator photogenerators: free radicals and cationic species. Accordingly, the mechanism of photopolymerization can be divided into two categories as described above.

The initiator, Irgacure 819, used for the research in this dissertation is a bis(acyl)phosphine oxide, which has several advantages as an initiator in the free radical photo polymerization. First, the optical absorption is in the UV region, therefore this allows the curing of pigmented formulations. Second, it is photo bleaching. Photo bleaching means after the aroyl-phosphinoyl chromophore is destroyed during the photo-induced cleavage of the carbonyl-phosphinoyl bond, the abosorption of the fragments is much smaller than the original absorption of the initiator before it breaks. This characterization makes it a good initiator for thick applications. Third, $\alpha$ cleavage of carbonyl-phosphinoyl bond in bis(acyl)phosphine oxides has a high efficiency. The quantum yield of consumption of bis(acyl)phosphine oxide initiators $\phi'$ was reported to be 0.5.[6] These characteristics attracted attention in recent years, and the photo-chemistry of this system has been studied extensively.[6-10] It has been reported that bis(acyl)phosphine oxides have the potential to produce four radicals, and all of them can initiate the chain polymerization.[8] It was also shown that bis(acyl)phosphine oxides undergo stepwise cleavage of both benzoyl residues upon irradiation (404.5nm).[10] The initiation process of bis(acyl)phosphine in a photo curable system will be discussed in detail in Chapter 4.

**Oligomers,** low molecular polymers, are the main component in the system that constitutes the backbone of the cured polymer. Therefore, they determine the physical and chemical properties of the product. Oligomers usually contain at least two functional groups, such as vinyl, acrylate, methacrylate, epoxy, etc. The molecular weight is from 500 to 3000 and the viscosity is from 5 to 25 Pa·s.

The oligomer used in this project is ethoxylated(4) Bisphenol-A dimethacrylate (CD540). This oligomer has many advantages, for example, it has high adhesion, flexibility, abrasion resistance, heat resistance, impact strength, water and chemical resistance and low shrinkage. Hence, it is widely used in photo-curable systems for making contact lenses, coating, inks, adhesives, elastomers, plastics, elecronics, etc.

**Monomers** are another active component in the system. It is added to the system to reduce the viscosity and facilitate the application of the material. Monomers have active groups that will participate in the polymerization. Monomers also affect the product properties and the cure speed. The monomer used in this project is styrene. It is cheap and cures quickly.

**Additives** are some non-active components in the systems. They are used in UV curable formulations at levels of up to 50%[11] to achieve some special requirements. For example, pigments are added to the UV curable ink system for color, dispersions for pigment dispersion, surfactants for substrate adhesion. Additives in the UV curable system may cause serious problems because they are opaque and hence the light penetration into the thick samples can be hindered. There is no additive in our system except toluene which was used to examine the effect of viscosity on rate of cure.

### 1.6    Mechanism of UV cure

A particularly comprehensive study of photo cure has been conducted by Odian who examined the rate of radical chain polymerization in his book "Principles of Polymerization".[12] Its contents are referenced here in the introduction regarding the theoretical background of the photo cure kinetics. The cure kinetics of our system is not completely the same as what is explained here. This is because a major assumption in the classic theory of UV cure kinetics is not valid as demonstrated in this dissertation. The differences will be elaborated in Chapter 3 and 4. As described in Odian's book, radical chain polymerization has been generally divided into three steps, initiation, propagation and termination.

The first step is initiation, which includes two reactions, the dissociation of photo initiators to produce radicals as shown in Equation 1-1 and the addition reaction of the radical with the first monomer molecule to form the chain initiating species $M_1 \cdot$ as shown in Equation 1-2

$$PI \xrightarrow{\;k_d\;} 2R \cdot \qquad\qquad\qquad \text{Equation 1-1}$$

$$R \cdot + M \xrightarrow{\;k_i\;} M_1 \cdot \qquad\qquad\qquad \text{Equation 1-2}$$

PI is the photo-initiator, $k_d$ is the rate constant of dissociation of the photo-initiator, $R \cdot$ is the free radical fragment, M is the functional group of the monomer, (for example, the C=C of methacrylate in CD540, the resin studied here), $k_i$ is the rate constant for the initiation step.

The second step is propagation, the successive addition of monomers to $M \cdot$ to form polymer radicals (from Equations 1-3 to 1-6).

$$M_1 \cdot + M \xrightarrow{\;k_p\;} M_2 \cdot \qquad\qquad\qquad \text{Equation 1-3}$$

$$M_2 \cdot + M \xrightarrow{k_p} M_3 \cdot \qquad\qquad \text{Equation 1-4}$$

$$M_3 \cdot + M \xrightarrow{k_p} M_4 \cdot \qquad\qquad \text{Equation 1-5}$$

$$\vdots$$

$$M_n \cdot + M \xrightarrow{k_p} M_{n+1} \cdot \qquad\qquad \text{Equation 1-6}$$

$k_p$ is the rate constant of propagation.

The third step is termination with annihilation of the radical centers. Usually, the termination is defined as a bimolecular reaction between radicals as shown in Equation 1-7.[12]

$$M_n \cdot + M_m \cdot \xrightarrow{k_t} dead\ polymer \qquad\qquad \text{Equation 1-7}$$

$k_t$ is the rate constant of termination, which is the combination of coupling and disproportionation termination.

Since the consumption number of monomers in the initiation step is much less than the number in the propagation step, therefore

$$-\frac{d[M]}{dt} = R_i + R_p \approx R_p \qquad\qquad \text{Equation 1-8}$$

$R_i$ and $R_p$ are rate of initiation and propagation. Assume $k_p$ is a constant which does not change with the length of the polymer radical, hence the propagation rate can be expressed as

$$R_p = k_p [M\cdot][M] \qquad\qquad \text{Equation 1-9}$$

For a bimolecular termination reaction, the rate of termination can be expressed as

$$R_t = 2k_t [M\cdot]^2 \qquad\qquad \text{Equation 1-10}$$

Note that the bimolecular termination reaction is only one type of termination, it is accepted that some radicals terminate by uni-molecular mechanism due to the

discovery of trapped radicals. The effect of uni-molecular termination on the cure kinetics will be discussed in Chapter 4.

According to the steady-state assumption, it is known that

$$R_i = R_t \qquad \text{Equation 1-11}$$

Therefore,

$$R_i = 2k_t[M\cdot]^2 \qquad \text{Equation 1-12}$$

Combining Equations 1-9 and 1-12, it is easy to get Equation 1-13.

$$R_p = k_p[M](\frac{R_i}{2k_t})^{1/2} \qquad \text{Equation 1-13}$$

It is known that

$$R_i = 2\phi I_a \qquad \text{Equation 1-14}$$

where $\phi$ is quantum yield of initiation, which represents the number of propagation chains formed for each photon absorbed. $I_a$ is the absorbed light intensity in moles of light quanta. The factor of 2 is used for those initiator systems, which yield 2 radicals instead of one.

From Lambert-Beer's law

$$\log(\frac{I_t}{I_i}) = -\varepsilon b[PI] \qquad \text{Equation 1-15}$$

$I_t$ is transmitted light intensity, $I_i$ is the incident light intensity, $\varepsilon$ is the absorption coefficient of photoinitiator, b is the thickness of the sample, [PI] is the concentration of photoinitiator. The absorbed light intensity can be expressed by

$$I_a = I_i(1 - 10^{-\varepsilon b[PI]}) \qquad \text{Equation 1-16}$$

If the absorption of the light is very small or the sample is very thin, Equation 1-16 can be written more conveniently as

$$I_a = 2.3\varepsilon I_i b[PI]$$ 

<div align="right">Equation 1-17</div>

Therefore the rate of propagation, $R_p$, can be written as

$$R_p = k_p[M](\frac{2.3\phi\varepsilon I_i[PI]b}{k_t})^{1/2}$$

<div align="right">Equation 1-18</div>

Substitute Equation 1-8 to Equation 1-18

$$-\frac{d[M]}{dt} = k_p[M](\frac{2.3\phi\varepsilon I_i[PI]b}{k_t})^{1/2}$$

<div align="right">Equation 1-19</div>

## 1.7    Characterization techniques

There are many methods to study UV cure kinetics. The most popular two are DSC (Differential Scanning Calorimeter) and FTIR (Fourier Transform Infrared).

DSC is a good method to study cure kinetics by measuring the heat flow of the exothermal reaction. But the traditional DSC has some disadvantages in measuring the UV polymerization. One is due to the surface tension of the aluminum pan, which makes it hard to make a sample with a homogeneous thickness. The second problem is the error is larger since the weight of the sample is small for a very thin sample. The third problem is the reflection of light from the surface of the pan bottom, which affects the measurement of the real incident intensity.

Transmitted Near FTIR is a reliable method to quantitatively measure the cure extent of organic functional groups, such as C=C in methacrylate oligomers and it is easy to use. The strength of the signal is proportional to the sample thickness and the accumulation time of the scan. In order to measure the fast photocure with high

resolution using transmitted FTIR, people use samples with a thickness more than 1 mm[13-15] to get a strong signal. However for an initiator like Irgacure 819, which has a high extinction coefficient, this will result in a heterogeneous reaction due to the varying absorption of light through the depth of the sample. This definitely affects the cure kinetics of the system. In order to study the cure kinetics accurately, a sample as thin as $0.05 \pm 0.01$ mm is used for the experiments in this paper. In this case, the decrease of light intensity through the depth is less than 4.6% for a composition with less than 0.2% Irgacure 819. The calculation of light intensity through the depth will be shown later in Chapter 4. Hence the reaction can be regarded as homogeneous. To get a good signal in a thin sample of 0.05 mm, a relatively low intensity of radiation ($<32.5$ uw/cm$^2$) is used to slow down the cure process and permit a longer accumulation time of the scan. Because the reaction is relatively slow under low power radiation, one is able to more accurately measure parameters related to absolute time, such as inhibition period (delay time) compared with fast cure under high exposure intensities.[16,17]

Even though FTIR is a good method to measure the UV cure kinetics of thin samples, it is not enough to measure the cure at particular depths for thick samples. It monitors only the bulk cure kinetics (average cure throughout depth) of a sample. Dielectric measurement is especially suited to measuring the cure kinetics at a particular depth. Therefore, it is used in the dissertation as an important monitoring method. Detailed discussion of dielectric measurements will be introduced in Chapters 5 and 6.

## 1.8 Motivation of the dissertation

Although the kinetics of UV cure has been studied a lot over the past fifty years, most of those studies were based on the average reaction in the systems. [18-21] However, the outcomes are not always correct if the sample is thick. For example, for a thin sample, the initiator concentration will usually increase the reaction rate. While for thick samples, the average polymerization rate may decrease when the initiator concentration is high. This is due to the strong absorption of initiator at upper layers which will be shown in Chapters 3 and 6. Another difference is due to the oxygen inhibition effect. For the free radical polymerization of thin samples in an open environment, the diffusion of oxygen from the air affects the cure significantly in the surface layers so that the surface stays wet (uncured). However, for thick samples, the diffusion of oxygen has little effect on the cure at deep layers.

The intensity gradient through the depth induces spatial non-homogeneous conversion[22] and resulting properties. This special property is an advantage on one hand since it can be used to make gradient materials for optical products. However it creates a problem on the other hand for some thick applications such as printing plates, stereolithography,[5] and dental restorative materials. For these materials, a homogeneous property and a complete cure throughout the entire depth is needed. The surface-to depth cure gradient and the resulting insufficient polymerization at the coating-substrate interface often results in poor adhesion. For this reason a photoinitiator that undergoes an effective bleaching reaction upon photolysis is a good choice because it allows UV radiation to penetrate deeper into the sample as curing proceeds. Irgacure 819 used in this project is a photo-bleaching initiator as described above.

Due to these thick applications, people pay more and more attention to the cure kinetics versus depth in thick films. They try to understand the spatial[5] and temporal[23,24] variation of light intensity and product properties to make desired products. But, these studies are mainly theoretical calculations with a model based on an ideal situation and using some assumed parameters. The real situation is usually much more complex.

In this dissertation, the theoretical calculations and experimental methods are combined. They complement and support each other.

In Chapter 3, the intensity versus **depth and exposure time** is studied first since photo-initiated curing follows a surface-to-depth gradient due to the absorption of light throughout depth and the photo-bleaching of initiator. Here, UV radiation is mainly absorbed by photo-initiator, so the intensity through depth is directly controlled by the PI concentration. Irgacure 819 is a photo-bleaching initiator so that the intensity at deeper layer increases with exposure time as the initiator at upper layer is photo degraded. The rate of the intensity increase is determined by the degrading speed of the initiator.

In Chapter 4, the intensity (365 nm), initiator concentration, and temperature effect on the cure kinetics will be studied using thin samples (0.05 mm) by FTIR. The cure through the depth of these thin samples can be regarded as homogeneous since the light absorption through depth is less than 4.6%. A model is developed to predict the cure at a given intensity, initiator concentration, and temperature based on thin sample kinetics experimental results.

In Chapter 5, dielectric measurement is used to measure the cure kinetics of thin samples and to correlate the dielectric output with the FTIR results.

In Chapter 6, a calculation method is developed based on the experimental and modeled results described in Chapters 3 and 4 to predict the UV cure kinetics as a function of depth and the average cure through depth. The predicted result will be compared with the experimental data measured by transmitted FTIR and dielectric sensors.

In Chapter 7, the diffusion of reactive species from exposure area to dark area is studied by monitoring the cure in a non-irradiated region under a mask by FDEMS. In addition, a free radical thermal cure of an acrylic resin will be researched to study the oxygen diffusion from the surface layers to deeper layers.

## References:

1    Marignier, J.-L. In Processes in photoreactive polymers; Krongauz, V. V.; Trifunac, A. D., Eds.; Champman&hall: New York, 1995, p 3-34.

2    Hoyle, C. E. In Organic coatings: their origin and development; Seymour, R. B.; Mark, H. F., Eds.; Eslevier Scinece Publishing Co., 1990, p 233-43.

3    Baikerikar, K. K.; Scranton, A. B. Polymer 2001, 42, 431-41.

4    Sipani, V.; Coons, L. S.; Rangarajan, B.; Scranton, A. B. In RadTech Report; RadTech International North America, 2003, p 22-26.

5    Lee, J. H.; Prudhomme, R. K.; Aksay, I. A. J. Mater. Res. 2001, 16, 3536-44.

6    Jockusch, S.; Koptyug, I. V.; McGarry, P. F.; Sluggett, G. W.; Turro, N. J.; Watkins, D. M. Journal of American Chemical Society 1997, 119, 11495-501.

7    Sluggett, G. W.; McGarry, P. F.; Koptyug, I. V.; Turro, N. J. J. Am. Chem. Soc. 1996, 118, 7367-72.

8    Jockusch, S.; Turro, N. J. Journal of American Chemical Society 1998, 120, 11773-77.

9    Rutsch, W.; Dietliker, K.; Leppard, D.; Kohler, M.; Misev, L.; Kolczak, U.; Rist, G. Progress in Organic Coatings 1996, 27, 227-39.

10    Kolczak, U.; Rist, G.; Dietliker, K.; Wirz, J. J. Am. Chem. Soc. 1996, 118, 6477-89.

11    Hoyle, C. E. In Radiation Curing of Polymeric Materials; Hoyle, C. E.; Kinstle, J. F., Eds.; American Chemical Society: Washington, DC, 1990.

12    Odian, G. Principles Of Polymerization; John Wiley&Sons, INC., 1991.

13      Berchtold, K. A.; Randolph, T. W.; Bowman, C. N. ACS meeting, 2003, pp 213-14.

14      Berchtold, K. A.; Randolph, T. W.; Bowman, C. N. Macromolecules 2005, 38, 6954-64.

15      Rey, L.; Galy, J.; Sautereau, H.; Lachenal, G.; Henry, D.; Vial, J. Applied Spectroscopy 2000, 54, 39-43.

16      Scherzer, T.; Decker, U. Polymer 2000, 41, 7681-90.

17      Scherzer, T.; Decker, U. Radiation Physics and Chemistry 1999, 55, 615-19.

18      Lecamp, L.; Youssef, B.; Bunel, C.; Lebaudy, P. Polymer 1997, 38, 6089-96.

19      Lecamp, L.; Youssef, B.; Bunel, C.; Lebaudy, P. Nuclear Instruments and Methods in Physics Research B 1999, 151, 285-89.

20      Lecamp, L.; Youssef, B.; Bunel, C.; Lebady, P. Polymer 1999, 40, 6313-20.

21      Lecamp, L.; Youssef, B.; Bunel, C.; Lebaudy, P. Polymer 1999, 40, 1403-09.

22      Schrof, W.; Beck, E.; Koniger, R.; Reich, W.; Schwalm, R. Progress in Organic Coatings 1999, 35, 197-204.

23      O'Bren, A. K.; Bowman, C. N. Macromolecules 2003, 36, 7777-82.

24      Terrones, G.; Pearlstein, A. J. Macromolecules 2004, 37, 1565-75.

25      Chong, J. S. Journal of Applied Polymer Science 1969, 13, 241-47.

26      Decker, C.; Jenkins, A. D. Macromolecules 1985, 18, 1241-44.

27      Studer, K.; Decker, C.; Bech, E.; Schwalm, R. Progress in Organic Coatings 2003, 48, 92-100.

28      Studer, K.; Decker, C.; Bech, E.; Schwalm, R. Progress in Organic Coatings 2003, 48, 101-11.

29      Wight, F. R. J. Polym. Sci., Polym. Lett. Ed 1978, 16, 121-27.

# Chapter 2.   The UV cure instruments

## 2.1    Introduction

The UV cure project was a new one when I entered the lab. Ordering and assembling the cure instruments (from the catalog of ORIEL INSTRUMENTS) was the first thing I did with another graduate student, Nick. This chapter describes the instruments I selected, their function, price, and why I chose them from other related products.

When ordering the equipment, several factors were considered. First is the function of the part that should satisfy the objectives of the project. Second is that these parts should work together. Third is the price.

The objective of the project is to study the cure kinetics of a dimethacrylate resin at particular depths and non-irradiation regions using the UV light at 365 nm wavelength and within a narrow band pass. Based on this objective, I examined literature reports on the UV cure kinetics of methacrylate's oligomers. It was found that the instruments need at least the following 5 components:

1.  light source,

2.  filter,

3.  shutter,

4.  light guide (fiber optic cable),

5. radiant detector.

The diagram of the instrument is shown in Figure 2.1.
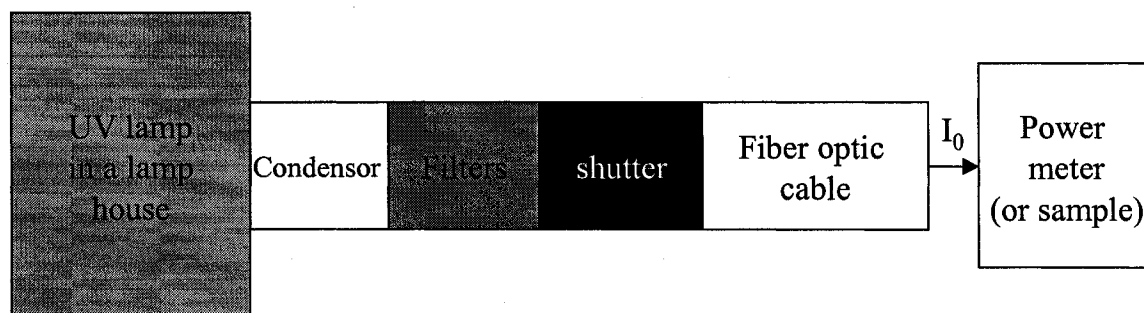


Figure 2.1 The graph of the instrument

After acquiring this general knowledge, we started to look through the catalog of ORIEL INSTRUMENTS and order the components. This process was harder than what was expected since there were so many choices for each part. In addition, it was found that each instrument also needed some accessories, such as power supplies, sockets, holders and connection parts, etc. This made the ordering process even more complex.

The detailed information about all components and accessories, their functions, and the reason for ordering them will be described in section 2.2. In Section 2.3 the prices will be described.

## 2.2    The composition of instruments

### 2.2.1    UV light source

A UV light source is composed of a lamp, a lamp housing with a condenser, a power supply and a socket adapter.

**The lamp** is the most important part that emits UV light and offers energy to induce the polymerization. It was found from the catalog that there are many kinds of lamps, such as QTH lamps, DC ARC lamps, Pulsed Xe ARC lamps, and $D_2$ lamps and all of them have irradiation in the UV wavelength from 200 to 400 nm. From the papers we researched, the most popular lamp is mercury (Hg) HBO/ARC lamp and Xe lamps for studying the UV cure kinetics of methacrylate's oligomer and the wattage is 100 or 200 W. It also found from the catalog that Hg ARC lamps give the strongest irradiation at 365 nm. So we decided to use Hg (ARC) lamp. The wattage of the mercury (ARC) lamps in the catalog is from 50 to 1000 watts. The lamp with a higher power is more expensive. We eventually chose the 200 W lamps since the price of 200W lamp is $162 that is not much more expensive than 100 W ($136) but the horizontal intensity is 4 times higher. We believe 200 W is enough for our research subject because it is what others used in many published papers for similar research topics.

**The lamp housing** covers the lamp and blocks the UV light to protect the people around from the strong UV exposure and keep the lamp clean and safe. It is the next item ordered after the lamp has been selected. There are two types of proper lamp houses for 200 W Hg lamp, PHOTOMAX™ and RESEARCH ARC lamp housing. Although the RESEARCH ARC lamp housing is more expensive, it has many advantages compared with PHOTOMAX™ lamp housing. For example, it has improved lamp adjustment with the rear reflector. Further, it has a temperature sensor to control fan operation and hence the radiation is more stable. In addition, the condensing lens assemblies are built in and have a locking screw to prevent accidental disturbances. Due to all these advantages, we decided to order the RESEARCH ARC lamp housing. There are two sizes of aperture,

1.5 and 3 inches, for the RESEARCH ARC lamp housing. The house with 3 inches aperture is $800 more expensive. In addition, other parts such as filters and shutters are also more expensive if the aperture is larger. So we decided to order the lamp house with 1.5 inches aperture and UV grade fused silica condenser. The house with 1.5 inches aperture is 66902 as shown in Figure 2.2.

**The power supply** converts AC power into DC power and supply energy to the lamp and the lamp housing. For the 200 W Hg lamp, there are two types of power supplies in the catalog. One is 68907 Universal Supply that operates lamps from 50-200 W and the other is 68910 Mercury Supply that operates lamps from 200-500 W. We chose 68907 because it is a universal supply that is also good for other type of lamps. In addition, 68910 was out of stock at that time and we would have to wait for several months to get it.

**The socket adapter** is used to connect the lamp to the lamp house. The type of the socket adapter is given clearly in the catalog for the 200 W Hg lamp. The product number is 66144.

**The cable** connects the lamp house (lamp) to the power supply. For the 200 W Hg lamp, the proper cable is also given in the catalog, as the part number is 70051.
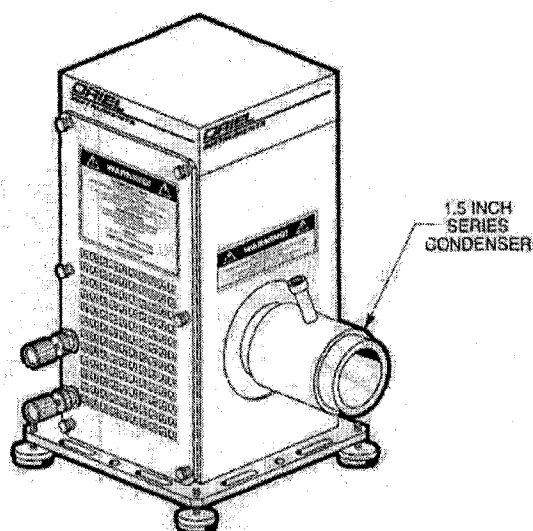
Figure 2.2 The picture of the lamp house for 200 W Hg lamp with a condenser.

## 2.2.2 Filters

There are many kinds of filters in the catalog, such as Colored Glass Filters, Neutral Density Filters, Interference Filters, Long and Short Pass Filters, Liquid Filters, Dichroic Filters. These filters either reduce the intensity of light homogeneously throughout the whole wavelength range (such as Neutral Density Filters) or reduce the intensity of light at some wavelength range and pass the light at other wavelength range. According to the requirements of our project, we need a filter that passes the light at 365 nm and with a narrow band pass. There are two choices, UV interference filters or analytical and mercury line filters. Both of them have a bandwidth of 10nm. The UV interference filter series include one with the center wavelength at 360nm and the minimum peak transmission is 25. The analytical and mercury line filter series include one with the center wavelength at 365 nm and the minimum peak transmission is 20. I would like the analytical and mercury line filters because its center wavelength is at 365nm which is the exact wavelength we need. In addition, the lamp radiation spectrum

also has a sharp peak at this wavelength. But the UV interference filter has a higher peak transmission and it was already ordered before I joined the group. So we kept it. I think that is probably the reason that our lamp gives relatively low intensity compared with some reported values for similar lamps. A 1.5 inch quick change filter holder was ordered to hold the UV interference filter.

The instrument also can include a liquid filter that passes UV and VIS and reduces IR. We did not order the liquid filter at the beginning because it is $347 and it is described in the catalog that the liquid filter is necessary for <u>more than 500 W</u> ARC radiation sources to protect the optics from the damaging heat of the IR. So we thought it was not necessary for the <u>200 W</u> ARC lamp which has lower radiation. However, this proved to be wrong after a UV interference filter was burned. So, we ordered a water filter later.

### 2.2.3 Shutter

Shutters are used to control the exposure time and frequency. There are several parameters that need to be considered when ordering the shutter. They are minimum exposure time, aperture diameter, delay time, and minimum pulse width. These parameters are very important for super fast cure that occurs at high light intensities. Our light intensity is less than $1\ mw/cm^2$ at 365 with 10nm bandwidth and therefore the reaction rate is relatively slow. A low cost electronic shutter, 71455, satisfies the requirement of our experiments. So we ordered it and a 68945 Digital Timer was also ordered to drive the shutter. This shutter has the 0.2s minimum exposure time, 0.5 Hz maximum repetition rate, and 1.5 inch aperture.

### 2.2.4  Light Guides

Light Guides are used for directing the light to the sample cell of the FTIR, DSC, or dielectric sensor and hence the cure and the characterization can be carried on at the same time. The material that is used to make the optic fibers determines the spectral range. For example, glass fibers have good transmittance for the light at the wavelength range of 400-1500 nm. So it is not good for 365 nm. Fused Silica works well from 280-2200nm which covers 365 nm. A Liquid Light Guide works well from 300 to 650 nm. Both Fused Silica Fiber and the Liquid Light Guide satisfy the requirement of our project. Comparing the price and the diameter, it was found that the Liquid Light Guide was $400 cheaper than Fused Silica Fibers and the diameter of Liquid Light Guide is larger which makes it easier to transmit more light into the fiber. Furthermore, a Liquid Light Guide has excellent UV transmittance and high throughput. So, the Liquid Light Guide was ordered.

### 2.2.5  Radiant detector

Radiant detector is usually composed of two parts: a radiant power meter and a probe. A radiant power meter displays the power of the light detected by the probe (detector) connected to it.

There are four kinds of probes in the catalog, such as Silicon, Germanium, Pyroelectric, and Thermopile. And for each kind of probe, there are many products that have different sensitive intensity ranges and wavelength ranges. After comparing different products, we found the Silicon probe to be a good choice since its spectral coverage is from 200 to 1100 nm and the signal level is from 100 pW to 3 W. But I did not make the decision to order it because I had no information about other probes, such as

Thermopile and Pyroelectric probes that are much cheaper. So I asked Dr. Luepke and his students for suggestions before we made the final decision since they use laser and different kinds of detectors frequently in his lab. From them I learned that Thermopile and Pyroelectric probes detect the power by different mechanisms. They are usually used to detect the light intensity at a higher intensity. The error of the measured data is usually large if they are used to measure an intensity less than 1 mw. And a photo-multiplier may be needed to make them work well. This is more complex. Thus the Silicon probe is the most convenient system for us even though it is expensive. So we eventually ordered the 70282 silicon detector. The power meter we ordered is a universal 70260 Radiant Power Meter.

## 2.3    The Price of the instruments

It has been described above that price of the instrument is also an important factor that we considered when we ordered them. In this section, the prices of all parts and the total prices are listed in Table 2.1. Table 2.1 gives a general idea of the total cost for the equipment of our UV cure project. Note that these prices are the data listed in the catalog and the real price was 10% more when we ordered them. In addition, the price actually increases a certain percent every year. Furthermore, lamps and UV Interference Filters are consumable parts and an extra lamp and UV interference filters were ordered during the research process.

Table 2.1 Prices of all parts

| Name of the component | | Model number | Size (inch) | Price ($) |
|---|---|---|---|---|
| Light | 200 W Hg Lamp | 6283 | | 162 |
| source | Lamp House (with a condenser) | 66902 | 1.5 | 2,212 |
| | Power Supply | 68907 | | 2,881 |
| | Socket Adapter | 66144 | | 55 |
| | Cable | 70051 | | 82 |
| Filter | UV interference Filters | 53410 | 1 | 298 |
| | Filter holder | 71260 | 1.5 | 229 |
| | Liquid Filter | 61945 | 1.5 | 347 |
| Shutter | Low Cost Electronic Shutter | 71455 | 1.5 | 550 |
| | Digital Timer | 68945 | | 997 |
| Light Guide | Liquid Light Guide | 77628 | 0.3 | 593 |
| Power Meter | UV Silicon Probe | 70282 | | 662 |
| | Radiation Power Meter with Charger | 70260 | | 1,175 |
| Total price | | | | 10,243 |

## 2.4    Conclusion

The equipment for doing UV cure was after much work eventually successfully set up and it worked well for the whole project even though the light intensity is not as high as we expected. But the lower intensity was later proved to be better to study the cure kinetics of thin sample since the reaction rate is lower so that the heat released from the exothermal reaction was balanced by the environment and did not significantly affect the cure kinetics.

The process of ordering equipment was like walking in the darkness at the beginning. But after I received them and assembled them, it became much clearer. I learned a lot from this process. I found it was much easier to solve a problem by asking those persons who have experience than working on it by myself. If I do it again, I would have more communication with technicians from the instrument company and other experts in the department.

# Chapter 3. Study of the light intensity and [PI] versus exposure time and depth in thick samples

## 3.1　Introduction

Photo bleaching means the photo initiator becomes transparent or has a lower absorption coefficient at a certain exposure wavelength. The photolysis of a set of aryl phosphine oxides including Irgacure 819 has been studied.[1,2] The outcome shows that the initiators exhibit pronounced photo bleaching at the 365 nm wavelength. The reason for this phenomenon is that the initiator undergoes $\alpha -$ breakage to produce a benzoyl-phosphinoyl pair. The optical absorption spectrum of the benzoyl-phosphinoyl radical pair (afer 8 ns laser excitation) shows that the absorption at 365 nm is almost 0, but at this wavelength, the absorption of the initiator is strong before the exposure starts. Therefore, the initiator concentration can be calculated by the intensity absorbance of the system at 365 nm according to the Beer-Lambert Law if the absorption coefficient, $\varepsilon$ , is known. Further, it is possible to monitor the photolysis of the initiator by monitoring the change of the absorbance of the system during the cure process.

In this chapter, the absorption coefficient, $\varepsilon$ , of the initiator is measured first. Second, the photo bleaching is studied by calculating the intensity and the initiator concentration versus time at different depths. Third, the transmitted intensity was measured by a radiometer and the experimental data are compared with the calculated data.

## 3.2 Experiment

**Materials.** The photoinitiator bis(2,4,6-trimethybenzoyl)-phenylphosphine oxide (Irgacure 819, Ciba) was dissolved in an oligomer, ethoxylated (4) Bisphenol-A dimethacrylate (CD540, Sartomer, from INSA France). The structure of the initiator and oligomer are shown in Figure 3.1. The system was stirred at room temperature for one hour. The initiator concentration in the system is 0.05 to 0.2wt%.
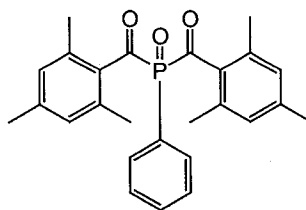
Irgacure 819, bis(2,4,6-trimethylbenzoyl)phenylphosphine oxide
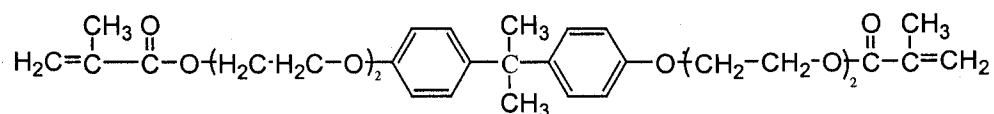
CD540, ethoxylated(4) Bisphenol-A dimethacrylate

**Radiation Source.** The radiation source was a 200 watt Hg HBO lamp equipped with a monochromator at 365 nm.

Other equipment used is listed in table 2.1 in Chapter 2.

## 3.3 Results and discussion

### 3.3.1 Measuring the absorption coefficient,ε , of initiator

The absorption coefficient can be calculated according to the Beer-Lambert Law as shown in Equation 3-1

$$A = \log(I_i / I_t) = \varepsilon \, b \, c \qquad\qquad \text{Equation 3-1}$$

$I_i$ is the incident intensity to the surface of the thick sample, $I_t$ is the transmitted intensity through the sample, $\varepsilon$ is the absorption coefficient (Molar absorbtivity) ($1 \, mol^{-1} \, cm^{-1}$), b is the path length of the sample (cm), c is the concentration of the IC819(mol/l).

The typical method for measuring the absorbance of a chemical involves using a reference solvent, which can dissolve the chemical and does not absorb the light. Acetone is a good solvent for the initiator Irgacure 819 as it dissolves the initiator very well and it is transparent for the UV light of 365 nm. So acetone was used first as the solvent, then the monomer, CD540, was used as the solvent.

### 3.3.1.1 Using acetone as the solvent to measure the absorption coefficient of the initiator

Using acetone as the solvent, two solutions with different initiator concentration were made and experiments were conducted for two thicknesses. The absorbance was measured by an UV spectrometer and the outcome is shown in table 3.1

Table 3.1 Absorption and extinction coefficient of IC819 at 365nm (using acetone as solvent)

| C (mol/l) | B (cm) | A | Absorption coefficient $\varepsilon$ ($1 \, mol^{-1} \, cm^{-1}$) |
|---|---|---|---|
| 0.012766 | 0.1755 | 1.9548 | 873 |
| 0.006383 | 0.1755 | 1.0397 | 928 |
| 0.012766 | 0.0815 | 0.9543 | 917 |
| 0.006383 | 0.0815 | 0.4287 | 824 |

C is the concentration of [PI], b is the thickness of the mode, A is value of absorbance.

Using data in table 3.1, the absorbance versus the cell thickness and the initiator concentration is plotted in Figure 3.1.
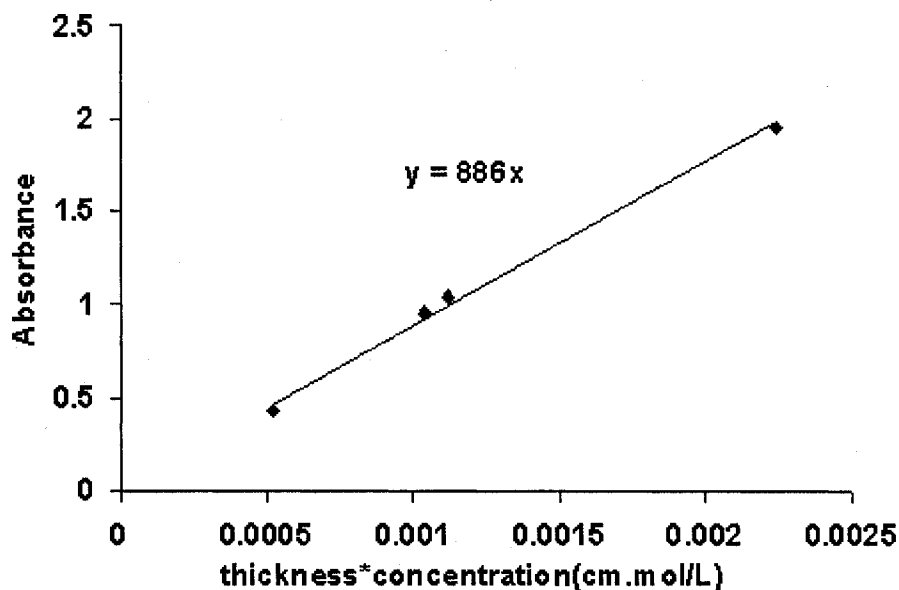


Figure 3.1 Measurement of initiator absorption coefficient using acetone as the solvent

Figure 3.1 shows that four data points fit well on a straight line through point (0,0), the fitted Equation gives the average value of $\varepsilon$, 886.32 l mol$^{-1}$ cm$^{-1}$, which approaches the value of 879 l mol$^{-1}$ cm$^{-1}$ in another paper.[3]

### 3.3.1.2 Using the monomer, CD540 as solvent to measure the absorption coefficient

Besides acetone, CD540 was also used as solvent directly to study the absorption coefficient of the initiator. Samples used for measuring the absorption coefficient are the same as the samples used for studying the cure kinetics. For a system with more than two components that absorb the light, Equation 3-1 can be written as

$$A = \log (I_i / I_O ) = b * ( \varepsilon_1 c_1 + \varepsilon_2 c_2 + \varepsilon_3 c_3 + \cdots + \varepsilon_n c_n ) \qquad \text{Equation 3-2}$$

Since the system is composed of initiator Irgacure 819 and the oligomer CD540, the absorption coefficient of CD540 was measured first. Pure CD540 was put into cell with different thicknesses and the transmitted intensity at 365nm was measured and the data are plotted in Figure 3.2.



$$y = 0.0755x$$
$$R^2 = 0.9896$$
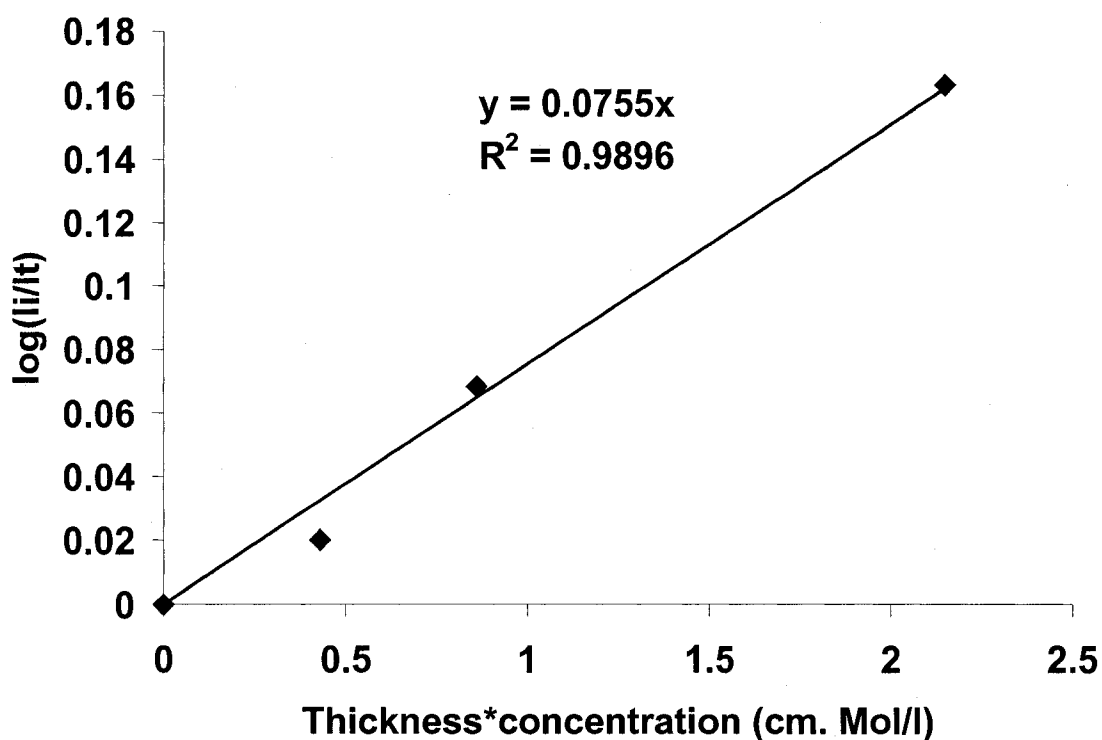
Figure 3.2 measurement absorption coefficient of CD540

From Figure 3.2, it is found that the absorption coefficient of CD540 is 0.0755 l mol$^{-1}$ cm$^{-1}$. This value is very similar to a previously reported value, $0.08 \pm 0.01$.[4]

A series of CD540 solutions with different concentrations of Irgacure 819 was made. The absorbance of the solution in the molds of different thickness was measured. Two different methods were used to calculate the absorption coefficient. One method used Equation 3-2 to deduct the absorbance of CD540 from the total absorbance. The absorbance of initiator versus thickness*[Irgacure 819] is shown in Figure 3.3.
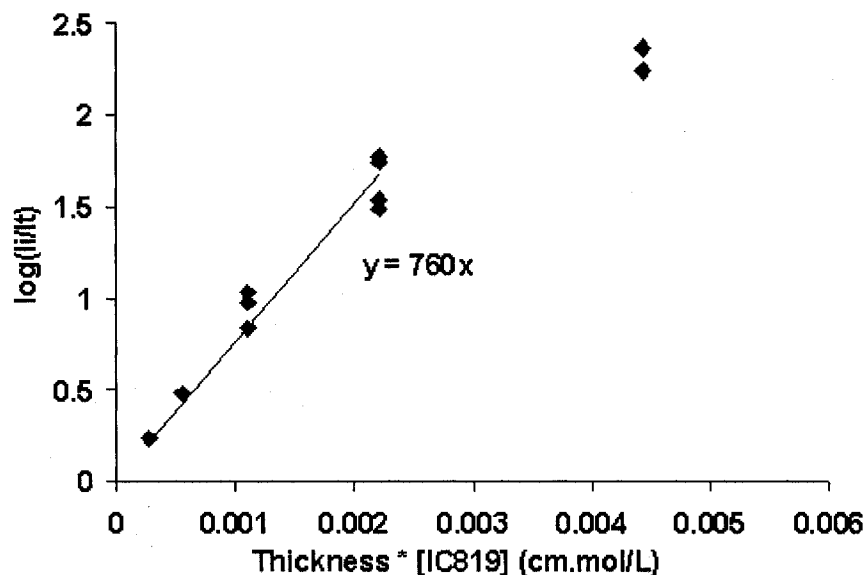
Figure 3.3 Measurement of initiator absorption coefficient using CD540 as solvent where absorption of CD540 was deducted.

The other method shown in Figure 3.4 disregards the absorption of the initiator.
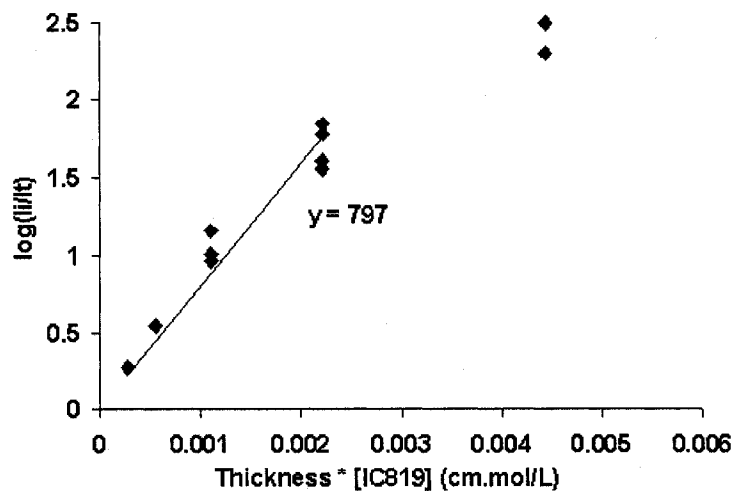


Figure 3.4 Measurement of total absorbance due to initiator and CD540.

Both Figure 3.3 and 3.4 show that the absorbance of initiator satisfies the Beer-Lambert Law when the multiplication of thickness and [IC819] is less than 0.003 cm mol $l^{-1}$. However when the multiplication value is high, both Figures show that the

experimental values deviated from the straight line. It does not fit Beer-Lambert Law any more. This is probably because the error of measuring the thickness of the sample or there were some bubbles in the system which did not absorb the UV light. This will be discussed in details in Chapter 6.

The absorption coefficient is calculated from Figure 3.3 using the points, which have a value of thickness times concentration on the axis less than 0.003 cm mol $l^{-1}$. The absorption coefficient of the initiator is 760 l $mol^{-1}$ $cm^{-1}$ as shown in Figure 3.3 when the absorption of the monomer is considered. If the absorption of the monomer is neglected since the absorption coefficient of CD540 is much smaller than Irgacure 819, the absorption coefficient is 797 l $mol^{-1}$ $cm^{-1}$ as shown in Figure 3.4. When the absorption of monomer is neglected, the error of the absorption coefficient of initiator is less than 5%. The value of 760 is used as the absorption coefficient of the initiator Irgacure 819 in the model calculations.

### 3.3.2 Study of the photo bleaching of Irgacure 819.

### 3.3.2.1 Theoretical background

The rate of initiator degradation can be express by Equation 3-3.

$$-\frac{d[PI]}{dt} = \phi' I_a \qquad \text{Equation 3-3}$$

$\phi'$ is the quantum yield of the **photo initiator consumption**, the mole number of photo-initiator degraded per Einstein photon absorbed. The value of $\phi'$ for $\alpha$ -cleavage of bis(acyl)phosphine oxides is reported to be 0.5[1] to produce a benzoyl-phosphinoyl radical pair. (Note: $\phi'$ is different from $\phi$, the quantum yield of **initiation**, the number of radicals which activate propagation formed for each photon absorbed as defined in

Odian's book[5].) $I_a$ is the absorbed photon number by **photo initiator** in units of Einstein $s^{-1} l^{-1}$. (Note that even though the monomer also absorbs light, it does not contribute to the consumption of the initiator.) The calculation of $I_a$ is shown below.

$$I_a = \frac{I_i - I_t}{b}$$
Equation 3-4

b is the thickness of the sample, $I_i$ is the incident intensity and $I_t$ is the transmitted intensity, both are in unit of $\mu w/cm^2$ as read from radiometer.

If the absorption of monomer is disregarded, then Equation 3-1 can be written as Equation 3-5.

$$I_t = I_i * 10^{-\varepsilon_i bc}$$
Equation 3-5

c is the concentration of Irgacure 819, [PI], $\varepsilon_i$ is the absorption coefficient of the initiator and its value is $760\ l\ mol^{-1}\ cm^{-1}$, as shown in section 3.2.2.

Substitute Equation 3-5 into Equation 3-4,

$$I_a = \frac{I_i * (1 - 10^{-\varepsilon bc})}{b}$$
Equation 3-6

Combine Equation 3-3 and 3-6, it gives Equation 3-7.

$$-\frac{d[PI]}{dt} = \frac{\phi' I_i (1 - 10^{-\varepsilon_i b[PI]})}{b}$$
Equation 3-7

Which can be written as Equation 3-8 when the time interval is very small

$$[PI]_{t2} = [PI]_{t1} - \frac{\phi' I_i (1 - 10^{-\varepsilon b[PI]_{t1}})}{b}(t_2 - t_1)$$
Equation 3-8

However, if the absorption of the monomer is considered, then according to Equation 3-2

$$I_t = I_i * 10^{-b(\varepsilon_i [PI]_t + \varepsilon_m [M])}$$     Equation 3-9

Here $\varepsilon_i$ is 760 l mol$^{-1}$ cm$^{-1}$ and $\varepsilon_m$ is 0.0755 l mol$^{-1}$ cm$^{-1}$ as shown in section 3.2.2. In equation 3-7 and 3-8 the absorption of monomer is not considered because the definition of I$_a$ in Equation 3-3 refers to the absorbed photon number **by [PI], not by monomer**.

### 3.3.2.2 Development of a model to calculate the change of the intensity and the initiator concentration versus exposure time at different depths.

The change of light intensity and the initiator concentration versus exposure time at different depths has been studied before.[6-10] However most of these papers regarded absorption of the monomer as 0 because the extinction coefficient of monomers is usually much smaller than the extinction coefficient of initiators. However, the fraction of monomers in the system is usually much larger than initiators, therefore the absorbance of the monomers may be important and affect the whole absorbance of the system. In this case, disregarding the absorbance of the monomer will affect the calculation of the transmitted intensity and [PI] versus exposure time at different depths.

In this section, two calculation models are set up. In the first model, the absorbance of the monomer is regarded as 0 as is the case in most other research reports. In the second model, the absorbance of the monomer is considered. Then, the calculation outcomes from two models are compared to see difference between them.

## 1)  Without considering the absorption of monomer

For the model, which regards the absorbance of the monomer as 0, the proper equations used for calculation are Equation 3-5 and 3-8. A Matlab program (appendix 2) is written to calculate the change of the intensity at the bottom and the average initiator concentration with the exposure time. Here, $\varepsilon_i$=760 1 mol$^{-1}$ cm$^{-1}$ from Figure 3.3 and $\phi'$=0.5$^1$.

First, the effect of the step size of time, st, on the outcome was studied by calculating using different value of st. The model predicted intensity at the bottom of the sample is shown in Figure 3.5a when st is 100 minutes, 10 minutes, and 1 minute.
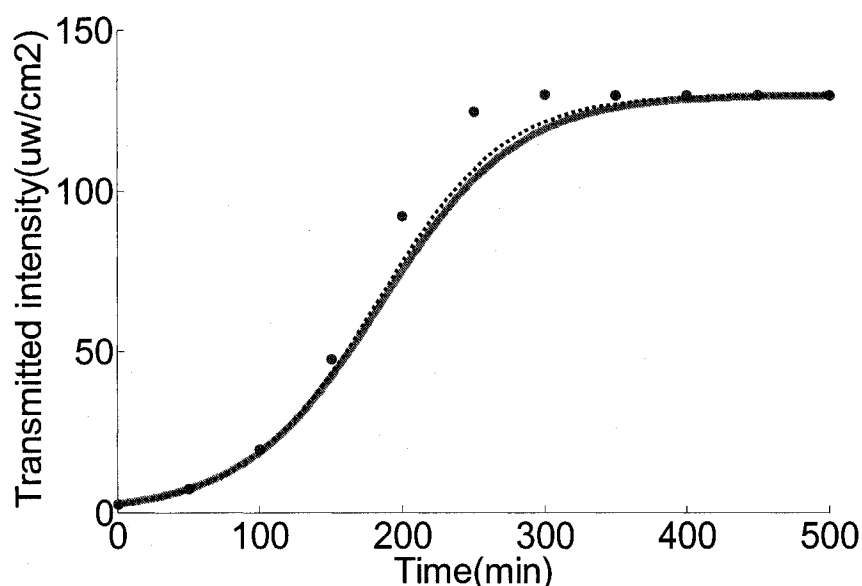


Figure 3.5a The model predicted transmitted intensity versus time at the bottom of a sample. CD540-0.2wt%Irgacure 819, Ii=130 uw/cm$^2$, Thickness of sample is 4 mm, [PI]=0.2wt%, $\varepsilon$ =760 1 mol$^{-1}$ cm$^{-1}$; $\phi'$=0.5. The values of step size of time, st, used for calculations are marked in the figure. ($\bullet$) st=100 minutes; (---) st=10 minutes; (—) st=1 minute.

The model predicted intensity at the bottom of the sample is shown in Figure 3.5b when st is 1 minute and 0.1 minutes.
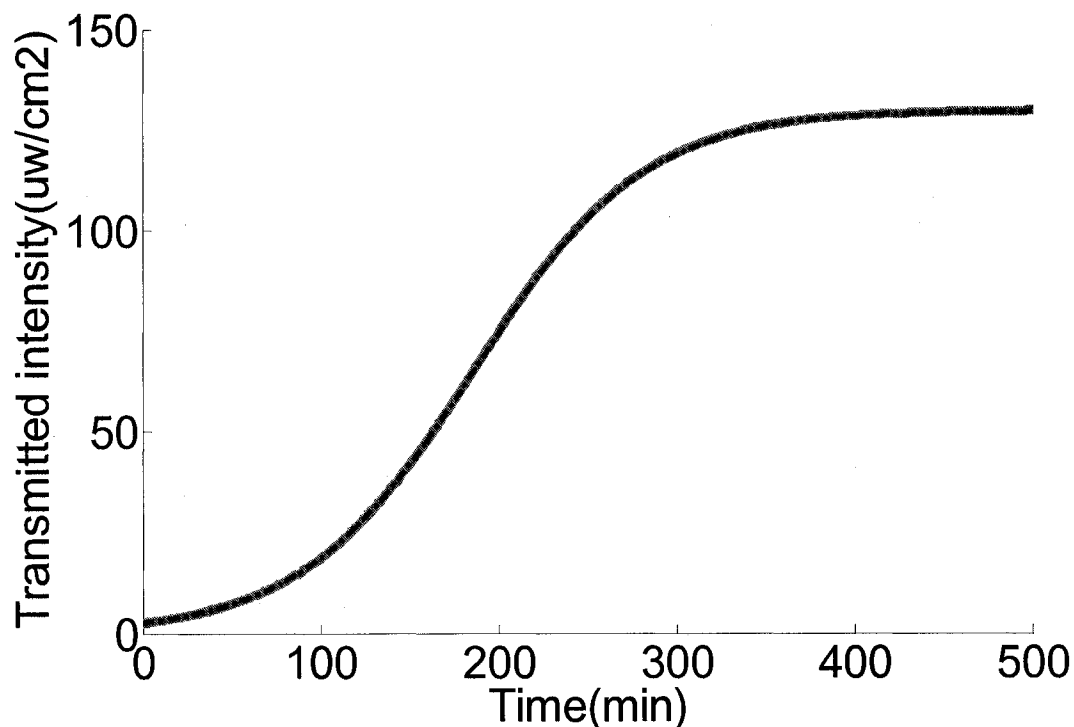


Figure 3.5b The model predicted transmitted intensity versus time at the bottom of a sample. CD540-0.2wt%Irgacure 819, Ii=130 uw/cm$^2$, Thickness of sample is 4 mm, [PI]=0.2wt%, $\varepsilon$ =760 1 mol$^{-1}$ cm$^{-1}$; $\phi'$=0.5. The values of step size of time, st, used for calculations are marked in the figure. (—) st=1 minute; (– · — · –) st=0.1 minutes.

After the intensity at the bottom of the sample is calculated, initiator concentration, [PI], versus exposure time is calculated too. The data are shown in Figure 3.6a when st is 100 minutes, 10 minutes, and 1 minute.
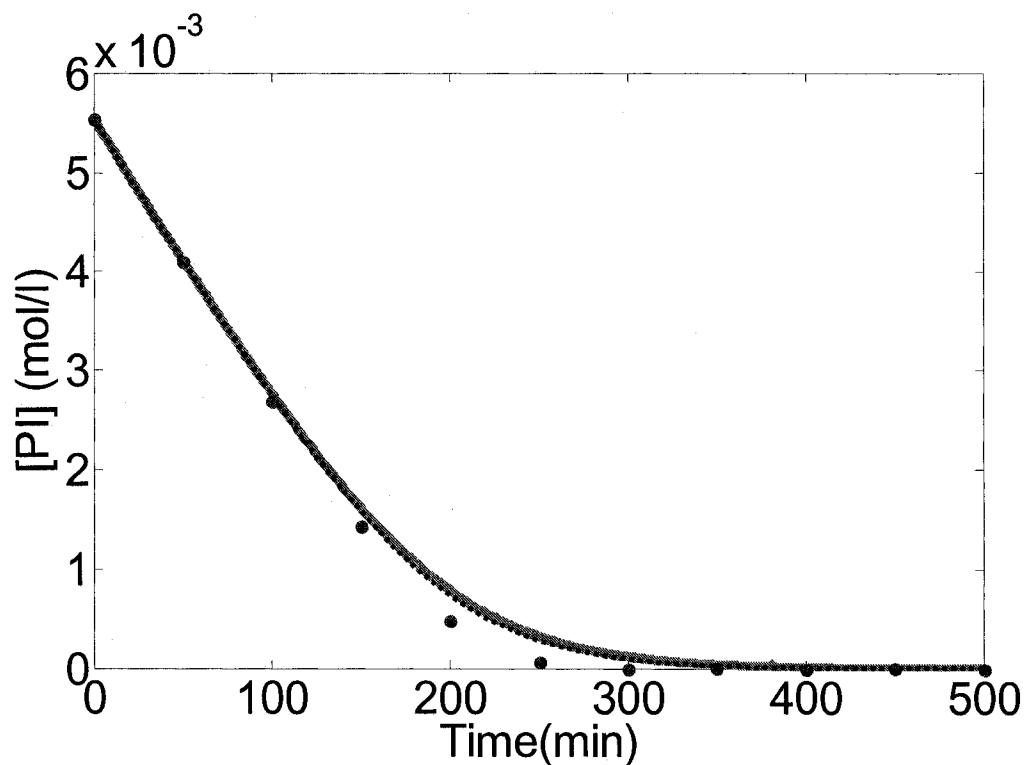
Figure 3.6a The model predicted average of [PI] versus exposure time in a thick sample. CD540-0.2wt%Irgacure 819, Ii=32.5 uw/cm$^2$, Thickness of sample is 4 mm, [PI]=0.2wt%, ε =760 l mol$^{-1}$ cm$^{-1}$; φ'=0.5. The values of step size of time, st, used for calculations are marked in the figure. (●) st=100 minutes; (---)st=10 minutes; (—)st=1 minute.

The model predicted [PI] versus exposure time of the sample is shown in Figure 3.6b when st is 1 minute and 0.1 minutes.
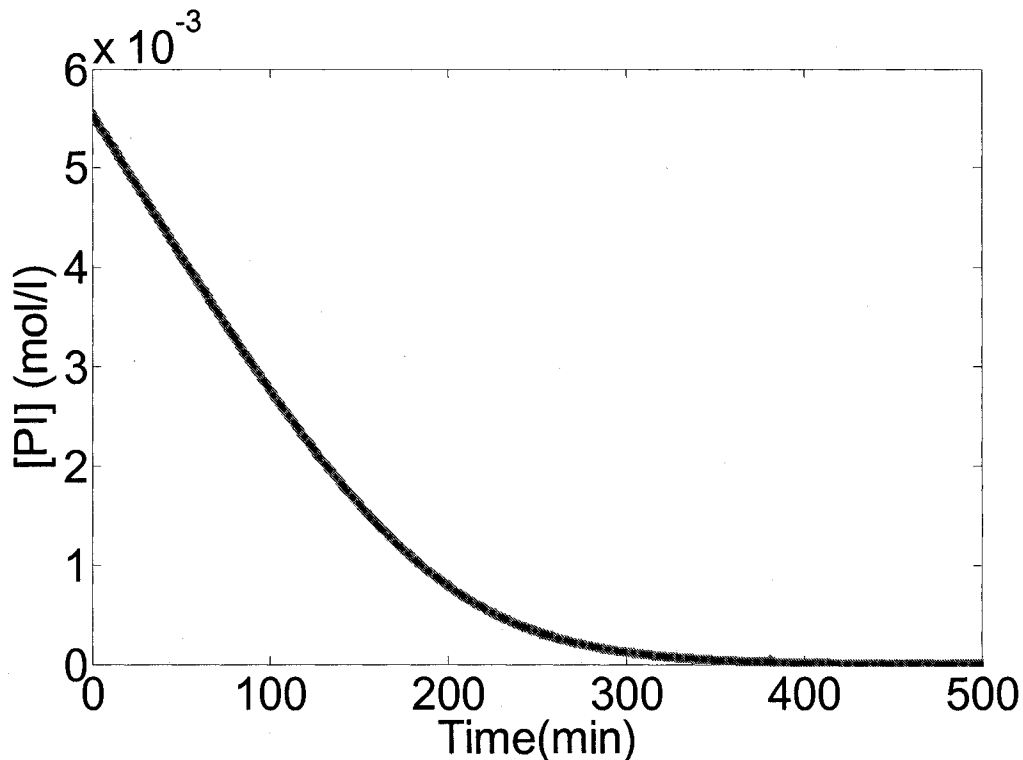
Figure 3.6b. The model predicted average of [PI] versus exposure time in a thick sample. CD540-0.2wt%Irgacure 819, Ii=32.5 uw/cm$^2$, Thickness of sample is 4 mm, [PI]=0.2wt%, ε =760 1 mol$^{-1}$ cm$^{-1}$; φ'=0.5. The values of step size of time, st, used for calculations are marked in the figure. (—) st=1 minute; (– · – · –) st=0.1 minutes.

Figures 3.5 and 3.6 show the effect of the time interval, st, on the calculated data of changing transmitted intensity and the average [PI]. Figures 3.5a and 3.6a show that there is some difference between the curves calculated using the step size of 100 minutes and 10 minutes. However there is a small difference between the curves calculated using the step size of 10 minutes and 1 minutes. Figure 3.5b and 3.6b shows that the model predicted curves using a value of st=1 and 0.1 minutes have little difference. It is known that decreasing the step size can minimize the error of calculation. However, decreasing

the step size will increase the calculation time, and therefore decrease the efficiency. Eventually **1 minute** is chosen as the step size in the later calculation, which produces less error compared with 10 and 100 minutes step size and the calculation efficiency is 10 times faster than the one with 0.1 minutes.

(Note: the step size here is only correct for the present reaction conditions. If the reaction is very fast, then it needs a smaller step size of time for the model calculation.)

After the proper step size was determined, the change of the intensity and the initiator concentration with the exposure time at different depths in a sample was studied. The effect of the number of layers on the transmitted intensity at the bottom was studied too. The program is designed to divide the thickness of the sample, TH, into NL (number of layers) thin layers and dividing the exposure time t into nt (total number of time points) with a step size of time, st. A matrix, I (NL, nt), is used to represent the intensity at NL depths through the exposure time and another matrix C (NL, nt) is used to represent the initiator concentration at all depths and throughout the exposure time t.

The initiator concentration versus time in the first layer is expressed in the program as C (1, 1:nt) which can be calculated using Equation 3-8. For these model trial calculations, the absorption of monomer is ignored. The values of parameters in the equation are that $\varepsilon_i$ is 760 1 mol$^{-1}$ cm$^{-1}$, b is equal to TH/NL, $[PI]_0$ is given from the original sample composition, t is the step size of time, $I_i$ is the incident intensity, which is a constant for the first thin layer, $\phi'$ is 0.5 from the published result[1]. Then using Equation 3-5, the transmitted intensity versus time of the first layer expressed as I (2, 1:nt) can be calculated, which is then the incident intensity of the second layer. Then [PI] versus time of the second layer can be calculated using Equation 3-8 again. This time $I_i$ is

I (2, 1:nt). So on and on, the transmitted intensity and initiator can be calculated at any depth for thick samples. The program is listed in appendix 2.

The effect of the number of layers, NL, is studied using a fixed step size of time, st=1 minute. First, the value of NL is set as 1,which means the sample is regarded as 1 thick layer. The model predicted transmitted intensity at the bottom is shown in Figure 3.7.
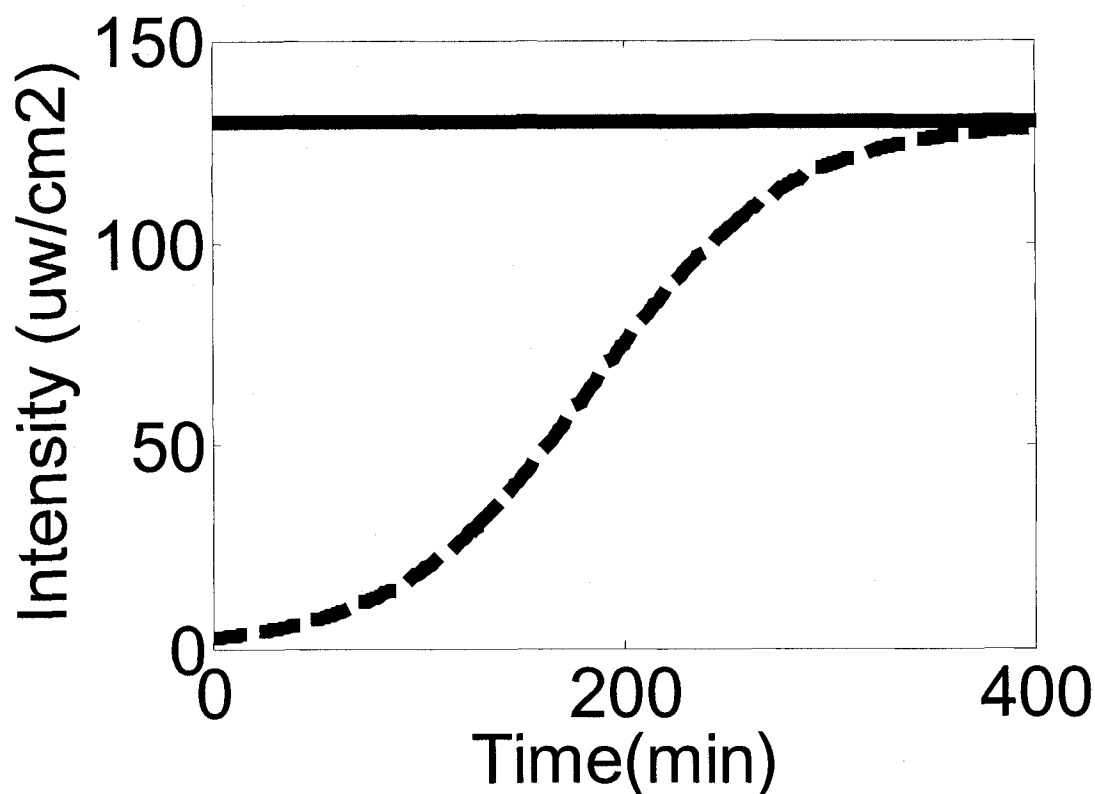


Figure 3.7 The model predicted transmitted intensity versus time. NL=1, the whole sample are regarded as one layer, CD540-0.2wt%Irgacure 819, $I_i$=130 uw/cm$^2$, Thickness of the sample=4 mm, [PI]=0.2wt%, $\varepsilon$ =760 1 mol$^{-1}$ cm$^{-1}$, $\phi'$=0.5, st=1minute. (——) Incident intensity at the surface; (– – –) transmitted intensity at the bottom.

Figure 3.7 shows that the transmitted intensity versus time at the bottom increases with the exposure time due to the photo bleaching of the initiator.

Next, NL is set as 10, which means the sample is divided to 10 homogeneous thinner layers. The transmitted intensity of each layer is shown in Figure 3.8.
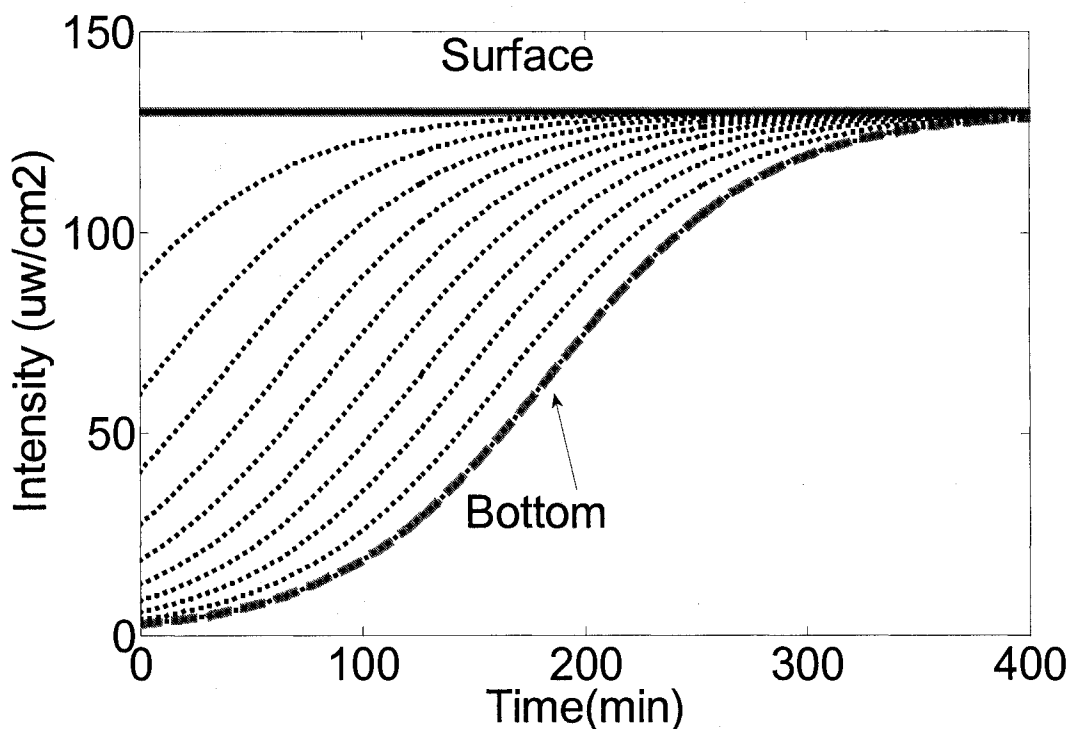


Figure 3.8 The model predicted transmitted intensity versus time at different depths in a thick sample. CD540-0.2wt%Irgacure 819, Ii=130 uw/cm$^2$, Thickness of the sample=4 mm, [PI]=0.2wt%, $\varepsilon$ =760 1 mol$^{-1}$ cm$^{-1}$,$\phi$'=0.5, st=1minute. (—) Incident intensity at the surface; NL=10, the sample thickness is divided to 10 layers: (---), Transmitted intensity at the bottom of each layer; NL=1, the whole sample is regarded as 1 thick layer: (— — —) transmitted intensity at the bottom.

Figure 3.8 shows the calculated transmitted intensities increase with the exposure time at all layers. The transmitted intensity at the bottom layer when NL=10 overlaps the

transmitted intensity when NL=1(thicker lines in figure 3.7 and 3.8). Which means the number of layers (NL) used for the calculation does not affect the calculation of the transmitted intensity at the bottom of the sample for this case when the absorbance of monomer is regarded as 0.

Next, the model predicted changing concentration of [PI] versus time at different layers is studied. First, the value of NL is set as 1,which means the sample is regarded as 1 thick layer. The model predicted [PI] of the whole sample is shown in Figure 3.9.
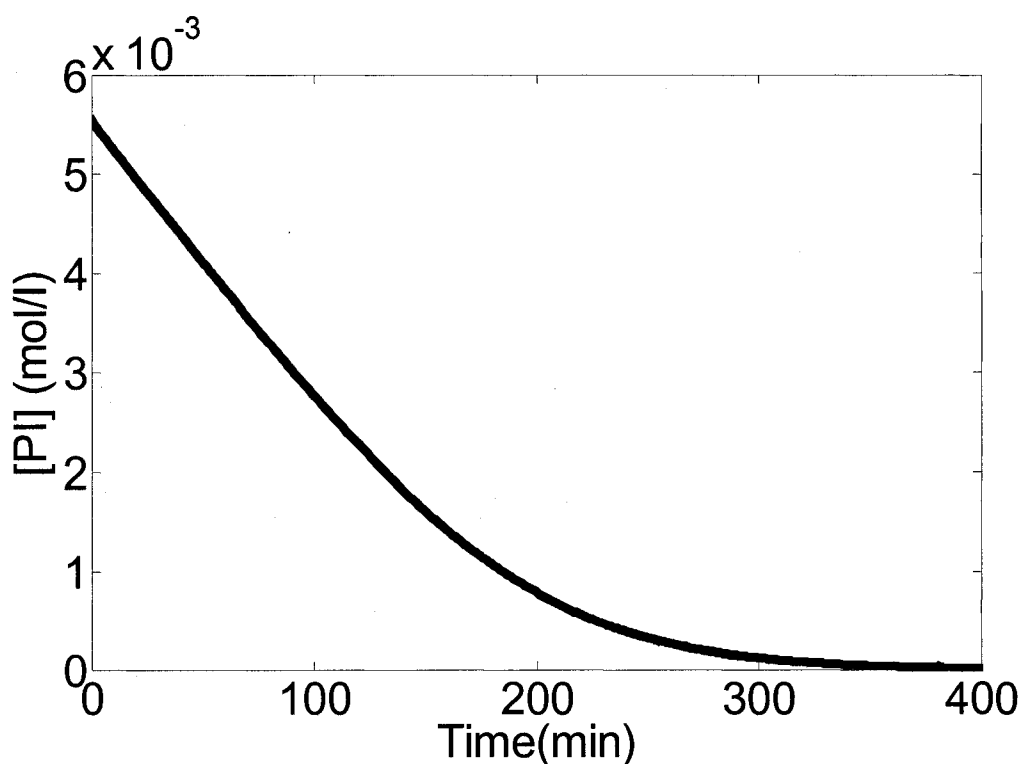


Figure 3.9 The model predicted changing of [PI] versus exposure time in a thick sample. CD540-0.2wt%Irgacure 819, Ii=130 uw/cm$^2$, Thickness of sample is 4 mm, [PI]=0.2wt%, $\varepsilon$ =760 l mol$^{-1}$ cm$^{-1}$, $\phi'$=0.5, st=1minute, NL=1.

Figure 3.9 shows that the total concentration of initiator decreases with the exposure time due to the photo bleaching of the initiator.

Next, NL is set as 10, which means the sample is divided into 10 homogeneous thinner layers. The changing of [PI] versus exposure time of each layer is shown in figure 3.10.
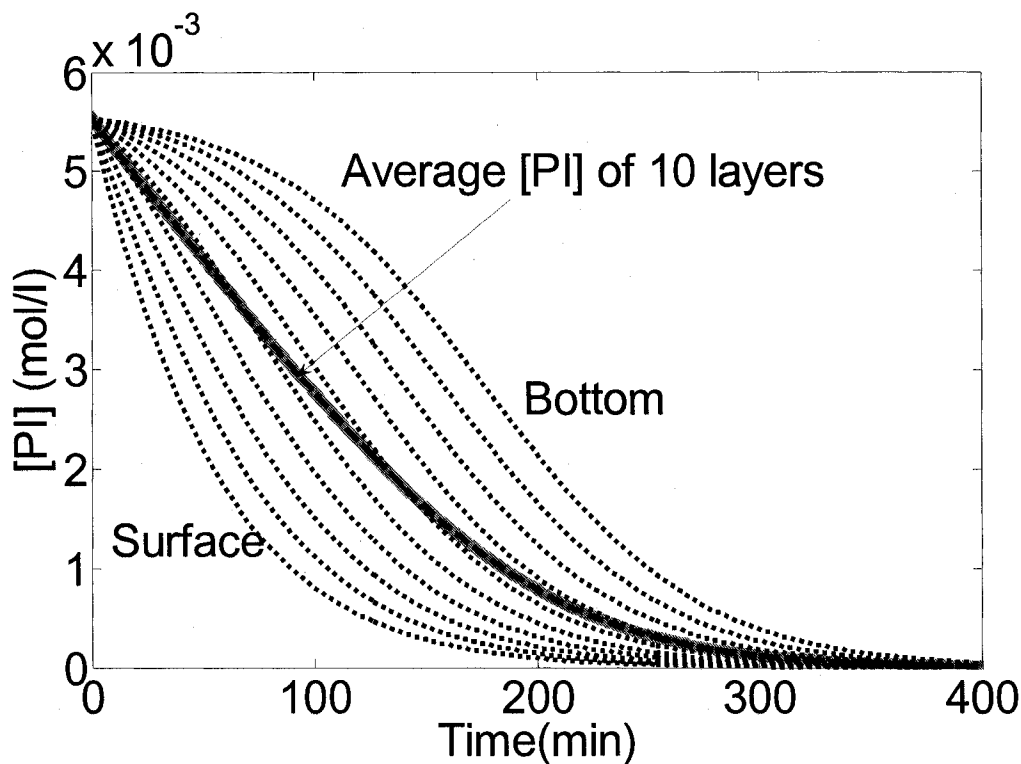


Figure 3.10 The model predicted changing of [PI] versus exposure time at different depth in a thick sample. CD540-0.2wt%Irgacure 819, Ii=130 uw/cm$^2$, Thickness of sample is 4 mm, [PI]=0.2wt%, $\varepsilon$ =760 1 mol$^{-1}$ cm$^{-1}$, $\phi$'=0.5, st=1minute. NL=10, the sample thickness is divided to 10 layers: (- - -) [PI] versus time at the bottom of each layer; (– – – ) average data of [PI] versus time of 10 layers; (—) the total changing of [PI] versus time when NL=1, the whole sample is regarded as 1 thick layer as shown in figure 3.9.

Figure 3.10 shows the data of the changing [PI] versus time in 10 thin layers and the average data of these 10 layers. It is found the initiator is consumed faster in the upper

layers than in the bottom layers. The average concentration of [PI] calculated when NL=10 overlap the data when NL=1 (solid thick curves in figure 3.9 and 3.10).

From the study in this section, it is concluded that when the absorbance of monomer is regarded as 0, **nt=1minute** is a reasonable step size of time for the model calculation. The intensity at different depths of a sample can be predicated by dividing the sample into NL layers. The total transmitted intensity at the bottom of the sample is not affected by the number of layers, NL.

### 2) Considering the absorption of monomer

In the section above, the absorption of monomer is disregarded in the calculation model. In this section, the absorption of the monomer is considered and therefore Equations 3-8 and 3-9 are used for the calculation. In order to simplify the calculation, the absorption of the monomer is approximated as a constant. This means the $\varepsilon$ of the monomer units before and after polymerization are the same. In this case, $\varepsilon_m$ is 0.0755 l mol$^{-1}$ cm$^{-1}$ as shown in Figure 3.2 and $\varepsilon_i$ is 760 l mol$^{-1}$ cm$^{-1}$.

The effect of st, step size of time, and NL, number of layers, on the model calculation is also studied here. It was found that similar with the first model in section 3.4.2.1, **st=1** is also a reasonable step size of time for the second model which considered the absorption of monomer. Since the result is very similar with Figure 3.5 and 3.6, it is not shown again here. However the effect of NL, number of layers, on the transmitted intensity at the bottom is different from the results above. The model predicted transmitted intensities using different number of layers are shown in Figure 3.11.
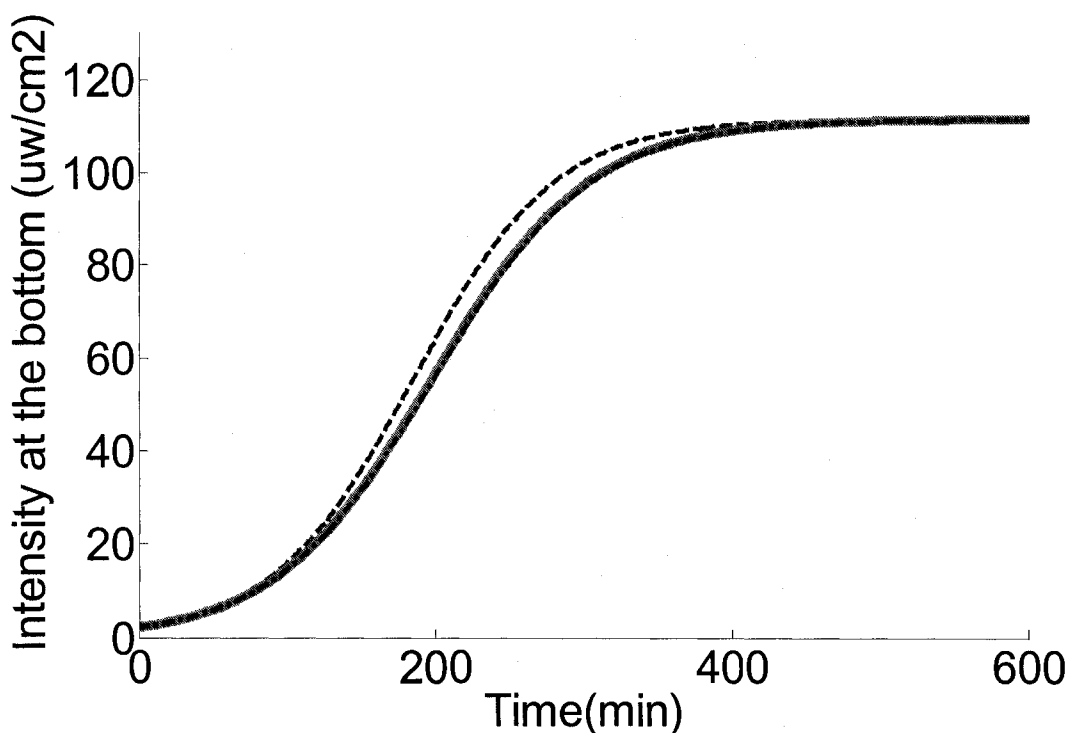
Figure 3.11 The transmitted intensity at the bottom of a thick sample. CD540-0.2wt%Irgacure 819, Ii=32.5 uw/cm$^2$, Thickness of sample is 4 mm, [PI]=0.2wt%, $\phi'$=0.5, $\varepsilon_i$=760 1 mol$^{-1}$ cm$^{-1}$, $\varepsilon_m$ is 0.0755. (– – –) NL=1; (—) NL=10; (– · – · –), NL=50

Figure 3.11 shows that, there is an obvious difference between the curve of NL=1 and NL=10. This means when the number of layers is lower than 10, the calculation error is statistically significant. However, the curve of NL=50 overlap with the curve of NL=10, and the difference between them is little. Therefore when the number of layers, NL, is set at more than 10, so the thickness of each layer is less than 0.4 mm, the error of calculation is trivial. The layer thickness used for calculation later is 0.05 mm to match the thin sample thickness in Chapter 4 and minimize the calculation error.

### 3) Comparing the predicted data using two different models.

Figure 3.11 and 12 shows the difference between the two models, (1) not considering the absorbance of monomers, and (2) considering the absorbance of the monomer. The step size of time, st, is 1 minute and the number of layers, NL, is 10 for both models. (NL is set as 10 here to give a clear view of the curves)
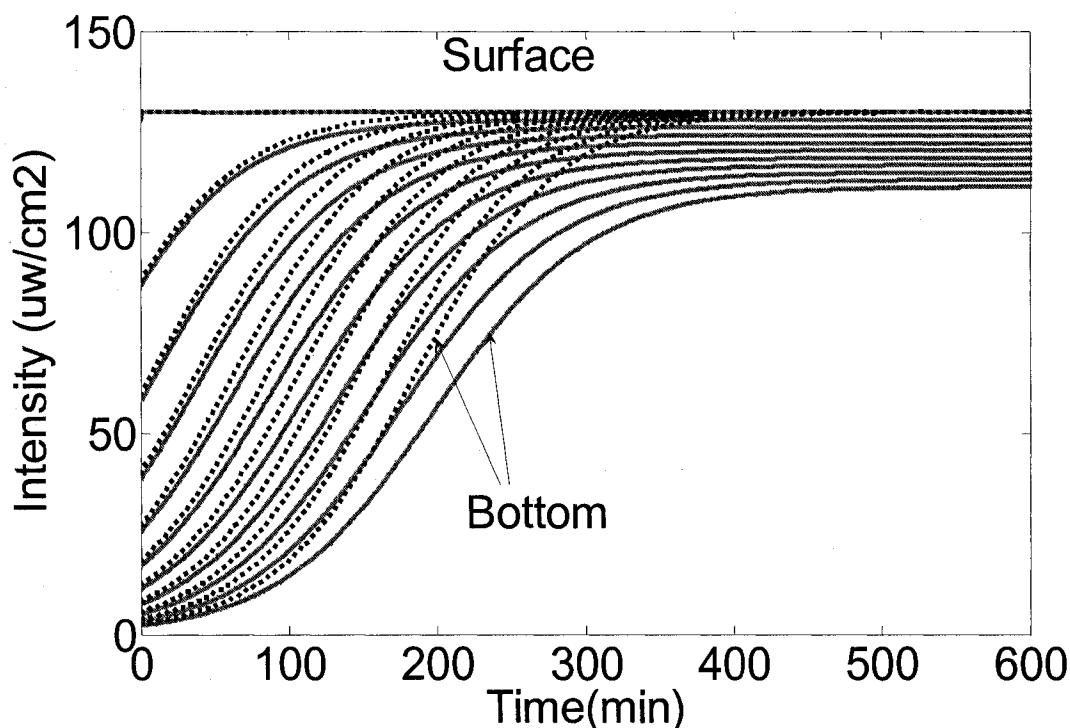


Figure 3.12 The model predicted intensity at different depths in a thick sample. CD540-0.2wt%Irgacure 819, Ii=130 uw/cm$^2$, Thickness of sample is 4 mm, [PI]=0.2wt%, $\phi'$=0.5, NL=10. (—) Considering the absorption of the monomer, $\varepsilon_i$=760 1 mol$^{-1}$ cm$^{-1}$, $\varepsilon_m$ is 0.0755; (---) without considering the absorption of the monomer, $\varepsilon$ =760 1 mol$^{-1}$ cm$^{-1}$.

It is seen from Figure 3.12 that when the absorption of the monomer is considered, the transmitted intensity increases slower than the one without considering

the absorption of the monomer. Further, the final transmitted intensity is lower and is determined only by the absorption of the monomer since all initiator is consumed then.

The predicted changing of initiator concentration versus time at different depths is shown in Figure 3.13 for both models.
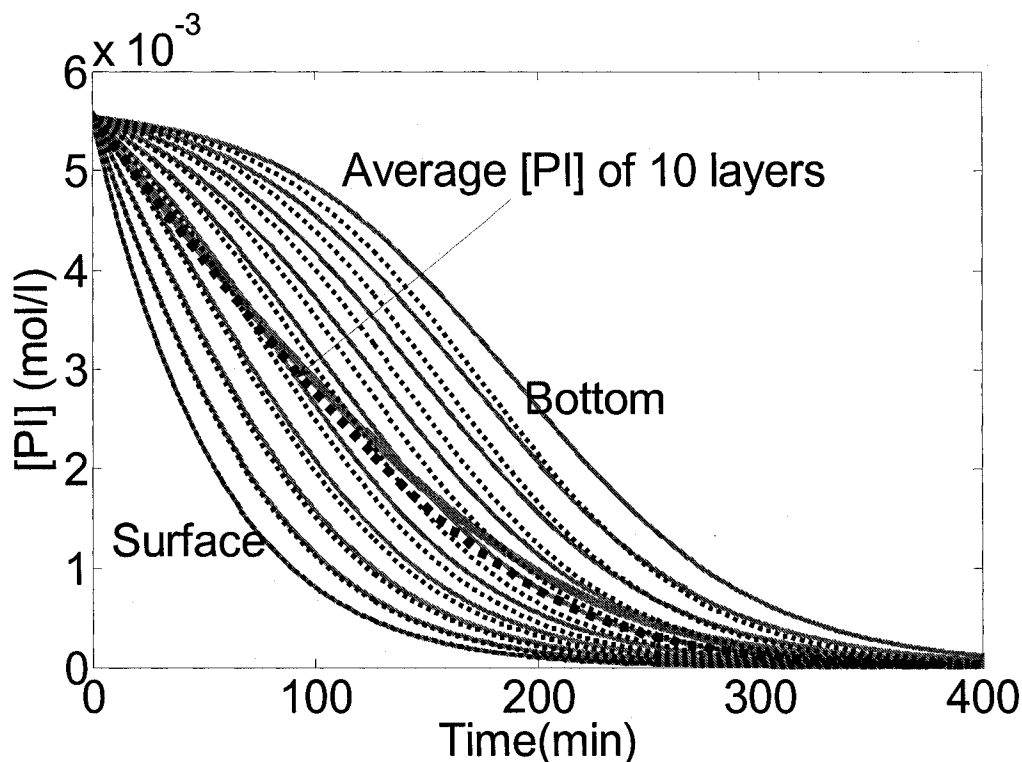


Figure 3.13 [PI] versus time at different depths in a thick sample. CD540-0.2wt%Irgacure 819, $I_i$=32.5 uw/cm$^2$, Thickness of sample is 4 mm, [PI]=0.2wt%, $\phi'$=0.5, NL=10. (—) Considering the absorption of monomer, $\varepsilon_i$=760 l mol$^{-1}$ cm$^{-1}$, $\varepsilon_m$ is 0.0755; (---) without considering the absorption of monomer, $\varepsilon$ =760 l mol$^{-1}$ cm$^{-1}$. Two darker curves in the middle of other curves are the average of all 10 layers.

Figure 3.13 shows that when the absorption of the monomer is considered, the initiator concentration in every layer decreases with exposure time. Comparing the solid curves and the dotted curves, it is found in the surface layer, the dotted curves overlay the

solid curve. However, at deeper layers, the dotted curves decrease faster than the solid curves. This means, the predicted consumption of [PI] at deeper layers is slower when the absorption of the monomer is considered than when absorption of the monomer is regarded as 0.

Both figure 3.12 and 3.13 show the difference of the predicted data calculated by the two different models. The deeper the layer (or the thicker the sample), the larger the difference. Therefore, it is necessary to consider the absorption of the monomer especially when the sample is thick, and the initiator concentration is large.

### 3.3.3 Calculation of transmitted intensities of thick samples and comparison with experimental data

Using the second model, which considers the absorbance of the monomer, the transmitted intensities of several thick samples under varying conditions were calculated using equation 3.8 and 3.9. Here $\varepsilon_i$=760 1 mol$^{-1}$ cm$^{-1}$, $\varepsilon_m$=0.0755 1 mol$^{-1}$ cm$^{-1}$, $\phi'$=0.5. The results are listed in Figures 3.14 to 3.16. The transmitted intensity was also measured by a radiometer. The experimental data are listed in the same Figure and compared with the calculated outcome.

The transmitted intensity of a system CD540-**0.4wt%**Irgacure 819 was studied first. The incident light intensity is 60uw/cm2, sample thickness is $3\pm0.5$ mm. The experimental data and the model predicted data are shown in figure 3.14a.
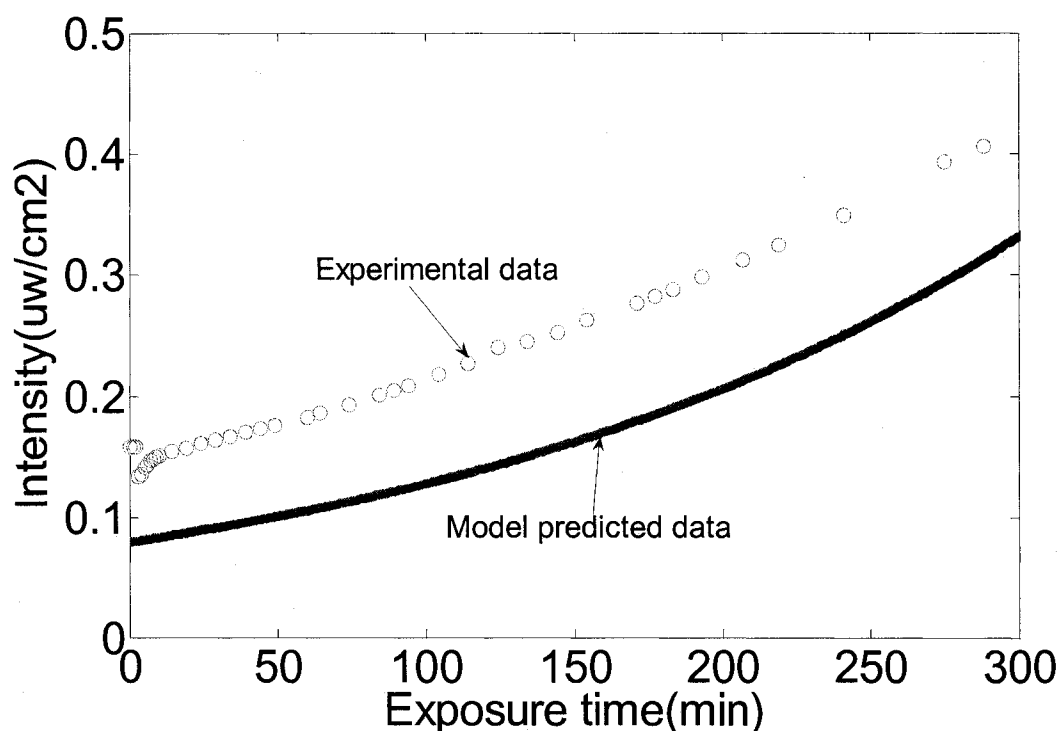
Figure 3.14a Transmitted intensity of a thick sample. CD540-0.4wt%Irgacure 819, Ii=30

uw/cm$^2$, Thickness of sample is 3 mm, $\phi'$=0.5, NL=50, $\varepsilon_i = 760$ 1 mol$^{-1}$ cm$^{-1}$,

$\varepsilon_m$=0.0755 1 mol$^{-1}$ cm$^{-1}$. (•••) Experimental data; (—) calculated data.

Figure 3.14a shows that for the system CD540-0.4wt%IC819, the calculated

intensity is lower than the experimental data at the beginning, which may due to the error

of measuring the thickness of the sample. Then, the thickness was calculated based on the

light absorbance of the sample and Equation 3.9. It was found that the correct thickness is

0.27 mm instead of 0.3 mm, a value which is determined by the spacer thickness of the

sample mold and the cell gap was assumed to be the exact value of the spacer. Using the

corrected thickness, 0.27 mm, the transmitted intensity was calculated again. The

predicted data are shown in Figure 3.14b.
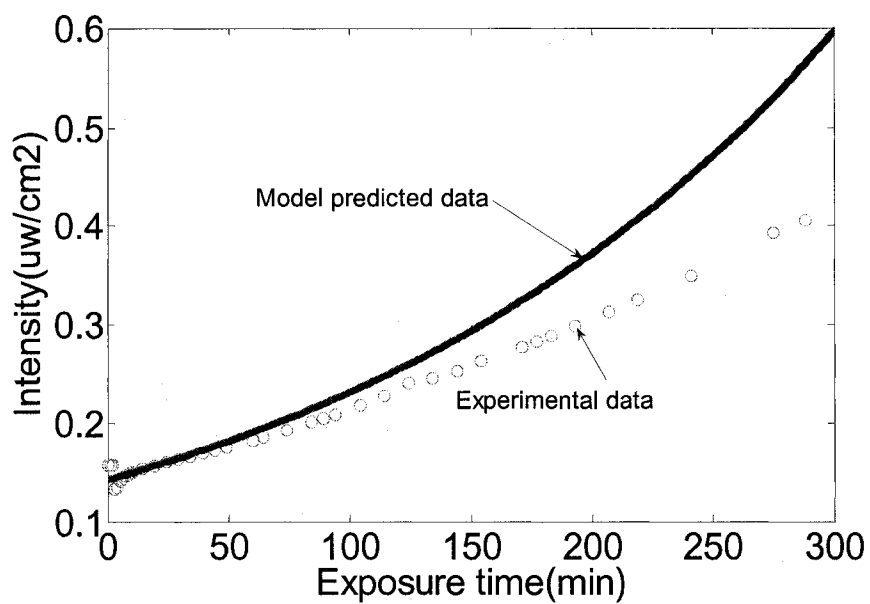
Figure 3.14b Transmitted intensity of a thick sample. CD540-0.4wt%Irgacure 819, Ii=30

uw/cm$^2$, Thickness of sample is 0.27 mm, $\phi'$=0.5, NL=50, $\varepsilon_i$ = 760 1 mol$^{-1}$ cm$^{-1}$,

$\varepsilon_m$=0.0755 1 mol$^{-1}$ cm$^{-1}$. (•••) Experimental data; (—) calculated data.

Figure 3.14b shows that the calculated outcome fits well with experimental data at

the beginning using the correct thickness. However when the exposure time is longer than

50 minutes, the difference between the experimental data and the predicted data increases

with time. This may be because the real $\phi'$ is less than 0.5. So using a smaller $\phi'$, 0.4, the

transmitted intensity is calculated again and the result is shown in Figure 3.14c.
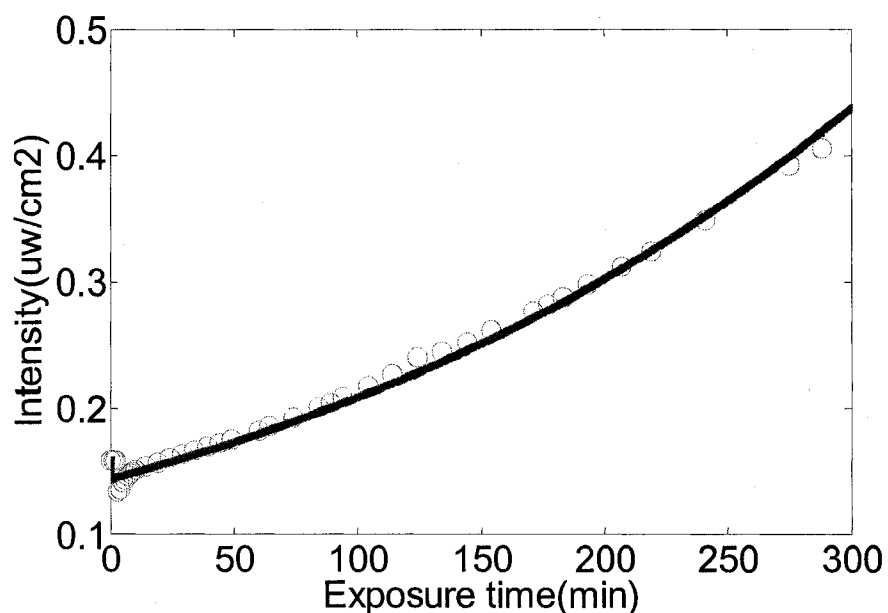
Figure 3.14c Transmitted intensity of a thick sample. CD540-0.4wt%Irgacure 819, $I_i$=30

uw/cm$^2$, Thickness of sample is 0.27 mm, $\phi'$=0.4, NL=50, $\varepsilon_i = 760$ 1 mol$^{-1}$ cm$^{-1}$,

$\varepsilon_m$=0.0755 1 mol$^{-1}$ cm$^{-1}$. ($\bullet\bullet\bullet$) Experimental data; (—) model prediction.


Figure 3.14c shows that using 0.4 as the $\phi'$ value, the model prediction matches

the experimental data well.

Next, the transmitted intensity of another system that has less initiator

concentration (CD540-**0.2wt%IC819**) was studied under two different incident

intensities, 130 and 65 uw/cm$^2$. The thickness of the sample is the same, $4 \pm 0.5$ mm for

the two measurements here. The experimental and predicted data are shown in Figure

3.15a with the calculated data.
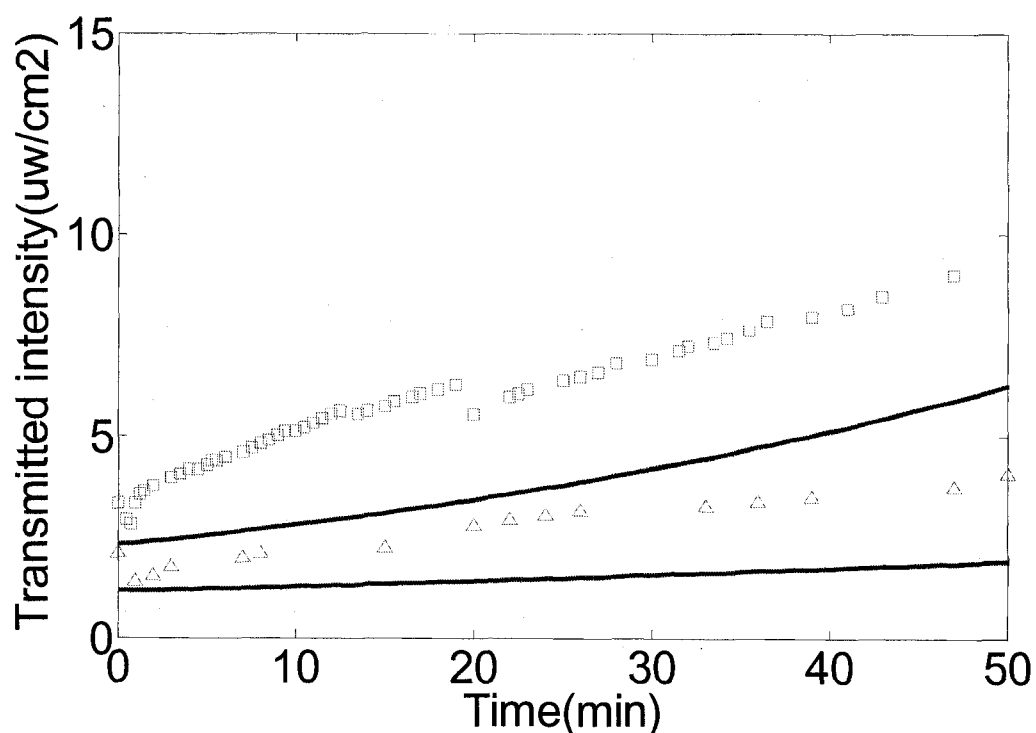
Figure 3.15a Transmitted intensity of thick samples. CD540-0.2wt%Irgacure 819,

Thickness of sample is 4 mm, $\phi'$=0.5, NL=50, $\varepsilon_i$ = 760 1 mol$^{-1}$ cm$^{-1}$, $\varepsilon_m$=0.0755 1 mol$^{-1}$

cm$^{-1}$. ( □ ) I$_i$=130 uw/cm$^2$, ( Δ ) I$_i$=65uw/cm$^2$, (—) model predictions.

Figure 3.15a shows that the calculated data is lower than the experimental data at

the beginning, which may due to the error of measuring the thickness of the sample.

Therefore, the thickness was calculated based on the light absorbance of the sample and

Equation 3.9. It was found the correct thickness is 0.35 mm instead of 0.5 mm, the value

determined by the spacer thickness of the sample mold and assuming the cell gap was the

exact value of the spacer. Using the corrected thickness, 0.35 mm, the transmitted

intensity was calculated again. The predicted data are shown in Figure 3.15b.
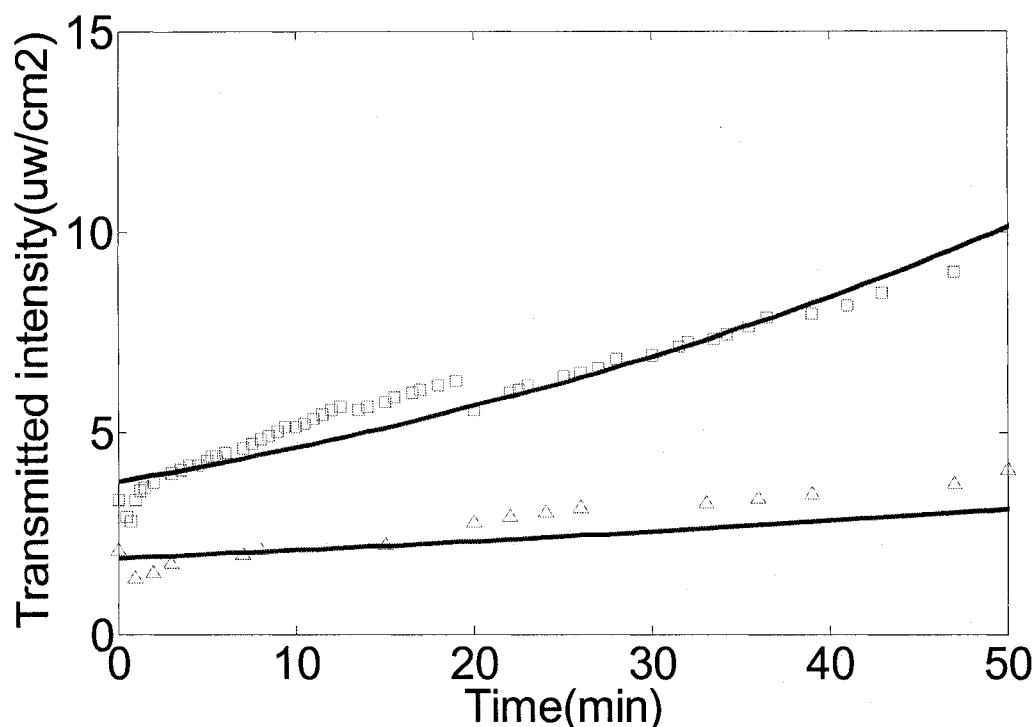
Figure 3.15b Transmitted intensity of thick samples. CD540-0.2wt%Irgacure 819,

Thickness of sample is 3.5 mm, $\phi'$=0.5, NL=50, $\varepsilon_i$ = 760 l mol$^{-1}$ cm$^{-1}$, $\varepsilon_m$=0.0755 l mol$^{-1}$ cm$^{-1}$. ( □ ) I$_i$=130uw/cm$^2$, ( △ ) I$_i$=65uw/cm$^2$, (—) model predictions.

Figure 3.15b shows that the model predicted data fit the experimental data well

under two different incident intensities using the correct sample thickness.

The transmitted intensity of another system with less [PI], <u>CD540-0.05wt%IC819</u>,

was studied too. Here the thicknesses of the samples are different, $4 \pm 0.5$ and

$8 \pm 0.5$ mm. The incident light intensities are the same, 130uw/cm$^2$. The model predicted

data and the experimental data are shown in Figure 3.16a with the calculated data.
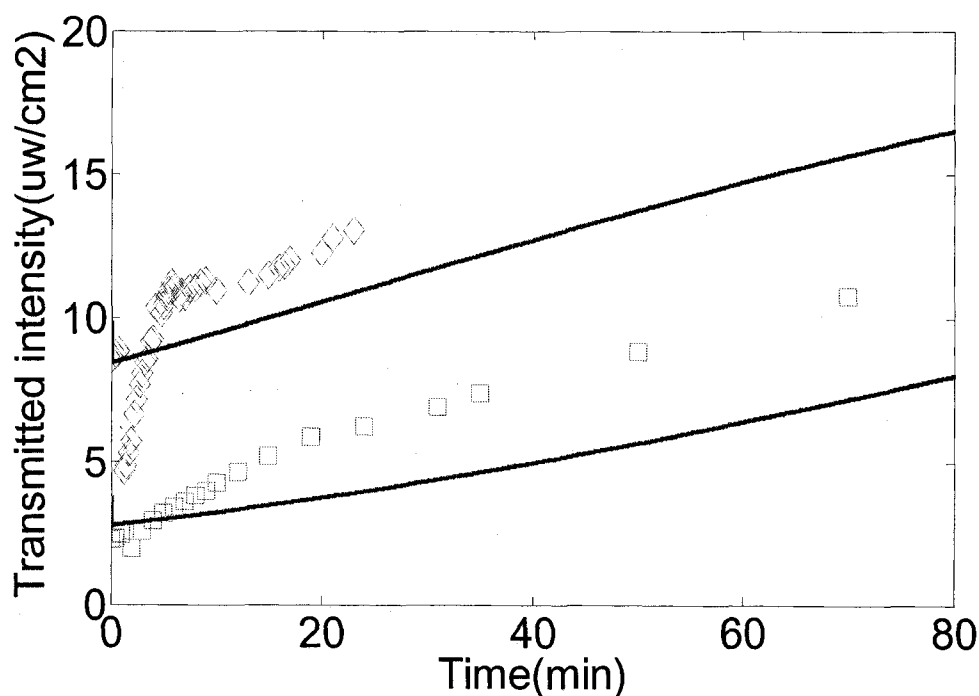
Figure 3.16a Transmitted intensity of thick samples. CD540-0.05wt%Irgacure 819, Ii=130 uw/cm$^2$,$\phi'$=0.5, NL=50, $\varepsilon_i$ = 760 1 mol$^{-1}$ cm$^{-1}$, $\varepsilon_m$=0.0755 1 mol$^{-1}$ cm$^{-1}$. ( $\Diamond$ ), Thickness of sample is 4 mm, ( $\square$ ) Thickness of sample is 8 mm.

Figure 3.16a shows that the calculated intensities fit well the experimental data at the beginning for the system CD540-0.05wt%IC819. In this case, the predicted value of the gap thickness based on light absorbance and Equation 3-9 agrees with the experimental gap based on the spacer thickness. But the calculated curves increase slower than experimental data. This may be because the real $\phi'$ is larger than 0.5. So using a larger $\phi'$, 0.8, the transmitted intensity is calculated again and the result is shown in Figure 3.16b.
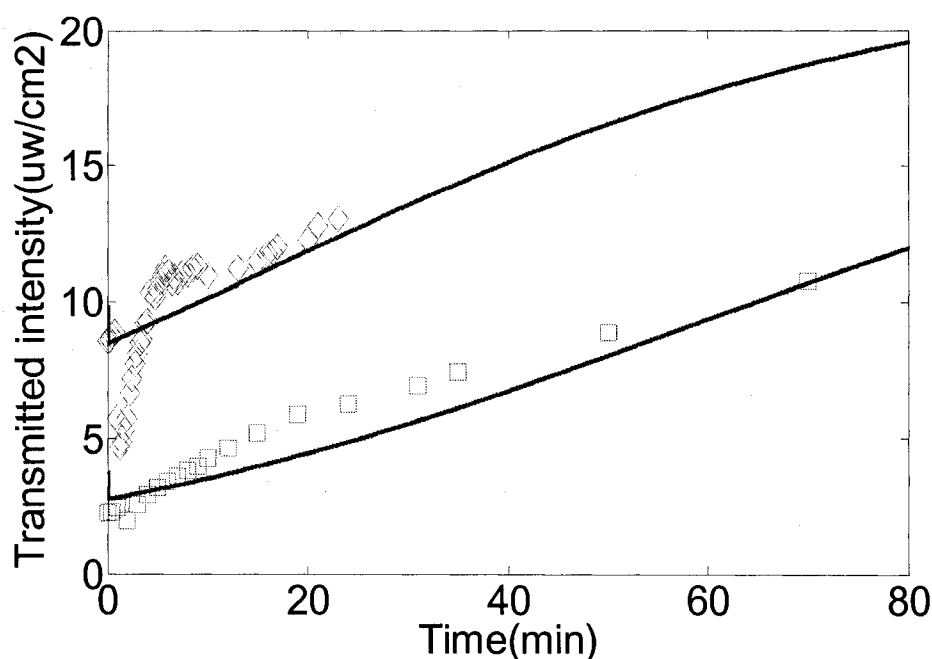
Figure 3.16b Transmitted intensity of thick samples. CD540-0.05wt%Irgacure 819,

$Ii=130uw/cm^2$, $\phi'=0.8$, NL=50, $\varepsilon_i = 760$ 1 $mol^{-1}$ $cm^{-1}$, $\varepsilon_m=0.0755$ 1 $mol^{-1}$ $cm^{-1}$. ( $\Diamond$ ) ,

Thickness of sample is 4 mm, ( $\Box$ ) Thickness of sample is 8 mm.

Figure 3.16b shows that the calculated intensities fit well the experimental data

for the system CD540-0.05wt%IC819 when $\phi'=0.8$.

Comparing all the data above in this section, it was found that there is two likely

reasons for a difference between the experimental data and the calculated one. One error

is in assuming the spacer thickness exactly determines the gap thickness of the sample.

This error is up to 12%. Another error is using literature value $\phi'$, 0.5 and assuming $\phi'$ is

a constant and does not affected by the concentration of initiator in the system. However,

it was observed that the value of $\phi'$ increases when the initiator concentration decreases.

This is probably because the more initiator in the system, the more chance for the initiator

radicals to meet each other and recombine. So the $\phi'$ value is smaller for the system with

more initiator concentration. However, the change of $\phi'$ only affect the prediction of transmitted intensity in a long time range but its effect is not significant in a short period during which the most of the cure occurs. So 0.5 will be used as the value of $\phi'$ in the model for future calculations.

## 3.4    Conclusion.

Using the Matlab program, the intensity and the initiator concentration versus time at different depths in a thick sample can be calculated.

An increased $\phi'$ value was observed when the initiator concentration decreases. This has little effect for the calculation of transmitted intensity in a short period during which most of the cure occurs. A literature value of $\phi'$, 0.5, is used for the later calculation.

# References

1	Steffen Jockusch, I. V. K., Peter F. McGarry, Gregory W. Sluggett, Nicholas J. Turro, and Diana M. Watkins. Journal of American Chemical Society 1997, 119, 11495-501.

2	Steffen Jockusch, N. J. T. Journal of American Chemical Society 1998, 120, 11773-77.

3	Aurelie Botella, J. D., Alain-Andre Roche, Henry Sautereau,Vincent Verney. Macromol. Rapid Commun 2004, 25, 1155–58.

4	Sacco, A. B. In L's Institut National des Sciences Appliquees de Lyon; Ingenieur Maitre es Sciences: Materiaux de Lyon, 2004.

5	Odian, G. Principles Of Polymerization; John Wiley&Sons, INC., 1991.

6	Ivanov, V. V.; Decker, C. Polym Int 2001, 50, 113-18.

7	Guilermo Terrones, T., Arne J. Pearlstein. Macromolecules 2001, 34, 3195-204.

8	Guillermo Terrones, A. J. P. Macromolecules 2001, 34, 8894-906.

9	Guilermo Terrones, r. J. P. Macromolecules 2004, 37, 1565-75.

10	O'Bren, A. K.; Bowman, C. N. Macromolecules 2003, 36, 7777-82.

**Appendix**

**1. Calculation of absorbed photon number**

Since the unit of radiation intensity is uw/cm2 from the radiometer, one needs the following calculation to transfer to Einstein $s^{-1}$ $l^{-1}$. It is known the definition of 1 Einstein is one mole photon regardless of its wavelength, therefore, the energy of 1 mole photon at the wavelength of 365nm needs be calculated using the following Equation.

It is known that

$$E = hv = h\frac{c}{\lambda}$$  Equation 3-10

For one photon at 365 nm, E=$5.446*10^{-19}$ J. ( h = $6.626*10^{-34}$ J s, c=$3*10^{8}$ m $s^{-1}$, $\lambda = 365*10^{-9}$ m). Therefore, E=N*$5.446*10^{-19}$ = $3.28*10^{5}$ J. (N=$6.02*10^{23}$)

If the decrease of light intensity through the sample is $I_a$=1uw $cm^{-2}$=$10^{-6}$ J $s^{-1}$ $cm^{-2}$, and the sample thickness is 0.005cm, the absorbed photons per liter can be calculated by

$$\overline{I_a} = \frac{I_a}{T} = \frac{10^{-6} J.s^{-1}.cm^{-2} *10^{3}}{0.005cm} = 0.2 \text{ J } s^{-1} l^{-1}$$  Equation 3-11

T is the thickness of the sample that the light pass through. $\overline{I_a}$ is the absorbed light intensity per liter. Since the energy of 1 Einstein photon at 365nm is $3.28*10^{5}$ J, the number of absorbed photons for the decreased intensity of 1 1uw $cm^{-2}$ through a 0.005cm sample is $\frac{0.2}{3.28*10^{5}}$. This is equal to $6.1*10^{-7}$ Einstein $s^{-1}$ $l^{-1}$.

2. **An example Matlab program for calculation of intensity versus exposure time at particular depth of thick samples.** (the present situation: incident intensity is $13*5uw/cm^2$, the sample thickness is 0.4 mm, initiator concentration is 0.2wt%, absorption coefficient is 659, quantum yield of initiator consumption is 0.5)

```
clear;

%Initial conditions:

II=65;              %Incident intensity at the surface(uw/cm2)

TH=0.4;             %Thickness (cm) (or depth)

PI=0.2;

IC=PI*0.011087216/0.4;   %Initiator concentration in the system (mol/l)

e=659;              %Absorption coefficient

q=0.5


%Time allocation, whole process is divided into nt time points

nt=600;             %Number of time point

dt=1;               %interval of time 1 minute

t=zeros(1,nt+1);

for k1=1:nt+1

   t(1,k1)=dt*(k1-1);     %Value of time points

end


%Space allocation: sample is divided into NL layers of thin sample
```

```
sL=0.004;              %thickness of layers(cm)

NL=round(TH/sL)        %number of layer

dt=zeros(1,NL+1);      %allocation of thickness

for k2=1:NL+1

   dt(k2,1)=sL*(k2-1);  %value of depth

end

I=zeros(NL+1,nt+1);    %I is Intensity(uw/cm2);x is layer, y is time;

C=zeros(NL,nt+1);      %C is the concentration of photo initiator

I(1,1:nt+1)=II;        %Intensity of light at the surface of the sample

C(1:NL,1)=IC;          %Initial concentration of initiator

for k5=1:NL+1

   z=(k5-1)*sL;

   I(k5,1)=II/10^(e*z*IC);

end



%Calculation of the change intensity versus time at different depth



for k4=1:NL

   for k3=2:nt+1

      IE=(I(k4,k3-1)*3.05e-9/sL);  %Convert unit of I to Einstein/l-s

      C(k4,k3)=C(k4,k3-1)-q*st*60*IE*(1-10^(-e*sL*C(k4,k3-1)));

      I(k4+1,k3)=I(k4,k3)/10^(e*sL*C(k4,k3));

   end
```

```
end

plot(t,I(NL+1,1:nt+1),'k')

xlabel('Time(min)')

ylabel('Transmitted intensity(uw/cm2)')

title('Transmitted intensity versus time for thick sample');

hold on
```

# Chapter 4.  Study of UV cure kinetics of thin samples by FTIR

## 4.1 Introduction

### 4.1.1 Experimental background

This chapter is focused on studying the UV cure kinetics of thin samples (CD540-Irgacure 819) as a function of intensity, initiator concentration, and temperature.

The research of thin samples has been done extensively based on thin film applications but the conclusions are not always applicable to thick applications. For example, the cure of thin samples in an open environment of air (oxygen or nitrogen) was studied in some papers.[1-5] In these papers, one side of the sample contacts a support surface and the other side is exposed to the air. In this situation, the oxygen diffusion from the environment into the system strongly affects the cure. However, for thick applications, the bulk cure is not affected by the diffusion of oxygen as much as the cure of thin samples[2] because the diffusion of oxygen has less effect on the cure of layers far from the surface. Reactions in the layers far from the surface are mainly affected only by the oxygen already dissolved in them. Therefore, in this paper, thin samples were placed between two pieces of glass to get rid of the diffusion of oxygen from the air. This imitates the cure environment of thin layers inside thick samples since only oxygen that inhibits the cure is the oxygen already dissolved in it.

The UV cure process is monitored by FTIR (Fourier Transform Infrared). Transmitted Near FTIR is a reliable method to quantitatively measure the cure extent of

organic functional groups, such as C=C in methacrylate oligomers. The strength of the signal is proportional to the thickness of the sample and the accumulation time of the scan. In order to measure the fast photocure with a high resolution using transmitted FTIR, researchers[6-8] used samples with a thickness more than 1mm to get a strong signal. However, for an initiator like Irgacure 819, which has a high extinction coefficient, this will result in a heterogeneous reaction due to the varying absorption of light through the depth of the sample. Besides, the temperature of the system may increase significantly when the sample is thick. All these affect the study of the cure kinetics of the system. In order to study the cure kinetics accurately, a sample as thin as $0.05 \pm 0.01$ mm is used for the experiments in this paper. In this case, the decrease of light intensity through the depth is less than 4.6% for a composition with less than 0.2% Irgacure 819. (The calculation of light intensity through the depth is shown in appendix 1. Hence, the reaction can be regarded approximately as homogeneous. To get a good signal in a thin sample of 0.05mm, a relatively low intensity of radiation ($<32.5$ $\mu$w/cm$^2$) is used to slow down the cure process and permit a longer accumulation time for the scan. Because the reaction is relatively slow under a low power radiation, one is able to more accurately measure parameters related to absolute time, such as inhibition period (delay time) compared with fast cure under high exposure intensities.[9-12]

## 4.1.2   Theoretical background

The photo-polymerization of the system, CD540 (ethoxylated(4) Bisphenol-A dimethacrylate) with Irgacure 819 (bis(2,4,6-trimethylbenzoyl)phenylphosphine oxide), studied in this dissertation is a radical chain polymerization. The general kinetics and mechanism of free radical chain polymerization and photo cure has been studied by

Odian[13] as discussed in the first chapter. In this chapter, the research focuses on the specific system of CD540 with Irgacure 819.

Similar to other free radical polymerizations, the cure kinetics of the system CD540-Irgacure 819 can be divided into three important steps, initiation, propagation, and termination.

### (i) Initiation

As described in Chapter 1, Irgacure 819 has several advantages as an initiator in the free radical photo polymerization. These characteristics attracted attention in recent years,[14-18] and the photo chemistry of this system has been studied extensively. It was reported that bis(acyl)phosphine oxides had the potential to produce four radicals, and all of them can initiate the chain polymerization.[16] The bis(acyl)phosphine oxides undergo stepwise cleavage upon irradiation (404.5nm).[14] The degradation process of bis(acyl)phosphine in a photo curable system is shown below.



(1)                Step 1            (2)            (3)



(4)                Step 2            (5)            (6)
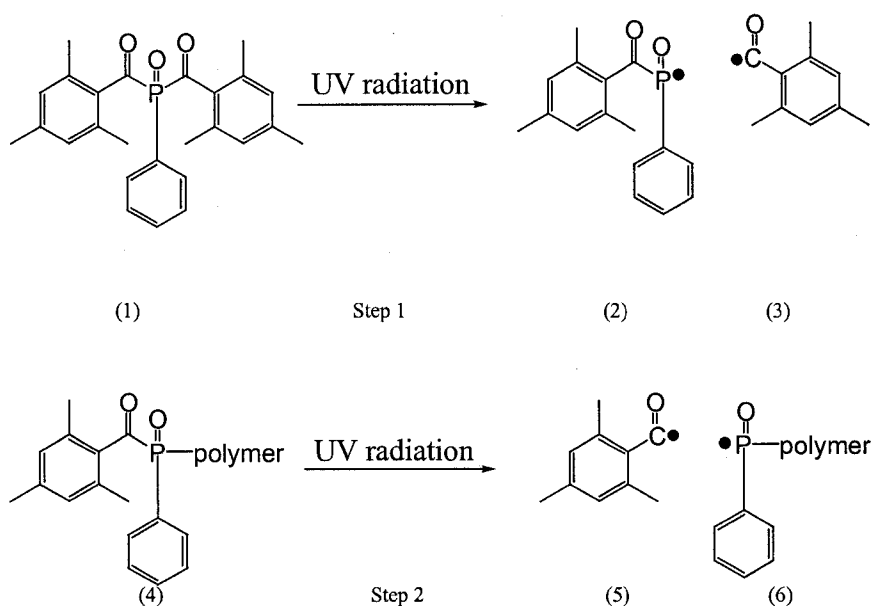
Figure 4.1 Photochemistry of the initiator, Irgacure 819

Since the photo chemistry of bis(acyl)phosphine oxides is more complex compared with mono(acyl)phosphine oxides and other traditional radical initiators that produce only two radicals, the kinetics of the cure of the system CD540-Irgacure 819 is a little different from what was reported in classic photo polymer text books such as in Odian's book.[13]

The initiation step of the polymerization can be expressed in Equations 4-1 and 4-2.

$$PI \xrightarrow{k_d} 4R\bullet \qquad\qquad \text{Equation 4-1}$$

$$R\bullet + M \xrightarrow{k_i} M_1\bullet \qquad\qquad \text{Equation 4-2}$$

Where PI is photo-initiator, $k_d$ is the rate constant of dissociation of the photo-initiator, $R\bullet$ is the free radical fragment, M is the functional group of the monomer (for Monomer, CD540, M is the C=C), $k_i$ is the rate constant for the initiation step. Here the factor, 4, is used in Equation 4-1 because four radicals are formed per Irgacurecure 819 consumed.

This complex initiation mechanism results in a different initiate kinetics from other traditional radical initiators that produce only two radicals. For traditional radical initiators, the rate of initiation is usually expressed using Equation 4-3 (see Equation 1-10)

$$R_i = 2\phi I_a \qquad\qquad \text{Equation 4-3}$$

$R_i$ is the rate of initiation, $\phi$ is quantum yield of initiation, which represents the number of propagation chains formed for each photon absorbed. $I_a$ is the absorbed light intensity in moles of light quanta. The factor of 2 is used for those initiator systems, which yield 2 radicals instead of one.

For the initiator, Irgacure 819, there are two possible kinetics for the initiation. CASE I: two radicals were formed first for each photon absorbed with the breakage of one C-P bond of Irgacure 819 as shown at step 1 in Figure 4.1. Then the other C-P bond will break to form another two radicals in the second step with the absorption of another photon. For this case, Equation 4-3 is still correct since two radicals are formed for every photon absorbed. **However, the initiator concentration here is not the concentration of Irgacure 819, but the concentration of C-P bond, in Irgacure 819, which is twice the concentration of Irgacure 819.** So, $[PI]_{CASE1} = 2 \times [Irgacure\ 819]$. This will be applied to the calculation later. However, the mechanism of step 2 in Figure 4.1 is not completely understood. Hence, the kinetic study here also considers another possible situation that four radicals are formed in sequence for each photon absorbed. (The possibility for this situation is very small) This is set as CASE II. If CASE II is true, then

$$R_i = 4\phi I_a \qquad\qquad \text{Equation 4-4}$$

The factor of 4 is used for initiator systems, which yield 4 radicals per photon absorbed.

The absorbed intensity, $I_a$, can be calculated using Equations 4-5 and 4-6. According to Lambert-Beer's law

$$\ln(\frac{I_i}{I_i}) = -2.3\varepsilon b[PI] \qquad\qquad \text{Equation 4-5}$$

$I_i$ is the incident light intensity in units of $\mu w/cm^2$, $I_a$ is in units of $\mu w/cm^2$, $\varepsilon$ is the absorption coefficient of photoinitiator, b is the thickness of the sample, [PI] is the concentration of photoinitiator. **Note that for CASE II, [PI] is exactly the concentration of Irgacure 819, [Irgacure 819]. However for CASE I, $[PI]_{CASE1} = 2 \times [Irgacure\ 819]$ as discussed above in CASE I.**

Therefore, absorbed intensity, $I_a$, can be calculated using Equation 4-6.

$$I_a = I_i - I_t = I_i(1 - e^{-2.3\varepsilon b[PI]})$$     Equation 4-6

Where, $I_t$ is transmitted light intensity in units of $\mu w/cm^2$. For CASE I discussed above,

(Note that in Equation 4-6, the units need to be converted to Einstein $s^{-1}$ $l^{-1}$ by

multiplying a constant C. C is equal to $6.1*10^{-7}$ for the light path length of 0.05mm for

strict quantitative calculations. The detailed calculation of this conversion has been

shown in the appendix 1 in Chapter 3. However, the conversion of units is not necessary

for most of the relative studies in this chapter. The units of $\mu w/cm^2$ will be used in this

chapter for most cases unless otherwise mentioned to use the unit of Einstein $s^{-1}$ $l^{-1}$. )

The calculation results using Equations 4-5 and 4-6 for the sample of CD540-

Irgacure 819 with 0.05mm thickness are shown in table 4.1.

Table 4.1 Transmitted and absorbed intensities of samples with different initiator

concentration, at 0.05mm depth, $I_i$=32.5 $\mu w/cm^2$

| [PI] | $I_t$ ($\mu w/cm^2$) | $I_a$ ($\mu w/cm^2$) |
|---|---|---|
| 0.2wt% | 31.05 | 1.45 |
| 0.1wt% | 31.77 | 0.73 |
| 0.05wt% | 32.13 | 0.37 |

From table 4.1, the change of intensity through depth is less than 4.6% when the

initiator concentration is less than 0.2wt%. The cure of the sample can be regarded as

homogeneous in this case.

If the sample is thin, the incident light intensity does not vary appreciably

throughout the thickness of the sample, $I_a$ is often conveniently expressed by Equation 4-

7.

$$I_a = 2.3\varepsilon I_i b[PI] \qquad\qquad \text{Equation 4-7}$$

**Similar to Equation 4-5, [PI] in Equation 4-7 is exactly the concentration of Irgacure 819 for case II, [Irgacure 819]. However for CASE I, [PI]$_{CASE1}$=2×[Irgacure 819] as discussed above in CASE I.**

In order to study the difference between the data calculated using Equations 4-6 and 4-7, the transmitted intensity was calculated again using Equation 4-7. The data is shown in Table 4.2

Table 4.2 Transmitted intensities of samples with different initiator concentration, at 0.05mm depth, Ii=32.5 $\mu$w/cm$^2$.

| [PI] | $I_t$ ($\mu$w/cm$^2$) | $I_a$ ($\mu$w/cm$^2$) |
|---|---|---|
| 0.2wt% | 31.02 | 1.48 |
| 0.1wt% | 31.76 | 0.74 |
| 0.05wt% | 32.13 | 0.37 |

Comparing the data in Tables 4.1 and 4.2, the calculated values of $I_t$ and $I_a$ are quite similar under the same conditions using Equations 4-6 and 4-7. (The difference of the calculated $I_t$ is less than 0.1% between the data in two tables and the difference of $I_a$ is less than 2.2%.) Therefore, it is reasonable to use Equation 4-7 instead of Equation 4-6 here to simplify the calculation of $I_a$, hence, the kinetic study of UV curing.

Substituting Equation 4-7 into Equation 4-3(CASE I) yields

$$R_i = 2\phi \times 2.3\varepsilon I_i b(2 \times [Irgacure819]) = 9.2\varepsilon I_i b[Irgacure819] \qquad \text{Equation4-8a}$$

The reason for $2 \times [Irgacure819]$ is because $[PI]=2 \times [Irgacure819]$ as explained above for

CASE I.

For CASE II, substituting Equation 4-7 into Equation 4-4 gives

$$R_i = 4\phi \times 2.3\varepsilon I_i b \times [Irgacure819] = 9.2\varepsilon I_i b[Irgacure819] \qquad \text{Equation4-8b}$$

The outcome of Equation 4-8b is exactly the same as Equation 4-8a. This means

the kinetics of initiation can be expressed by the same equation for two different possible

initiation mechanisms.

### (ii) Propagation

This process is the same as what was described in Chapter 1 from Equations 1-3

to 1-6. The propagation rate can be expressed as Equation 4-9. (See Equation 1-9)

$$R_p = k_p[M\bullet][M] \qquad \text{Equation 4-9}$$

$R_p$ is the rate of propagation. $k_p$ is the rate constant of propagation. **M is C=C in the**

**monomer**, CD540, $[M\bullet]$ is polymer radicals. Even though $k_p$ is always defined as the

rate constant of propagation, it was often found as a function of conversion.[6,19-26] The

changing of $k_p$ versus conversion will be studied at the end of this chapter.

Usually the consumption number of monomer in the initiation step is much less

than the number in the propagation step for free radical polymerization. Therefore,

$$-\frac{d[M]}{dt} = R_i + R_p \approx R_p \qquad \text{Equation 4-10}$$

For the cure of the system of CD540-0.2wt%IC819 by 32.5 $\mu w/cm^2$ UV radiation,

it was found that the calculated kinetics chain length is larger than 3811. (The detailed

calculation is shown in appendix 2.) It is reasonable to calculate approximately using Equation 4-10. Combining Equations 4-9 and 4-10,

$$-\frac{d[M]}{dt} = k_p[M][M\bullet]$$

Equation 4-11

### (iii) Termination

The termination kinetics of free radical polymerization is very complex and is not well understood, particularly at high conversions. It is usually believed that a radical stops propagation by recombining with another polymer radical. This process is known as the classic **bimolecular** termination mechanism. However the discovery of **"trapped"** radicals[6,27-31] in many systems strongly suggests that there is another possible way to terminate by a **unimolecular mechanism,** because trapped radicals are enclosed in polymer chains and hence they have no opportunity to meet other radicals to terminate. What is the difference between these two termination mechanisms and what is their influence on the cure kinetics? This question will be discussed in this section. First, the bimolecular termination mechanism and its effect on the whole cure kinetics will be discussed in part 1. Then the unimolecular termination mechanism of "trapped" radicals and its effect on the cure kinetics will be discussed in part 2.

### 1. Bimolecular termination mechanism

In part 1, we assume that the bimolecular reaction is the only mechanism for termination as most other researches do. It means there is no trapped radicals in the system. This is an extreme situation that may happen only at very low conversions and low viscosity before reaching the gel point. Hence, the termination process can be expressed using Equation 4-12.

$$M_n\bullet + M_m\bullet \xrightarrow{\ k_t\ } dead\ polymer$$
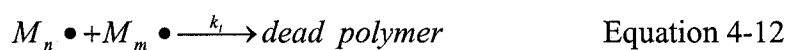
Equation 4-12

where $k_t$ is the rate constant of termination, which includes the combination and disproportionation termination.

According to the mechanism in Equation 4-12, the rate of termination can be expressed as

$$R_{t2} = 2k_{t2}[M\bullet]^2 \qquad \text{Equation 4-13}$$

where $R_{t2}$ is the termination rate and $k_{t2}$ is termination rate constant, $[M\bullet]$ is the concentration of free radicals in the system. (Note that 2, the subscript of the $R_t$ and $k_t$, is used to indicate the <u>bi</u>molecular termination mechanism here.)

For free radical polymerization, which has a fast initiation and termination speed, a steady-state assumption is extensively used to study the cure kinetics. It assumes the concentration of free radicals, $[M\bullet]$, in the system is a constant, therefore,

$$R_i = R_t \qquad \text{Equation 4-14}$$

This assumption was believed to be not correct because it was discovered that the concentration of radicals, $[M\bullet]$, monitored by ESR, increased with exposure time. [27,30,31] However, the steady-state assumption is still the basic assumption and it is widely used by most kinetic studies of free radical polymerization. Based on the steady-state assumption and the bimolecular termination reaction,

$$R_i = R_t = 2k_{t2}[M\bullet]^2 \qquad \text{Equation 4-15}$$

Therefore, Equation 4-15 can be written as

$$[M\bullet] = (\frac{R_i}{2k_{t2}})^{0.5} \qquad \text{Equation 4-16}$$

Substitute Equation 4-16 into Equation 4-11,

$$-\frac{d[M]}{dt} = k_p[M]\left(\frac{R_i}{2k_{t2}}\right)^{0.5}$$
Equation 4-17

Substituting Equation 4-8 into Equation 4-17,

$$-\frac{d[M]}{dt} = k_p[M]\left(\frac{4.6\phi\varepsilon I_i[PI]b}{k_t}\right)^{0.5}$$
Equation 4-18

Here initiator is in **excess** and its concentration is regarded as **constant** throughout the cure process because it does not decrease much. The change of initiator concentration versus exposure time under different conditions is shown in appendix 1. We found that the decrease of the **initiator concentration is less than 4.1%** while the **conversion of C=C is less than 50%** for the cure of all systems studied in this chapter. However, [M] (the concentration of C=C) changes a lot with conversion, so we moved it to the left side of the equation to simplify the variables on the right side of the equation.

$$-\frac{1}{M}\frac{d[M]}{dt} = -\frac{d(\ln[M(t)])}{dt} = k_p\left(\frac{4.6\phi\varepsilon I_i[PI]b}{k_t}\right)^{0.5}$$
Equation 4-19

Equation 4-19 shows that the exponent is 0.5 for the ideal bimolecular termination. However, the real situation often deviates from ideal. The exponent was found higher than 0.5 in several reports.[10,22,32-36] This has been attributed to the unimolecular termination mechanism due to the formation of trapped radicals.[22,37-39] This will be elaborated in part 2.

## 2. Unimolecular termination mechanism

The discovery of "trapped" radicals in many radical polymerization systems[6,27,29-31] strongly suggests that bimolecular termination is not the only termination mechanism. Trapped radicals have no opportunity to meet other radicals to terminate because they are

enclosed in polymer chains. Therefore, the <u>unimolecular termination</u> theory is applicable here to explain the UV cure kinetics of CD540-Irgacure 819.

The unimolecular termination mechanism of trapped radicals can be expressed by Equation 4-20

$$R_{t1} = k_{t1}[M_f \bullet]$$ 

Equation 4-20

Where $R_{t1}$ is the termination rate and $k_{t1}$ is termination rate constant by single polymer radical. The termination rate here is equal to the formation rate of trapped radicals. $[M_t \bullet]$ is the trapped radicals in polymer chains. $[M_f \bullet]$ represents the concentration of **free** radicals. It is used here to separate from trapped radicals that also exist in the system. The subscript 1 of $R_t$ and $k_t$ is used to indicate the <u>unimolecular</u> termination mechanism instead of bimolecular.

Similar to the assumption in part 1 that bimolecular reaction is the only termination mechanism, we assume here that uni-molecular termination is the only way to terminate. This means that all radicals eventually become trapped radicals to terminate the propagation. This is another extreme situation that may happen at very high conversion or in the glass transition region. According to the steady-state assumption,

$$R_i = R_t = k_{t1}[M_f \bullet]$$ 

Equation 4-21

Therefore,

$$[M_f \bullet] = \frac{R_i}{k_{t1}}$$ 

Equation 4-22

Since trapped radicals are enclosed by polymer chains, a solid environment, they have no opportunity to meet liquid monomer to propagate. So Equation 4-11 can be written as

$$-\frac{d[M]}{dt} = k_p[M][M_f\bullet]$$

Equation 4-23

Note that the radicals here are <u>free</u> radicals. Its concentration is the difference of the concentration of total radicals minus the concentration of trapped radicals

Equation 4-23 should be written as,

$$-\frac{1}{M}\frac{d[M]}{dt} = -\frac{d(\ln[M(t)])}{dt} = k_p(\frac{9.2\phi\varepsilon I_i[PI]b}{k_t})$$

Equation 4-24

Comparing Equation 4-19 with 4-24, the exponent of $R_i$, is 0.5 for the case that the termination is by bimolecular mechanism, but the exponent is 1 for the case that the termination is by unimolecular mechanism. This means the trapped radical in the system results in a higher exponent than the classic 0.5.

Trapped radicals in the system not only affect the exponent but also may change the reaction rate during the cure process. This will be discussed in section 4.3.2.

## 4.2 Experiment

### 4.2.1 Materials

The photo-initiator and the monomer used in this chapter is the same as what was used in Chapter 3

**4.2.2 Instrumentation**

The radiation Source is listed in Table 2.1 in Chapter 2. The radiation source is equipped with a water filter to remove the IR radiation and a 356-365 band pass filter. A fiber optic cable guides the light to the sample chamber of FTIR equipment.

In real-time near FTIR Measurement, a FTS 7000 Series FTIR spectrometer (Digilab) is used to measure the transmitted spectrum of the thin samples. It can in-situ monitor the changes of the absorption peak (6160 $cm^{-1}$) area of carbon double bonds of the CD540 resin during the cure process. The sample was prepared by putting it between two pieces of glass (absorption of IR<5%, absorption of UV (365 nm)<10%) using (0.05 mm) Kapton tape as the spacer. At a thickness of 0.05mm, the light absorption of thin samples is less than 4%, therefore, it is reasonable to regard it as a system with homogeneous light intensity and cure kinetics.

In order to study of the temperature effect on the cure kinetics, a hair dryer is used to heat the sample. The sample temperature is controlled by the position of the hair dryer from the sample and the sample environment. Because of the balance of heat transmitted to the sample from the hair dryer and the heat transferred to environment from the sample, the sample reaches a constant temperature.

**4.3** Results and discussion

4.3.1 **Calculation of the conversion of C=C versus time**

The absorption peaks of C=C between 6110-6230 $cm^{-1}$ at different exposure times are shown in Figure 4.2.
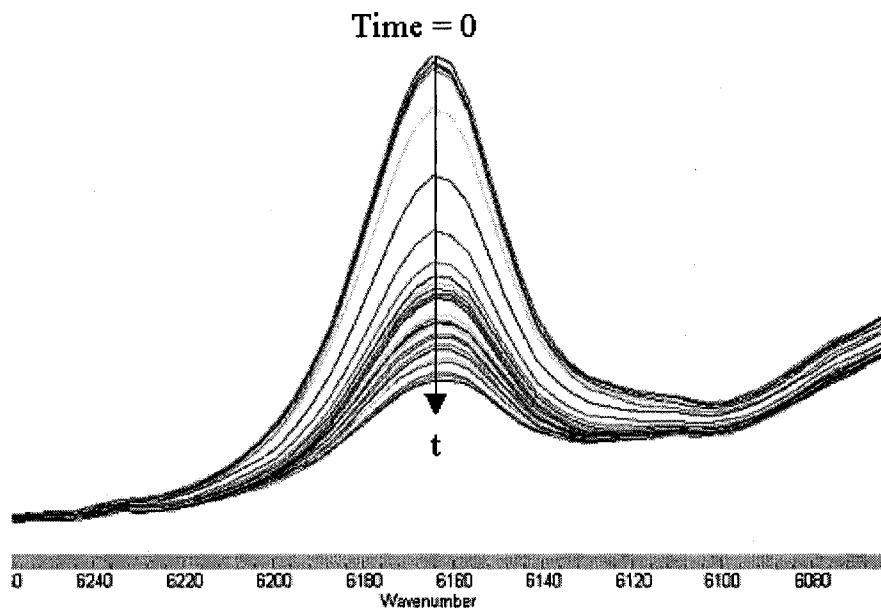
Figure 4.2 Absorption peak of C=C during the UV cure process of CD540-0.2wt%IC819,

incident intensity=32.5 $\mu$w/cm$^2$, Thickness=0.05 mm.

The baseline for calculating the area of the peak is decided automatically by the

software with a given value of left and right limitation of the peak. A reference peak used

before does not change much with exposure time, so we did not use a reference peak

here. The area of the peak is known to be proportional to the concentration of C=C, [M],

in the system.[6,40] The definition of the conversion of C=C is the fraction of C=C

consumed. It can therefore be calculated using Equation 4-25.

$$\alpha_t = 1 - \frac{[M]_t}{[M]_0} = 1 - \frac{A_t}{A_0} \qquad \text{Equation 4-25}$$

$\alpha_t$, the conversion of C=C at time t. A$_t$, the peak area of C=C at time t. A$_0$, the peak area

of C=C at time 0. [M]$_0$ is the concentration of C=C before the cure starts. It is equal to

3.92 mol/l, according to the original composition and the density of the system. [M]$_t$ is

the concentration of C=C at time t. Figure 4.2 shows that the area of the peak decreases with time. This means the concentration of C=C decreases with exposure time. Therefore, the conversion of C=C in CD540 increases with exposure time.

### 4.3.2  Light intensity effect on the cure kinetics of thin samples

A series of thin samples with the composition of CD540-0.2% Irgacure 819 were cured at various intensities from 32.5 to 1 $\mu w/cm^2$. The thickness of the samples is 0.05mm. The cure process was monitored by real-time near FTIR. The result of conversion versus time is shown in Figure 4.3.



♦ I=1uw/cm2      × I=8uw/cm2      ● I=16uw/cm2      + I=32.5uw/cm2
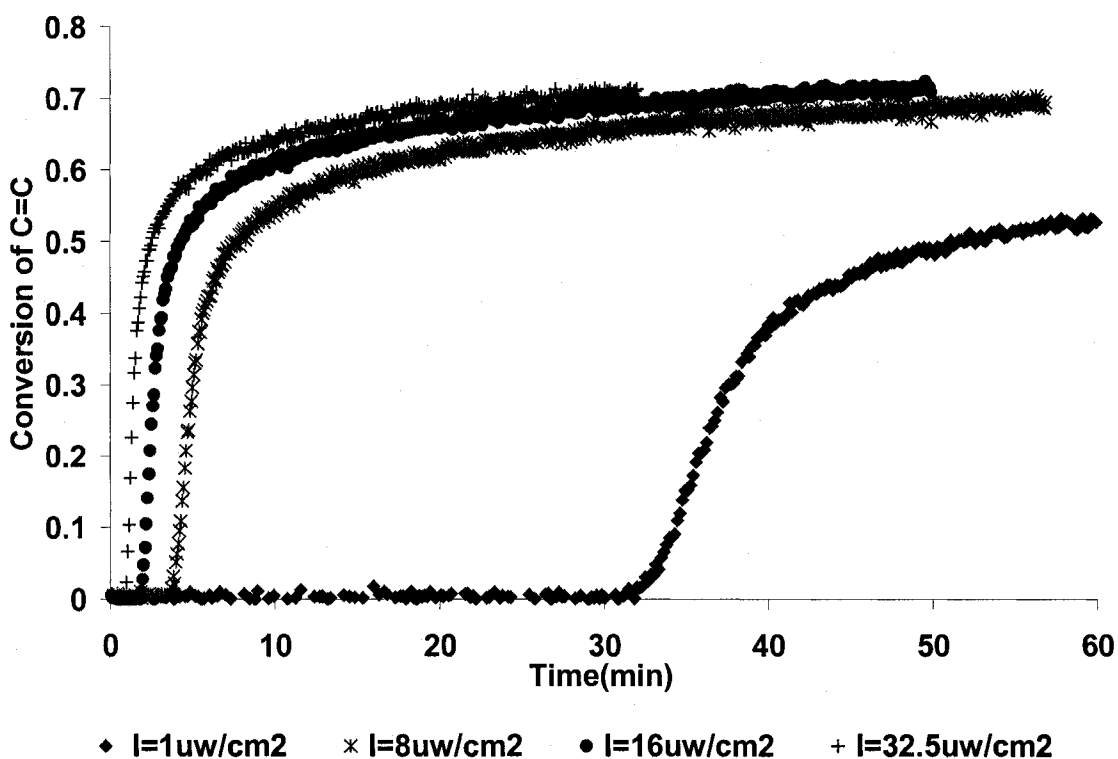
Figure 4.3 UV cure of CD540 with 0.2% Irgacure 819 at different intensities from 32.5 to 1 $\mu w/cm^2$.

It is found that before the polymerization starts, there is a delay period that is due to the oxygen inhibition. The inhibition period is a function of the incident light intensity. After the oxygen in the system was consumed, the polymerization started. The slope of curves in Figure 4.3 represents the polymerization rate at different intensities. The slope is steep initially and then it levels off before the conversion of C=C reaches 100%. The degree of the initial slope decreases with a decrease in light intensity. This means the cure rate is initially rapid and then becomes extremely slow. The cure rate is also a function of light intensity.

The reason for the curves leveling is believed to be due to the formation of the glassy state in the system. This has been verified by studying the temperature effect on the final conversion of the cured sample. Figure 4.4 shows the experimental result of the temperature effect on the final conversion for tetraethoxylated Bisphenol-A dimethacrylate (CD540) reported by Wayne D. Cook (Polymer, 1992).
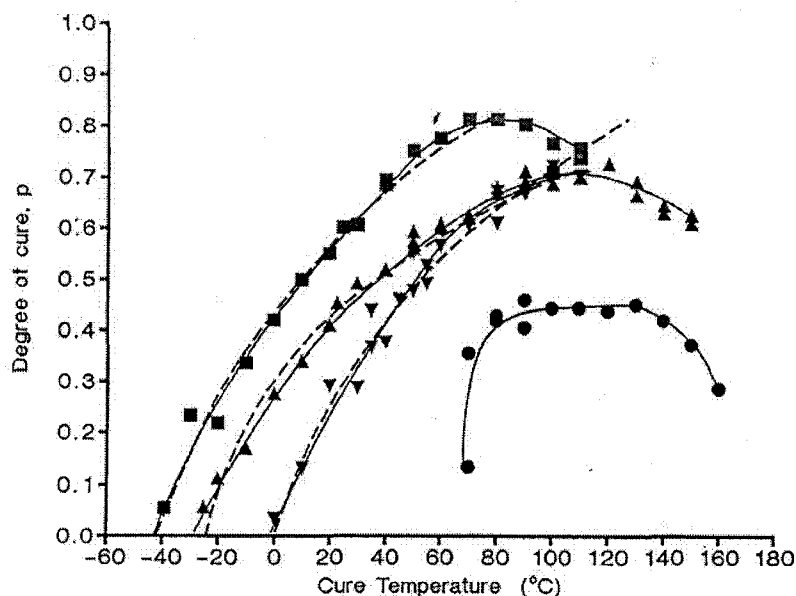
Dependence of the limiting conversion on curing temperature for BPADMA(●), DEBPADMA (▲), bisGMA (▼) and TEBPADMA (■). The broken lines are predicted from equations (2), (3) and (A3) for the data in the following ranges: DEBPADMA, −25 to 110°C; bisGMA, 0 to 120°C; TEBPADMA, −39 to 80°C. The solid lines are guides for the eye

Figure 4.4 "Degree of cure versus cure temperature." [41] This figure is reported by Wayne D. Cook in Polymer 1992, Volume 33, P 2154. TEBPADMA is tetraethoxylated bisphenol-A dimethacrylate (CD540).

Figure 4.4 shows that increasing the temperature can increase the final degree of cure. It was also found in another report[20] that $T_g$ (onset) of the cured product increases with reaction temperature for a dimethacrylate oligomer (M=575) that has almost the same structure as CD540. This is shown in Figure 4.5.
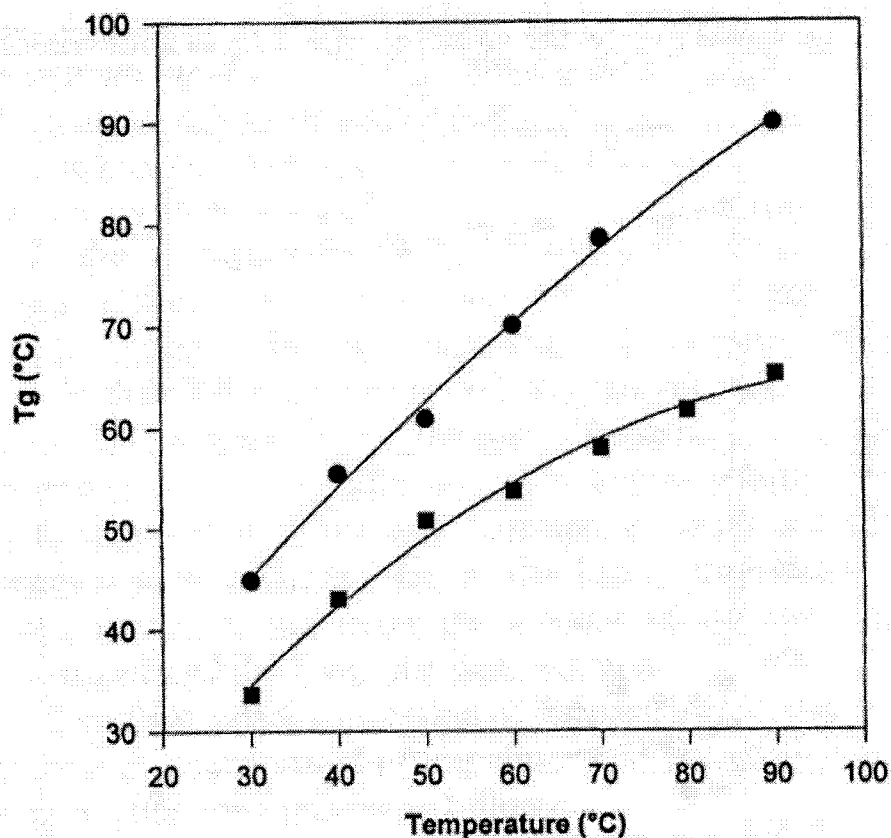
Figure 4.5 "$T_g$ versus ultimate reaction temperature: (■) photopolymerization at 30°C and thermal postcuring from 30°C to ultimate reaction temperature (2°C); (●) photopolymerization during 7 min at the corresponding temperature." This figure is reported in Bunel's paper in Polymer (1999).[20]

Figure 4.5 shows that the $T_g$ of cured product increases with cure temperature. Comparing the result in Figure 4.4 and 4.5, it is found that a product with a higher conversion has a higher $T_g$. This means that final conversion of a cured product is strongly affected by the $T_g$ of the material and the cure temperature.

In addition, the final conversion is also affected by the incident light intensity. Figure 4.3 shows that at the lower intensity the reaction rate starts to slow down at a

relatively low conversion. This has been explained by volume relaxation theory.[20] According to this theory, the shrinkage process due to the formation of network can not keep up with the C=C conversion. If partly polymerized samples are allowed to shrink, their capability for further polymerization is reduced. Since the reaction rate is slower at the lower intensity and it gives the sample more time to shrink during the cure process, its capability for further polymerization is reduced.

In this section, the effect of intensity on the inhibition period (delay time) will be studied first in part (1). Then the intensity effect on the reaction rate will be discussed in part (2). In part (3), the cure rate versus conversion will be modulated by sigmoid equations. In part (4), a calculation method will be developed based on the results from part (1), (2), and (3) to predict the cure kinetics at different incident intensities.

## (1) The effect of intensity on the inhibition period

In order to study quantitatively the effect of intensity to the inhibition period, the inhibition time versus the value of 1/intensity is plotted in Figure 4.6.
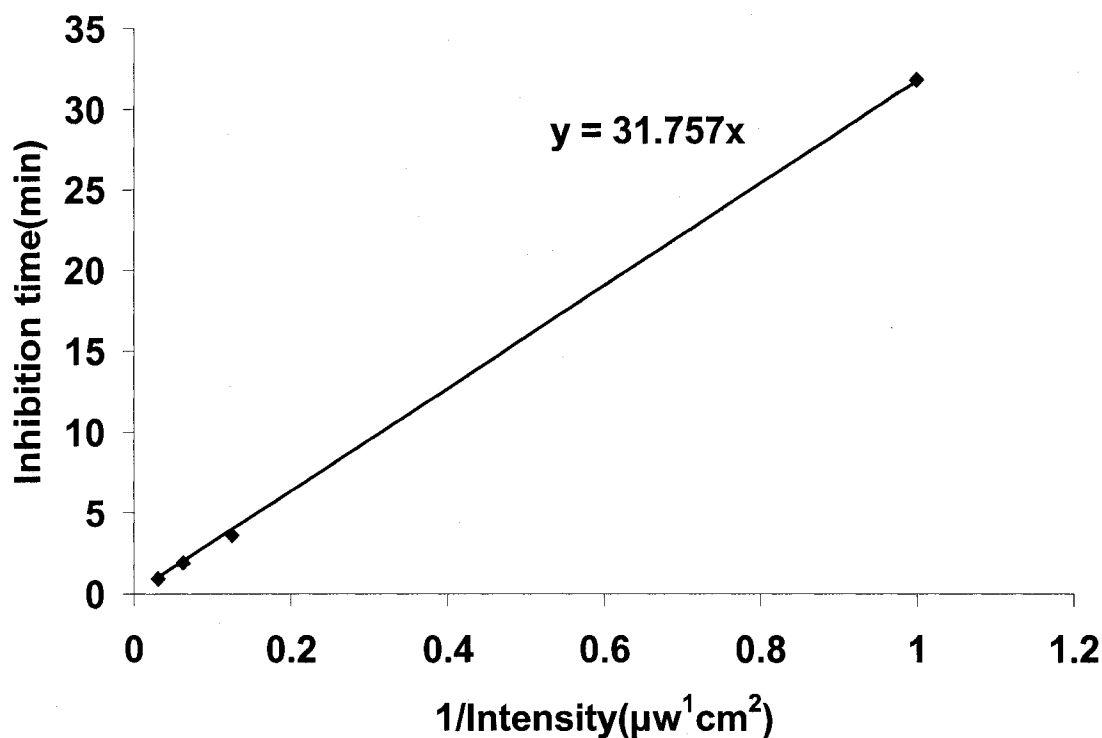
Figure 4.6 Delay time as a function of intensity. CD540-0.2wt%IC819, thickness=0.05mm.

Figure 4.6 shows that the delay time is inversely proportional to the incident intensity as in Equation 4-26.

$$Td = \frac{31.76}{Intensity(uw/cm^2)}$$  Equation 4-26

This result is similar to the result that was observed by Wight.[5] In Wight's paper, plots of delay time versus 1/I produced straight lines. The difference is that Wight found extrapolating those straight lines back to 1/I=0 gave nonzero values for the delay time. I believe this is because Wight did the experiment with the sample exposed to the air. Therefore, oxygen could diffuse into the sample during the polymerization process to change the total amount of the oxygen, which scavenged initiator radicals in the system.

However, the concentration of the oxygen in the sample here can be regarded as a constant because there is no diffusion of oxygen as discussed above. In this case, extrapolating the lines back to 1/I=0 gives a zero value for the delay time.

**(2) The effect of intensity on the polymerization rate**

After the oxygen in the system is consumed the polymerization starts. In order to study the effect of incident light intensity on the polymerization rate of thin samples, Equation 4-19 is used to study the value of $-\dfrac{d(\ln[M(t)])}{dt}$ as a function of conversion at different intensities as shown in Figure 4.8. Note, the reason for using $-\dfrac{d(\ln[M(t)])}{dt}$ (or $-\dfrac{1}{[M(t)]}\dfrac{d([M(t)]}{dt}$) as y axis here instead of $-\dfrac{d[M(t)]}{dt}$ was explained in section 4.1.2. By moving the variable [M(t)] to the left of the equation, the variables on the right side of the equation is simplified. The curves of $-\dfrac{d(\ln[M(t)])}{dt}$ versus conversion at different intensities are shown in Figure 4.7. The time interval for doing the **derivation** of data in Figure 4.7 is $0.320 \pm 0.007$ minutes.
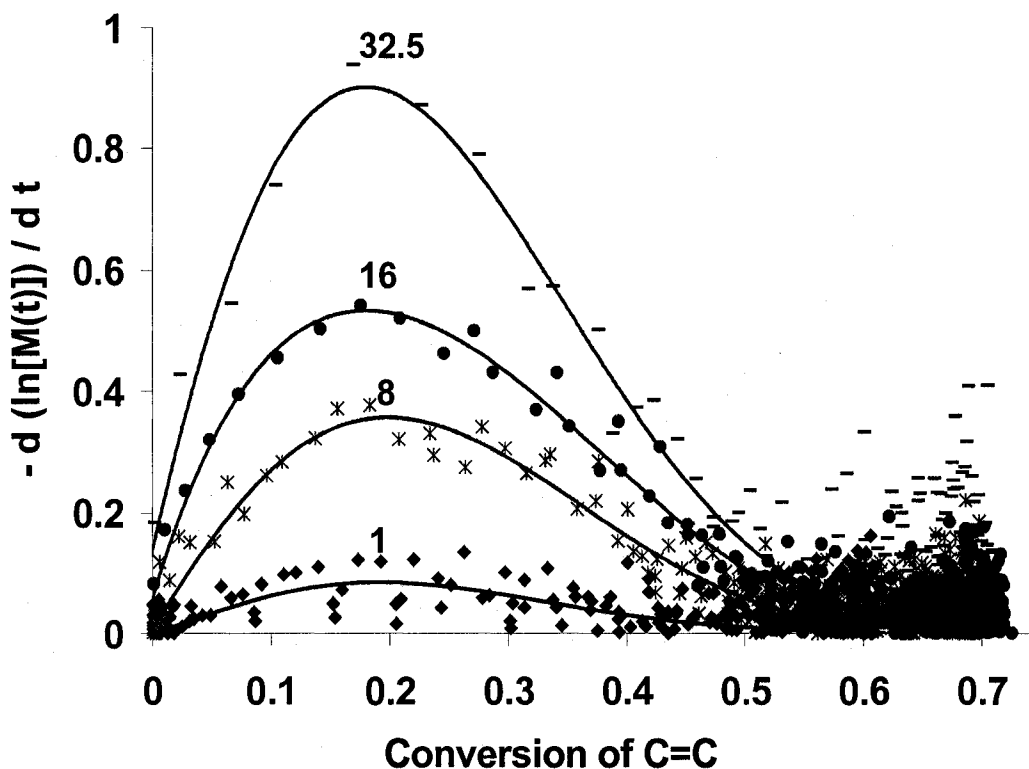
Figure 4.7 dlnM/dt versus conversion at different intensities from 32.5 to 1 μw/cm$^2$. CD540-0.2wt%IC819, thickness=0.05mm. Dotted curves are experimental data; solid curves are the fit results.

Figure 4.7 shows that the experimental curves (dotted curves) are not smooth due to the experimental uncertainty, especially when the reaction rate is slow. In order to get the values of $-\dfrac{d(\ln[M(t)])}{dt}$ with less experimental error at different conversions, the experimental data are fit into average curves using a polynomial and Excel software. The fit results are shown as solid curves in Figure 4.7. (Note: The polynomial curves here have no physical meaning, they only give the values of $-\dfrac{d(\ln[M(t)])}{dt}$ through conversion with reduced experimental variation than any single experimental point. The

experimental data at the intensity of 32.5 $\mu w/cm^2$ will be fit again according to the cure

kinetics of the system using a MATLAB program later.)

Figure 4.7 shows that the curves of $-\dfrac{d(\ln[M(t)])}{dt}$ versus conversion of C=C at

different intensities exhibit similar behavior. All four reactions experience an

autoacceleration process at the low conversion that is known as Trommsdorff or gel

effect. After the conversion of C=C reaches about 18%, it starts to drop. After 50% of

conversion of C=C, the reaction rate becomes very slow. The reason for the increase and

decrease of reaction rate will be explained according to the trapped radical theory later in

part (3). Here the effect of intensity on the polymerization rate will be discussed first at

different conversion. The value of $-\dfrac{d(\ln[M(t)])}{dt}$ at the conversions from 0.1 to 0.6 are

read at different intensities from the solid curves in Figure 4.7. Note that in the region of

0.5 to 0.6, the reaction becomes very slow as the glass transition is reached. Plotting

$-\dfrac{d(\ln[M(t)])}{dt}$ versus intensity at different conversions in Figure 4.8.
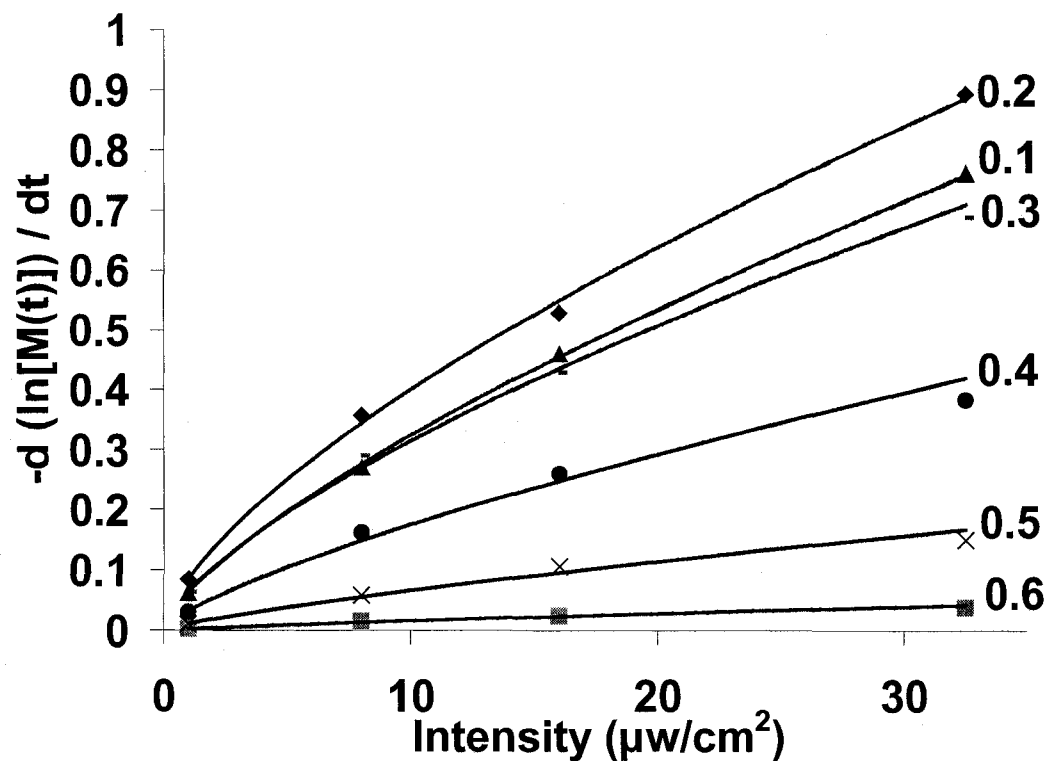
Figure 4.8  $-\dfrac{d(\ln[M(t)])}{dt}$  versus intensity at different conversions (0.1 to 0.6). CD540-

0.2wt%IC819, thickness=0.05mm.

From Figure 4.8, it is found that the relationship of  $-\dfrac{d(\ln[M(t)])}{dt}$  and intensity

can be fit using Equation 4-27 at different degrees of conversion.

$$\frac{d(\ln[M(t)])}{dt} \propto a * Intensity^{b}$$  Equation 4-27

Where a and b are constants and their values are listed in Table 4.3 at different degrees of

conversion.

Table 4.3 The value of a and b of Equation 4-27 at different degrees of conversion.

| Conversion of C=C | a*1000 | b |
|---|---|---|
| 10% | 62.1 | 0.72 |
| 20% | 85.2 | 0.67 |
| 30% | 64.6 | 0.69 |
| 40% | 31.9 | 0.74 |
| 50% | 10.9 | 0.78 |
| 60% | 2.5 | 0.82 |

Note: The consumption of initiator is not been considered in this section because it is less than 1.2% for all the systems studied here when the conversion of C=C is less than 50%. The effect of the consumption of initiator will be considered in Section 4.3.3, where the decreasing of initiator is more significant.

It is found from Table 4.3 that the value of b is $0.70 \pm 0.04$ for the conversion range from 10% to 40% where reaction rate is fast as shown in Figure 4.5. After 40% conversion, the value of **b increases considerably**. Comparing the b value in Table 4.3 with the value of the exponent in Equation 4-19, it is found that b is higher than the classic value, 0.5. Why is the value of b larger than 0.5 and t**he difference of b and 0.5 even more significant at high conversions**? We believe it is due to the formation of trapped radicals in the system as discussed in the <u>section 4.1.2</u>. Trapped radicals have been extensively discovered in many free radical polymerization systems.[27,30,31,42,43] These trapped radicals have little chance to meet liquid monomers to propagate or meet other radicals to terminate because they are enclosed in polymer chains, an immobile

environment.[31] Therefore, trapped radicals terminate themselves by the unimolecular termination mechanism instead of by a bimolecular termination mechanism. For the case that unimolecular termination is the only termination mechanism, the cure kinetics can be expressed by Equation 4-24. Where, the exponent value is equal to 1. For the system studied here, the gel point starts at a very low conversion ($\alpha < 5\%$), it is then possible that the trapped radicals exist through most of the cure process ($\alpha > 5\%$). Therefore, both bimolecular termination and unimolecular termination kinetics exist. The value of b approaches 0.5 if bimolecular termination is the main kinetics and it approaches 1 if unimolecular termination is the main kinetics. The reason that the exponent, **b, increases fast** after 40% conversion is because of the **fast increase in the fraction of trapped radicals** in the total radicals at higher conversions, higher viscosity and the approach to glass formation. This has been observed in an ESR experimental result.[6] In the glass transition region, the concentration of trapped radicals is found almost equal to the total radical concentrations. From Equations 4-19 and 4-24, **more trapped radicals in the system** (Or the more uni-molecular termination relative to bimolecular termination) **correlates to a b value approaching 1 and deviating from 0.5**.

From Equation 4-27, Equation 4-28 can be derived for the intensity effect on the cure rate of the UV polymerization.

$$\frac{\left( -\dfrac{d(\ln[M(t)])}{dt} \right)_{I_1}}{\left( -\dfrac{d(\ln[M(t)])}{dt} \right)_{I_2}} = (\frac{I_1}{I_2})^b \qquad \text{Equation 4-28}$$

Where, I1 and I2 are two intensities. b is $0.70 \pm 0.04$ for the conversion range from 10% to 40% where reaction rate is fast. After 50% conversion, the reaction rate is very small,

having less effect on the total cure kinetics. Therefore, for the latter calculation, b is approximately regarded as 0.7 for the whole cure process.

## (3) Modeling polymerization rate versus conversion at one intensity

In this section, a model will be developed to fit the experimental curve of $-\dfrac{d(\ln[M(t)])}{dt}$ versus conversion at the intensity of 32.5 μw/cm$^2$ in Figure 4.7. The trapped radical theory will be used here as the theoretical basis for the modeling. In this theory, we assume that all radicals in the system are divided into two groups, completely "free" radicals and completely "trapped" radicals. It is assumed that the reaction rate constant of "Free" radicals is only decided by the radical itself and not affected by changes in mobility and environment at all. On the other hand, "trapped" radicals are completely enclosed by polymer chains and have no chance to contact monomers and other radicals to react. **Radicals under a condition between two extreme situations can be divided into A% complete "free" radicals and B% complete "trapped" radicals.** And the value of A and B is determined by the diffusion ability of the molecule. According to these descriptions, Equation 4-11 should be written as

$$-\frac{1}{[M(t)]}\frac{d[M(t)]}{dt} = -\frac{d(\ln[M(t)])}{dt} = k_p[M_f\bullet] \qquad \text{Equation 4-29}$$

The changing of $-\dfrac{d(\ln[M(t)])}{dt}$ versus conversion in Figure 4.8 is the same as the changing of the value of $k_p$ times $[M_f\bullet]$, the completely free radical concentration. $k_p$ is propagation **rate constant** and here, it is a **real** constant that does not change with

conversion according to the definition of "free" radicals above. The curves in Figure 4.8

represents the changing concentration of free radicals, $[M_f\bullet]$. The concentration of free

radicals is equal to the total radicals minus the trapped radicals as shown in Equation 4-30.

$$[M_f\bullet] = [M\bullet]_{total} - [M_t\bullet]$$ 
Equation 4-30

Equation 4-29 can be written as

$$-\frac{d(\ln[M(t)])}{dt} = k_p[M\bullet]_{total} - k_p[M_t\bullet]$$ 
Equation 4-31

According to Equation 4-31, the UV cure curve of CD540-0.2wt%IC819 at

intensity 32.5 μw/cm$^2$ in Figure 4.8 can be fit by Equation 4-32, which is the difference

of two Sigmoid Equations.

$$-\frac{d(\ln([M(t)])}{dt} = \frac{1}{1+e^{-30(\alpha-0.05)}} - \frac{1}{1+e^{-13.7(\alpha-0.36)}}$$ 
Equation 4-32

$\alpha$ is the conversion of C=C. The first factor, $\dfrac{1}{1+e^{-30(\alpha-0.05)}}$, represents the contribution

of $k_p$ times $[M\bullet]_{total}$, the concentration of all radicals in the system. The second factor,

$\dfrac{1}{1+e^{-13.7(\alpha-0.36)}}$, represents the contribution of $k_p$ times $[M\bullet]_t$, the concentration of

trapped radicals **(that is the sum of complete "trapped" radicals and B% of radicals**

**under a condition between two extreme situations)**. The coefficient of 30 and 13.7

determines the increasing rate of the concentration of total radicals and trapped radicals

versus conversion. The number of 0.05 and 0.36 is the conversion where the total and

trapped radical concentration is equal to the half of their maximum concentration during

the exposure process.

The reason for using the sigmoid function as the model to represent the changing concentration of total radicals and trapped radicals is because the sigmoid function models the S-curve of growth. The standard sigmoid function is a solution of a first-order non-linear differential equation. The initial stage of growth is exponential, then it is linear, by the end, it shows an exponential decay and eventually becomes a constant. This model curve represents and describes the increase of total radical and trapped radical concentration with conversion or exposure time.

Using Equation 4-32, the modeled curve is shown in Figure 4.9 and compared with the experimental data of $-\dfrac{d(\ln[M(t)])}{dt}$ versus conversion.
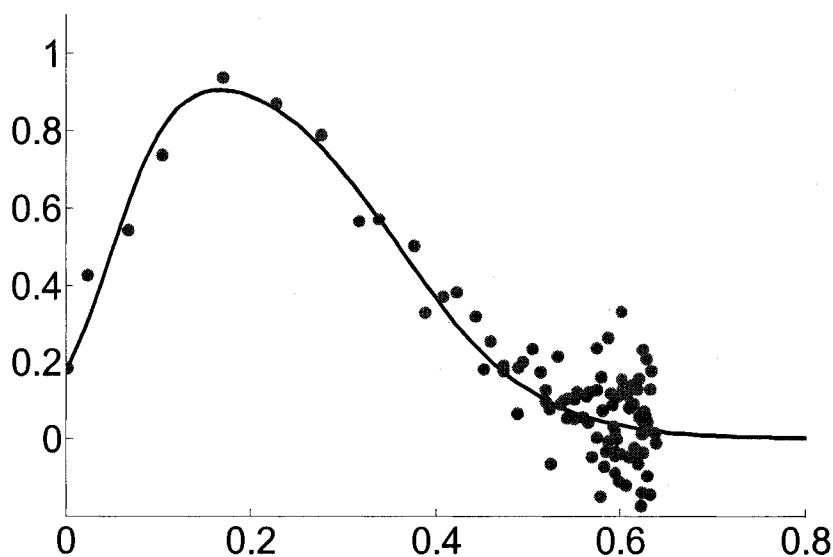


Figure 4.9 $-\dfrac{d(\ln[M(t)])}{dt}$ versus conversion for cure of the sample at room temperature under intensity of 32.5 $\mu w/cm^2$, CD540-0.2wt%Irgacure 819, thickness=0.05mm. ($\bullet$) the experimental data, (—) the fitted curve.

Figure 4.9 shows that the calculated curve fits the experimental data well. This

means Equation 4-32 can be used to fit the curve of $-\dfrac{d(\ln[M(t)])}{dt}$ versus conversion for

the cure of the system CD540-0.2wt% Irgacure 819 at room temperature, Ii=32.5

$\mu$w/cm$^2$, thickness=0.05mm.

According to the two factors in Equation 4-32, the changing concentration of total

radicals and "trapped" radicals are shown in Figure 4.10a and b.
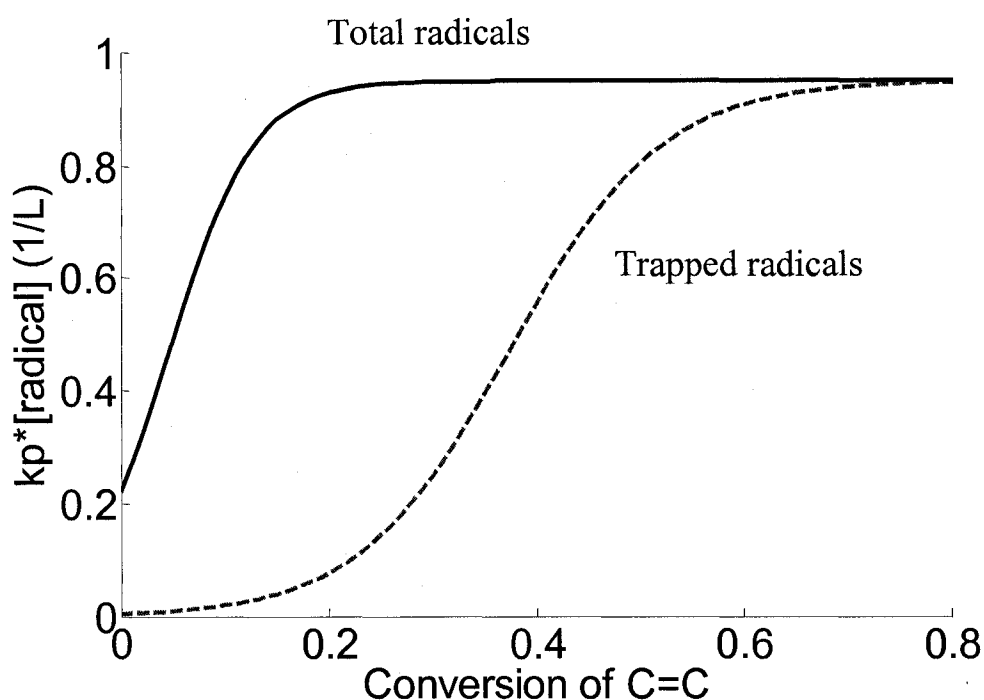


Figure 4.10a The model's changing concentration of total radicals and trapped radicals

versus conversion for the cure of a sample, CD540-0.2wt%Irgacure 819, at room

temperature under intensity of 32.5 $\mu$w/cm$^2$, thickness=0.05mm. (———) The total radical

concentration, (– – –) the trapped radical concentration (that is a sum of complete

"trapped" radicals and B% of radicals under a condition between two extreme situations).

Data in (b) are for the log scale ordinate of (a)
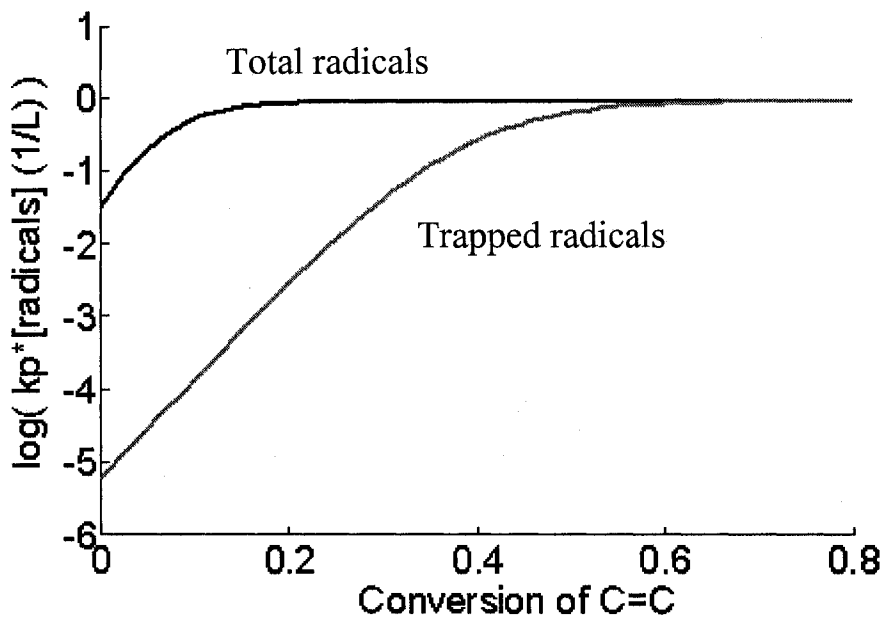
Figure 4.10b The model's changing concentration of total radicals and trapped radicals

versus conversion for the cure of a sample, CD540-0.2wt%Irgacure 819, at room

temperature under intensity of 32.5 $\mu$w/cm$^2$, thickness=0.05mm. (———) The total radical

concentration, (– – –) the trapped radical concentration (that is a sum of complete

"trapped" radicals and B% of radicals under a condition between two extreme situations).

Data in (b) are for the log scale ordinate of (a).

From Figure 4.10, the concentration of total radicals in the system increases very

fast at the beginning. After 20% conversion, total radical concentration becomes constant.

Figure 4.10a also shows that the fraction of trapped radicals in all radicals is low when

the conversion is less than 20%; however after that, the fraction of trapped radicals

increases significantly till 50% conversion. From 50% to 70% conversions, most radicals

in the system are trapped radicals. This is due to the vitrification of the sample. At this

time the reaction rate becomes extremely slow due to the formation of a glass.

Figure 4.10a and b give the model's result of the concentration of total radicals and "trapped" radicals. We do not have the experimental result to study the exactness of this model prediction. We did not find any reported data under the same conditions to compare. However Bowman[6] reported the measured concentration of total radical and complete "trapped" radicals versus conversion for the cure of another dimethacrylate monomer, TEGDMA at a higher intensity in Macromolecules (2005). The reported results are shown in Figure 4.11. (Figure 4.10b is a log scale of data in Figure 4.10a to make it easier to compare with the reported experimental results[6] that is also in a log scale in Figure 4.11. )
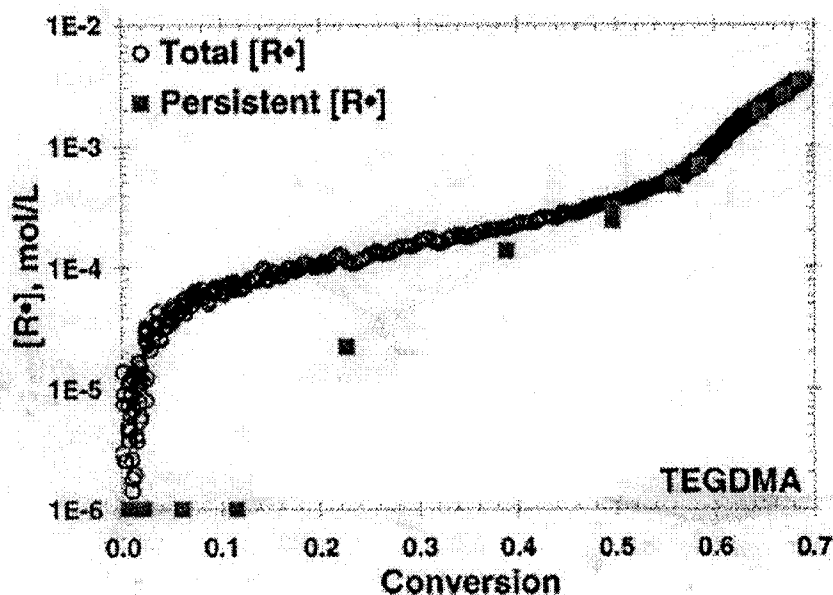


Figure 4.11 "The persistent (or trapped) radical population (■) compared with the total radical population (○) as a function of conversion. TEGDMA polymerization. Polymerization conditions: light intensity, $5mw/cm^2$; initiator concentration, 0.1wt%." Reported by Bowman in Macromolecules (2005) [6]

Comparing Figure 4.11 and the measured total and trapped radicals in the report,[6] it is found that the experimental data show a linear increase of the concentration of both trapped radicals after the fast increase at the very beginning of the reaction. This can not be expressed by the sigmoid function in Equation 4-32 because the sigmoid function of total radical concentration becomes constant after 20% conversion and the trapped radical concentration becomes constant after 70% conversion. So a linear first-order factor, $c*\alpha$ is added to both factors as shown in Equation 4-33. **The addition of $c*\alpha$ in Equation 4-33 does not change the outcome of Equation 4-32.**

$$-\frac{d(\ln([M(t)]))}{dt} = (\frac{1}{1+e^{-30(\alpha-0.05)}} + c*\alpha) - (\frac{1}{1+e^{-13.7(\alpha-0.36)}} + c*\alpha) \quad \text{Equation 4-33}$$

c is a constant, which is set as 0.3 to fit the reported experimental curves in Figure 4.11.[6] According to the two factors in Equation 4-33, the changing concentration of total radicals and trapped radicals in log scale are shown in Figure 4.12.
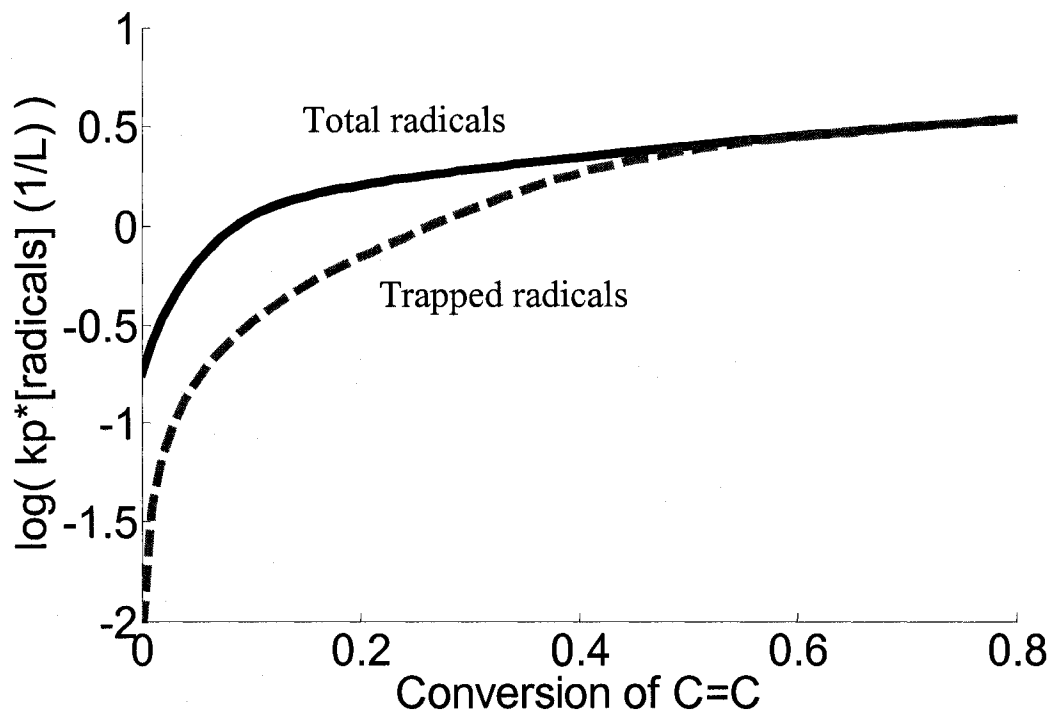
Figure 4.12 The model's changing concentration of total radicals and trapped radicals versus conversion for the cure of a sample, CD540-0.2wt%Irgacure 819, at room temperature under intensity of 32.5 μw/cm², thickness=0.05mm. (——) The total radical concentration, (– – –) the trapped radical concentration. Data in (b) are for the log scale ordinate of (a)

Although Figure 4.12 is different from Figure 4.11 due to the different reaction conditions, Figure 4.12 shows a constant increase after a fast increase of the concentration of free radicals in the system. This is more similar to the reported experimental curves in Figure 4.11[6] than Figure 4.10.

The outcome in this section suggests that the changing concentration of "free" and "trapped" radicals in the system strongly influences (or determines) the increase and the decrease of reaction rate versus conversion.

## (4) Prediction of UV cure kinetics at different intensities

With the results from part (1), (2), and (3), the cure kinetics at different intensities can be predicted. The calculation method is elaborated below.

From Equation 4-32,

$$-\frac{d(\ln([M(t)]))}{dt} = f(\alpha) \qquad \text{Equation 4-34}$$

Where

$$f(\alpha) = \frac{1}{1+e^{-30(\alpha-0.05)}} - \frac{1}{1+e^{-13.7(\alpha-0.36)}} \qquad \text{Equation 4-35}$$

Step 1, integrating Equation 4-34 from time ($t_1$) to time ($t_2$)

$$\ln[M]_{t2} = \ln[M]_{t1} - f(\alpha_1)*(t_2 - t_1) \qquad \text{Equation 4-36}$$

Time $t_1$ is the beginning of the cure and also the end of the inhibition period. Time $t_2$ is another time after $t_1$ and the difference between them is so small that the conversions at two time points have little difference. (A large interval of time ($t_2$-$t_1$) can induce large calculation error as shown in appendix 3.) $[M]_{t1}$, the concentration of monomer at $t_1$ is equal to the original concentration of C=C in the system, $[M]_0$. $[M]_0$ is approximately equal to 3.92 mol/l according to the original composition of the system. The conversion of C=C, $\alpha_1$ can be calculated using Equation 4-25 and it is equal to 0 at $t_1$. Therefore, $f(\alpha_1)$ can be calculated using Equation 4-35 by substituting $\alpha_1$ with 0. So, $[M]_{t2}$ can be calculated using Equation 4-36.

Step 2, integrating again from t$_2$ to t$_3$,

$$\ln[M]_{t_3} = \ln[M]_{t_2} - f(\alpha_2) * (t_3 - t_2)$$ Equation 4-37

Where $[M]_{t_2}$ is given from the calculation above using Equation 4-36. Similar to what was done above, $\alpha_2$ can be calculated using Equation 4-25 at time $t_2$, and $f(\alpha_2)$ can be calculated using Equation 4-35. With these values, $[M]_{t_3}$ can be calculated using Equation 4-37.

Step 3 through step n continue on the same way, the conversion of C=C,$\alpha$ , from time, $t_1$ to time $t_n$ can be calculated for the cure of CD540-0.2wt%Irgacure 819 at room temperature when the incident light intensity is 32.5 $\mu w/cm^2$ and the sample thickness is 0.05mm.

Combining Equation 4-28 and 4-34, the value of $-\dfrac{d(\ln([M(t)]))}{dt}$ versus conversion at other incident intensities ($I_i$) can be calculated using Equation 4-38.

$$-\frac{d(\ln([M(t)]))}{dt} = A * f(\alpha)$$ Equation 4-38

Where $A = (\dfrac{I_i}{32.5})^{0.7}$, the units of $I_i$ is $\mu w/cm^2$. The reason of using 0.7 as the exponent is that b in Table 4.3 is $0.70 \pm 0.04$ for the conversion range from 10% to 40% where reaction rate is fast as shown in Figure 4.5. After 50% conversion, the value of b increases considerably, the reaction is very slow then as shown in Figure 4.5. Therefore, the increase of b after 50% conversion should have little effect on the total cure kinetics.

The conversion of C=C,$\alpha$ versus **cure time** can be calculated for the cure of CD540-0.2wt%IC819 at different light intensities using Equation 4-38 and the method described above from step 1 to step n.

Note that the **cure times**, $t_1$ to $t_n$, take the cure starting point, instead of the exposure starting point, as 0. The **exposure time** can be calculated by adding the inhibition period (the delay time due to oxygen inhibition) to the cure times.

The time length of inhibition period can be calculated for any given intensity using Equation 4-26 for cure of the system, CD540 with 0.2wt% Irgacure 819 at room temperature with a thickness of 0.05mm.

Now the conversion of C=C,$\alpha$ versus **exposure time** can be calculated and predicted for the cure of CD540-0.2wt%IC819 thin film of 0.05mm thickness at different light intensities.

A Matlab program (in the appendix 2) is written to do all the calculations above. The step size used for the calculation is 0.005 minutes. The reason for choosing this step size is shown in appendix 3.

Using the method above, the cure kinetics of CD540-0.2wt%Irgacure 819 thin films at different exposure intensities (32.5, 16, 8, and 1 $\mu w/cm^2$) are calculated and the results are shown in Figure 4.13. The experimental data are listed in the same figure to compare with the predicted curves.
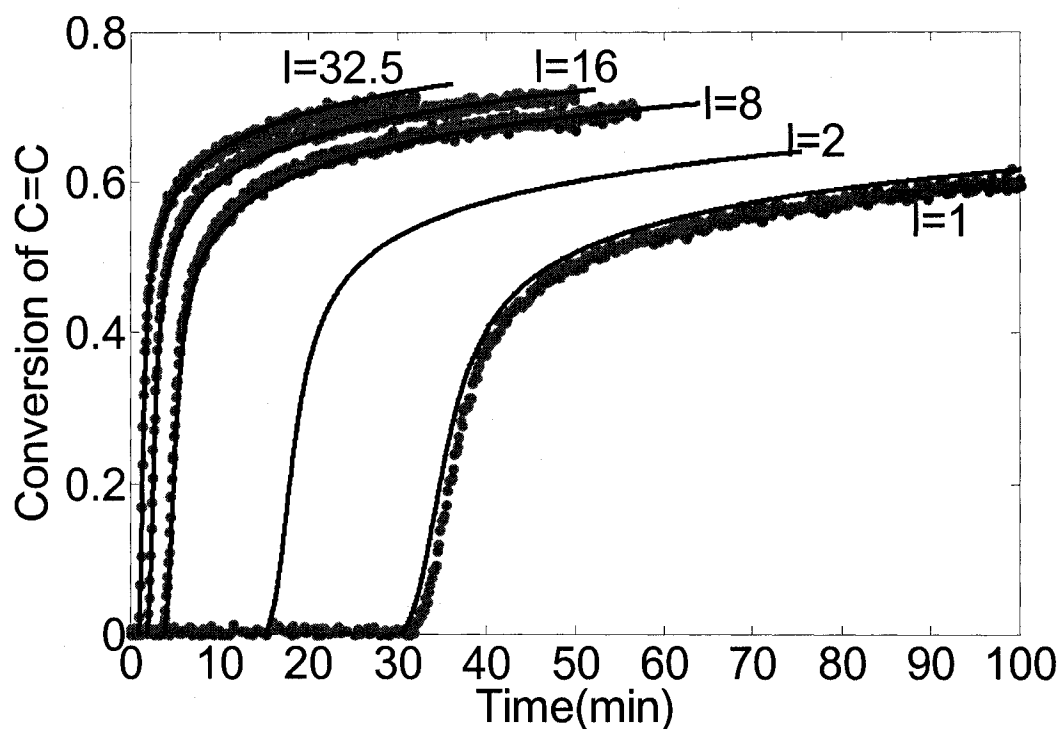
Figure 4.13 Calculation of cure conversion at different times for different intensities. (—) the calculated data, (●)the experimental data

Figure 4.13 shows that the predicted curves fit the experimental data very well. The outcome is encouraging. It suggests that it is possible to predict the cure kinetics of a thick sample at different depths since the changing intensity versus depth and exposure time is the main reason for the change of cure kinetics in the thick samples. The changing intensity versus depth and exposure time has been studied in Chapter 3.

### 4.3.3   Initiator concentration effect on the cure kinetics of thin samples

A series of thin samples with the composition of CD540 with Irgacure 819 (at varying concentration of 0.05 to 0.2wt%) were cured at the intensity of 32.5 $\mu w/cm^2$. The

thickness of the samples here is 0.05mm. The cure process was monitored by real-time

near FTIR. The conversion of C=C versus exposure time is shown in Figure 4.14.
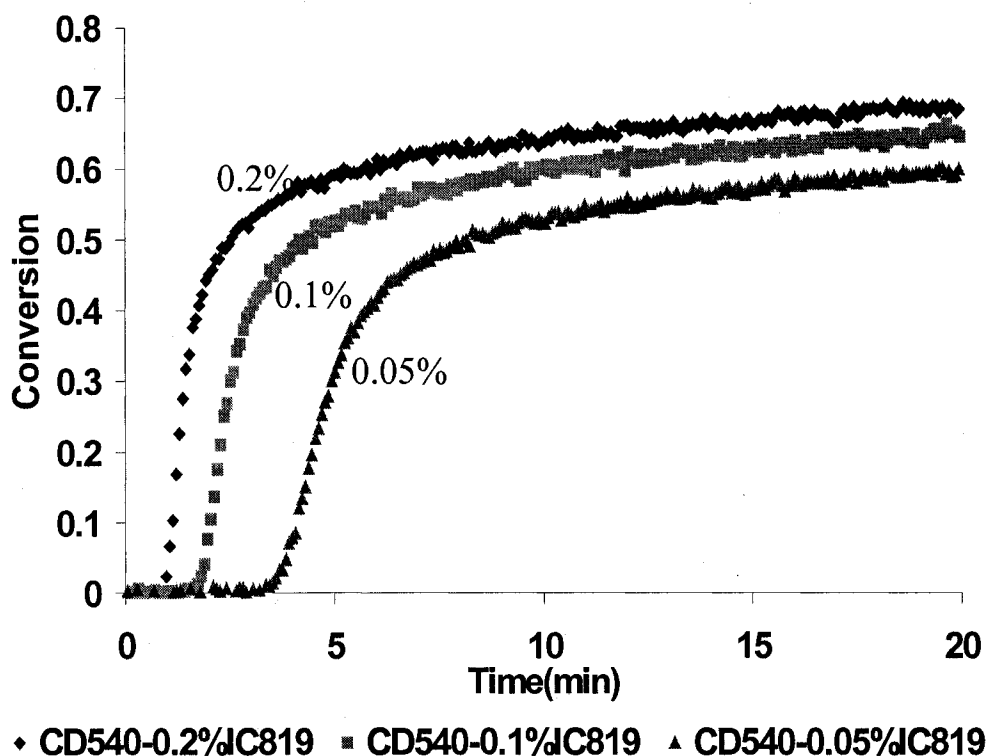


Figure 4.14 UV cure of CD540 with Irgacure 819 at the intensity of 32.5 $\mu$w/cm$^2$.

Figure 4.14 shows similar phenomena to Figure 4.3, the inhibition period, reaction rate and the final conversion are also functions of initiator concentration, [PI]. Additionally, increasing the initiator concentration has the similar effect on the cure kinetics to increasing the light intensity.

In this section, the effect of initiator concentration on the inhibition period (delay time) will be studied first in part (1). The initiator concentration on the reaction rate will

be discussed in part (2). In part (3) A calculation method will be developed based on the results from part (1), (2) here and part (3) in section 4.3.2 to predict the cure kinetics of the sample with different initiator concentrations at the same light intensity.

## (1) The effect of initiator concentration on the inhibition period

In order to study quantitatively the effect of [PI] on the delay time, the delay time versus the value of 1/[PI] is plotted in Figure 4.15.



$y = 0.1745x$
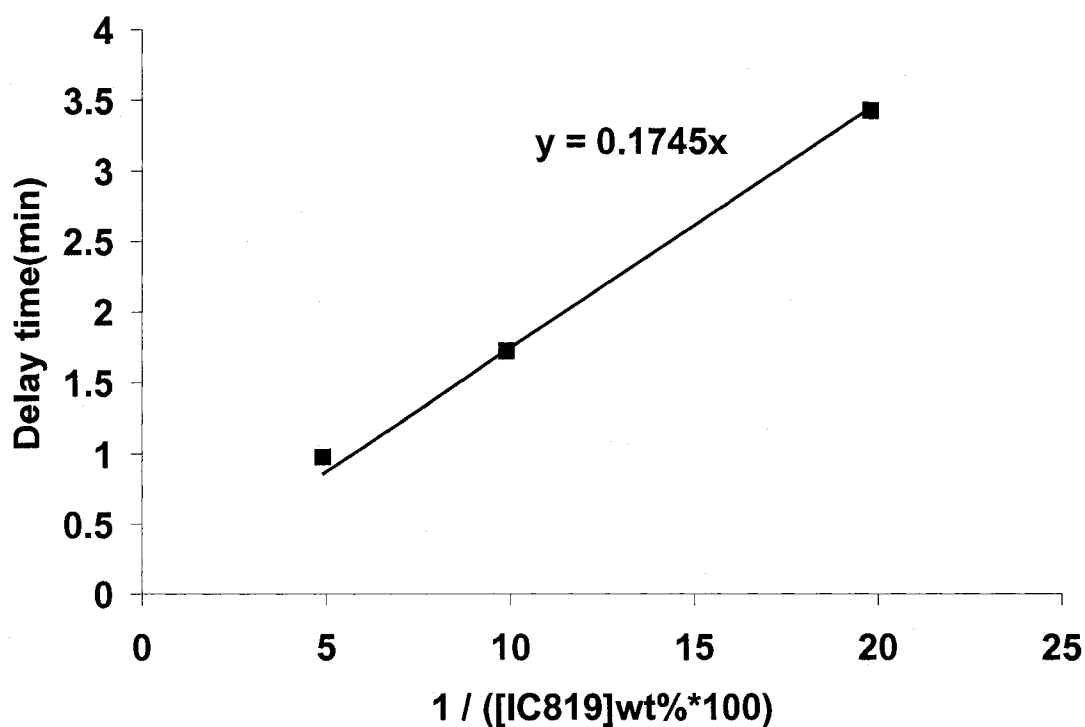
Figure 4.15 Delay time as a function of [PI], I=32.5 $\mu$w/cm$^2$.

Figure 4.15 shows that the delay time is longer for the system with less initiator concentration. Similar phenomena are observed in Decker's paper[9] for the polymerization

with much higher cure rate, but he did not study this quantitatively. Studying the relationship of delay time and [PI] gives Equation 4-39.

$$Td = \frac{0.1745}{[PI]wt\%*100}$$

Equation 4-39

From Equations 4-39 and 4-26, the delay time (inhibition period) is inversely proportional to both the _incident intensity_ and [PI] in the range studied in this dissertation. In order to understand the reason, the mechanism and kinetics of oxygen inhibition is studied as below.

The delay of the polymerization is known due to the existing oxygen in the system scavenging the initiating radicals.[4,5,5]Usually one radical reacts with one $O_2$ as shown in Equation 4-40 at room temperature,

$$R\bullet + O_2 \xrightarrow{\ ko\ } RO_2\bullet$$
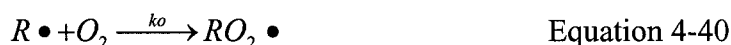
Equation 4-40

$R\bullet$ is the initiator radical, $k_o$ is the kinetic rate constant that oxygen molecules react with fragmental initiator radicals, $k_o \sim 5*10^5 k_p$.[4]

Because of the high reactivity of oxygen to free radicals,

$$k_o[O_2]>>k_p[M]$$

Equation 4-41

Initiator radicals tend to react with oxygen to form $RO_2\bullet$ instead of with monomer to induce polymerization at the beginning. Besides, $RO_2\bullet$ has a low reactivity and does not induce the polymerization of CD540.[4] Therefore, the polymerization won't start until the concentration of oxygen in the system is decreases to $2*10^{-6}*[M]$ to make

$$k_p[M]=k_o[O_2]$$

Equation 4-42

This happens at the end of the inhibition period and that is also the starting time of polymerization.

From Equation 4-40, it is proper to describe the reaction rate of oxygen with radicals as

$$R_o = -\frac{d[O_2]}{dt} = k_0[R\bullet][O_2]$$ 

Equation 4-43

Define the rate of the formation of radicals ($R_r$) that react with oxygen to form peroxy radical initiation as

$$R_r = 2\phi_o I_a$$ 

Equation 4-44

where $\phi_o$ is similar to the definition of $\phi$ [13] (the number of propagating chains initiated per light photon absorbed), $\phi_o$ is defined as the number of peroxy radicals (non-active) formed per photon absorbed. Since peroxy radicals are relatively stable compared with initiating radicals, $[R\bullet]$ can be regarded as a constant according to the assumption of steady-state during the inhibition period. Therefore,

$$\frac{d[R\bullet]}{dt} = R_r - R_O = 0$$ 

Equation 4-45

Substitute Equations 4-43 and 4-44 into Equation 4-45 gives

$$\frac{d[R\bullet]}{dt} = 2\phi' I_a - k_o[R\cdot][O_2] = 0$$ 

Equation 4-46

Therefore,

$$[R\bullet] = \frac{2\phi_o I_a}{k_0[O_2]}$$ 

Equation 4-47

Substitute into Equation 4-43,

$$-\frac{d[O_2]}{dt} = 2\phi_o I_a$$ 

Equation 4-48

Integrating Equation 4-48 from time 0 to the time $T_d$. Where $T_d$ is the end of the inhibition period and also the starting time of the polymerization

$$\int_{[O_2]_0}^{[O_2]_{T_d}} d[O_2] = -\int_0^{T_d} (2\phi_o I_a)dt \qquad \text{Equation 4-49}$$

Substitute $I_a$ using Equation 4-1 gives Equation 4-50,

$$\int_{[O_2]_0}^{[O_2]_{T_d}} d[O_2] = -\int_0^{T_d} (4.6\phi_o I_i \varepsilon b[PI])dt \qquad \text{Equation 4-50}$$

Since only a little amount of initiator is consumed during the inhibition period, [PI] can

be regarded as a constant. In addition, $\phi_o, \varepsilon, I_i$ are all constants.

$$[O_2]_{td} - [O_2]_0 = -4.6\phi_o \varepsilon I_i [PI] * T_d \qquad \text{Equation 4-51}$$

Therefore,

$$T_d = \frac{[O_2]_0 - [O_2]_{T_d}}{4.6\phi_o \varepsilon I_i [PI]} \qquad \text{Equation 4-52}$$

In these experiments, the samples were placed between two pieces of glass as described

in the experiment section. Therefore, oxygen could not diffuse into the sample through

the glass and it is reasonable to assume that the concentration of oxygen $[O_2]_0$ dissolved

in the three samples is the same. For Equation 4-42, $k_p$ and $k_o$ are constants at the same

temperature during the inhibition period, and [M] varies only a little due to the small

difference of composition for the three systems. At the end of the induction period,

$k_o[O_2]_{Td} = k_p[M]_0$. The residual oxygen, $[O_2]_{Td}$ can be regarded as a constant for these

three experiments. The delay time is inversely proportional to [PI] and incident intensity

as shown in Equation 4-52.


## (2) The effect of initiator concentration on the polymerization rate

Figure 4.14 also shows that increasing the initiator concentration results in a

larger polymerization rate and the final conversion. In order to study the connection

between the polymerization rate and [PI], the value of $-\dfrac{d(\ln[M(t)])}{dt}$ as a function of [PI]

is plotted in Figure 4.16.
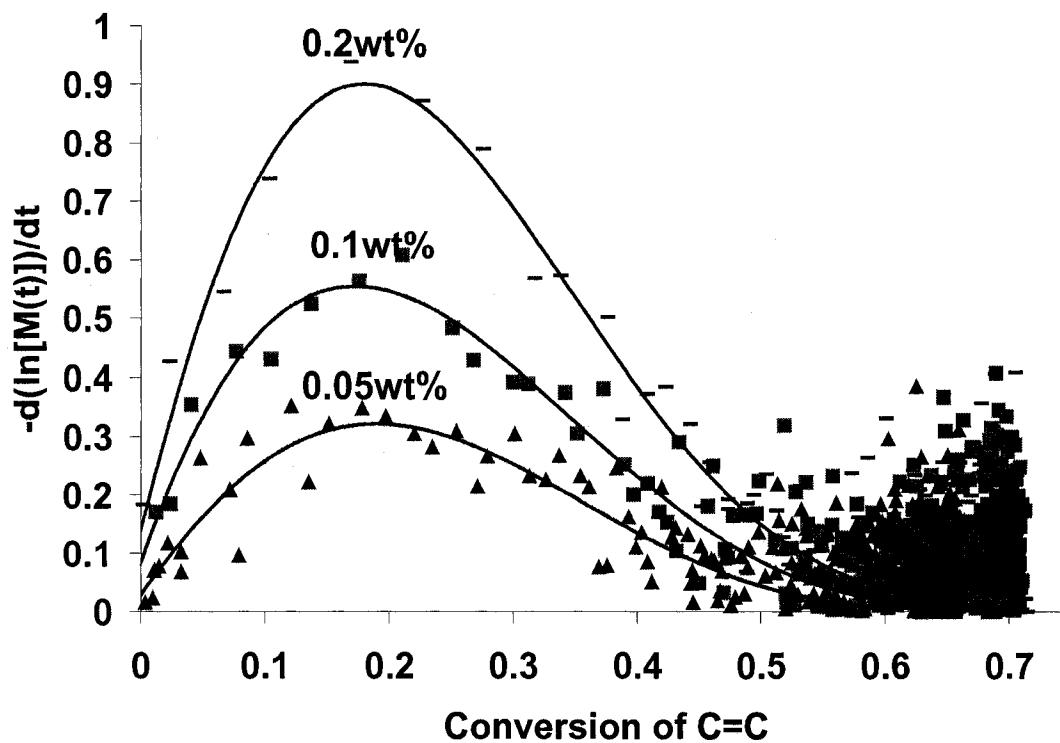


Figure 4.16   $-\dfrac{d(\ln[M(t)])}{dt}$ versus conversion for system with different initiator

concentration, [PI], Ii=32.5 μw/cm², thickness=0.05 mm. Point curves are experimental

data; solid curves are the fitting curves.

Similar to Figure 4.7, the experimental data in Figure 4.16 are also fit to average

curves using a polynomial and Excel software to give the values of $-\dfrac{d(\ln[M(t)])}{dt}$ with

less experimental error at different conversions. The value of $-\dfrac{d(\ln[M(t)])}{dt}$ versus [PI],

the photo initiator concentration at different conversions of C=C is shown in Figure 4.17.
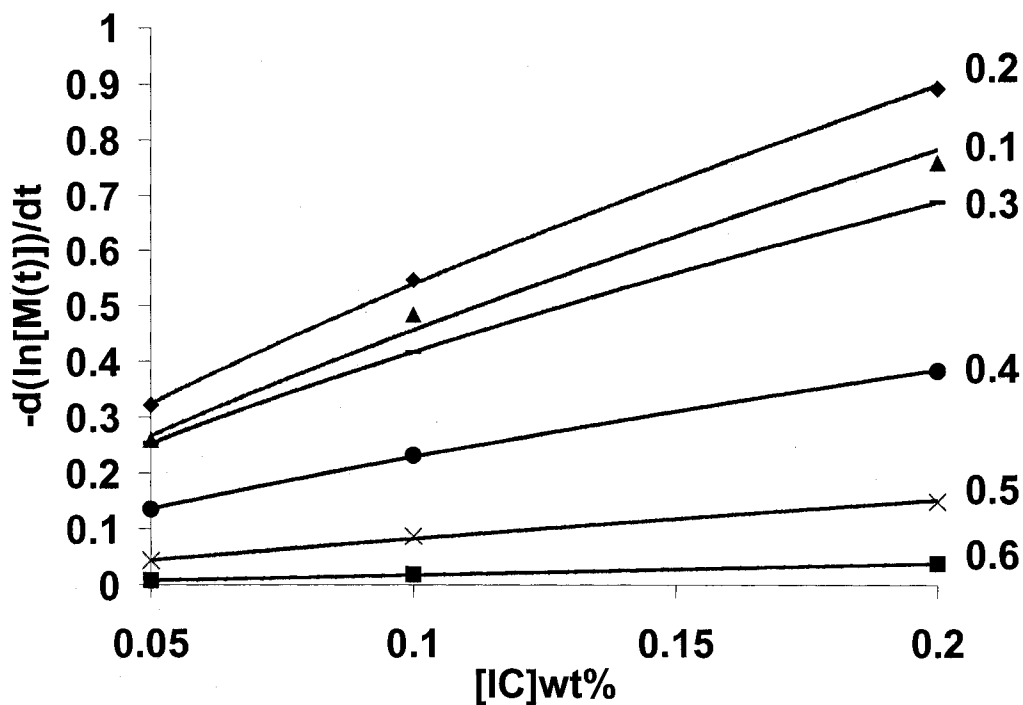


Figure 4.17 [PI] effect on the value of –d(ln[M(t)])/dt at different degrees of conversion.(0.1 to 0.6 marked in the figure)

From Figure 4.17, it is found that the relationship of $-\dfrac{d(\ln[M(t)])}{dt}$ and [PI] can

be written as

$$-\frac{d(\ln[M(t)])}{dt} \propto c*[PI]^d \qquad\qquad \text{Equation 4-53}$$

Similar to Equation 4-27, c and d here are constants. Their values are calculated first using the original initiator concentration. The results are listed in Table 4.4 at different conversions of C=C. They are then calculated again using the exact value of initiator

concentration as shown in Appendix 1. The data calculated using the corrected initiator concentration are also listed in Table 4.4 in parentheses.

Table 4.4 The value of c and d of Equation 4-53 at different degrees of conversion.

| Conversion of C=C | c | | d | |
|---|---|---|---|---|
| 0.1 | 2.74 | (2.71) | 0.78 | (0.77) |
| 0.2 | 2.94 | (2.90) | 0.79 | (0.73) |
| 0.3 | 2.20 | (2.18) | 0.72 | (0.71) |
| 0.4 | 1.29 | (1.28) | 0.75 | (0.74) |
| 0.5 | 0.63 | (0.62) | 0.88 | (0.86) |
| 0.6 | 0.22 | (0.21) | 1.09 | (1.03) |

Note: the values in parentheses are calculated using corrected initiator concentrations at different conversions.

Table 4.4 shows that d $(0.75 \pm 0.04)$ is almost a constant for the conversion range from 10% to 40% where the reaction rate is large. Using the corrected initiator concentrations, both c and d value decreases but not much. The value of d, 0.75, is about the same as the value of b, 0.7 in Equation 4-27. The deviation of the value of b and d from 0.5 has been attributed to the unimolecular termination kinetics due to trapped radicals in the system. **It also shows when the conversion of C=C is higher than 0.3, d increases with exposure time and after 0.5 conversion it increases even faster.** As discussed in section 4.3.2, this is due to the increase of trapped radicals in the system as it becomes more viscous. From Equations 4-19 and 4-24, **more trapped radicals in the**

**system** (Or more uni-molecular termination relative to bimolecular termination) **correlates to a b (and d) value approaching 1 and deviating from 0.5**. According to this theory, d should be less but approaching 1 by the end of the reaction. However, d, 1.09 is a little higher than 1 at 0.6 conversion. One reason is the decrease of initiator concentration. Using the correct initiator concentration, the value decreases to 1.03. Another reason is probably due to the experimental error especially at very low or high conversions where reaction rate is relatively slow.

From Equation 4-53,

$$\frac{\left(-\dfrac{d(\ln[M(t)])}{dt}\right)_{[PI]_1}}{\left(-\dfrac{d(\ln[M(t)])}{dt}\right)_{[PI]_2}} = \left(\frac{[PI]_1}{[PI]_2}\right)^d \qquad \text{Equation 4-54}$$

$[PI]_1$ and $[PI]_2$ are two concentrations of initiator. d is approximately set as 0.75 since d is $0.75 \pm 0.04$ for the conversion range from 10% to 40% where the reaction rate is large.

### (3) Prediction of UV cure kinetics at different intensities

From the Equations 4-39 and 4-54 in this section, 4.3.3 and the Equation 4-32 in section 4.3.2, the cure kinetics of CD540 with different initiator concentration, [PI], at 32.5 $\mu$w/cm$^2$ intensity can be calculated. The calculation method is similar to that in section 4.3.2. The difference is the varying parameter here is initiator concentration, [PI], instead of intensity, $I_i$. The Matlab program for the calculation is in appendix 4. The calculation result is shown in Figure 4.18.
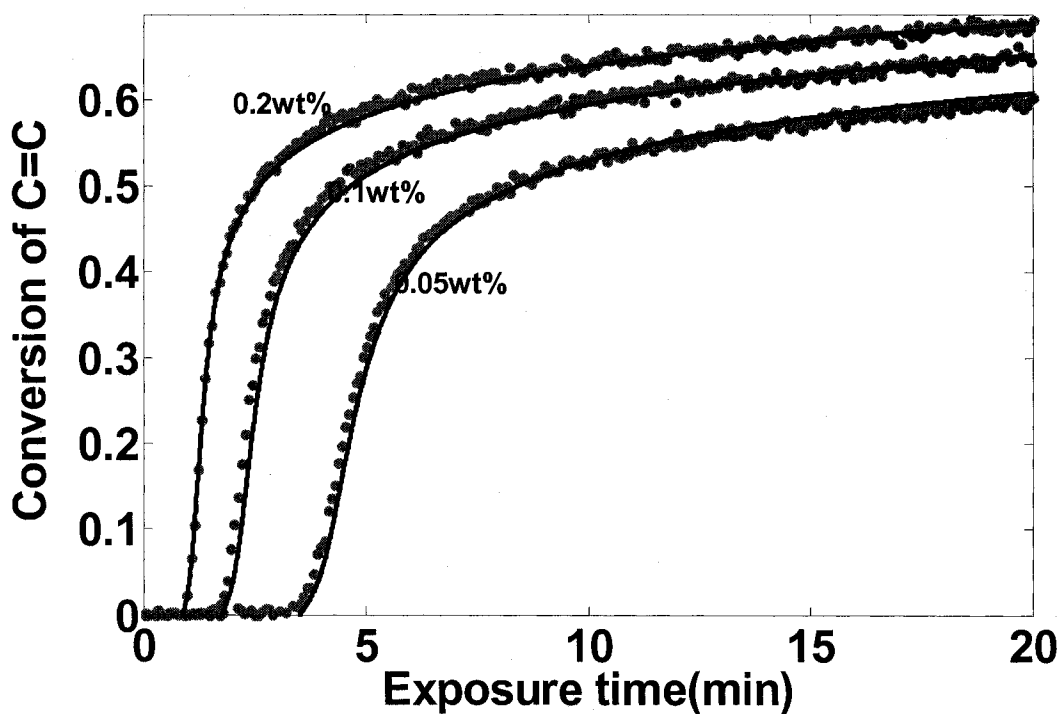
Figure 4.18 Calculation of cure conversion versus time for different [PI], photoinitiator concentration. (—) the calculated data, (●) the experimental data

Figure 4.18 shows that the calculated predictions fit the experimental results very well. This result leads to a method to predict the cure kinetics of a thin sample of CD540 and Irgacure 819 with varying Irgacure 819 concentration under the same radiation intensity. Combining Equations 4-26 and 4-39 gives the Equation 4-55,

$$Td = \frac{5.542}{I \times [PI]wt\% \times 100}$$

Equation 4-55

Combining Equations 4-28 and 4-54 gives the Equation 4-38,

$$\frac{\left(-\dfrac{d(\ln[M(t)])}{dt}\right)_{I_1[PI]_1}}{\left(-\dfrac{d(\ln[M(t)])}{dt}\right)_{I_2[PI]_2}} = \left(\frac{I_1}{I_2}\right)^{0.7}\left(\frac{[PI]_1}{[PI]_2}\right)^{0.75}$$

Equation 4-56

With Equations 4-55, 4-56, and 4-32, the cure kinetics of CD540-Irgacure 819 can be predicted at any intensity with any amount of initiator concentration when the sample thickness is 0.05mm.

### 4.3.4 Temperature effect on the cure kinetics of thin samples.

In order to study the temperature effect on the cure kinetics, a series of experiments was done with the system composed of CD540 and Irgacure 819 under the same radiation, 32.5 $\mu w/cm^2$, at different temperatures 27, 35, and 55°C. The thickness of the samples remains the same, 0.05mm. The curing process was monitored by near FTIR and the result for the sample CD540 with 0.05% Irgacure 819 is shown in Figure 4.19.
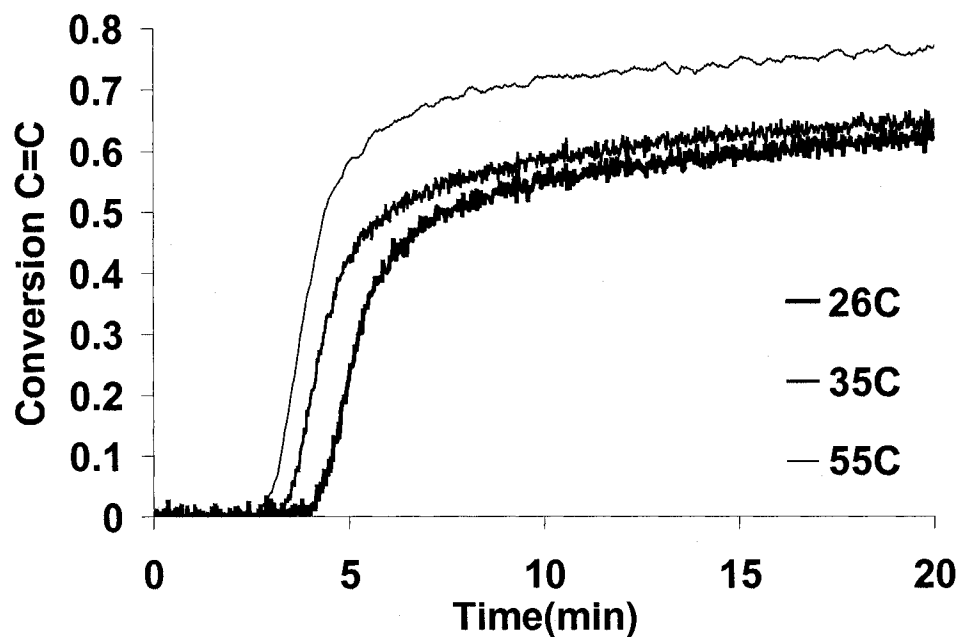


Figure 4.19 Conversion versus time for the system of CD540 with 0.05%IC 819 cured at different temperatures.

From Figure 4.19, it is found that increasing the temperature increased the final conversion of the system. This is because at higher temperatures, the viscosity of the system is lower and because the system can obtain a higher $T_g$. Therefore, the segmental mobility of the residual double bonds near a similar extent of cure will be increased to facilitate the polymerization. Figure 4.19 also shows that the cure rate as expected is also increased with increasing temperature.

**(1)     Calculation of the apparent activation energy**

Similar experiments were done for the system with different concentration of initiator. The kinetic dependence of initiator concentration was studied at different temperatures. The results are shown in Figure 4.20.
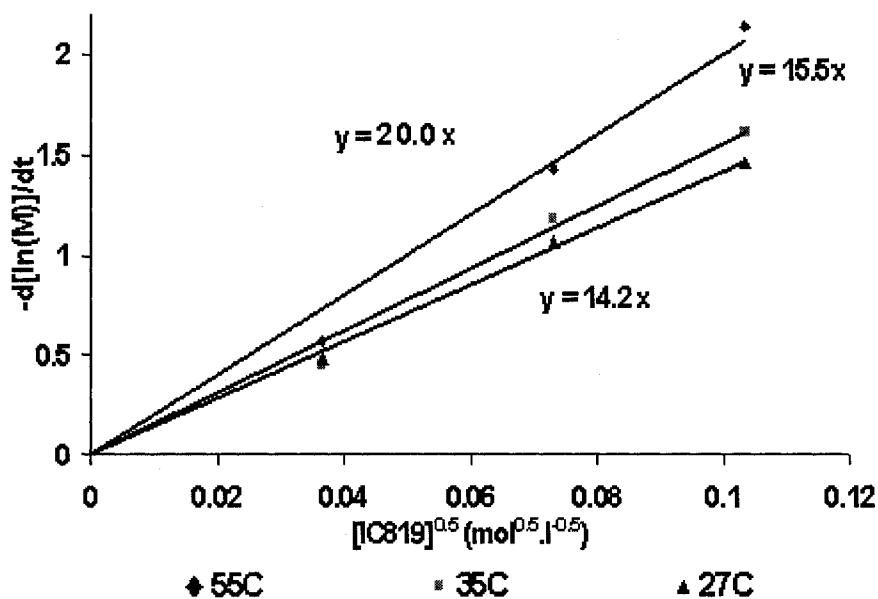


Figure 4.20 $-d(\ln[M(t)])/dt$ versus $[IC819]^{0.5}$ at different temperatures for the system composed of CD540 with Irgacure 819, Io=32.5 $\mu w/cm^2$, thickness=0.05mm.

It is found in Figure 4.20 that the value of the slope at the temperatures of 27, 35, and 55°C is 14.2, 15.5 and 20.0 cm $\mu w^{-0.5}$ $min^{-1}$ respectively. According to Equation 4-19, the slopes are the value of $\frac{k_p}{k_t^{1/2}}(4.6\phi\varepsilon I_i b)^{1/2}$ at different temperatures. With a given value of $\varepsilon$, $I_i$, and b, the value of $\emptyset^{0.5}$ $k_p/k_t^{0.5}$ was calculated for different temperatures and a plot $\emptyset^{0.5}$ $k_p/k_t^{0.5}$ versus 1/ Temperature is shown in Figure 4.21.

Figure 4.21  4.6 $\emptyset^{0.5}$ $k_p/k_t^{0.5}$ versus the inverse of temperature for the system composed of CD540 and Irgacure 819, intensity is 32.5 $\mu w/cm^2$, and thickness is 0.05mm.

The relationship of $4.6\phi^{0.5}\frac{k_p}{k_t^{0.5}}$ and 1/T can be fit to Equation 4-57.

$$y = 7.1e^{-1207(K) * x}$$

Equation 4-57

Where y represents $\emptyset^{0.5}$ $k_p/k_t^{0.5}$ and x represents $1/T(K^{-1})$.

Therefore,

$$\phi^{0.5}\frac{k_p}{k_t^{0.5}} = 30.9e^{\frac{-1207}{T}}$$

Equation 4-58

According to the Arrhenius' law, $k = Ae^{-\frac{E}{RT}}$, where k is a rate constant, A is a pre-exponential factor and E is the activation energy.

$$k_p = A_p e^{(-E_p/RT)}$$

Equation 4-59

$$k_t = A_t e^{(-E_t/RT)}$$

Equation 4-60

Therefore,

$$\phi^{0.5}\frac{k_p}{k_t^{0.5}} = \phi^{0.5}(\frac{A_p}{A_t^{0.5}})e^{\frac{0.5E_t - E_p}{RT}}$$

Equation 4-61

Comparing Equations 4-58 with 4-61, the value of $\phi^{0.5} \dfrac{A_p}{A_t^{0.5}}$ is 30.9 cm $\mu$w$^{0.5}$ min$^{-1}$ and

the value of $(E_p-0.5E_t)/R$ is 1207 (K). Therefore, $E_p-0.5E_t$, the value of the apparent

activation energy is 10.0 kJ/mol (R=8.3145 J mol$^{-1}$ K$^{-1}$). This value is not very far from

the value, 15.5 kJ/mol reported in Bunel's paper[44] on the system of dimethacrylate

oligomer with Darocur 1173.


**(2) Fit and predict the effect of temperature on the cure kinetics**

The value of dlnM/dt versus conversion of the cure of CD540-**0.2wt%**IC819 at

different temperatures from 25 to 55°C ($I_i$=32.5 $\mu w/cm^2$, thickness=0.05mm) are

calculated and the results are shown in Figure 4.22 as the solid curves.
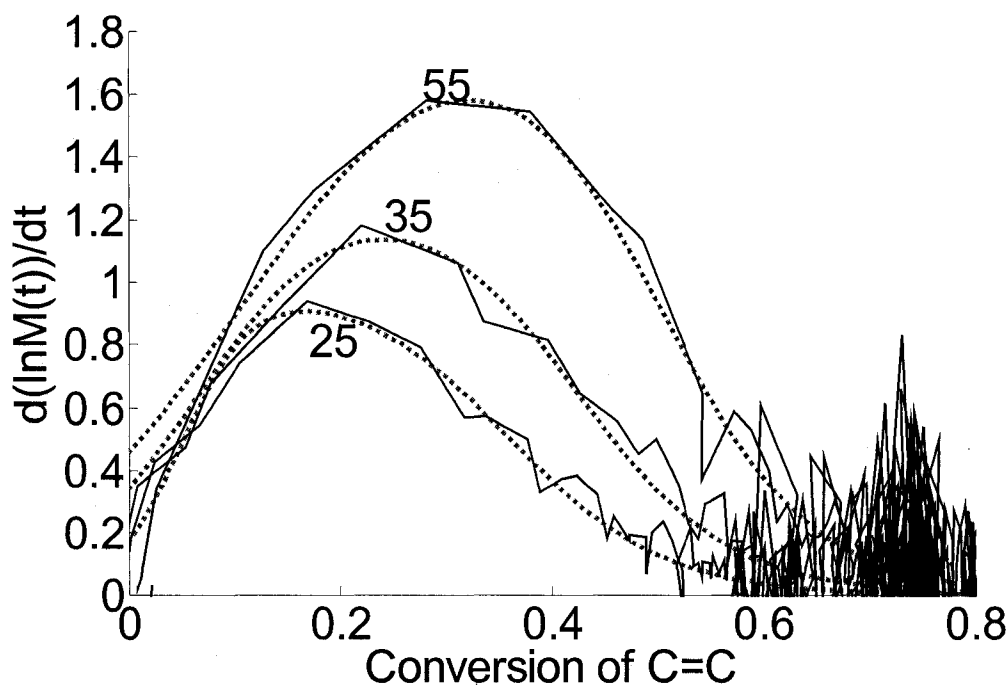
Figure 4.22 dlnM/dt versus conversion of the cure of CD540-**0.2wt%**IC819 at different temperatures from 25 to 55°C, $I_i$=32.5 $\mu w/cm^2$, thickness=0.05mm. (—) Experimental data (••••••) the fit results.

The experimental data at different temperatures are fit using the following equations. The best fit curves are shown in Figure 4.22 as the point curves.

T=25°C, $\qquad -\dfrac{d(\ln[M(t)])}{dt} = \dfrac{1}{1+e^{-30(\alpha-0.05)}} - \dfrac{1}{1+e^{-13.7(\alpha-0.36)}}$ $\qquad$ Equation 4-62

T=35°C, $\qquad -\dfrac{d(\ln[M(t)])}{dt} = \dfrac{1}{0.75+e^{-15(\alpha-0.05)}} - \dfrac{1}{0.75+e^{-13.7(\alpha-0.4)}}$ $\qquad$ Equation 4-63

T=55°C, $\qquad -\dfrac{d(\ln[M(t)])}{dt} = \dfrac{1}{0.51+e^{-10(\alpha-0.05)}} - \dfrac{1}{0.51+e^{-13.7(\alpha-0.45)}}$ $\qquad$ Equation 4-64

Where, $\alpha$ is the conversion of C=C bonds. Equations 4-62 to 4-64 can be expressed by a common equation below.

**Common equation:** $-\dfrac{d(\ln[M(t)])}{dt} = \dfrac{1}{f_1 + e^{-f_2(\alpha-0.05)}} - \dfrac{1}{f_1 + e^{-13.7(\alpha-f_3)}}$    Equation 4-65

This equation represents the cure rate versus conversion for the cure of the 0.05mm thickness sample, CD540-0.2wt%IC819, at $32.5\,\mu w/cm^2$ incident light intensity and different cure temperatures. As shown in Figure 4.10 the first factor , $\dfrac{1}{f_1 + e^{-f_2(\alpha-0.05)}}$ , represents the change of $k_p[M\bullet]_{total}$ versus conversion ($\alpha$ ) and the second factor, $\dfrac{1}{f_1 + e^{-13.7(\alpha-f_3)}}$ , represents the change of $k_p[M\bullet]_{trapped}$ versus conversion ($\alpha$ ). $f_1, f_2$, and $f_3$ are three parameters to describe the temperature dependence of the cure rate versus conversion. $\dfrac{1}{f_1}$ determines the highest concentration that the total and the trapped radicals can reach, $f_2$ determines the rate, $\dfrac{d[M\bullet]_{total}}{d\alpha}$ (or $\dfrac{-d(\ln[C=C])/dt}{d\alpha}$), for the total radicals as a function of temperature, $f_3$ determines the conversion value where the trapped radical concentration reaches the half value of its highest concentration. The value of the three parameters at different temperatures are shown in Table 4.5.

Table 4.5 Three parameters at different cure temperatures for Equation 4-65(CD540-

0.2wt%IC819, 0.05mm thickness, $I_i$=32.5 $\mu w / cm^2$)

| Temperature(°C) | $f_1$ | $f_2$ | $f_3$ |
| --- | --- | --- | --- |
| 25 | 1 | 30 | 0.36 |
| 35 | 0.75 | 15 | 0.4 |
| 55 | 0.51 | 10 | 0.45 |

It is found from Table 4.5 that the three parameters change with reaction

temperature as shown in Figures 4.23 to 4.25.
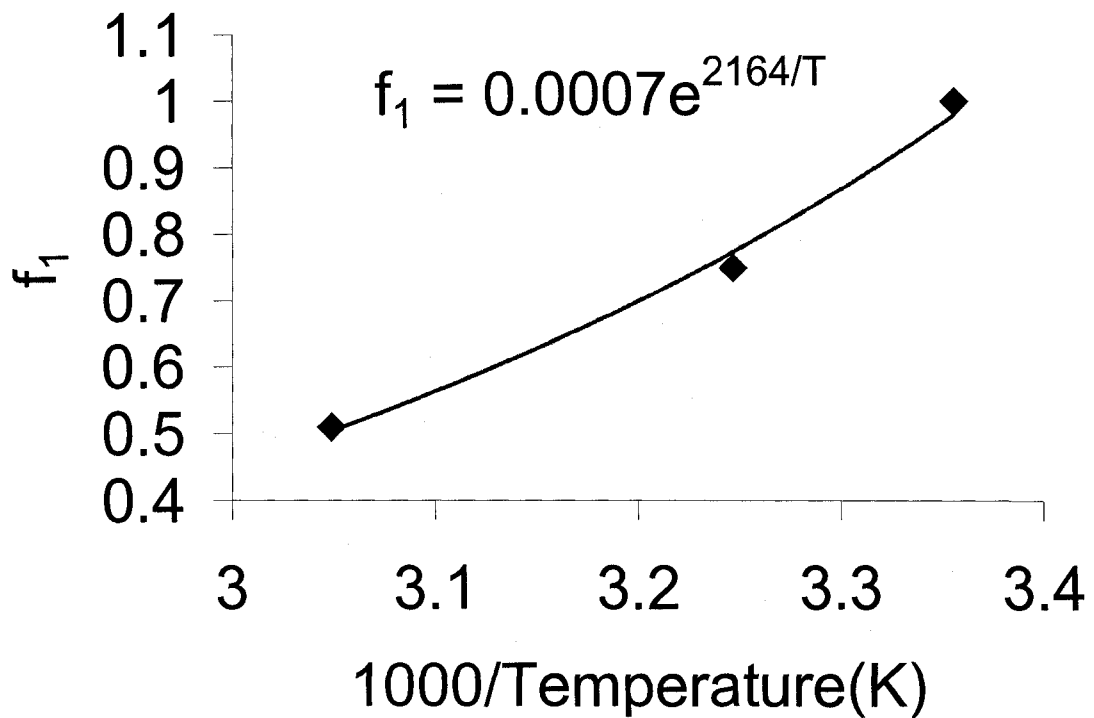


Figure 4.23 Parameter $f_1$ versus temperature (K) for the cure of CD540-0.2wt%IC819,

$I_i$=32.5 $\mu w / cm^2$, thickness=0.05mm.

$$f_2 = 0.0003e^{3394/T}$$
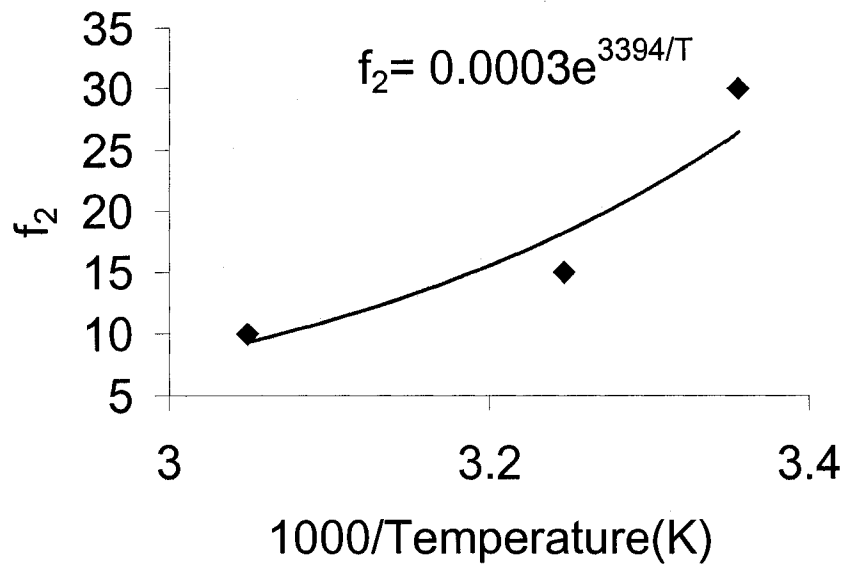
Figure 4.24 Parameter $f_2$ versus temperature (K) for the cure of CD540-0.2wt%IC819,

$I_i$=32.5 $\mu w/cm^2$, thickness=0.05mm.

$$f_3 = -219/T + 1.1$$
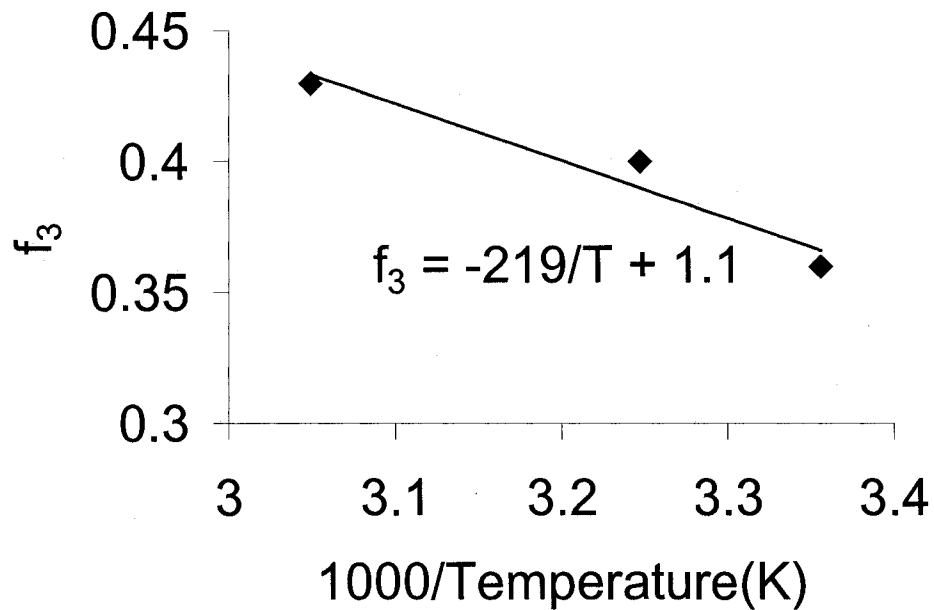
Figure 4.25 Parameter $f_3$ versus temperature (K) for the cure of CD540-0.2wt%IC819,

$I_i$=32.5 $\mu w/cm^2$, thickness=0.05mm.

From Figures 4.22 to 4.25, three parameters are functions of temperature as shown in the following equations.

$$x = \frac{1}{Temperature(K)}$$ 

Equation 4-66

$$f_1 = 0.0007e^{2164x}$$ 

Equation 4-67

$$f_2 = 0.0003e^{3394x}$$ 

Equation 4-68

$$f_3 = -219x + 1.1$$ 

Equation 4-69

Now the cure rate versus conversion at different temperatures for the cure of 0.05mm thickness sample, CD540-**0.2wt%**IC819, can be calculated using Equations 4-65 to 4-69.

Next, the temperature effect on the **delay time** (inhibition period) is studied for the cure of CD540-**0.05wt%**IC819 at 32.5 $\mu w/cm^2$. Note that the system used to study the delay time is CD540-0.05wt%IC819 instead of CD540-0.2wt%IC819. This is because the delay times for the system of CD540-0.2wt%IC819 are smaller. However the delay times for the system of CD540-0.05wt%IC819 are longer and have more variation at different temperatures from 25 to 55 $^{\circ}$C.

Figure 4.27 shows the delay time as a function of temperature for the cure of the 0.05mm thickness samples, CD540-0.05wt%IC819, at 32.5 $\mu w/cm^2$.
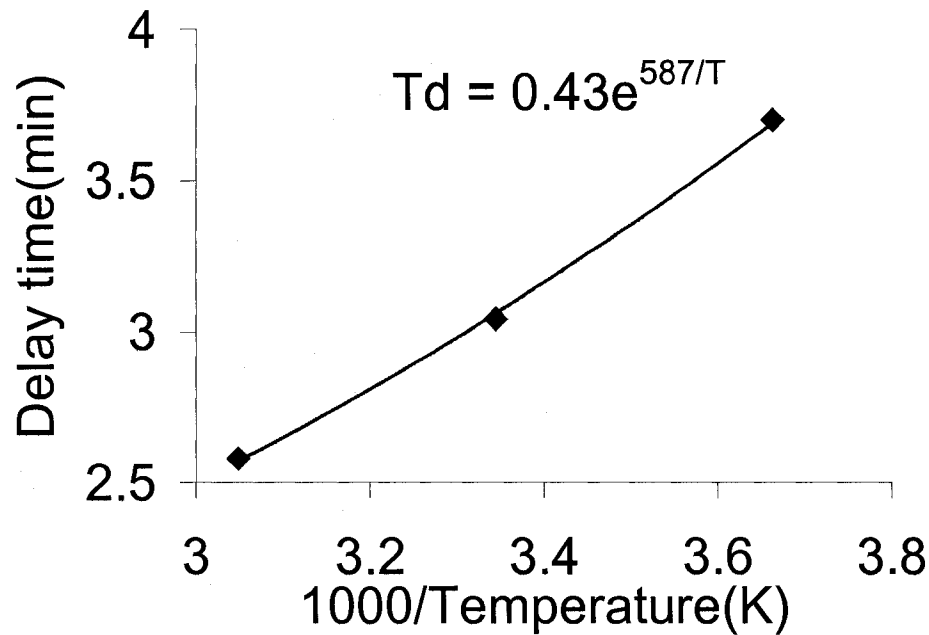
Figure 4.26 Inhibition period as a function of temperature for the system of CD540 with 0.05%IC819 cured at different temperatures from 25 to 55 °C, $I_i$=32.5 μ $w/cm^2$, thickness=0.05mm.

From Figure 4.26, we have the Equation 4-70,

$$T_d = 0.43e^{587 / Temperature(K)}$$

Equation 4-70

Combining Equations 4-65 to 4-70 and the results from Section 4.32 and 4.33 (Equations 4-55 and 4-56) for the intensity and initiator concentration effect on the cure kinetics of 0.05mm thin sample CD540-IC819, a Matlab program (Appendix 5) was written to calculate the cure kinetics at different temperatures for the system CD540-IC819 at different initiator concentrations and incident intensities. The predicted cure curves are separately shown in Figures 4.27 and 4.28 for two systems with different initiator concentrations. The corresponding experimental curves are listed together to compare.
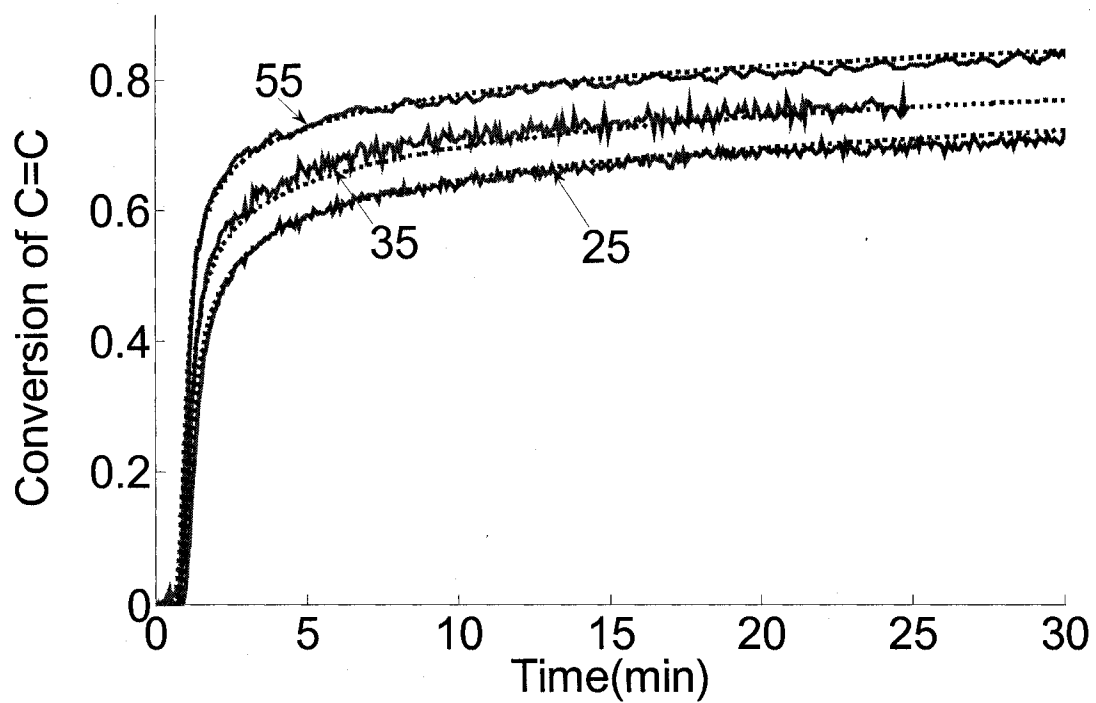
Figure 4.27 Conversion versus time for the system of CD540 with **0.2%IC 819** cured at

different temperatures from 25 to 55°C, $I_i$=32.5 uw/cm$^2$, thickness=0.05mm. (——)

Experimental data, (••••••) predict results.
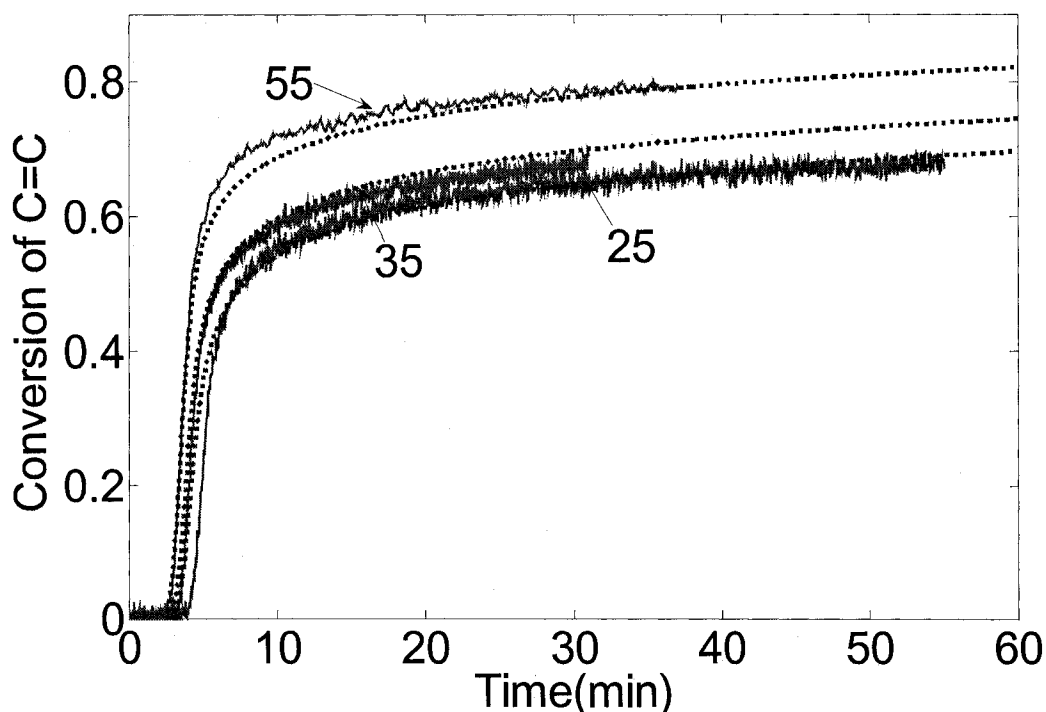
Figure 4.28 Conversion versus time for the system of CD540 with **0.05%IC 819** cured at

different temperatures from 25 to 55°C, $I_i=32.5$ uw/cm$^2$, thickness=0.05 mm. (━━)

Experimental data, (••••••) predict results.

Both Figures 4.27 and 4.28 show that the predicted curves match the experimental

curves well. This means the UV cure of CD540- IC819 thin samples (0.05mm) at

different temperatures, different intensities, and different photo-initiator concentrations

can be predicted.

### 4.3.5 Determination of $k_p$ and $k_t$

The effect of trapped radicals on UV cure kinetics was studied in section 4.1.2.

The presence of trapped radicals explains the deviation of the exponent from the classic

0.5 in Equation 4-19. In addition, a theory was developed in section 4.3.2 by dividing all

radicals in the system into two groups, "free" radicals and "trapped" radicals. This theory explained the changing reaction rate versus conversion.

Besides the "trapped" radical approach in this dissertation, another popular theory---diffusion-controlled reaction was proposed and researched widely for the cure of cross-linked systems.[6,19,21-26,45,46] In this section, diffusion-controlled reaction mechanism will be studied. This mechanism is supported by measuring the propagation and termination rate constants based on the assumptions of bimolecular termination and a steady-state concentration of radicals, which increases initially, but almost instantaneously reaches a constant, steady-state value.[13,47] With these assumptions, Polymerization rate of photo cure of CD540-Irgacure 819 is described by Equation 4-19. Equation 4-19 can be rewritten as

$$C^{0.5} \frac{k_p}{k_t^{0.5}} = -\frac{d(\ln[M(t)])}{dt}$$

Equation 4-71

Where

$$C = 4.6\emptyset \, \varepsilon \, I_i [PI] b$$

Equation 4-72

$\varepsilon \, I_i[PI]b$ is a constant when the experiment is done at the same light intensity with the same system composition at the same sample thickness. C is a function of $\emptyset$. It is difficult to measure $\emptyset$ and it often simply treated as an unknown constant.

With Equation 4-62, the value of $C* \, k_p/k_t^{0.5}$ can be measured through the process of photo polymerization. In order to determine the value $k_p$ and $k_t$ separately as they vary with the degree of conversion, the dark polymerization was monitored after the exposure is stopped at different conversions. Suppose the termination of one big molecular free radical will not happen until it meets another free radical.

$$-\frac{d[M\bullet]}{dt} = 2k_t[M\bullet]^2 \qquad\qquad \text{Equation 4-73}$$

$$-\frac{d[M\bullet]}{[M\bullet]^2} = 2k_t dt \qquad\qquad \text{Equation 4-74}$$

$$d[M\bullet]^{-1} = 2k_t dt \qquad\qquad \text{Equation 4-75}$$

If the exposure is stopped at time $t_0$ and $t_1$ is the time shortly after $t_0$, then we have the

Equation 4-76.

$$\frac{1}{[M\bullet]_{t=t_1}} - \frac{1}{[M\bullet]_{t=t_0}} = 2k_t(t_1 - t_0) \qquad\qquad \text{Equation 4-76}$$

Since Equation 4-9,

$$[M\bullet] = R_p / k_p [M] \qquad\qquad \text{Equation 4-77}$$

Substituting the $[M\bullet]$ into Equation 4-76 yields

$$(\frac{k_p[M]}{R_p})_{t=t_1} - (\frac{k_p[M]}{R_p})_{t=t_0} = 2k_t(t_1 - t_0) \qquad\qquad \text{Equation 4-78}$$

If the time difference is very short between $t_1$ and $t_0$ and the conversion only changes a

little, $k_p$ can be regarded as a constant at $t_1$ and $t_0$.

$$(\frac{k_p[M]_{t=t_1}}{R_{pt=t_1}}) - (\frac{k_p[M]_{t=t_0}}{R_p})_{t=t_0} = 2k_t(t_1 - t_0) \qquad\qquad \text{Equation 4-79}$$

Therefore, the value of $k_t$ at the conversion when the exposure was stopped can be

expressed as:

$$k_t^{0.5} = \frac{k_p / k_t^{0.5}}{2(t_1 - t_0)}[\frac{[M]_{t=t_1}}{R_{Pt=t_1}} - \frac{[M]_{t=t_0}}{R_{Pt=t_0}}]$$

or

$$C^{0.5}k_t^{0.5} = \frac{C^{0.5}k_p/k_t^{0.5}}{2(t_1-t_0)}[\frac{[M]_{t=t_1}}{Rp_{t=t_1}}-\frac{[M]_{t=t_0}}{Rp_{t=t_0}}] \qquad \text{Equation 4-80}$$

In order to satisfy the steady-state assumption, the difference between the conversion at $t_1$ and $t_0$ is limited to be less than 2.5%.

Combining Equations 4-71 and 4-80

$$C^{0.5}k_t^{0.5} = \frac{(-d\ln[M]/dt)_{t=t_0}}{2(t_1-t_0)}[\frac{[M]_{t=t_1}}{R_{P\,t=t_1}}-\frac{[M]_{t=t_0}}{R_{P\,t=t_0}}] \qquad \text{Equation 4-81}$$

Then the value of C*$k_p$ and C*$k_t$ can be calculated from the value of $C^{0.5}$ $k_t^{0.5}$, which is determined from Equation 4-81 and the value of $C^{0.5}k_p/k_t^{0.5}$, which can be calculated from Equation 4-71.

To measure the $k_p$ and $k_t$ during the process of photo polymerization, a series of experiments in which the exposure was stopped at different degrees of conversion were done for the system CD540 with 0.05wt% Irgacure 819 at the intensity of 32.5 $\mu$w/cm$^2$. Thickness of the samples here is 0.1mm in order to increase the time resolution and decrease the error of the experiment. Since the [PI] is very small here, the change of the intensity is still less than 4%. The results are shown in Figure 4.29.
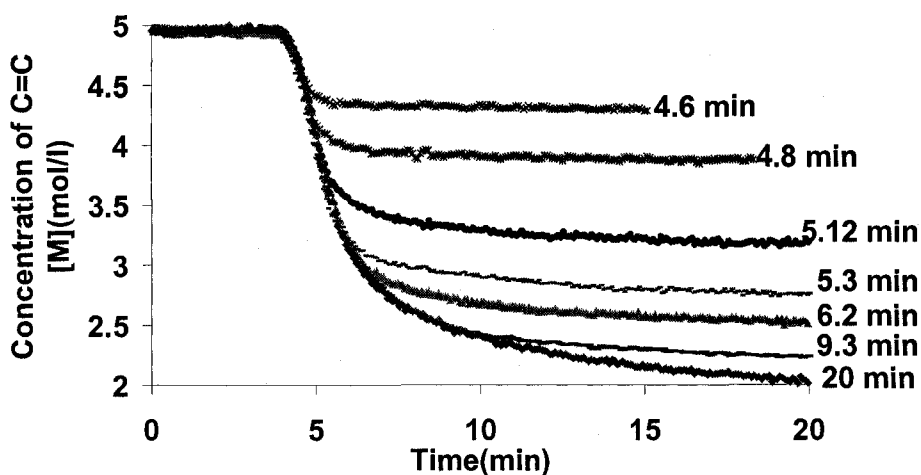
Figure 4.29 Concentration of carbon double bond as a function of time. CD540-0.05%IC819, intensity = 32.5 $\mu w/cm^2$, thickness=0.1mm, temperature=25°C. The exposure was stopped after certain exposure time as marked in the figure.

Using the method described, the value of $k_p$ and $k_t$ was calculated. The results are displayed in Figures 4.30 and 4.31 as a function of conversion.
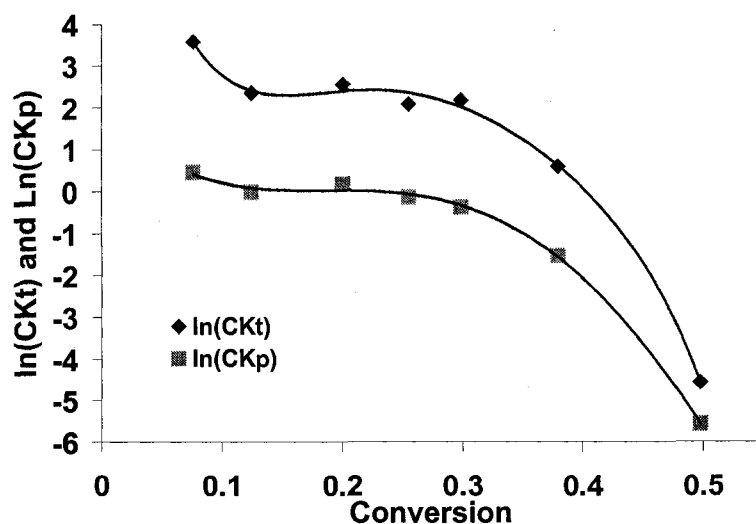


Figure 4.30. $k_p$ and $k_t$ versus conversion. CD540-0.05%IC819, intensity = 32.5$\mu w/cm^2$, thickness=0.1mm, temperature=25°C.
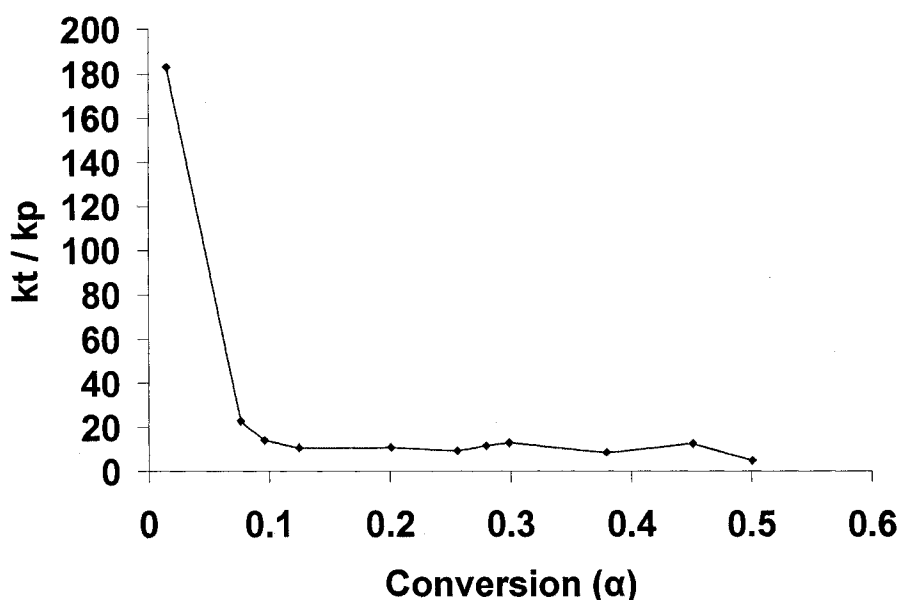
Figure 4.31. $k_t / k_p$ versus conversion. CD540-0.05%IC819, intensity = 32.5 $\mu w/cm^2$,

thickness=0.1mm, temperature=25°C.

The curve shape of $k_p$ and $k_t$ as a function of conversion is very similar to the

results observed by Bowman.[25,48]. The curve in Figure 4.30 can be divided into three

periods.

The first period is before the conversion of 7.6%. During this period, $k_t$ decreases

very fast while $k_p$ stays fairly constant as shown in Figure 4.30 and 4.31. It was believed

that the fast decrease of $k_t$ at the beginning of the reaction is due to the rapid increase of

viscosity[25], which reduces the diffusion of the macro radicals significantly. This reduces

the chance of their colliding into each other to terminate the propagation. The system

reached its gel point, which is observed below 5% conversion during this period. In

addition, the polymerization auto-accelerated because of the decrease of $k_t$ while $k_p$ is

relatively constant.

The second period is between 7.6% and 30% conversion. During this period, $k_t$ is proportional to $k_p$ as shown in Figure 4.30. The value of $k_t / k_p$ is almost constant as shown in Figure 4.31. This suggests the rate controlling factors of termination in this period are similar to the rate controlling factors of propagation. Both are controlled by the diffusion of radicals. Therefore, the rate of termination can not be simply written as Equation 4.19. The diffusion rate of the radicals needs to be considered.

The last period is between 30% to 50% conversion. It was also found that both $k_p$ and $k_t$ decrease rapidly during this period. This is probably because the sample approaches the glass transition point.

After 50% conversion, polymerization reaches a final period. Here the polymerization rate is very low for the cure of CD540-0.05%IC819 at room temperature and under the exposure of the radiation with the intensity of 32.5 $\mu w/cm^2$. Therefore, it is very hard to measure the $k_p$ and $k_t$ value after 50% conversion because the error is larger due to the small change of conversion. The system has reached its $T_g$ at which time the diffusion rate approaches zero. The exponent in Equation 4-16 during this period as shown in tables 4.3 and 4.4 is even further from 0.5 compared with the 0.7(0.75), the experimental value when the C=C conversion is less than 50%.

Comparing the diffusion-controlled reaction theory with the trapped radical theory, the former one regards all radicals in the system as active radicals with different diffusion abilities and the value of $k_p$ and $k_t$ is the average values of all radicals in the system. And it assumes the bimolecular termination is the only termination mechanism. This theory explains well the changing reaction rate versus conversion, but it can not explain directly the deviation of the exponent in Equation 4-19 from 0.5 that was found in

most diffusion-controlled reactions. The trapped radical theory developed in this dissertation divided all radicals into two types, "free" radicals whose reactions are not affected by the diffusion at all and "trapped" radicals that can not react at all. Radicals that have reactivity between two extreme conditions are divided into a% complete "free" radicals and b% complete "trapped" radicals. And the value of a and b is determined by the diffusion ability of the molecules. This theory not only explains the changing reaction rate versus conversion but also elaborates the reason for the deviation of exponent from classic value, 0.5. These two theories explain the UV cure kinetics from different perspectives.

## 4.4 Conclusion

UV cure kinetics are a function of incident intensity, initiator concentration, and temperature. The inhibition period of the free radical photopolymerization due to the existence of oxygen is inversely proportional to the initiator concentration and the incident intensity and it is also a function of temperature. The rate of polymerization ($\frac{d(\ln[M(t)])}{dt}$) is found proportional to $I^{0.7}$ and $[PI]^{0.75}$ during the cure conversion from 10% to 40%. Because of this, it is possible to predict the cure kinetics of the system CD540 with Irgacure 819 with varying incident intensities, initiator concentrations, and cure temperatures for most of the reactions up to the glass transition at about 50% C=C conversion. In addition, these results offer a method to study the cure kinetics as a function of thickness for thick samples.

The increase of the exponential value from the theoretical value of 0.5 in Equation 4-16 is proposed to be due to the unimolecular termination of some "trapped" radicals,

which has been observed by ESR spectrum. The unimolecular termination mechanism also explains well the change of cure rate versus conversion (auto-acceleration at low conversion and decreased cure rate near $T_g$). Another possible reason for the change of cure rate versus conversion is the diffusion-controlled termination, which has been supported by the experimental measurement of the $k_p$ and $k_t$ values versus conversion. Using this approach, the value of $k_t$ is found to start to be proportional to the $k_p$ value as early as less than 8% conversion. However, this calculation assumes that the bimolecular reaction is the only termination mechanism, which was proved not correct for many cross-linked systems. In addition, the diffusion-controlled termination mechanism does not explain the deviation of the exponential value from 0.5.

Increasing the reaction temperature results in an increase in the maximum cure rate and the final conversion since the final $T_g$, where the reaction is quenched increases with the cure temperature. The value of apparent activation energy, $E_p$-0.5$E_t$, for the polymerization of CD540 is 10.0 kJ/mol. This value is in the same order of magnitude as the value reported (15.5 kJ/mol ) for the system of dimethacrylate with Darocur 1173.[49]

# Reference

1    Chong, J. S. Journal of Applied Polymer Science 1969, 13, 241-47.

2    Studer, K.; Decker, C.; Bech, E.; Schwalm, R. Progress in Organic Coatings 2003, 48, 92-100.

3    Studer, K.; Decker, C.; Bech, E.; Schwalm, R. Progress in Organic Coatings 2003, 48, 101-11.

4    Decker, C.; Jenkins, A. D. Macromolecules 1985, 18, 1241-44.

5    Wight, F. R. J. Polym. Sci., Polym. Lett. Ed 1978, 16, 121-27.

6    Berchtold, K. A.; Randolph, T. W.; Bowman, C. N. Macromolecules 2005, 38, 6954-64.

7    Berchtold, K. A.; Randolph, T. W.; Bowman, C. N. ACS meeting, 2003, pp 213-14.

8    Rey, L.; Galy, J.; Sautereau, H.; Lachenal, G.; Henry, D.; Vial, J. Applied Spectroscopy 2000, 54, 39-43.

9    Decker, C.; Masson, F.; Keller, L. ACS meeting, 2003, pp 215.

10   Scherzer, T.; Decker, U. Radiation Physics and Chemistry 1999, 55, 615-19.

11   Scherzer, T.; Decker, U. Vibrational Spectroscopy 1999, 19, 385-98.

12   Scherzer, T.; Decker, U. Polymer 2000, 41, 7681-90.

13   Odian, G. Principles Of Polymerization; John Wiley&Sons, INC., 1991.

14   Kolczak, U.; Rist, G.; Dietliker, K.; Wirz, J. J. Am. Chem. Soc. 1996, 118, 6477-89.

15   Jockusch, S.; Koptyug, I. V.; McGarry, P. F.; Sluggett, G. W.; Turro, N. J.; Watkins, D. M. Journal of American Chemical Society 1997, 119, 11495-501.

16    Jockusch, S.; Turro, N. J. Journal of American Chemical Society 1998, 120, 11773-77.

17    Rutsch, W.; Dietliker, K.; Leppard, D.; Kohler, M.; Misev, L.; Kolczak, U.; Rist, G. Progress in Organic Coatings 1996, 27, 227-39.

18    Sluggett, G. W.; McGarry, P. F.; Koptyug, I. V.; Turro, N. J. J. Am. Chem. Soc. 1996, 118, 7367-72.

19    Anseth, K. S.; Bowman, C. N. Polymer Reaction Engineering 1993, 1, 499-520.

20    Lecamp, L.; Youssef, B.; Bunel, C.; Lebady, P. Polymer 1999, 40, 6313-20.

21    Lecamp, L.; Youssef, B.; Bunel, C.; Lebaudy, P. Nuclear Instruments and Methods in Physics Research B 1999, 151, 285-89.

22    Lovestead, T. M.; Berchtold, K. A.; Bowman, C. N. Macromolecules 2005, 38, 6374-81.

23    Berchtold, K. A.; Lovell, L. G.; Nie, J.; Hacioglu, B.; Bowman, C. N. Polymer 2001, 42, 4925-29.

24    Anseth, K. S.; Kline, L. M.; Walker, T. A.; Anderson, K. J.; Bowman, C. N. Macromolecules 1995, 28, 2491-99.

25    Anseth, K. S.; Wang, C. M.; Bowman, C. N. Macromolecules 1994, 27, 650-55.

26    Mateo, J. L.; Serrano, J.; Bosch, P. Macromolecules 1997, 30, 1285-88.

27    Kloosterboer, J. G.; Lijten, C. M.; Greidanus, F. J. A. Polymer reports 1986, 27, 268.

28    Kloosterboer, J. G.; Van de Hei, G. M. M.; Boots, H. M. J. Polymer communications 1984, 25, 354-7.

29    Kloosterboer, J. G.; Van de Hei, G. M. M.; Gossink, R. G.; Dortant, G. C. M. Polymer Communications 1984, 25, 322-5.

30    Zhu, S.; Tian, Y.; Hamielec, A.; Eaton, D. R. Polymer 1990, 31, 1726.

31    Zhu, S.; Tian, Y.; Hamielec, A. E. Macromolecules 1990, 23, 1144-50.

32    Berchtold, K. A.; Lovestead, T. M.; Bowman, C. N. Macromolecules 2002, 35, 7968-75.

33    Tryson, G. R.; Shutz, A. R. Journal of polymer science, Part B: Polymer Physics 1979, 17, 2059-75.

34    Kloosterboer, J. G.; Lijten, G. F. C. M. Polymer Communications 1987, 28, 2-5.

35    Decker, C.; Bendaikha, T. Makromol. Chem. 1988, 189, 2381-94.

36    Decker, C.; Bendaikha, T. Eur. Polym. J. 1984, 20, 753-58.

37    Young, J. S.; Bowman, C. N. Macromolecules 1999, 32, 6073-81.

38    Anseth, K. S.; Anderson, K. J.; Bowman, C. N. Macromol. Chem. Phys. 1996, 197, 833.

39    Kllosterboer, J. G. L., G. F. C. M. ACS Symposium Series 1988, 367, 409-26.

40    Sacco, A. B. In L's Institut National des Sciences Appliquees de Lyon; Ingenieur Maitre es Sciences: Materiaux de Lyon, 2004.

41    Cook, W. D. Polymer 1992, 33, 2152.

42    Truffier-boutry, D.; Gallez, X. A.; Demoustier-Champagne, S.; Devaux, J.; Mestdagh, M.; Champage, B.; Leloup, G. Journal of Polymer science: Part A: Polymer Chemistry 2003, 41, 1691-99.

43    Hara, S.; Yamamoto, K.; Shimada, S.; Nishi, H. Macromolecules 2003, 36, 5661-65.

44      Bunel, L. L. B. Y. a. C. Polymer 1997, 38, 6089-96.

45      Lovestead, T. M.; Burdick, J. A.; Anseth, K. S.; Bowman, C. N. Polymer 2005, 46, 6226-34.

46      Lecamp, L.; Youssef, B.; Bunel, C.; Lebaudy, P. Polymer 1999, 40, 1403-09.

47      Kondratiev, V. N. In Chain Reactions; C.F.H.Tipper, C. H. B. a., Ed.; American Elsevier: New York, 1969.

48      Berchtold, K. A.; Hacioglu, B.; Lovell, L. G.; Nie, J.; Bowman, C. N. Macromolecules 2001, 34, 5103-11.

49      Lecamp, L.; Youssef, B.; Bunel, C.; Lebaudy, P. Polymer 1997, 38, 6089-96.

**Appendix**

1. Calculation of changing initiator concentration versus exposure time and conversion for the cure under different conditions.

The changing concentration of initiator versus exposure time for thin samples are calculated using the Equations 4-82 and 4-83 with the method described in Chapter 3.

$$[PI]_{t2} = [PI]_{t1} - \frac{\phi' I_i (1 - 10^{-\varepsilon_i b [PI]_{t1}})}{b}(t2 - t1)$$ 

Equation 4-82

$t_1$ and $t_2$ are two exposure times, $[PI]_{t1}$ and $[PI]_{t2}$ are photo initiator concentrations at two different exposure time. $\phi'$ is the quantum yield of the consumption of photoinitiator, b is the thickness of the layers for the calculation. $I_i$ is the incident intensity, $\varepsilon_i$ is the absorption coefficient of initiator, Irgacure 819, 760 1 mol$^{-1}$ cm$^{-1}$. The unit of absorbed intensity here is in units of Einstein s$^{-1}$ l$^{-1}$.

$$I_t = I_i * 10^{-b(\varepsilon_i [PI]_t + \varepsilon_m [M])}$$ 

Equation 4-83

It is the transmitted intensity, $\varepsilon_m$ is the absorption coefficient of the monomer, 0.0755 1 mol$^{-1}$ cm$^{-1}$.

Using this method, the consumption of initiator concentration versus exposure time is shown in Figure 4.32 for the UV cure of CD540-0.2wt%Irgacure 819 at different incident light intensities.
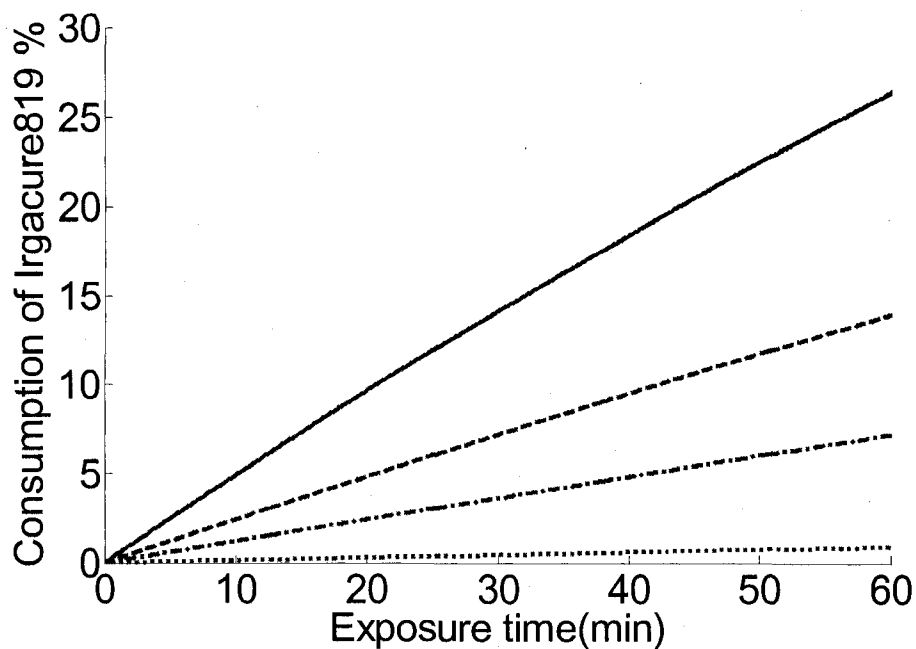
Figure 4.32 The degradation of initiator, Irgacure 819, at different incident intensities, $I_i$.

(——) $I_i$=32.5 $\mu$w/cm$^2$, (— — —) $I_i$=16 $\mu$w/cm$^2$, ( – · – ) $I_i$=8 $\mu$w/cm$^2$, (······)$I_i$=1 $\mu$w/cm$^2$.

Figure 4.32 shows that the initiator is consumed faster at higher intensities. Comparing Figure 4.3 and 4.32, the consumption of Irgacure 819 at different conversion of C=C are listed in Table 4.6 for the UV cure of CD540-0.2wt%Irgacure 819 at different incident light intensities.

Table 4.6 Consumption of Irgacure 819, at different conversion of C=C ($\alpha$) under different UV radiation intensities.

| Incident Intensity | Consumption of initiator, Irgacure 819 | | |
|---|---|---|---|
| ($\mu$w/cm$^2$) | $\alpha$ =0, (the end of delay time) | $\alpha$ =50% | $\alpha$ =60% |
| 32.5 | 0.4% | 1.2% | 3.0% |
| 16 | 0.4% | 1.0% | 2.2% |
| 8 | 0.4% | 1.0% | 1.9% |
| 1 | 0.5% | 0.8% | 1.5% |

It is found in Table 4.6 that the changing concentration of initiator in the system is less than 1.2% when the conversion of C=C is less than 50% which is the conversion range that the kinetics of the cure will be studied quantitatively in this dissertation. In addition, the amount of initiator consumed at different intensities is similar at the same conversion of C=C even though the consumption rate increases significantly with light intensity as shown in Figure 4.32. It is reasonable to regard [PI] as a constant for the study here.

Next, the consumption of initiator concentration versus exposure time is calculated for the UV cure of CD540-Irgacure 819(0.05, 0.1, and 0.2wt%) at 32.5 $\mu$w/cm$^2$ incident light intensity. The results are shown in Figure 4.33.
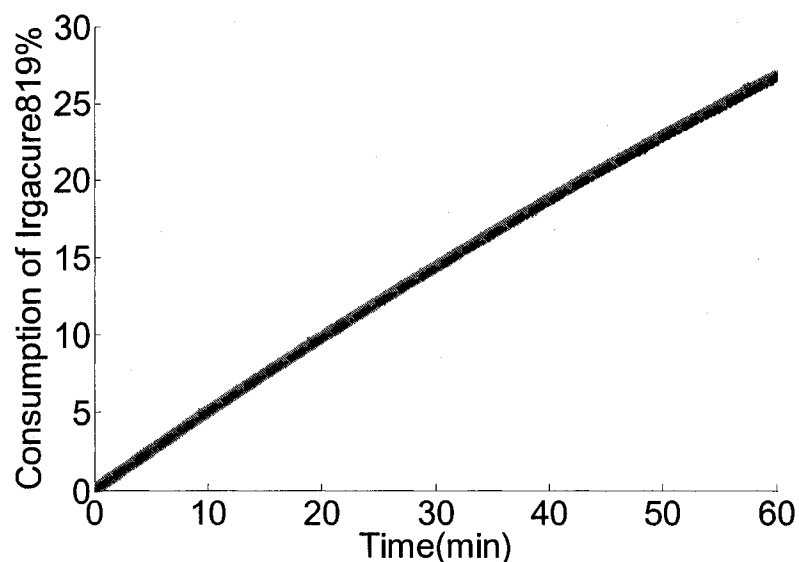
Figure 4.33 The degradation of initiator, Irgacure 819, at intensity of 32.5 $\mu w/cm^2$.

Concentration of Irgacure 819: (———) 0.05wt%, (— — —) 0.1wt%, (······) 0.2wt%.

Figure 4.33 shows that the percent consumption of initiator is almost the same for

the UV cure of the system, CD540-Irgacure 819, with varying initiator concentrations.

Comparing Figure 4.14 and 4.33, the consumption of Irgacure 819 at different conversion

of C=C are listed in Table 4.7 for the UV cure of CD540-0.2wt%Irgacure 819 at different

incident light intensities.

Table 4.7 Consumption of Irgacure 819, at different conversion of C=C ($\alpha$) for the system with different initiator concentration.

| The concentration of Irgacure 819 wt% | Consumption of initiator, Irgacure 819 | | | | | | |
|:---:|:---:|:---:|:---:|:---:|:---:|:---:|:---:|
| | $\alpha =0$ | $\alpha =10$ % | $\alpha =20$ % | $\alpha =30$ % | $\alpha =40$ % | $\alpha =50$ % | $\alpha =60$ % |
| 0.2 | 0.4% | 0.6% | 0.6% | 0.7% | 0.9% | 1.2% | 3.0% |
| 0.1 | 0.9% | 1.0% | 1.2% | 1.3% | 1.5% | 2.2% | 4.6% |
| 0.05 | 1.8% | 2.1% | 2.3% | 2.5% | 2.9% | 4.1% | 9.8% |

It is found in Table 4.7 that the fraction of the initiator that is consumed is considerably higher at the same conversion of C=C for the system with less initial initiator concentration. Consumption rate of initiator in the system increases when the initial concentration of initiator is less than 1.2% when the conversion of C=C is less than 50% which is the conversion range that the kinetics of the cure will be studied quantitatively in this dissertation. In addition, the amount of initiator consumed at different intensities is similar for the same conversion of C=C even though the consumption rate increases significantly with light intensity as shown in Figure 4.25. It is reasonable to regard [PI] as a constant for the study here.

2. Calculation of kinetic chain length.

The kinetic chain length can be calculated using the information in Table 4.6. It is known that the original concentration of C=C is 3.92 mol/l and the original concentration of initiator is 0.0107 mol/l. ( the data used for calculation: molecular weight of CD540 is

572, density is $1.12 \text{g/cm}^3$, the molecular weight of Irgacure 819 is 418.5) So for the system of CD540-Irgacure 819, the concentration of Irgacure 819 can be calculated using Equation 4-84

$$[PI](mol/l) = \frac{[PI]wt\%/418.5}{100/1.12} * 1000 \qquad \text{Equation 4-84}$$

For the system of CD540-0.2wt%Irgacure 819, the original concentration of Irgacure 819 is 0.0107 mol/l.

The kinetic chain length is calculated using the values at 50% conversion. This is after 50% conversion, reaction rate decreases substantially, which is possible due to the formation of the glassy state. Table 4.5 shows that at 50% conversion of C=C, 1.2% of initiator is consumed for the cure at the intensity of 32.5 $\mu\text{w/cm}^2$. Therefore, the kinetic chain length can be calculated using Equation 4-89.

$$N_k = \frac{[M]*0.5}{[PI]*4*0.012} = 3811 \qquad \text{Equation 4-85}$$

Factors 0.5 and 0.012 are the consumption of CD540 and Irgacure 819 when the conversion of C=C is 50%. Factor 4 is for the case that 4 radicals are formed per initiator consumed.

It can be figured out from Table 4.6 that increasing incident light intensity can increase the kinetic chain length. Table 4.7 shows that changing the initiator concentration in the system does not considerably affect the kinetic chain length.

3. Matlab program for calculating the conversion of C=C versus time for the UV cure of systems under varying radiation intensities.

```
clear;

IN=6;

I=zeros(1,IN);

I(1)=32.5;

p=10000;                        %total number of points for each curve

dt=0.005;        %step size (minutes)

for J=1:IN

    C=zeros(1,p);   %Conversion

    T=zeros(1,p);        %time of polymerization

    TR=zeros(1,p);  %Real exposure time=T+Td

    MC=zeros(1,p);  %MC is the calculated concentration of

            C=C

    S=zeros(1,p);   %-dlnM/dt for different intensities

    Td=31.76/I(J);  %Calculation of delay time

    MC(1)=3.92;     %Monomer concentration(mol/l)

    C(1)=0;      %Conversion is 0 at the beginning

    T(1)=0;

    A=(I(J)/I(1))^0.7;

    for g=1:p-1

        S(g)= A*1*((1/(1+exp(-30*(C(g)-0.05))))-(1/(1+exp(-13.7*(C(g)-0.36)))));

        ST(g)=S(g)*dt;

        MC(g+1)=exp(log(MC(g))-ST(g));

        T(g+1)=T(g)+dt;
```

```
C(g+1)=1-MC(g+1)/MC(1);

end

TR=T+Td;  %TR is the exposure time after adjusted by

        Inhibition time

plot(TR,C,'k-')

hold on

I(J+1)=I(J)/2;

End

xlabel('Time(min)')

ylabel('Conversion of C=C (mol/l)')

title('Predict the cure kinetics at the bottom of the mode(CD540 with 0.2wt%IC819,

I=32.5, 16, 8, 4, 2, 1 µw/cm2, T=0.05mm)')
```

Note: the step size of time used for the calculation here is dt=0.005 minutes. Different step sizes were used for the calculation as shown in Figure 4.34. The calculation is more exact with a smaller step size of time. But it needs longer time for the calculation. We found the calculation curve using 0.05 minutes step size almost overlaps the curve calculated using 0.005 minutes. This means when the step size is smaller than 0.05 minutes, the error of calculation is trivial. Therefore a step size of 0.005 minutes is used in the calculation in this chapter for thin samples.
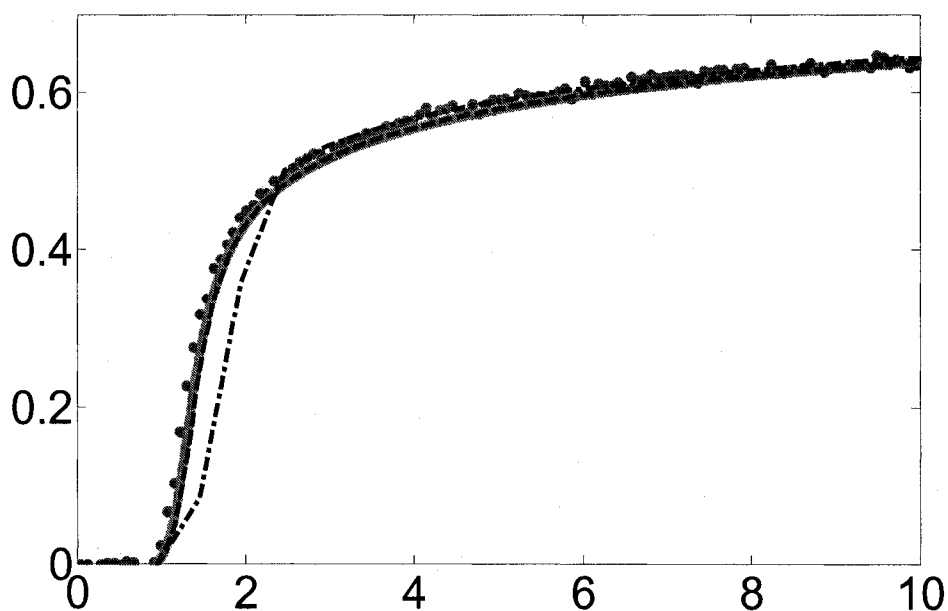
Figure 4.34 the conversion of C=C versus time calculated using different time step sizes. CD540-0.2wt%Irgacure 819, Ii=32.5 $\mu$w/cm$^2$, thickness=0.05mm. ( • ) Experimental data. Calculated curves: (—) step size=0.005 minutes (— — —), step size=0.05 minutes, (– • – • –) step size=0.5 minutes

4. Matlab program for calculating the conversion of C=C versus time for the UV cure of systems under varying radiation intensities.

CI=3;

PI=zeros(1,CI);          %The concentration of initiator

PI(1)=0.2;

p=10000;                 %Total number of points for each curve

dt=0.005;                %Step size of time for integration

for J=1:CI

```
C=zeros(1,p);          %Conversion

T=zeros(1,p);          %Cure time

TR=zeros(1,p);         %Exposure time(minute)

MC=zeros(1,p);         %Calculated concentration of C=C

S=zeros(1,p);          %-d(ln[M(t)]) / dt

Td=0.1745/PI(J);       %Calculation of delay time

MC(1)=3.92;            %The original concentration of C=C

C(1)=0;                %Conversion is 0 at the beginning

T(1)=0;

A=(PI(J)/PI(1))^0.75;  %The effect of concentration of initiator on the cure kinetics
%Integration calculation process from step 1 to step p

for g=1:p-1

    S(g)= A*1*((1/(1+exp(-30*(C(g)-0.05))))-(1/(1+exp(-13.7*(C(g)-0.36)))));

    ST(g)=S(g)*dt;

    MC(g+1)=exp(log(MC(g))-ST(g));

    T(g+1)=T(g)+dt;

    C(g+1)=1-MC(g+1)/MC(1);

end

TR=T+Td;               %TR is the real time after adjusted by inhibition

hold on

plot(TR,C,'k-')

PI(J+1)=PI(J)/2;       %Another intensity to calculate

end
```

5. Matlab program for calculating the conversion of C=C versus time for the UV cure of systems at varying cure temperatures, intensities and temperatures.

```
clear all;

%Initial conditions:

II=32.5;                    %Incident intensity value at the surface(uw/cm2)

PI=0.05;                    %Initiator concentration in the system (wt%)

IC=PI*0.011087216/0.4;      %Initiator concentration in the system (mol/l)

TEMP=273+55;

%Temperature effect

f=1/TEMP;

f1=0.0007*exp(2164*f);

f2=0.0003*exp(3394*f);

f3=-219*f+ 1.1;

%Time allocation, whole process is divided into nt time points

nt=50000;                   %Number of time point(minutes)

st=0.001;                   %step size of time

t=zeros(1,nt+1);

for k1=1:nt+1

    t(1,k1)=st*(k1-1);      %Value of time points

end


%Calculation of inhibition period considering the effect of temperatures and Initiator concentrations
```

```
td=(0.22*exp(791/TEMP))*(0.05/PI)*(32.5/II);

N=round(td/st);

C=zeros(1,nt);              %Conversion

MC=zeros(1,nt);             %calculated concentration of C=C(mol/l)

S=zeros(1,nt);             %-dlnM/dt

dC=zeros(1,nt);

I1=32.5;                   %Incident intensity of standard curve

MC(1,N)=3.92;              %Initial concentration of C=C(mol/l)

for g=N:nt

  A=((II/I1)^0.7)*((PI/0.2)^0.75);

  S(1,g)= A*1*((1/(f1+exp(-f2*(C(1,g)-0.05))))-(1/(f1+exp(-13.7*(C(1,g)-f3)))));

  dC(1,g)=S(1,g)*st;

  MC(1,g+1)=exp(log(MC(1,g))-dC(1,g));

  C(1,g+1)=1-MC(1,g+1)/MC(1,N(1,1));

end

plot(t(1,1:nt),C(1,1:nt),'b-')

xlabel('Time(min)')

ylabel('Conversion of C=C (mol/l)')

title('Modulate the cure kinetics at different temperature(SR540 with 0.2wt%IC819,

T=0.05mm, temperature=25,35,55C)')
```

# Chapter 5.  Study of UV cure kinetics of thin film samples by FDEMS

## 5.1     Introduction

The ability to monitor the cure of a film is particularly important for the coatings industry. Most measurements of a film as it cures utilize conventional laboratory techniques such as modulated differential scanning calorimeter (DSC), rheometer, spectroscopic techniques involving infrared, visible or UV absorption and simple physical tests, such as "dry to touch" and "dry to hard". The problem with DSC and Rheometry measurements is that it is difficult to monitor the cure process as a thin film with one side of the film in contact with the surface to be coated and one side exposed to the environment under the application conditions. Spectroscopic techniques overcome this problem. However, in general they lack sensitivity during the achievement of full cure. Monitoring the final build up to complete cure is particularly important when monitoring and verifying durability.  Physical criteria, such as "dry to hard" are subject to considerable variation from one person to another.

On the other hand, frequency dependent dielectric measurements using in situ micro sensors, FDEMS, is a particularly useful technique for monitoring the changing state of a coating during synthesis, cure and aging. Measurements can be made in the laboratory to monitor the polymerization process in a flask, to monitor cure as a coating in an oven or under a UV lamp, and to monitor the coating's durability and aging in a weather controlled environmental chamber or other degrading environment. Thus the

FDEMS micro sensor technique ought to be more widely used, particularly in monitoring cure and degradation of a coating. An important reason the planar micro sensor should be used more extensively is that it is ideally suited to monitoring coatings where only one side of a thin polymer film is exposed to the environment, a condition which is difficult to duplicate in most other measurements. Besides, it has high sensitivity and accuracy particularly at high cure extent. In addition, FDEMS can be used to measure the cure at particular depth and under real-application conditions.

A review of the FDEMS technique has been recently published.[1] Other articles describe its application to a variety of monitoring needs in the coating industry.[2-11] This chapter reports on the use of FDEMS sensors to monitor the cure of a methacrylic resin by UV radiation and comparing the dielectric loss data with the conversion data measured by transmitted real time near FTIR under the same conditions firstly. Secondly, a correlation curve of dielectric data, $\varepsilon"\omega$ , versus conversion is derived. Thirdly, the relation between the dielectric data (ion mobility) and the propagation and termination rate constant (diffusion ability of monomer and free radicals) is discussed. Fourthly, the temperature effect on the correlation curves is studied. Last, the changing viscosity and the value of $\varepsilon"\omega$ versus temperature are measured. This gives the connection between the temperature, the viscosity, and the ion mobility of the sample and it helps to understand the temperature effect on the correlation curves.

## 5.2    Experiment

### 5.2.1    Materials

The materials used in this Chapter are almost the same as what is used in Chapter 4. The only difference is the oligomer, CD540 used in this Chapter was bought from Akzo-Nobel. But the oligomer used in Chapter 3, 4, and 6 are obtained from INSA, which were bought from Sartomer. Even though the oligomer from two places was reported to have the same structure, they are not exactly the same due to different manufacture and storage process. This will be discussed in the experimental part.

## 5.2.2  Instrument

Radiation Source. A 200 Watt Hg arc lamp equipped with a water filter to remove the IR radiation and a 356-365 band pass filter. A fiber optic cable guides the light to the sample chamber of FTIR equipment and to the mold with the dielectric sensor. The sample mold here is similar to what was used in Chapter 4 for NIR experiments. The difference is a Kapton sensor was glued on the bottom of the mold as shown in Figure 5.1b. In addition, two layers of Kapton tape are used here as the spacer instead of one layer to compensate for the thickness of the Kapton sensor. The surface diagram of a Kapton dielectric sensor is shown in Figure 5.1a. Figure 5.1b is the cross section diagram of a glass mold with a sensor and sample in it.



a                                                    b
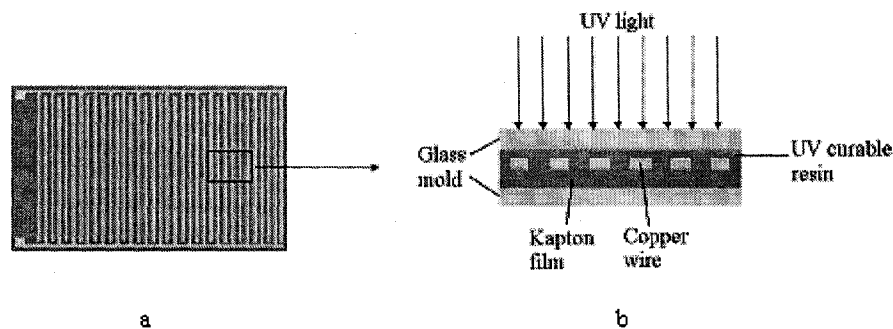
Figure 5.1 Kapton sensor (a) and the cross section diagram of a glass mold with sample and sensor in it.

Dielectric impedance measurements. A HP 4192A LF impedance analyzer is used to monitor the UV cure of CD540. A HP 4263A LCR meter is used to monitor the cure of CD540 with Irgacure 819 resin using UV radiation. The HP impedance analyzer and LCR meter were connected to a planar interdigitated Kapton dielectric sensor with an air replaceable capacitance, $C_o$. The sensor is used to monitor the changes in conductance and thereby the dielectric permittivity loss, $\varepsilon''$, of the sample during the polymerization process over a range of frequencies from 0.1 kHz to 100 kHz. The dielectric loss, $\varepsilon''$, is calculated for each frequency, f, where $\varepsilon'' = G/\omega C_o$ and $\omega = 2\pi f$.

The sensor is placed on the bottom of a mold as shown in Figure 5.1b. The mold was filled with liquid placed on the top of the sensor. Note: the Copper lines work as parallel capacitors that mainly measure the conductance of UV curable resin **between them**. Even if the light reflected from the surface of copper lines does affect the cure of sample on the surface of those wires it does **not** affect the cure of the sample between them. So, we believe the signal measured was not affected significantly by the reflection of the copper.

The thickness of the sample was determined by deducting the thickness of the Kapton sensor (0.05mm) from the spacer of the mold, which is a double layer of Kapton tape( thickness=0.05*2 mm), Therefore the thickness of the sample was 0.05 mm, which is the same as the sample thickness for the Near FTIR experiments. At a thickness of 0.05 mm, the light absorption of thin samples is less than 4%. Therefore it is reasonable to regard it as a system with a homogeneous light intensity and cure kinetics.

Real-time near FTIR Measurement here is exactly the same as described in Chapter 4.

An AR1000 rheometer was used to measure the viscosity of systems.

## 5.3    Results and discussion

### 5.3.1    Measurement of the UV cure of thin samples by FDEMS and real time near FTIR under the same conditions

Dielectric measurements were used to monitor the UV cure at room temperature. Using the Debye equation for a single dipolar relaxation time the frequency dependence of the loss parameter $\varepsilon''$ can be expressed as

$$\omega\varepsilon''(\omega) = \frac{\sigma}{8.85*10^{-14}} + (\varepsilon_0 - \varepsilon_\infty)\frac{\omega^2\tau}{1+(\omega\tau)^2}$$    **Equation 5-1**

$\sigma$ is the specific conductivity in units of $ohm^{-1}cm^{-1}$ and the permittivity of free space is $8.85*10^{-14}C^2J^{-1}cm^{-1}$.

The dielectric loss factor $\varepsilon''$ is a summation of two factors. The first factor is contributed by the ionic mobility and the second factor is contributed by the rotational mobility of dipoles. When the frequency is low and at low cure extent, the contribution of the dipolar rotational mobility is very small. Therefore at low frequencies, Equation 5-1 can be written as equation 5-2 where

$$\omega\varepsilon''(\omega) = \frac{\sigma}{8.85*10^{-14}}$$    Equation 5-2

A plot of $log(\omega\varepsilon'')$ versus time during the polymerization shows the ionic mobility contribution to the dielectric loss at a low frequency, 0.1kHz.

Our system composed of CD540-0.2wt% Irgacure 819 was cured under the UV wavelength of 365nm and the intensity of 32.5 $\mu w/cm^2$. The curing processes were

monitored separately by FDEMS and FTIR under the same conditions. The results are shown below.
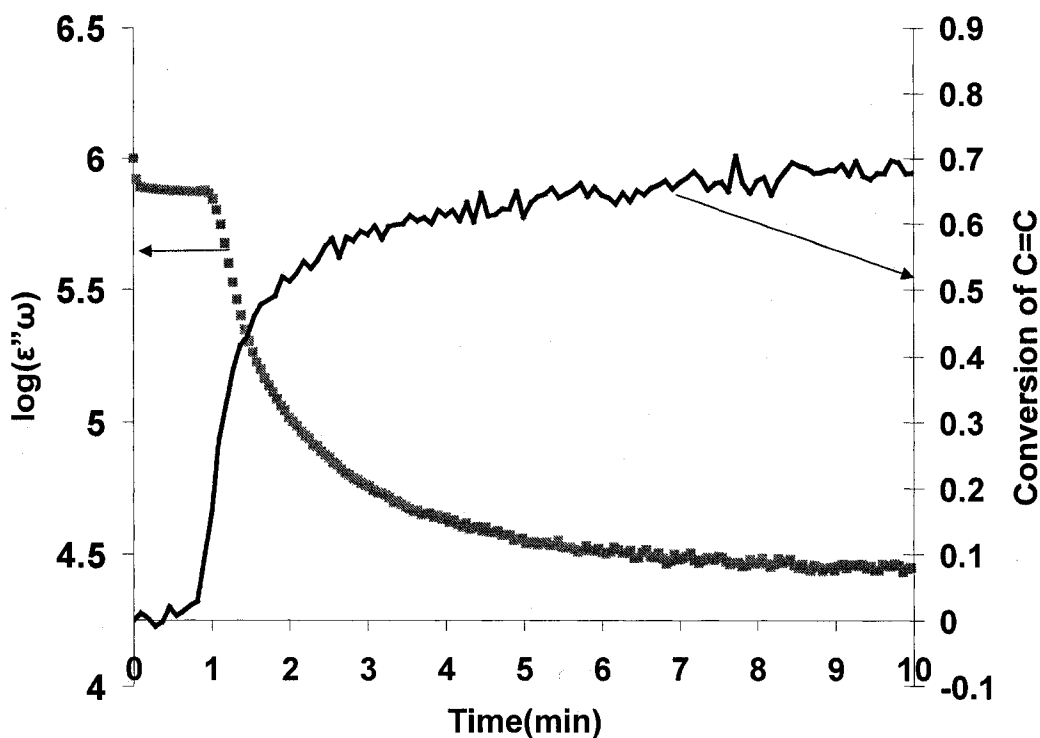


Figure 5.2 Monitoring UV cure of CD540-0.2wt%IC819 under 32.5 $\mu w/cm^2$ radiation intensities by FDEMS and FTIR.

Figure 5.2 shows the value of $\log(\varepsilon"\omega)$ decreases with exposure time while conversion of carbon double bonds increases with time. The FDEMS curve can be divided roughly into three periods. One is at the very beginning of the exposure, where almost no reaction was observed by FTIR measurement. But the value of $\log(\varepsilon"\omega)$ dropped a little suddenly as soon as the light was turned on. This may be due to reaction of C=C with some initiating radicals, which were not scavenged by oxygen. The amount of C=C that reacted is so little that it is hard to be detected by FTIR. However,

since the viscosity of pure CD540 is very high, even a little polymerization can result in a change in viscosity. After this sudden small change, there is no significant change in the FDEMS signal. The FDEMS output during this period is similar to the FTIR output and displays no change. The period up to 0.8 minutes is usually regarded as the inhibition period due to the oxygen dissolved in the system.[12,13]

The next period monitors the process of polymerization, which can be observed easily both by the increase of the conversion of C=C and the decrease of the ion mobility (log ($\omega\varepsilon$")). The polymerization almost stops near a conversion of 70% because the system approaches its glass transition point. Comparing Figure 5.2 and Figure 4.4 in Chapter 4, the conversion of C=C here at 10 minute exposure time is up to 0.05 higher than the value in Figure 4.4. The reason for the difference is that they are different samples as has been explained in section 5.2.1. The CD540 used in this Chapter and in Chapter 4 came from different sources even though their names and structure are reported to be the same. The different source and/or storage process may result in a small difference in structure. Since the sample here has a higher conversion, this suggests the CD540 from INSA (Sartomer, 2003) may have polymerized a little bit before the cure kinetics. However these differences in structure do not significantly affect the correlation result. This will be shown later.

From Figure 5.2, it is also observed that the dielectric measurement can be more sensitive than FTIR measurement as the y axis of the dielectric data is expressed using a log scale. This point will be discussed in section 5.3.2.

Similar experiments were done for the system of CD540 with 0.1 and 0.05wt%

under the same intensity of 32.5 $\mu$w/cm$^2$. The data are shown separately in Figures 5.3

and 5.4.
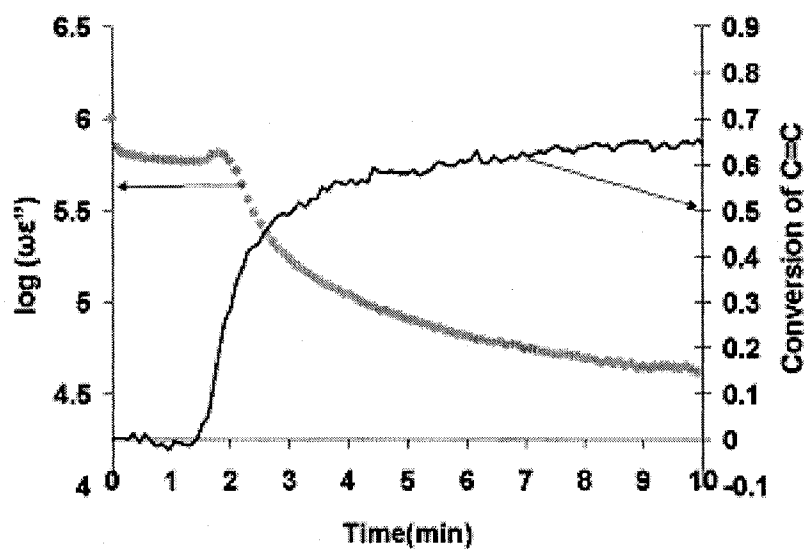


Figure 5.3 Monitoring UV cure of CD540-0.1wt%IC819 under 32.5 $\mu$w/cm$^2$ radiation

intensity by FDEMS and FTIR.
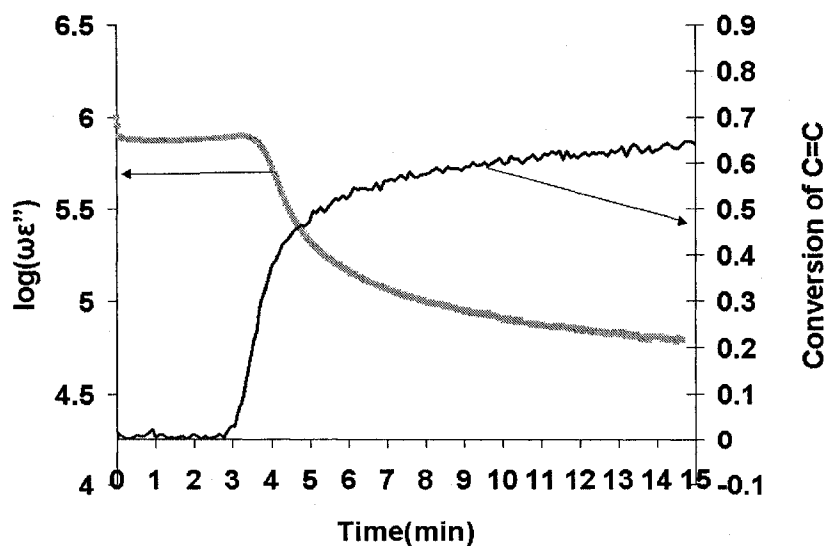


Figure 5.4 Monitoring UV cure of CD540-0.05wt%IC819 under 32.5 $\mu$w/cm$^2$ radiation

intensity by FDEMS and FTIR.

Figures 5.3 and 5.4 are similar to Figure 5.2 except the inhibition period is longer

and the polymerization rate is smaller for the system with less initiator concentration.

### 5.3.2 Correlation of the data of C=C conversion to log ($\omega\varepsilon$") for different initiator concentrations

The value of log ($\omega\varepsilon$") can be correlated with the C=C cure extent using the data

at the same point in time, where the degrees of conversion should be the same since the

FDEMS and FTIR experiments were done under the same conditions. The correlation is

displayed in Figure 5.5.
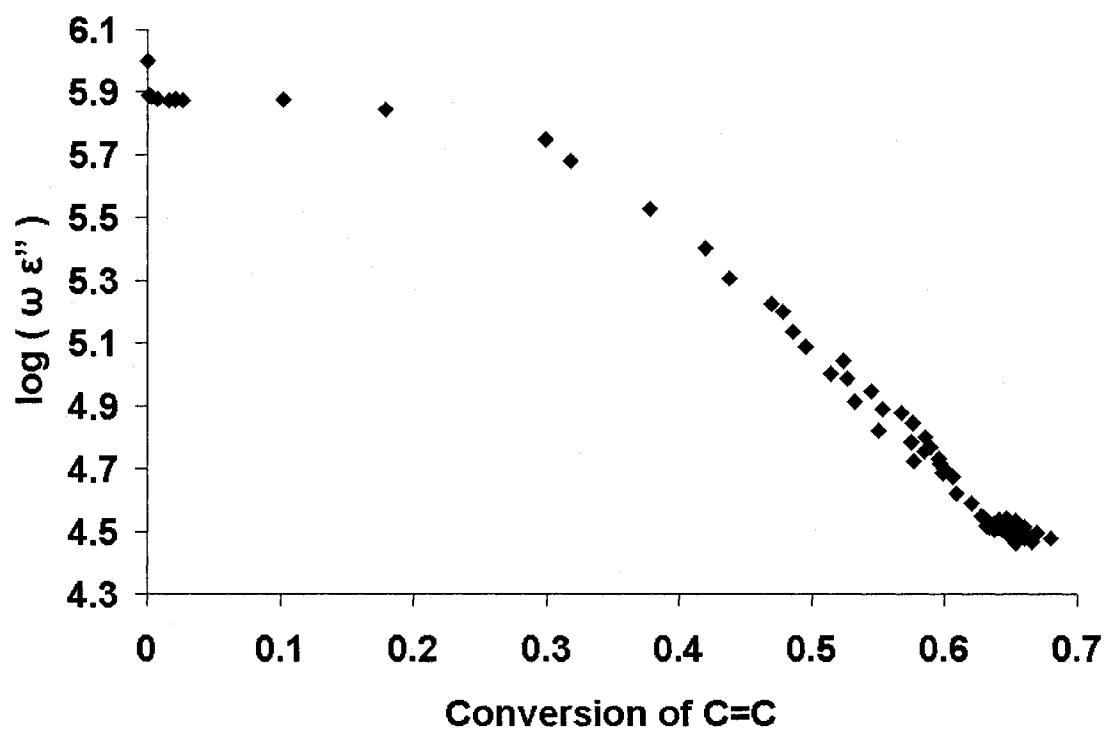


Figure 5.5 The correlation of FDEMS data (log($\omega\varepsilon$") ) and FTIR data (Conversion of

C=C). System composition: CD540-0.2wt%IC819, intensity: 32.5 $\mu w/cm^2$.

The value of $\log(\varepsilon''\omega)$ decreases with conversion of C=C, the extent of cure. The reason that the ion mobility decreases during the film formation process is due to the viscosity increase with the extent of cure. It is reasonable to assume that at the same C=C conversion, the viscosity of the system is the same regardless of the change in conditions described in Figures 5.2, 5.3, and 5.4 since the composition of the system changes a negligible amount when varying the amount of initiator. Therefore, these correlation curves should overlap. The correlation curves of Figures 5.2, 5.3, and 5.4 are shown in Figure 5.6.
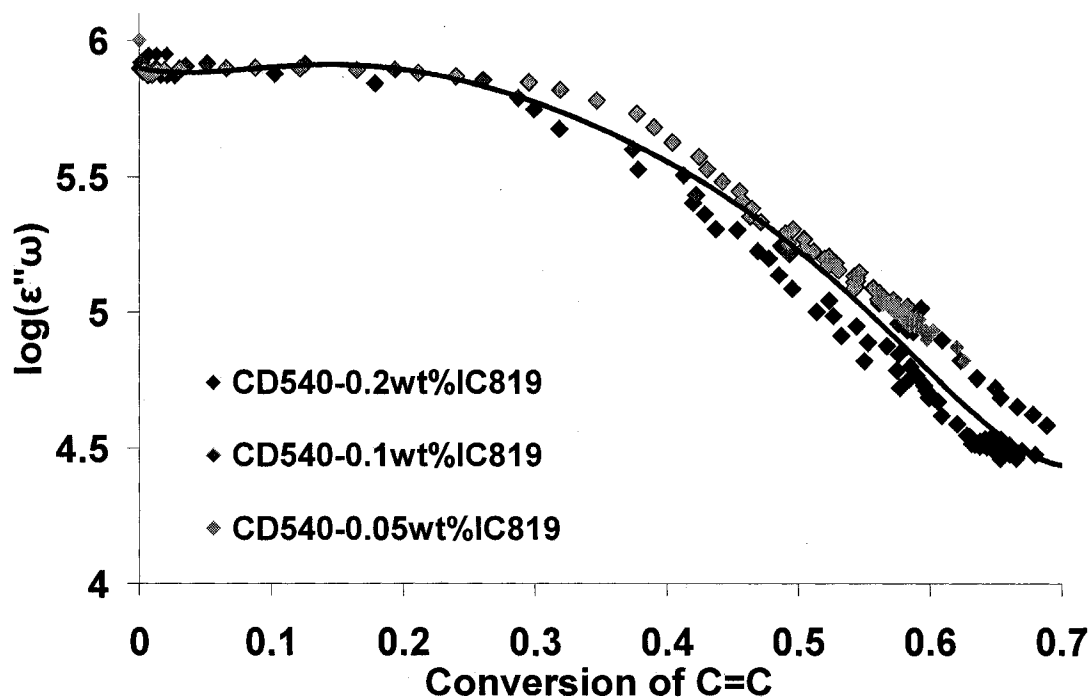


Figure 5.6 The correlation curves for different [PI]=0.05~0.2%, Ii=32.5 $\mu$w/cm$^2$.

The points overlapped and they can be fit to the polynomial equation,

$$y=-12.658x^6-31.852x^5+81.614x^4-59.146x^3+12.868x^2-0.8397x+5.9$$

Here y represents $\log(\varepsilon''\omega)$, x represents the conversion of C=C. The coefficients in the equation do not have any physical meaning, but the equation represents well the relationship of FDEMS data and conversion of C=C during the cure extent from the very beginning, 1% to 70% conversion. This correlation curve is for the sample bought from Akzo-Nobel.

But how much is the difference compared with the correlation curve of the sample from INSA (Sartomer)? In order to answer this question, two other experiments were done for the cure of CD540 from INSA (Sartomer). The results are shown in Figures 5.7 and 5.8.
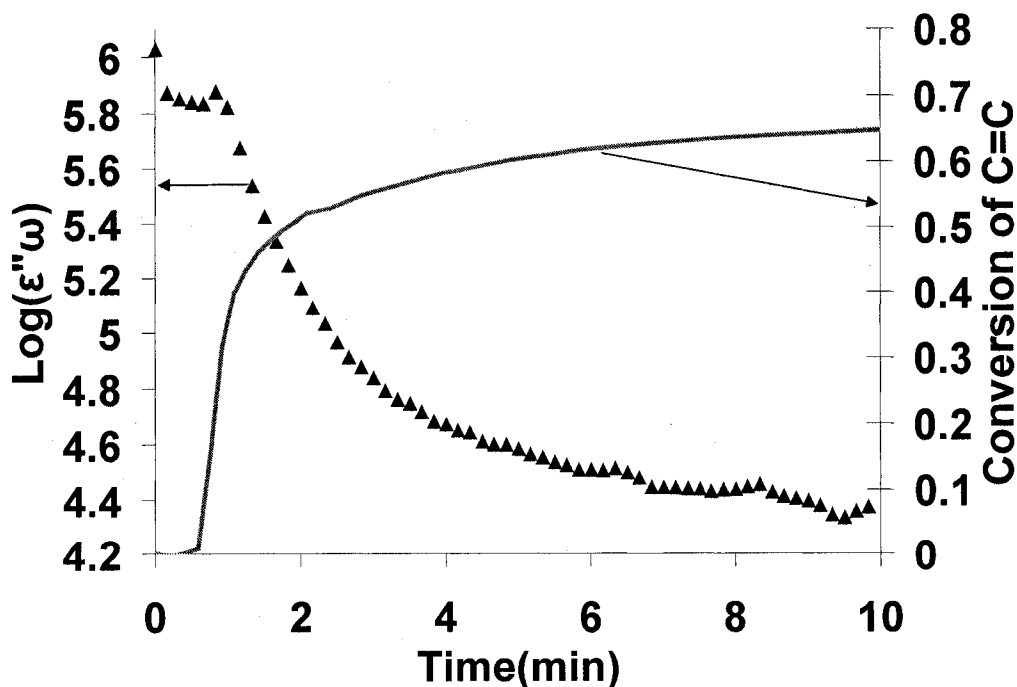


Figure 5.7 UV cure of CD540 (INSA)-0.2%IC819, I=65 $\mu w/cm^2$, T=0.05mm, f=0.1kHz.
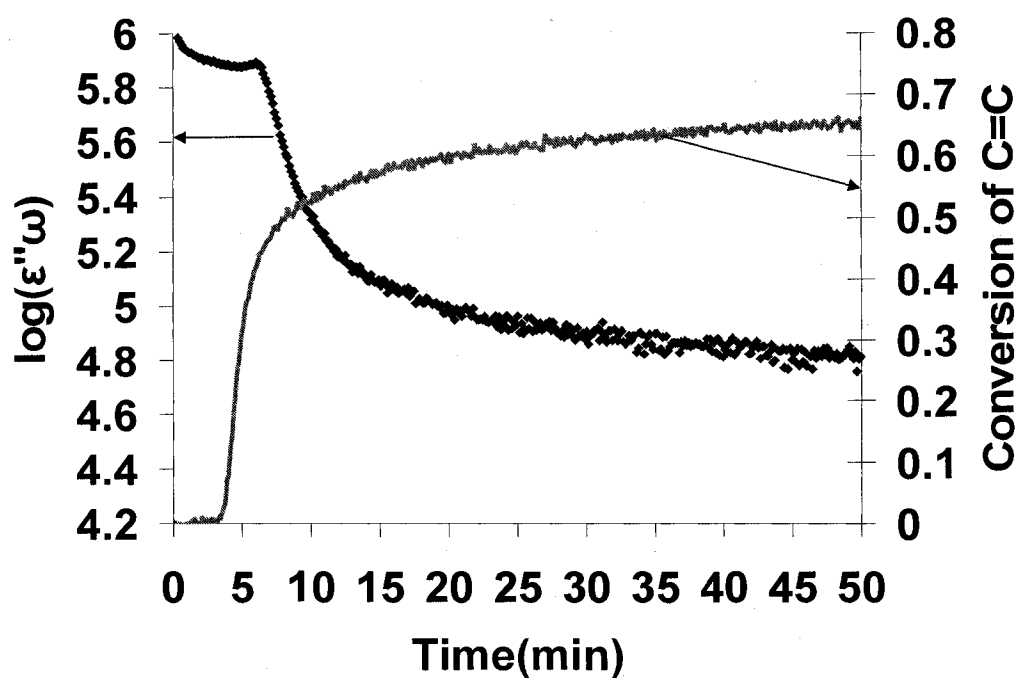
Figure 5.8 UV cure of CD540 (INSA)-0.05wt%IC819, I=32.5 μw/cm², T=0.05mm, f=0.1kHz.

Correlating the FDEMS and C=C conversion curves in Figures 5.7 and 5.8 and comparing the outcome to Figure 5.6 is displayed in Figure 5.9. The correlation curves of CD540 based on the two different samples are shown as two solid lines in Figure 5.9 as,
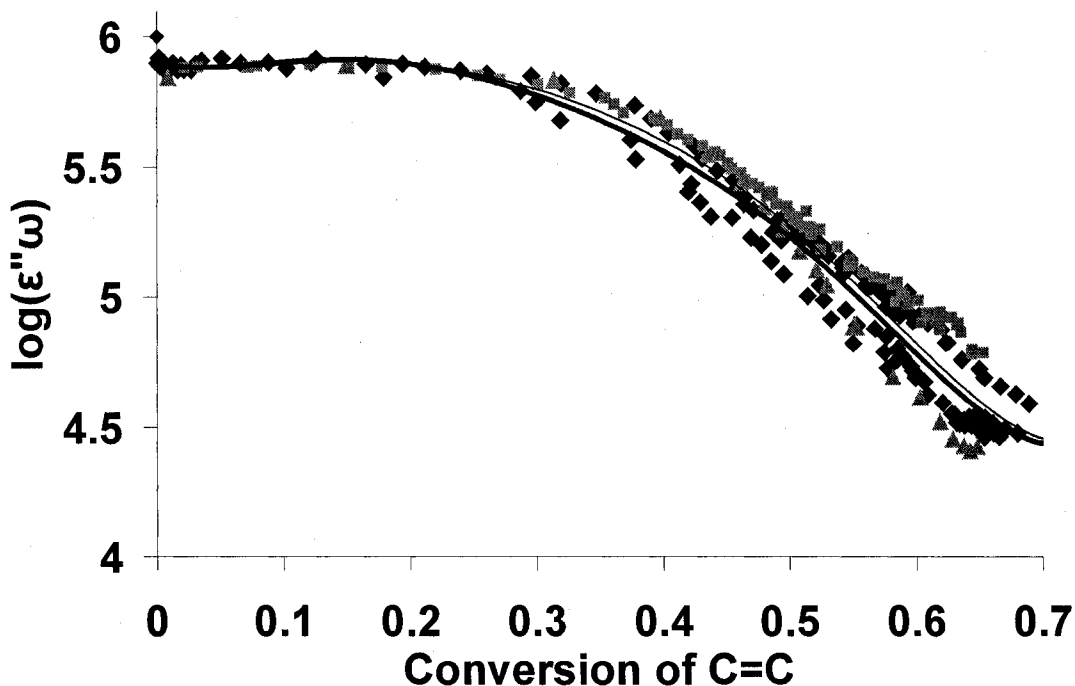
Figure 5.9 The correlation curves under different conditions. T=0.05mm, f=0.1kHz (♦)

CD540 (Akzo-Nobel) with Irgacure 819, [PI]=0.05~0.2%, $I_i$=32.5 μw/cm$^2$; (▲) CD540

(INSA)-0.2%IC819, I=65 μw/cm$^2$; (■) CD540 (INSA)-0.05wt%IC819, I=32.5 μw/cm$^2$

CD540 (INSA)-0.05wt%IC819, I=32.5 μw/cm$^2$; (———) average of correlation curves of

UV cure of CD540 only from Akzo-Nobel; (——) average of correlation curves of UV

cure of CD540 both from Akzo-Nobel and from INSA

Figure 5.9 shows that two correlation curves of the cure of CD540 (INSA) under

different conditions overlap with all data points. This second new average correlation

curve which considers the correlation of samples from INSA has a little difference from

the curve based on the sample from Akzo-Nobel. The difference is less than the error of

the experimental data, so it is not considered in the following calculations.

### 5.3.3 Relation between the change of ωε" and the change of $k_p$ and $k_t$ versus conversion

Comparing Figure 5.6 (or 5.9) with Figure 4.24 in Chapter 4, it was found that they share some common characteristics. In order to study this, two figures are combined to make a new figure below.
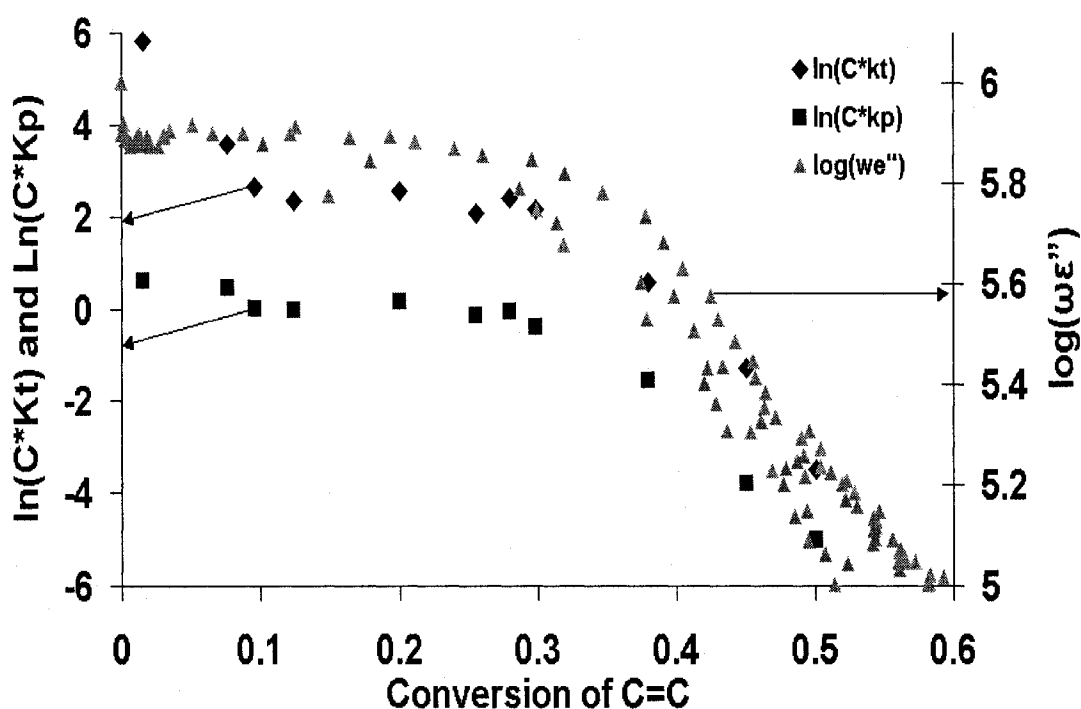


Figure 5.10 Comparison of the correlation curves with the $C^*k_p$ and $C^*k_t$ during the cure of the film. (C is regarded as a constant as described in Chapter 4.)

From Figure 5.10, it is found that the change of log(ωε") that represents the ion mobility at low frequency (0.1kHz) decreases slowly at the very beginning of the reaction until 30% conversion. After 30% conversion, it drops rapidly with the conversion. Similar phenomena are found for the change of $\ln(C^*k_p)$ and $\ln(C^*k_t)$ versus conversion

during the period of 30% to 50% conversion of C=C. The rapid drop of $\ln(C^*k_p)$ and $\ln(C^*k_t)$ is believed due to a buildup in viscosity and the approach to vitrification of the sample as discussed in Chaper 4. The diffusion ability of free radicals and monomer decreases significantly due to the approach to the glassy state. Thus, the rate of diffusion-controlled propagation and termination drops quickly during this period. Similarly, the ion mobility decreases significantly too upon approach to formation of glassy state of the sample. The rapid decrease of both the ion mobility and the diffusion ability of free radicals and monomers in the system strengthen the conclusion that the sample approaches the glassy state during the period of 30% to 50% conversion. In addition, the dielectric correlation curve offers insight into the role of radical and monomer diffusion during the C=C conversion.

### 5.3.4 Temperature effect on the correlation curves of dielectric data and the conversion of C=C

The polymerization was also done at different temperatures to develop the correlation as described above. The outcome is shown in Figures 5.11 and 5.12 separately for two systems that have different initiator concentrations.
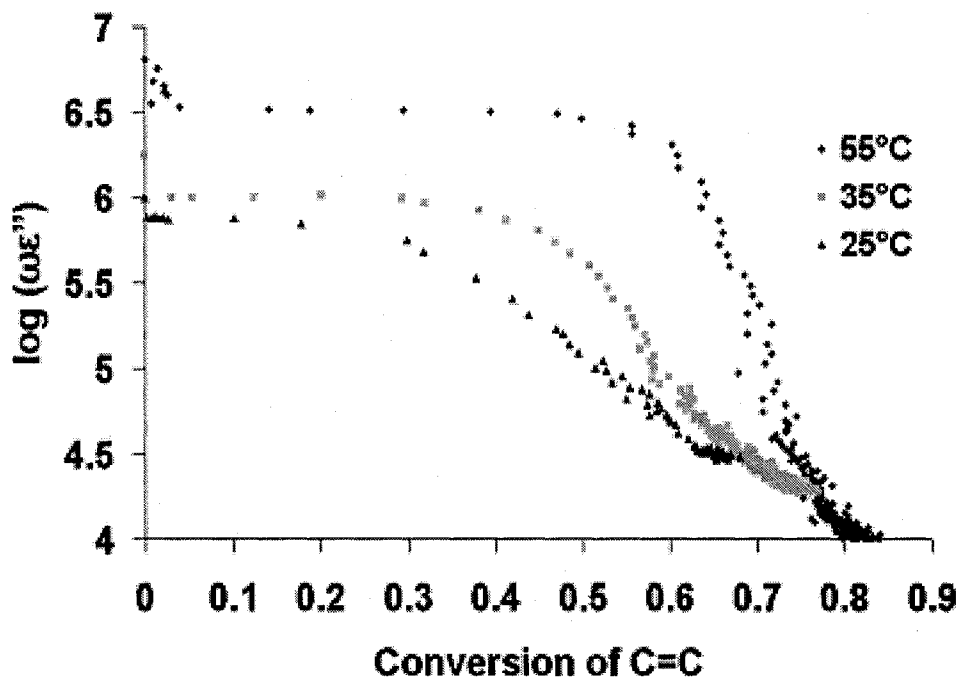
Figure 5.11 Correlation curves at different temperature. CD540 + 0.2% IC819, Ii=32.5 uw/cm².
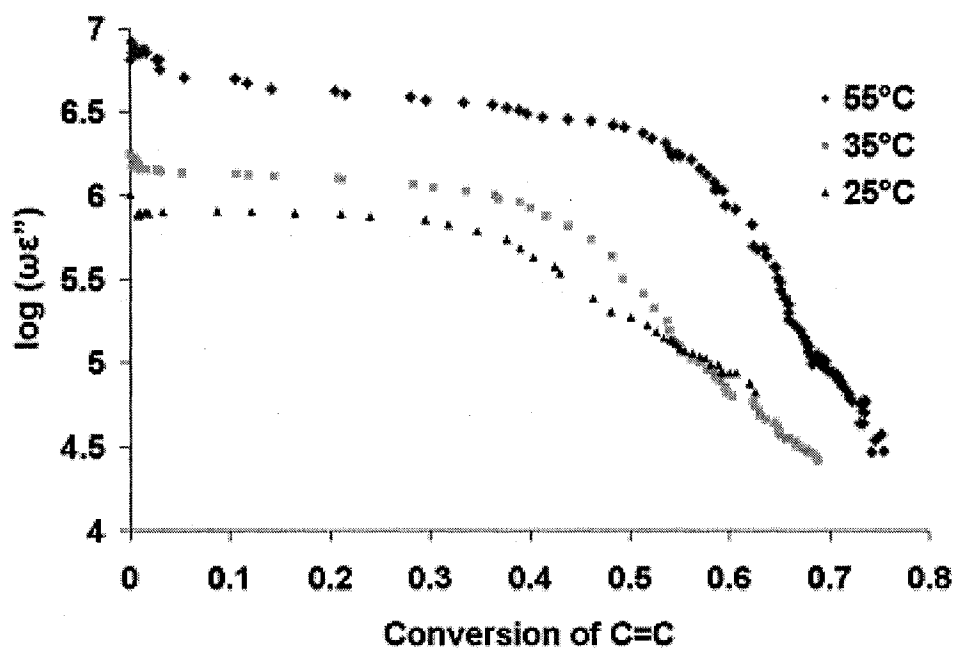


Figure 5.12 Correlation curves at different temperature. D121-0.05%IC819, I=32.5 uw/cm².

Figures 5.11 and 5.12 show that the final conversion is higher for the cure at a higher temperature. This is because increasing the temperature decreases the viscosity of the system at the same conversion hence postpones the vitrification of the sample to a higher conversion. In addition, at a higher temperature, the value of $\log(\varepsilon''\omega)$ starts dropping rapidly at a higher conversion. It is found in Figure 5.11 that at 55°C, the ion mobility does not start dropping rapidly until 60% conversion. This means that the ion mobility is higher for the system at a higher temperature at the same conversion. This is because the viscosity is lower at a higher temperature, so the ion mobility is higher. The temperature effect on the viscosity and the ion mobility of the system will be discussed in Section 5.3.5.

### 5.3.5 The effect of temperature on the viscosity and FDEMS data of the system

An AR1000 rheometer was used to measure the changing viscosity of CD540 without initiator versus temperature in the darkness without UV exposure. The result is shown in Figure 5.13.
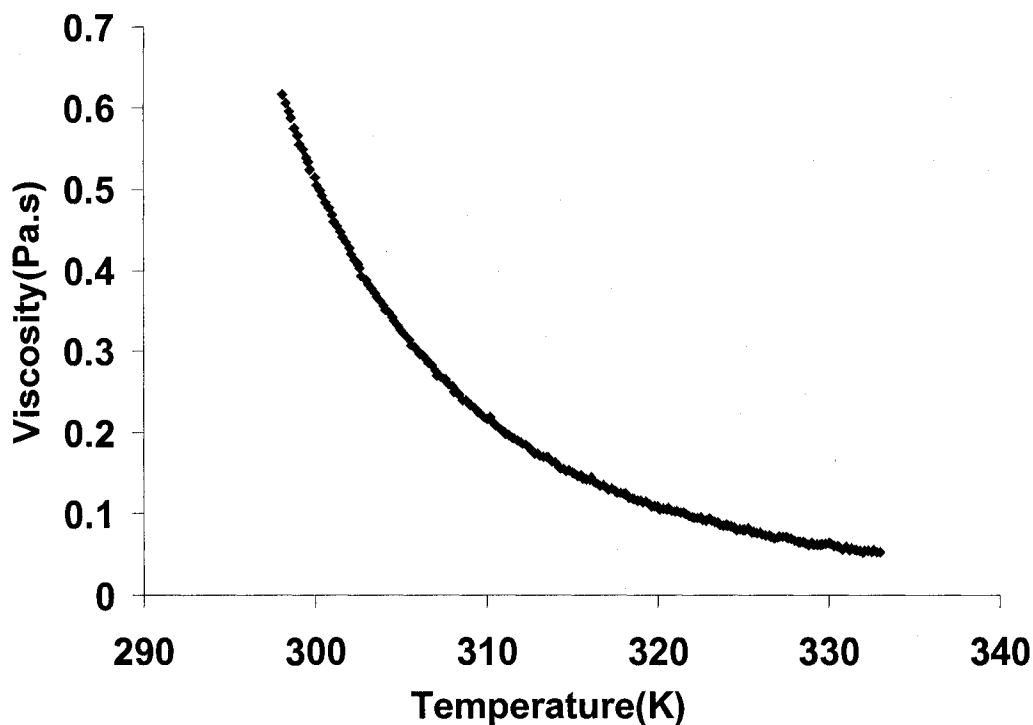
Figure 5.13 The changing viscosity of CD540 (without initiator) versus temperature measured in darkness without UV exposure.

It is found from Figure 5.13 that the viscosity of CD540 decreases with temperature. Combining this result with the one observed in Figures 5.11 and 5.12 that the system can reach a higher conversion at a higher cure temperature, it is found the viscosity of the sample affects its final cure conversion. This supports that the final conversion of less than 100% is due to the vitrification of the sample and the formation of a glassy state.

The temperature effect on the ion mobility of CD540 with initiator and UV exposure was also studied. The value of $\log(\varepsilon''\omega)$ and viscosity was correlated at the same temperature. The correlation curve is shown in Figure 5.14.
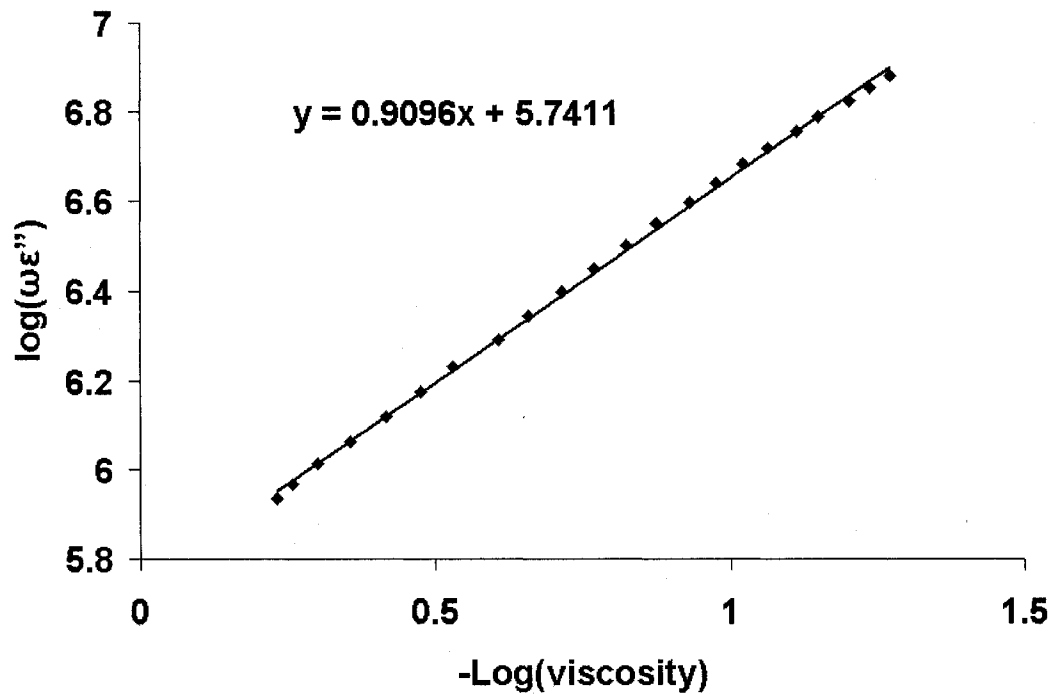
Figure 5.14 $\log(\varepsilon''\omega)$ versus log (viscosity)

Figure 5.14 shows that $\log(\varepsilon''\omega)$ and log (viscosity) satisfies equation 4-7

$$\log(\varepsilon''\omega) = - 0.91* \log (\text{viscosity}) + 5.74 \qquad \text{Equation 5-4}$$

Therefore for the sample CD540, the change of log(1/viscosity) is proportional to the change of $\log(\varepsilon''\omega)$ at the frequency of 0.1kHz, and the diffusion process is governed by Stokes (or Einstein) law that the movement of a spherical ball in a liquid is inversely related to viscosity. This result is very helpful for understanding the delay in the rapid drop of $\log(\varepsilon''\omega)$ at a higher temperature.

## 5.4 Conclusion

The value of $\log(\varepsilon''\omega)$ can be correlated with conversion during the formation of a thin film and this correlation does not change for systems with small differences in initiator concentration range studied here. The correlation curve shows how ion mobility and thereby radical mobility-diffusion change with extent of conversion for the system of CD540 as the reaction progresses and the glass transition is approached. This result offers evidence that diffusion controls the propagation and termination rate constant as well as the ion mobility. Thus the dielectric response can be used to monitor the progress of the reaction.

The correlation is affected by reaction temperature. Increasing the temperature increased the final conversion and the system reaches its glassy state at a higher conversion. For systems with the same conversion, the viscosity is lower at a higher temperature. Therefore the ion mobility and radical diffusion are higher, which facilitates the polymerization and increases the final degree of conversion.

# References:

1       Kranbuehl, D. E. Journal of Coating Technology 2004, 48-55.

2       Kranbuehl, D. E. Dielectric Spectroscopy of Polymeric Materials 1997, 303-28.

3       Kranbuehl, D. E. Processing of Composites, 2000.

4       Kranbuehl, D. E.; Warner, J.; Knowles, R.; Best, P. 60tnnual Technical
Conference, Soc. Plastic Engineers,, 2002, pp 3384-88.

5       Kranbuehl, D. E.; Rogozinski, J. Polymeric Materials Science and Engineering
1999, 81, 197-98.

6       Kranbuehl, D. E.; Hood, D.; Kellam, C.; Yang, J. In ACS Symposium Series;
Provder, T., Ed., 1996, p 96-117.

7       Kranbuehl, D. E.; Rogozinski, J.; Meyer, A.; Neag, M. 24th International
Conference in Organic Coatings, July 6-10 1998, pp 197-211.

8       Kranbuehl, D. E.; Hood, D.; Rogozinski, J.; Meyer, A.; Neag, M. Progress in
Organic Coatings 1999, 35, 101-07.

9       Kranbuehl, D. E.; Rogozinski, J.; Meyer, A.; Hoipkemeier, L.; Nikolic, N. In
ACS Symposium Series,, 2001, p 141-56.

10      Kranbuehl, D. E.; Hood, D.; McCullough, D.; L.Aandahl, H.; Haralampus, N.;
Newby, W.; Eriksen, M. Progress in Durability Analysis of Composite Systems,
Proceedings of the International Conference, Brussel, July, 16 1996, pp 53-59.

11      Kranbuehl, D. E.; Hood, D.; Rgozinski, J.; Meyer, A.; Powell, E.; Higgins, C.;
David, C.; Hoipkenmeier, L.; Ambler, C.; Elko, C.; Olukcu, N. 4th International
Conference on Durability Analysis of Composite Systems, Brussels, Belgium, July 11-14
1999, pp 413-20.

12      Wight, F. R.; Nunez, I. M. Journal of Radiation Curing 1989, 16, 3.

13      Decker, C.; Jenkins, A. D. Macromolecules 1985, 18, 1241-44.

# Chapter 6.  Study of the cure kinetics of thick samples

## 6.1 Introduction

The UV cure kinetics of thin samples was studied in Chapter 4 by real-time near FTIR. It was found that increasing intensity and initiator concentration always increases the cure rate for thin samples. However, the results for thin samples are not always correct if the sample is thick. The bulk polymerization rate of a **thick** sample may decrease when the initiator concentration increases. This phenomenon will be observed later in this chapter. It is due to the strong absorption of initiator at upper layers, which blocks the light, hence inhibiting the cure at the bottom layer. Furthermore, the intensity gradient through the depth induces spatial non-homogeneous conversions and properties. This fact can be used when making special materials with desired gradient properties.[1-3]

In order to control the cure process spatially and temporally, it needs to be understood how the cure kinetics change with depth and exposure time, and how some factors, such as incident intensity, initiator concentration, and temperature affect the cure kinetics. Due to the expanding use of thick film applications, there is a need to understand in more detail the cure kinetics versus depth for thick samples. Others have studied the spatial and temporal variation of light intensity,[4-8] cure kinetics and product properties based on Beer-Lambert's law and some assumptions. But, these studies are mainly theoretical calculations with a model based on an ideal situation. Most were not

verified by experimental data.[7-9] The real situation is usually much more complex than that which is assumed in models and therefore needs more experimental studies.

In this dissertation, UV cure kinetics will be studied using both theoretical calculations and experimental methods. These two outcomes complement and support each other.

The theoretical calculations are based on the results in Chapter 3 and Chapter 4. In Chapter 3, the intensity versus exposure as a function of depth was calculated for different systems and at different incident intensities. In Chapter 4, a calculation method was successfully developed to predict the curing at different light intensities and initiator concentrations based on the experiments with CD540 thin films (thickness=0.05 mm). Combining the research results in these two chapters, the cure curves at particular depths and the average bulk cure curves of thick samples can be calculated.

In the experimental part, the bulk curing of thick samples is studied first by real-time transmitted near FTIR to examine the differences from the typical cure kinetics of thin samples. The experimental results will be compared with theoretical calculation predictions. After that, the cure process at particular depths is measured by dielectric measurements. The dielectric data, $\log(\varepsilon''\omega)$, are converted into conversion of C=C, $\alpha$, using the correlation curve obtained in Chapter 5. The experimental data are also compared with theoretical calculation results at particular depths.

The results help to determine what is the proper initiator concentration for a desired bulk reaction and the product gradient structure properties.

## 6.2 Experiment

**Materials.** The photo-initiator, Irgacure 819, and the oligomer, CD540, are the same as what was used in Chapters 3, 4, and 5. The method of making the system is the same too.

**Sample preparation.** The mold was made of two pieces of glass (>90% IR transparent and >90% UV transparent) using plastic glass as the spacer for thick samples. A thin planar dielectric sensor was fixed to the bottom of the glass slide inside the mold as shown in Figure 6.1.
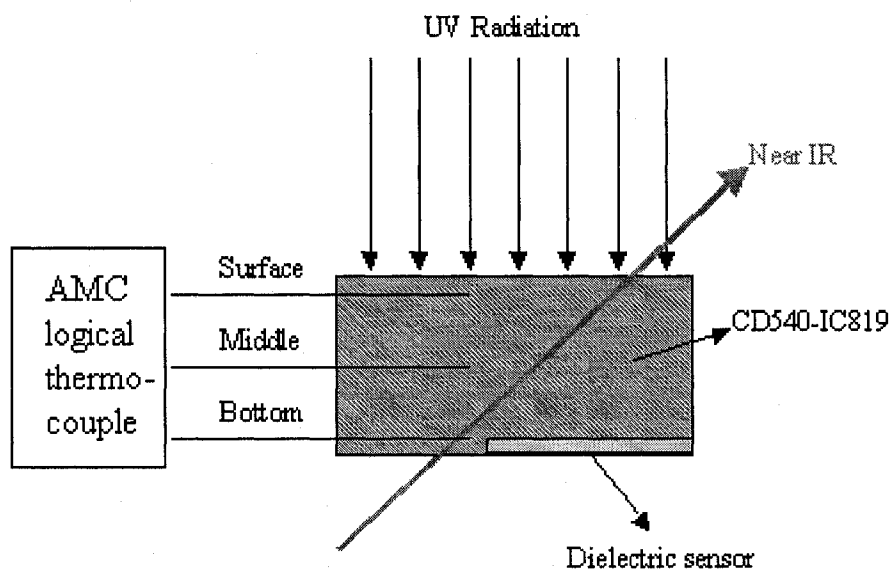


Figure 6.1 Experimental setup

**Radiation Source.** The radiation source is the same as what was used in Chapter 4.

**Real-Time near FTIR Measurement.** A near FTIR spectrometer (PIR at INSA, Lyon) connected with an optic fiber was used to measure the transmitted spectrum of the thin samples. The spectrum was analyzed by OPUS software. It can in-situ monitor the

changes of the absorption peak area of carbon double bonds of the thick samples during the cure process.

**FDEMS Measurement.** A Eumetric System III microdielectrometer (Micromet Instruments, Inc) (INSA, Lyon) connected to a planar inter-digitated Kapton dielectric sensor was used to monitor the changes in the capacitance and conductance of the sample during the cure process at a frequency of 0.1kHz at the bottom of the mold as shown in figure 5.1.

**Temperature Measurement.** A portable AMC logical thermocouple thermometer has three ports to connect with one end of three thermocouple lines separately and can monitor three temperatures simultaneously. The other ends of the three thermocouple lines were placed separately at the surface, bottom and middle of the mold inside the sample near the sensor to monitor the temperature at different depths during the cure process, as shown in figure 5.1. The AMC logical thermal thermometer recorded a value every two seconds.

## 6.3 Results and discussion

### 6.3.1 Study of UV cure kinetics of thick samples by theoretical calculations

In this section, UV cure kinetics in thick samples is studied by dividing the whole sample into many thin layers (layer thickness=0.05 mm). The cure kinetics for each thin layer at particular depths will be calculated first. Then the average bulk cure kinetics will be studied by calculating the average of cure kinetics of all layers.

### 6.3.1.1 Calculation of cure kinetics at particular depths

The radiation intensities versus exposure time at different depths in a thick sample can be calculated using Equations 3-8 and 3-9 as discussed in Chapter 3. Since those equations are very important for the calculation in this chapter, they are listed here again as Equations 6-1 and 6-2.

$$[PI]_{t_2} = [PI]_{t_1} - \frac{\phi' I_i (1 - 10^{-\varepsilon_i b [PI]_{t_1}})}{b}(t_2 - t_1)$$

Equation 6-1

$$I_t = I_i * 10^{-b(\varepsilon_i [PI]_t + \varepsilon_m [M])}$$

Equation 6-2

Here [PI] is the concentration of the initiator, Irgacure 819; [M] is the concentration of the C=C in CD540; $I_i$ is the incident light intensity; $I_t$ is the transmitted intensity; $\varepsilon_i$ (760 1 mol$^{-1}$ cm$^{-1}$) is the absorption coefficient of the initiator; $\varepsilon_m$ (0.0755 1 mol$^{-1}$ cm$^{-1}$) is the absorption coefficient of the CD540, b (0.05 mm) is the thickness of the sample/layer; and $t_2$-$t_1$ is the time interval for the calculation. The value of the time interval is determined by the cure rate (light intensity and initiator concentration) as discussed in Chapter 3.

In addition, the cure kinetics at a given intensity and initiator concentration can be calculated using Equations 6-3 to 6-6, as discussed in Chapter 4.

$$-\frac{d(\ln([M(t)]))}{dt} = \frac{1}{1 + e^{-30(\alpha - 0.05)}} - \frac{1}{1 + e^{-13.7(\alpha - 0.36)}}$$

Equation 6-3

$$\frac{\left(-\frac{d(\ln[M(t)])}{dt}\right)_{I_1 [PI]_1}}{\left(-\frac{d(\ln[M(t)])}{dt}\right)_{I_2 [PI]_2}} = \left(\frac{I_1}{I_2}\right)^{0.7} \left(\frac{[PI]_1}{[PI]_2}\right)^{0.75}$$

Equation 6-4

Equation 6-3 represents the value of $-\dfrac{d(\ln[M(t)])}{dt}$ versus conversions ($\alpha$) for

the cure of the system, CD540-0.2wt%IC819 under the light intensity of 32.5 $\mu w / cm^2$.

Combining Equation 6-3 and 6-4,

$$-\frac{d(\ln([M(t)])}{dt} = (\frac{I}{32.5})^{0.7}(\frac{[PI]}{0.2})^{0.75}(\frac{1}{1+e^{-30(\alpha-0.05)}} - \frac{1}{1+e^{-13.7(\alpha-0.36)}}) \quad \text{Equation 6-5}$$

The value of $-\dfrac{d(\ln[M(t)])}{dt}$ versus conversion ($\alpha$) at other intensities and

initiator concentrations can be calculated using Equation 6-5. Equation 6-6 is used to

calculate the delay time (the inhibition period), Td, for the systems with different initiator

concentrations and under different light intensities.

$$Td = \frac{5.542}{I \times [PI]wt\% \times 100} \quad \text{Equation 6-6}$$

**(Note that the equations and parameters above will be used for calculations**

**throughout this chapter.)**

A Matlab program is written to perform the calculation by dividing the sample

into many layers. Two assumptions are used to simplify the calculation process. **The first**

**one** is that there is no mass exchange (no diffusion of $O_2$, CD540 and IC819) between

any two adjacent layers. This is reasonable as the absorption of one layer is very small

and therefore the difference of the intensities and the cure process between two adjacent

layers is small. At the same exposure time, the difference of component concentration

between two layers is small. Hence the diffusion, which is proportional to the difference

of component concentrations (as shown in Fick's law[10]) between two thin layers, can be

neglected. Then, the reaction at each layer can be regarded as a thin sample reaction as in

Chapter 4. **The second** assumption is that the curing of all layers is at room temperature. The increase of temperature due to the exothermal reaction was not considered initially in the calculation. (Note: the temperature effect will be considered later for only some experiments that have a significant increase in temperature.) In addition, in order to use Equations 6-5 and 6-6, the layer thickness should be equal to 0.05 mm. With these assumptions and limitations, the method used in Chapters 3 and 4 for calculating cure kinetics can be used here. The calculation process is elaborated using Table 6.1. All parameters are expressed using two-dimensional matrices since they are functions of both exposure time and depth.

Table 6.1 Calculation of UV cure kinetics at different depths in a thick sample.

| | $t_1$ | $t_2$ | ...... | $t_m$ |
|---|---|---|---|---|
| | $I(1,1)=I_i$ | $I(1,2)=I_i$ | | $I(1,m)=I_i$ |
| $d_1$ | $PI(1,1)=[PI]_0$ | $PI(1,2)$ | ...... | $PI(1,M)$ |
| | $M(1,1)=[M]_0$ | $M(1,2)$ | | $M(1,m)$ |
| | $\alpha(1,1)=0$ | $\alpha(1,2)$ | | $\alpha(1,m)$ |
| | $Td[I(1,1),PI_0]$ | $Td[I(1,2),PI_0]$ | | |
| | $I(2,1)$ | $I(2,2)$ | | $I(2,m)$ |
| $d_2$ | $PI(2,1)=[PI]_0$ | $PI(2,2)$ | ...... | $PI(2,M)$ |
| | $M(2,1)=[M]_0$ | $M(2,2)$ | | $M(2,m)$ |
| | $\alpha(2,1)=0$ | $\alpha(2,2)$ | | $\alpha(2,m)$ |
| | $Td[I(2,1),PI_0]$ | $Td[I(2,2),PI_0]$ | | |
| : | : | : | : | : |
| | $I(n,1)$ | $I(n,2)$ | | $I(n,m)$ |
| $d_n$ | $PI(n,1)=[PI]_0$ | $PI(n,2)$ | ...... | $PI(n,m)$ |
| | $M(n,1)=[M]_0$ | $M(n,2)$ | | $M(n,m)$ |
| | $\alpha(n,1)=0$ | $\alpha(n,2)$ | | $\alpha(n,m)$ |
| | $Td[I(n,1),PI_0]$ | $Td[I(n,2),PI_0]$ | | |

t is the exposure time; d is the depth; I is the light intensity; M is the concentration of C=C; $\alpha$ is the conversion of C=C; PI is the concentration of photo initiator. $[M]_0$ and $[PI]_0$ are the initial concentration of C=C and photo-initiator before the cure starts. $I_i$ is the incident light intensity at the surface of the sample. $T_d$ is the time of delay (the length of the inhibition period).

The variables in Table 6.1 can be calculated in the following steps.

(1)      First, all intensities, I(x, y) and photo initiator concentrations, PI(x,y) at different depths and exposure times in table 6.1 are calculated using Equations 6-1 and 6-2. The method has been elaborated in Chapter 3.

(2)      Second, Td, the delay times (inhibition periods), of UV cure in thin layers at all depths are calculated using Equation 6-6 by substituting I with I (x, y) from step 1 and [PI] with $PI_0$. The increasing I(x,y) with exposure time in a given layer makes the calculation more complex. A loop is applied in the calculation process. Taking the sample at the $d_x$ layer as an example, the calculation process is shown below.

Td(x,1) is calculated first by substituting I(x,1), the value of intensity at time $t_1$ and layer x into Equation 6-6. If Td(x,1)-t1>0, then Td(x,2) at time $t_2$ is calculated by substituting I(x,2) into Equation 6-6. Now, the average value of delay time, ATd, is equal to [Td(x,1)+Td(x,2)]/2. If ATd-t2>0, then Td(x,3) at time $t_3$ is calculated by substituting I(x,3) into Equation 6-6. This is continued until the $y^{th}$ time point, where Td-t (x, y)$\leq$ 0. At this point, the value of Td best matches t (x, y). This is the end of the inhibition period (delay time) and also the starting point of the polymerization. The error of the calculation of the delay time is less than the time interval, $t_2$-$t_1$.

(3)     Third, the concentration of C=C, M(x, y) and the conversion of C=C, $\alpha$ (x, y) are calculated from the time of the end of the inhibition period. The process for calculating the polymerization is shown below.

According to the third assumption described above that [PI] is regarded as a constant during the curing process of the sample in the **same** thin layer,

$$PI(1,1)= PI(2,1)=\ldots\ldots PI(n,1)=[PI]_0 \qquad \text{Equation 6-7}$$

Before the polymerization starts, when $t<t_b$,

$$M(x,1)=M(x,2)=\ldots\ldots M(x,b-1) =[M]_0 \qquad \text{Equation 6-8}$$

Conversion of C=C, $\alpha$ , can be calculated using Equation 6-10,

$$\alpha =1-\frac{M}{M_0} \qquad \text{Equation 6-9}$$

So,

$$\alpha(x,1)=\alpha(x,2)=\ldots\ldots\alpha(x,b-1)=0 \qquad \text{Equation 6-10}$$

$[M]_0$ and $[PI]_0$ are calculated according to the initial composition of the system and they do not change with depth before the cure starts.

With these initial values, **M(x,b)** is calculated using Equation 6-5 by substituting $\alpha$ with 0, I with I(x,b), and [PI] with $[PI]_0$. $\alpha$ **(x,b)** is calculated using Equation 6-10 by substituting M with M(x,b). Then, M(x,b+1) can be calculated by substituting $\alpha$ **(x,b)**, I(x,b+1), and PI(1,2) into Equation 6-5. This is continued until time n. Then, all values of conversion of C=C from the $b^{th}$ time point to $n^{th}$ ($\alpha$ (x,b), $\alpha$ (x,b+1)...... $\alpha$ (x,n)) can be calculated for the $x^{th}$ thin layer.

Using the method described above from step (1) to (3), the cure kinetics at different depths are calculated for the 4 mm thick sample, CD540-**0.2**wt%IC819, under

$130\,\mu w/cm^2$ radiation intensity. The sample is divided into 80 0.05 mm thick layers. When different time intervals were considered in the calculation shown in Appendix 2, it was found that 0.01 minutes is a good increment giving a small error and a reasonable calculation time. Using 0.01minutes as the time interval, the cure curves at the surface, and at 1, 2, 3, and 4 mm depth are shown in Figure 6.2.
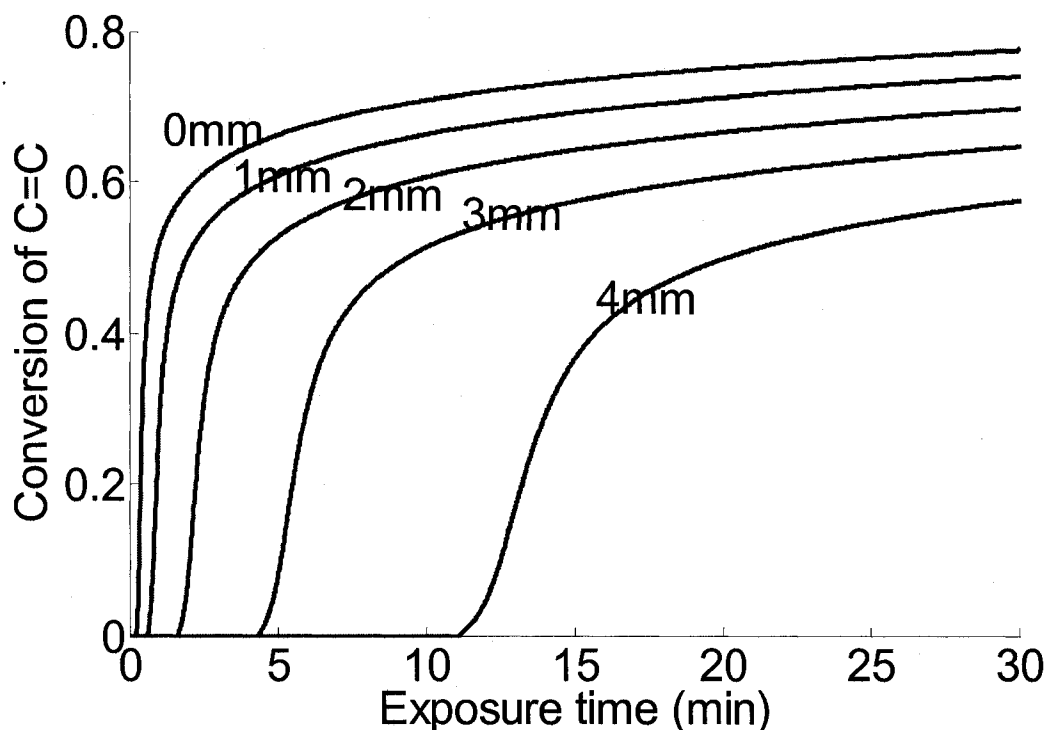


Figure 6.2 Predicted values using Equations 6.1 to 6.6. UV cure kinetics of CD540-0.2wt%Irgacure 819 at different depths. The depths are marked in the figure as 0 to 4 mm. $I_i = 130\,\mu w/cm^2$, time interval is 0.01minutes, layer thickness=0.05 mm.

Figure 6.2 shows that the cure kinetics are a function of depth. The polymerization at the surface layers is much faster than the reaction at the bottom layers. This is because the intensity decreases with depth as what was studied in Chapter 3.

Using the same method, the cure kinetics are predicted for another system, CD540-**0.05**wt%IC819 under the same conditions. The result is shown in Figure 6.3.
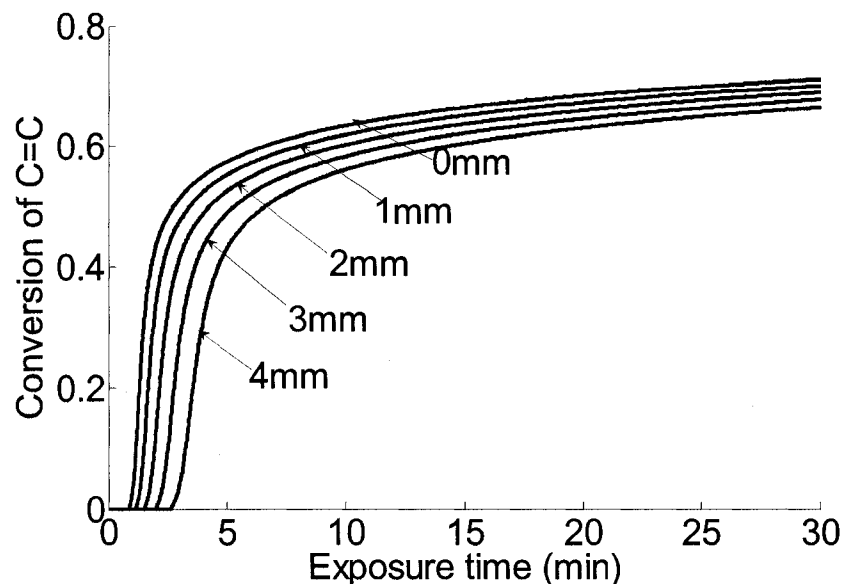


Figure 6.3 Predicted values using Equations 6.1 to 6.6. UV cure kinetics of CD540-0.05wt%Irgacure 819 at different depths. The depths are marked in the figure as 0 to 4 mm. $I_i = 130\mu w/cm^2$. Time interval is 0.01minutes, layer thickness=0.05 mm.

Similar to Figure 6.2, Figure 6.3 also shows that the cure kinetics are functions of depth and the polymerization is faster at surface layers than bottom layers. Comparing Figures 6.2 and 6.3, it is also found that the cure at the **surface** layer is faster for the system with more initiator (Figure 6.2). However, the cure at the **bottom** layer is even slower for the system with more initiator (Figure 6.2). It means the reaction is more homogeneous through depth for the sample with less photo initiator in it. This is because the absorption of light intensity is higher for the system with more initiator. Hence, the gradient of intensity versus depth for the sample with 0.2wt% initiator is more pronounced than the sample with 0.05wt% initiator and so is the cure rate.

## 6.3.1.2 Calculation of average cure kinetics (bulk cure) in thick samples

Using the result from section, 6.3.1.1, the bulk cure kinetics can be predicted by calculating the average of the conversion of C=C in all layers from the surface to the bottom at the same time. As discussed above, the sample is divided into 0.05 mm thin layers. So there are a total of 80 layers in a 4 mm thick sample. The cure curves at all layers from surface to bottom and the average cure curve (bulk cure kinetics) are shown in Figure 6.4.
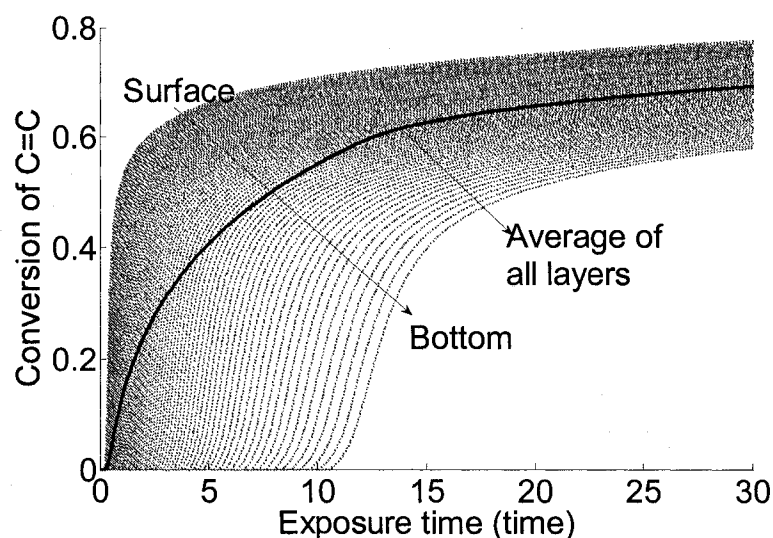
Figure 6.4 Predicted values using Equations 6.1 to 6.6. Cure kinetics of a 4 mm thick sample, CD540-0.2wt%Irgacure 819, $I_i = 130 \mu w / cm^2$. Time interval is 0.01minutes, layer thickness=0.05 mm. (••••••) Cure curves of sample in 0.05 mm thin layers at different depths; (——————) Average cure curve of all thin layers in thick sample.

Figure 6.4 shows that the inhibition period of the bulk cure curve is determined by the cure near the surface. But the bulk cure rate and the final conversion are affected by the cure of all layers through all the depths.

Next, the **intensity and initiator concentration** effects on the bulk cure kinetics are studied using the same calculation method. The bulk cure curves of 4 mm thick samples, CD540-0.2wt%Irgacure 819, under different radiation intensities are shown in Figure 6.5.
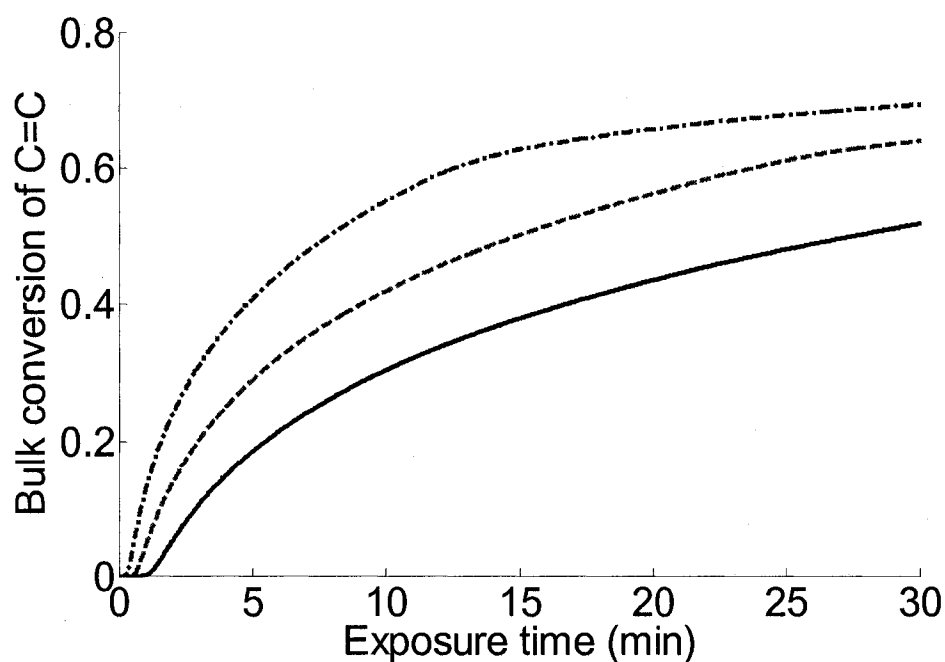


Figure 6.5 Predicted values using Equations 6.1 to 6.6. Bulk cure kinetics of 4 mm thick sample, CD540-0.2wt%Irgacure 819 under different radiation intensities. Time interval is 0.01minutes, layer thickness=0.05 mm. (—•—•—)$I_i = 130 \mu w / cm^2$; (— —)$I_i = 65 \mu w / cm^2$; (————)$I_i = 32.5 \mu w / cm^2$.

It is shown in Figure 6.5 that increasing the light intensity can increase the cure rate and decrease the inhibition period of 4 mm thick samples, CD540-0.2wt%Irgacure 819. These phenomena mean that the effect of **radiation intensity** on bulk cure kinetics of 4 mm thick samples is similar to that of 0.05 mm thin samples.

Next, the initiator concentration effect on the bulk cure kinetics of 4 mm thick samples, CD540-Irgacure 819, with varying [PI] and under the same radiation intensity is calculated. The results are shown in Figure 6.6.
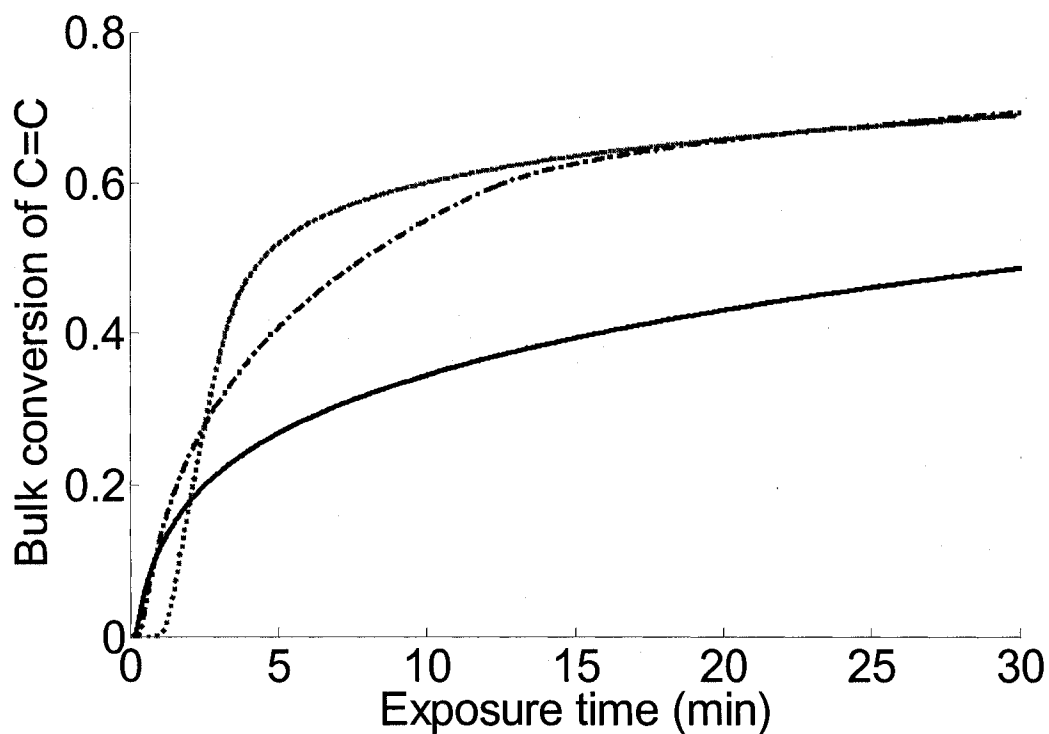


Figure 6.6 Predicted values using Equations 6.1 to 6.6. Bulk cure kinetics of 4 mm thick sample, CD540-Irgacure 819 with varying initiator concentrations. $I_i = 130 \mu w / cm^2$. Time interval is 0.01minutes, layer thickness=0.05 mm. (••••••) [PI]=0.05wt%; (—•—•—) [PI]=0.2wt%; (————) [PI]=0.4wt%.

It is found from Figure 6.6 that the inhibition period is shorter for the system with more initiator for the [PI] range studied here. This is similar to the 0.05 mm thin samples. However, Figure 6.6 shows that increasing initiator concentration does not increase the average polymerization rate of the 4 mm thick samples. This is different from the

conclusion for thin samples. The reason for the abnormal phenomena is the significant decrease of light intensity through the depth in a thick sample with a higher initiator concentration. This results in an extremely slow reaction rate at the bottom. Since the bulk cure kinetics are the average of cures in thin layers at all depths, the slow reaction rate and long delay time at the bottom decrease the bulk cure rate. But the inhibition period is determined only by the reaction in the layers near the surface (as shown in Figure 6.4) where the intensity is not significantly decreased but the initiator concentration is higher. So the inhibition period in the surface layers is shorter, as is the inhibition period for the bulk cure.

### 6.3.2 Bulk cure kinetics studied by real-time transmitted near FTIR and compared with predicted curve

In section 6.3.1, the cure kinetics of CD540-Irgacure 819 were studied by theoretical calculation. In this section, the cure kinetics are monitored using real-time transmitted near FTIR. First, the exposure intensity effect on the cure kinetics will be studied by experimentally measuring cure curves under varying intensities. Second, the initiator concentration effect on the cure kinetics will be studied by experimentally measuring UV cure of the system with different [PI]. Last, the experimental data will be listed together with the theoretical predicted data in the same figure to compare the differences among them and to evaluate the predictions using the calculation method based on Equation 6-1 to 6-6. Note that the transmitted FTIR gives only **bulk cure kinetics** instead of the cure at a particular depth.

(1) The experimental bulk cure curves of CD540-0.2wt%Irgacure 819 at two different radiation intensities are shown in Figure 6.7.
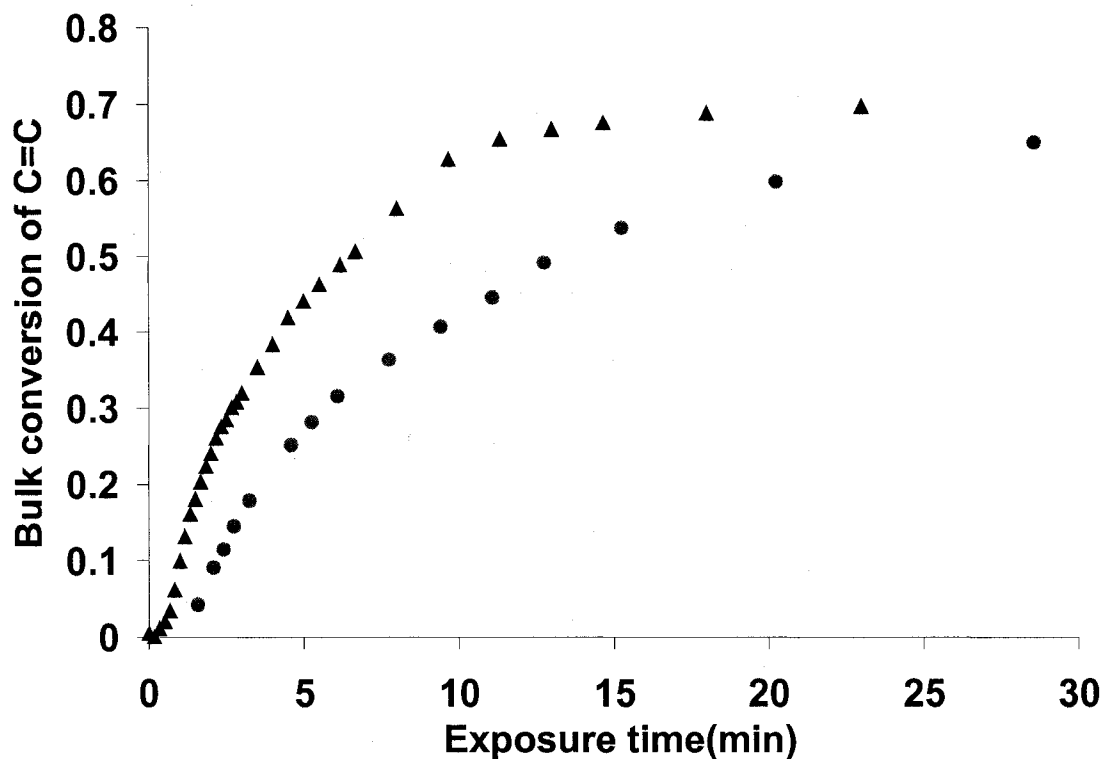
Figure 6.7 FTIR measured bulk conversion versus time for the cure of 4 mm thick

system, CD540-0.2wt%Irgacure 819. $(\blacktriangle)I_i = 130\mu w/cm^2$; $(\bullet)I_i = 65\mu w/cm^2$.

Figure 6.7 shows that increasing radiation intensity increases the bulk cure rate of

a 4 mm thick sample. This agrees with the theoretically predicted result in Figure 6.5.

(2) Next, the initiator concentration effect on the bulk cure kinetics is studied.

Figures 6.8 shows the cure curves of CD540-Irgacure 819 with 0.2 and 0.05wt% initiator

concentration at $130 \mu w/cm^2$ radiation intensities.
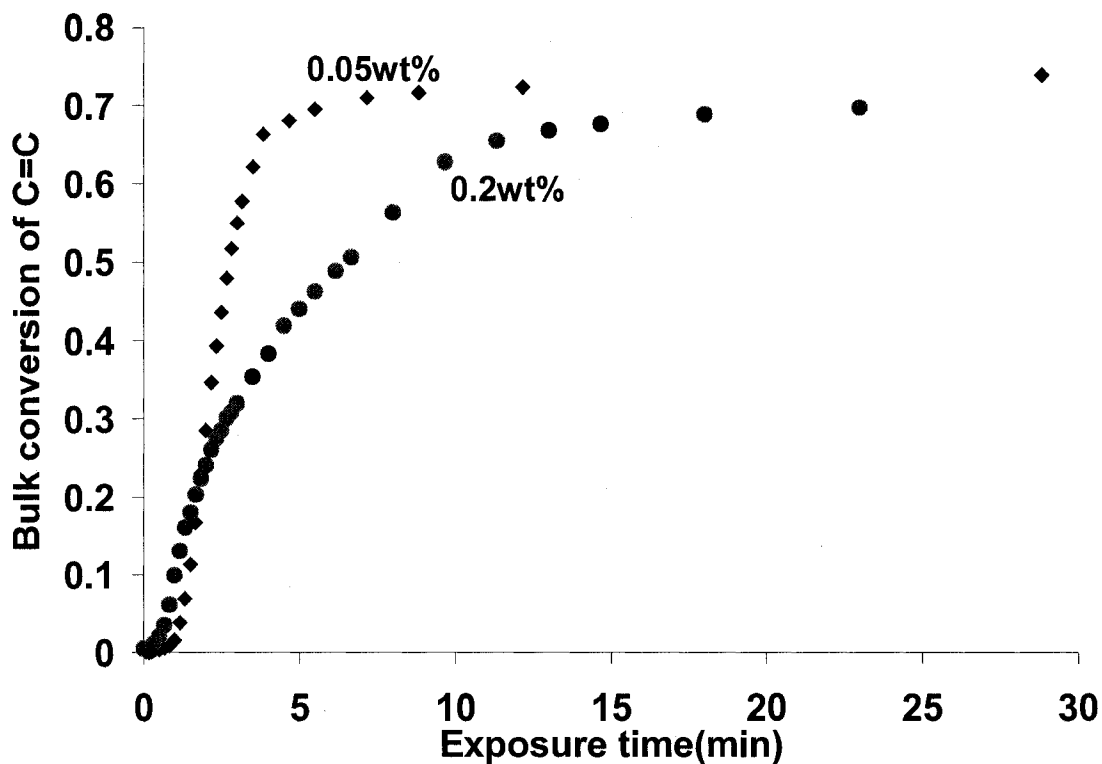
Figure 6.8 FTIR measured bulk conversion versus time for the cure of 4 mm thick system, CD540-Irgacure 819 under the exposure intensity, $I_i = 130 \mu w / cm^2$. Initiator concentration are marked in the figure, (♦) [PI]=0.05wt% ; (●)[PI]=0.2wt%.

Figure 6.8 shows that increasing initiator concentration results in a shorter inhibition period but a slower cure rate. This is the same as the predicted results in Figure 6.6 under the same conditions.

Next, the cure kinetics of systems, CD540-Irgacure, with 0.2 and 0.4wt% photo initiator concentration are studied for the cure under another exposure intensity, $I_i = 65 \mu w / cm^2$ as shown in Figure 6.9.
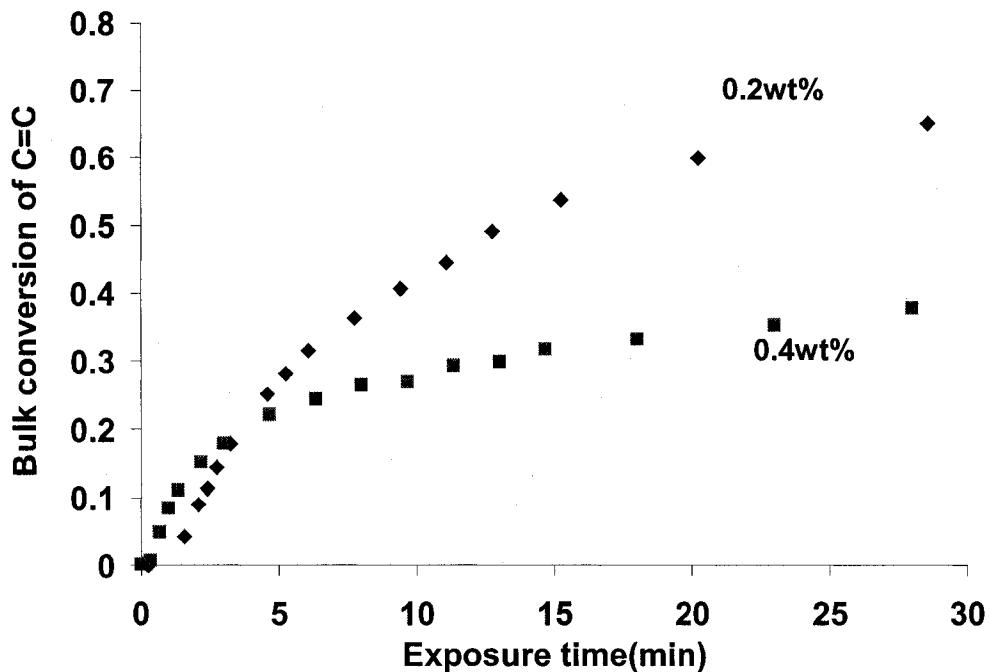
Figure 6.9 FTIR measured bulk conversion versus time for the cure of 4 mm thick system, CD540-Irgacure 819, under the exposure intensity, $I_i = 65\mu w/cm^2$. Initiator concentrations are marked in the figure, (♦) [PI]=0.2wt% ; (■)[PI]=0.4wt%.

Figure 6.9 shows again that increasing initiator concentration results in a shorter inhibition period but a slower cure rate for the UV cure of a 4 mm thick sample, CD540-Irgacure 819 under another radiation intensity. Both Figures 6.8 and 6.9 show that for a thick sample, increasing initiator concentration may not always increase the bulk cure rate but it can shorten the inhibition period.

(3) Next, the experimental data will be plotted together with the corresponding predicted data from Figures 6.10 to 6.14 to evaluate the calculation method. The cure conditions of these figures and relationships between the experimental data and the predicted data are listed in Table 6.2 following these figures.
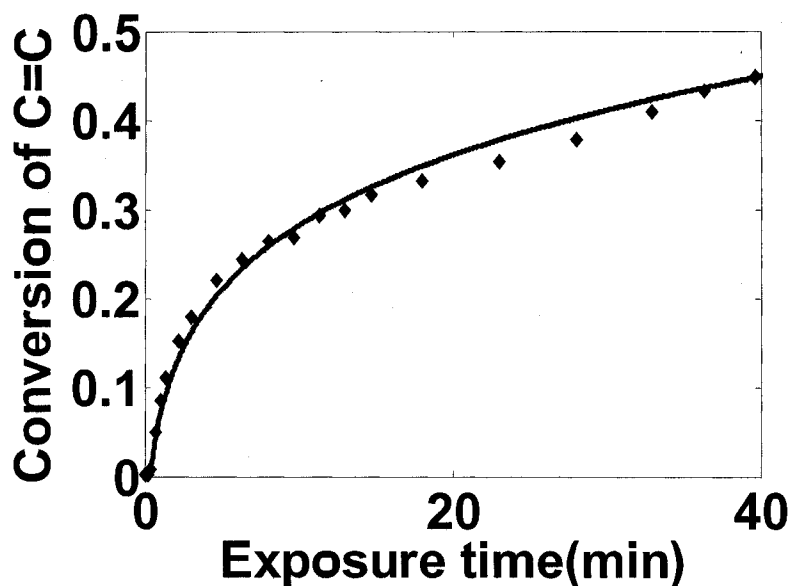
Figure 6.10 Bulk conversion versus time for the cure of 4 mm thick system, CD540-0.4wt%Irgacure 819. $I_i = 65 \mu w / cm^2$. (♦) FTIR measured data; (———) Predicted cure curve using Equations 6-1 to 6-6.
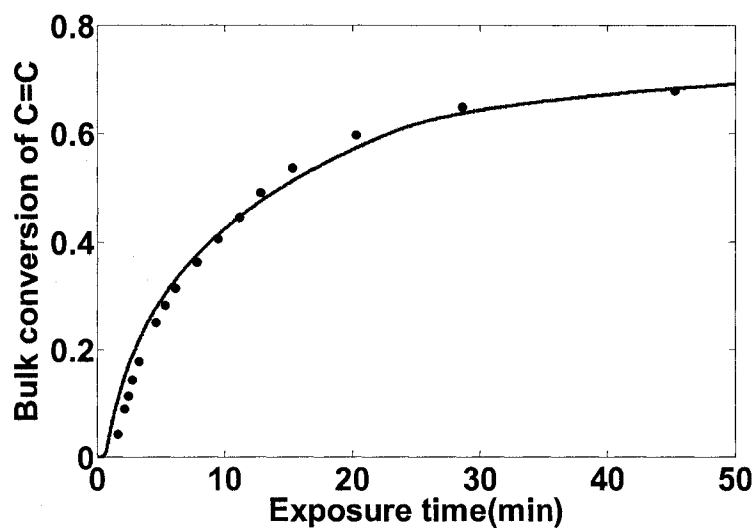


Figure 6.11 Bulk conversion versus time for the cure of 4 mm thick system, CD540-0.2wt%Irgacure 819. $I_i = 65 \mu w / cm^2$. (●) FTIR measured data; (———) Predicted cure curve using Equations 6-1 to 6-6.
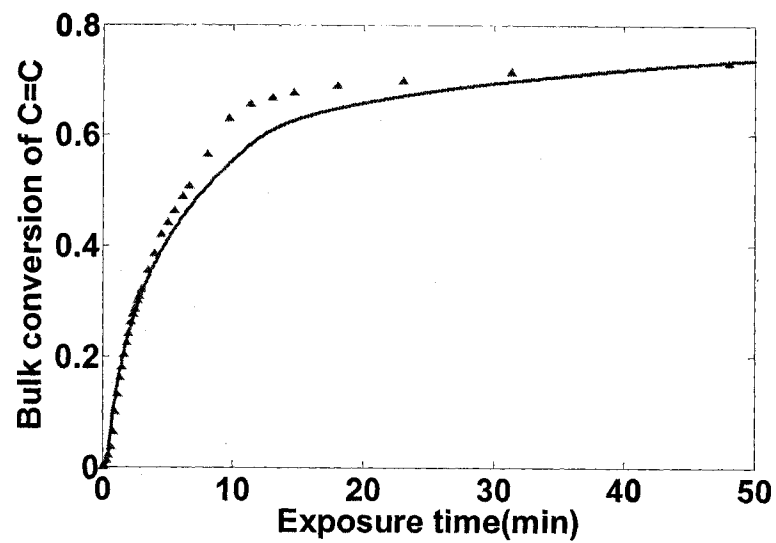
Figure 6.12 Bulk conversion versus time for the cure of 4 mm thick system, CD540-0.2wt%Irgacure 819 at $130\mu w/cm^2$. (▲) FTIR measured data; (———) Predicted cure curve using Equations 6-1 to 6-6.
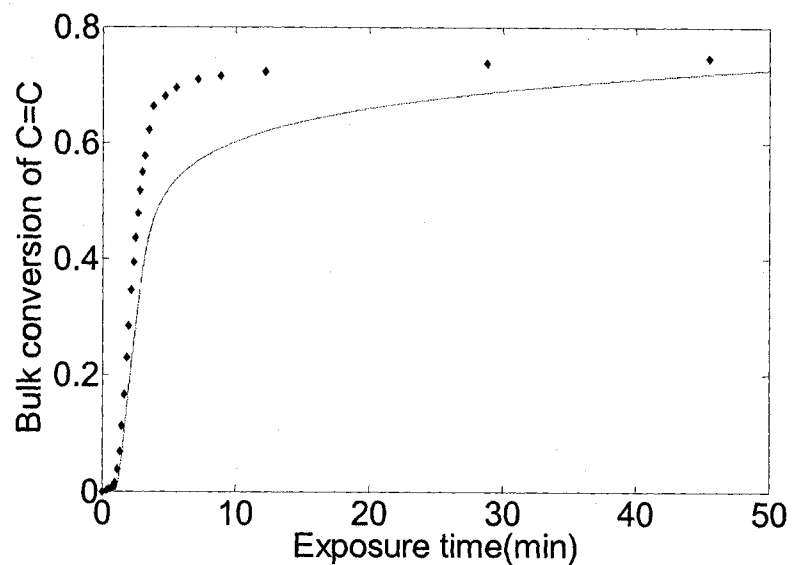


Figure 6.13 Bulk conversion versus time for the cure of 4 mm thick system, CD540-0.05wt%Irgacure 819. $I_i = 130\mu w/cm^2$. (♦) FTIR measured data; (———) Predicted cure curve using Equations 6-1 to 6-6.
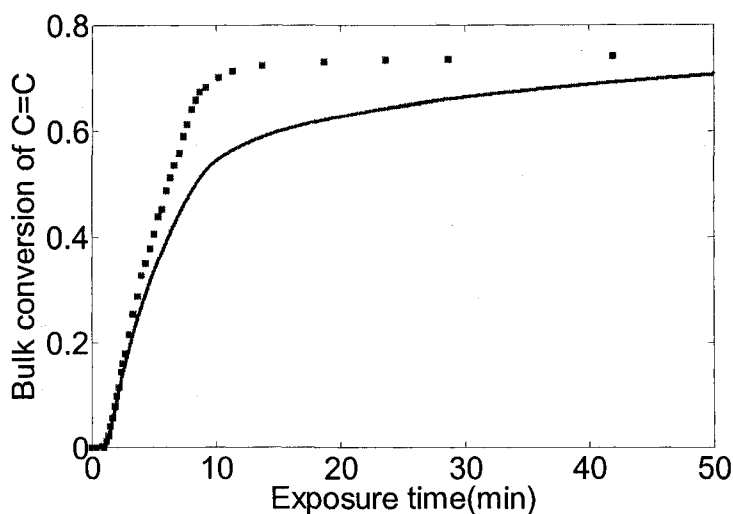
Figure 6.14 Bulk conversion versus time for the cure of <u>8 mm</u> thick system, CD540-0.05wt%Irgacure 819. $\underline{I_i = 130 \mu w/cm^2}$. (■) FTIR measured data; (━━━) Predicted cure curve using Equations 6-1 to 6-6.

The cure conditions and the relationship between the experimental data and the corresponding predicted data of the UV polymerization from Figure 6.10 to 6.14 are listed in Table 6.2.

Table 6.2 UV cure of CD540-Irgacure 819 under different conditions

| Figure number | [PI] wt% | Intensity $\mu w/cm^2$ | Thickness (mm) | Experiment/predicted data agreement |
|---|---|---|---|---|
| 6.10 | 0.4 | 65 | 4 | Good |
| 6.11 | 0.2 | 65 | 4 | Good |
| 6.12 | 0.2 | 130 | 4 | Ok |
| 6.13 | 0.05 | 130 | 4 | Good up to $\alpha = 0.4$, then lags experimental values. Final cure value agrees. |
| 6.14 | 0.05 | 130 | 8 | Good up to $\alpha = 0.4$, then lags experimental values. Final cure value agrees. |

Table 6.2 shows that the predicted data match the experimental data well in Figures 6.10 and 6.11 where the initiator concentration is high and the radiation intensity is lower. This result is very encouraging. However, in Figures 6.12, 6.13 and 6.14, the predicted data match the experimental data up to $\alpha = 0.4$. At higher conversions, the experimental data are higher than predicted data in Figures 6.13 and 6.14. This is due to the exothermal reaction that results in an increase of temperature during the cure process. It has been seen from Chapter 4 that UV cure rate is faster and the final conversion is slightly higher at a higher temperature. The changing temperature inside the sample at different depths will be studied in Section 6.3.4.

### 6.3.3 UV cure kinetics at particular depths studied by in-situ dielectric measurement and compared with predicted outcome

While transmitted FTIR is a good method to monitor the UV cure process, it can only give the **bulk cure** information, not the cure at particular depths. Dielectric measurement using a planar inter-digitated sensor has advantages in measuring the reaction at a particular depth. In this section, the UV cure kinetics are monitored under different cure conditions using dielectric sensors and the results will be compared with the corresponding predicted results using the model of Chapter 4.

Typical FDEMS data measured at the bottom of thick samples are shown in Figure 6.15 for the system of CD540-0.2wt%IC819 cured under the radiation intensity of $65 \, \mu w / cm^2$. The depth where cure of the sample is measured is determined by the spacer thickness of the mold. The depth (spacer thickness) is 4 mm where the FDEMS sensor is located. The temperature was also measured at the bottom of the mold near the sensor by a thin thermocouple wire as shown in Figure 6.1.
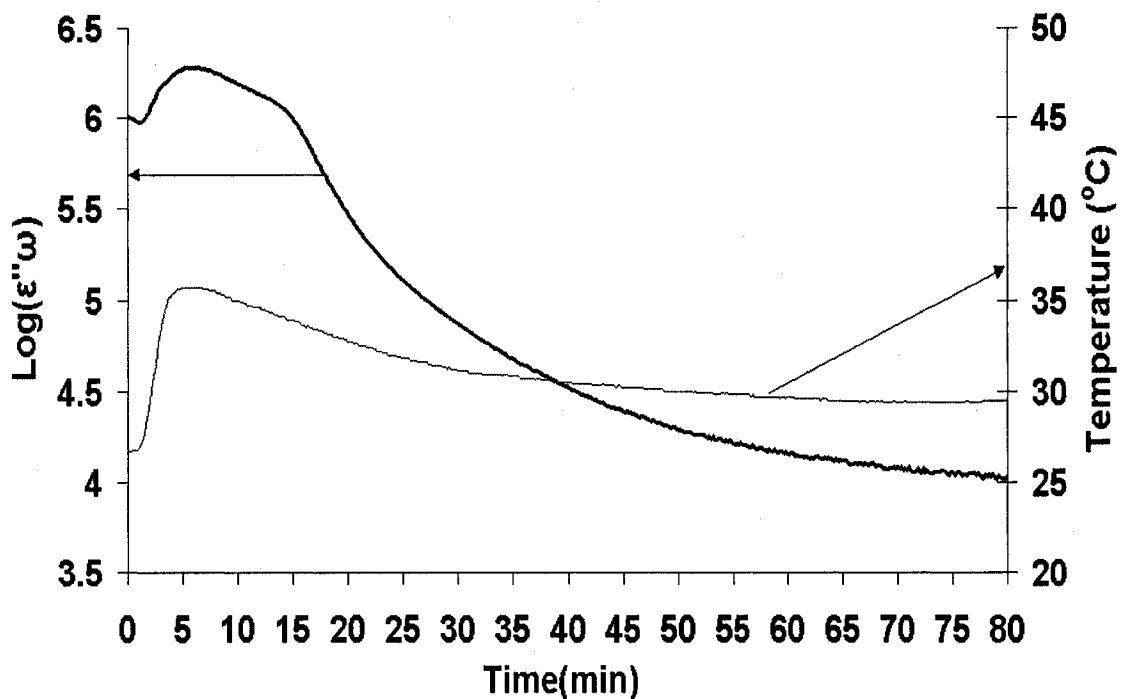
Figure 6.15 dielectric and temperature data measured at the bottom of the sample, CD540-0.2wt%IC819, Ii=65 $\mu w$/cm$^2$, thickness=4 mm, f=0.1kHz.

An unusual result is observed in Figure 6.15. The value of log($\varepsilon''\omega$) does not keep decreasing with exposure time as observed for thin samples in Chapter 4. Instead, it increased soon after the exposure started. This increase is induced by the increase of the temperature of the system due to the exothermal reaction. The change of the value of log($\varepsilon''\omega$) with temperature was studied by monitoring the log($\varepsilon''\omega$) of CD540 as a function of temperature. The result is shown in Figure 6.16.
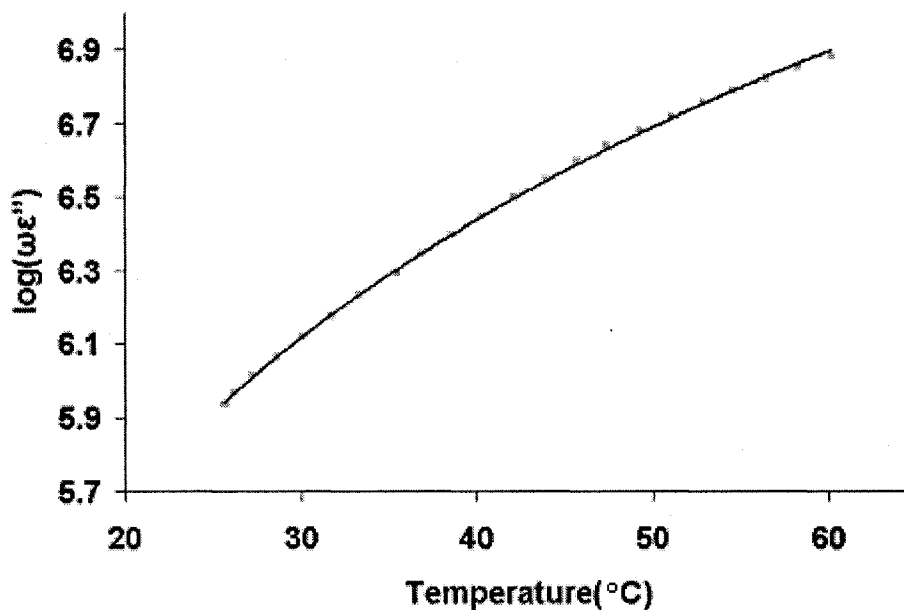
Figure 6.16 $\log(\varepsilon"\omega)$ versus temperature for pure CD540 without UV radiation

It is found from Figure 6.16 that the value of $\log(\varepsilon"\omega)$ is a function of temperature for pure CD540 as shown in Equation 6-11.

$$\log(\varepsilon"\omega) = 1.12 \times T + 2.3 \qquad \text{Equation 6-11}$$

T represents the temperature in the unit of $^\circ$C here.

Since the systems that are studied in this chapter only have a little initiator dissolved in them, it is reasonable to assume that Equation 6-11 is also correct for other systems with less than 0.4wt% [PI] studied in this chapter. Using Equation 6-11 to calculate the change of $\log(\varepsilon"\omega)$ due to the change of temperature at the bottom of the sample, the FDEMS data curve after temperature correction is shown in Figure 6.17. This correction has some error as the cure proceeds since Equation 6-11 is for the uncured CD540. Fortunately, the temperature at the bottom of the mold is not much higher than

room temperature during the cure. Therefore the correction for the effect of the temperature on FDEMS output during the curing process is small at the bottom of the mold.
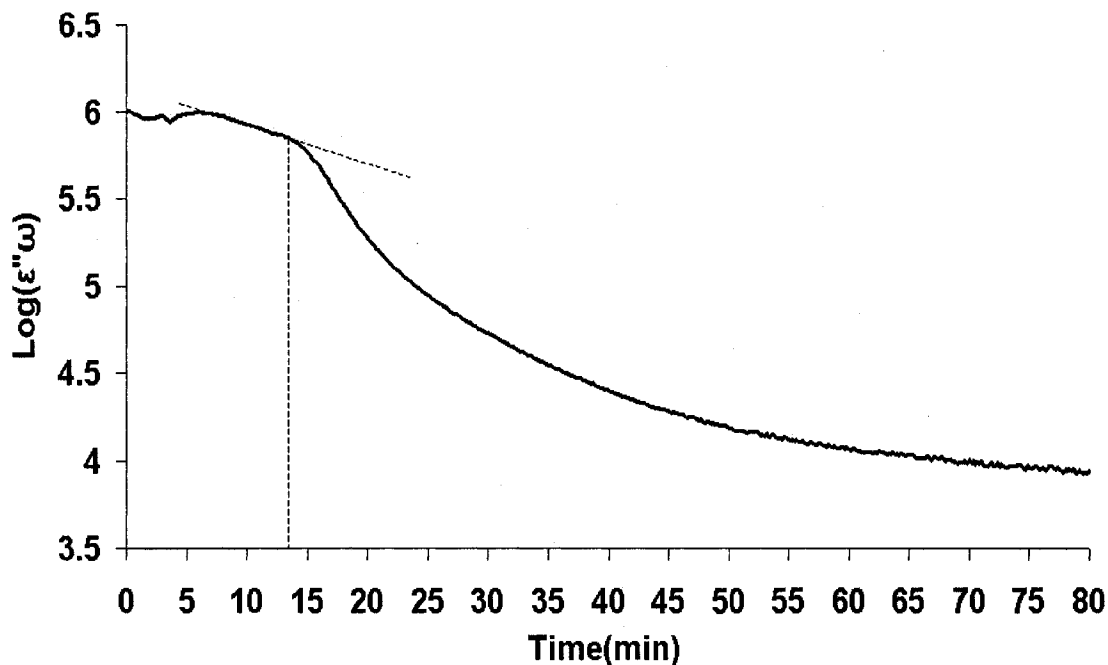


Figure 6.17 The values of log($\varepsilon$"$\omega$) versus exposure time after temperature correction at the bottom of the sample, CD540-0.2wt%IC819, Ii=65 $\mu w$/cm$^2$, thickness=4 mm, f=0.1kHz.

Figure 6.17 shows the FDEMS data measured at the bottom of the sample after the temperature correction. It looks much more reasonable since log($\varepsilon$"$\omega$) decreases with exposure time. It is known from chapter 5 that log($\varepsilon$"$\omega$) stays constant or drops slowly during the inhibition period. After that it experiences a fast decrease which is matched by the increase of C=C conversion measured by FTIR.

The start point of the reaction is where the value of log($\varepsilon$"$\omega$) starts decreasing sharply, at about 5.9, a value which varies little for different samples. The start point for

the experiment in Figure 6.17 is shown as the break point where two dashed lines cross. Sometimes the break point is not sharply defined. In this case the point of 5.9 is taken as the start of the reaction.

Once the reaction started at the location of the sensor, the bottom of the sample, the conversion value of each point in time in Figure 6.17 can be determined according to the $\log(\varepsilon''\omega)$ value and using the correlation curve of $\log(\varepsilon''\omega)$ versus C=C conversion shown in Figure 5.6 in Chapter 5. Therefore, the curve of conversion for each film thickness versus exposure time can be determined. In order to simplify this process, a simple Matlab program (Appendix 4) is written using Equation 5-3 to calculate the conversion versus exposure time according to $\log(\varepsilon''\omega)$ values.

Using the method described above, the cure kinetics as a function of depth are studied first by monitoring the cure of samples with the same composition but **different thicknesses**. Second, the exposure **intensity** effect on the cure kinetics at a particular depth is measured by the dielectric measurement. Third, the **initiator concentration** effect on the cure kinetics at a particular depth is studied. Last, the **experimental** data will be compared with the **theoretical model predicted** data in the same figure to compare the difference between them.

(1) The cure curves of CD540-Irgacure 819 at two different depths under the same incident radiation intensities are shown in Figures 6.18 and 6.19. Figure 6.18 is for the cure of the system with 0.05wt% photo initiator concentration under $130 \mu w / cm^2$ radiation intensity and Figure 6.19 is for the cure of the system with 0.2wt% photo initiator concentration under $65 \mu w / cm^2$ radiation intensity.
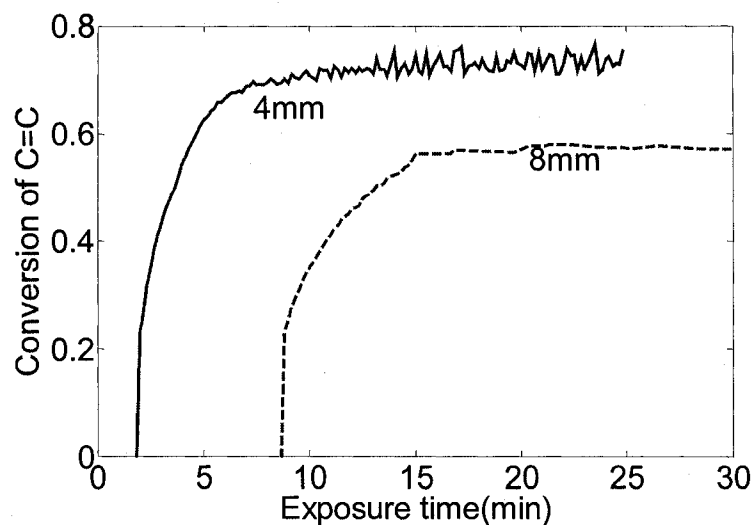
Figure 6.18 Dielectric converted values using Equation 5-3. Cure kinetics of CD540-0.05wt%Irgacure 819 at the depth of 4 and 8 mm under the radiation intensity of $130 \mu w / cm^2$. (———) Sample thickness=4 mm. (— — —) Sample thickness=8 mm.
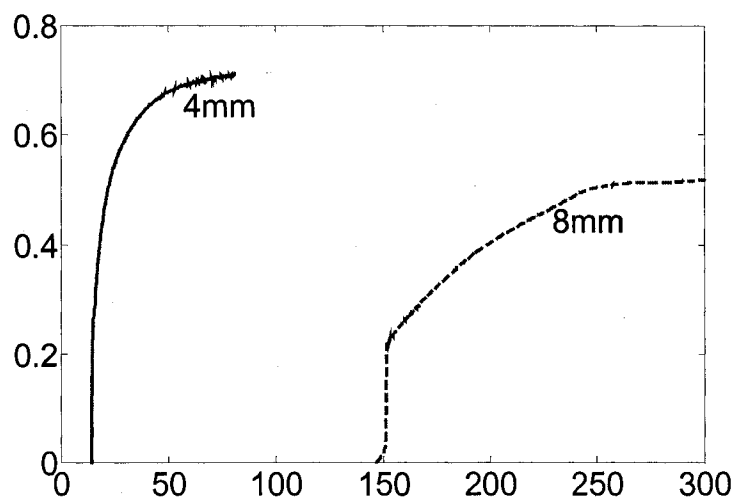


Figure 6.19 Dielectric converted values using Equation 5-3. Cure kinetics of CD540-0.2wt%Irgacure 819 at the depth of 4 and 8 mm under the radiation intensity of $65 \mu w / cm^2$. (———) Sample thickness=4 mm. (— — —) Sample thickness=8 mm.

Both Figures 6.18 and 6.19 show that the cure at 4 mm depth starts earlier and the cure rate is faster than the cure at 8 mm depth. This result is because the light intensity decreases with depth. It is similar to what was predicted in Section 6.3.1.

(2) Next, the exposure intensity effect on the cure kinetics at a particular depth is measured by the dielectric sensor. The cure curves of an 8 mm thick sample CD540-0.2wt% Irgacure 819 under two different incident radiation intensities is shown in Figure 6.20.
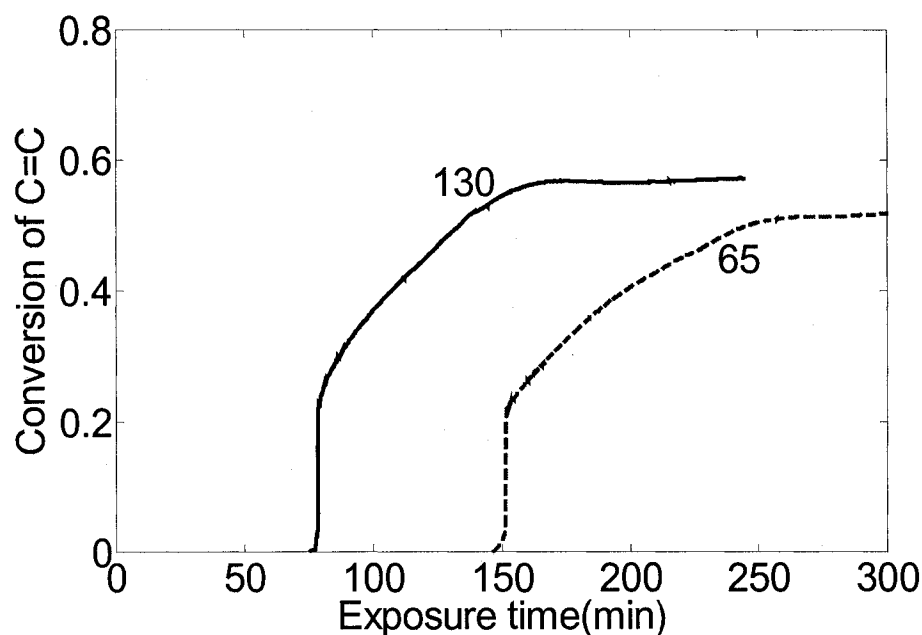
Figure 6.20 Dielectric converted values using Equation 5-3. Cure kinetics of CD540-0.2wt%Irgacure 819 at the depth of 8 mm under two different radiation intensities.
(——)130 $\mu w / cm^2$, (— — — —) $65 \mu w / cm^2$.

It is found from Figure 6.20 that the cure at a particular depth of a thick sample is very similar to the cure of a thin sample and the delay time is approximately inversely proportional to the incident light intensity. This is because the transmitted intensity at a particular depth is proportional to the incident intensity according to the Beer-Lambert Law (Equation 3-1) in Chapter 3.

(3) The initiator concentration effect on the cure kinetics at particular depth is studied next. Figure 6.21 shows cure curves at 4 mm depth of two samples with different photo initiator concentration but under the same incident radiation intensity.
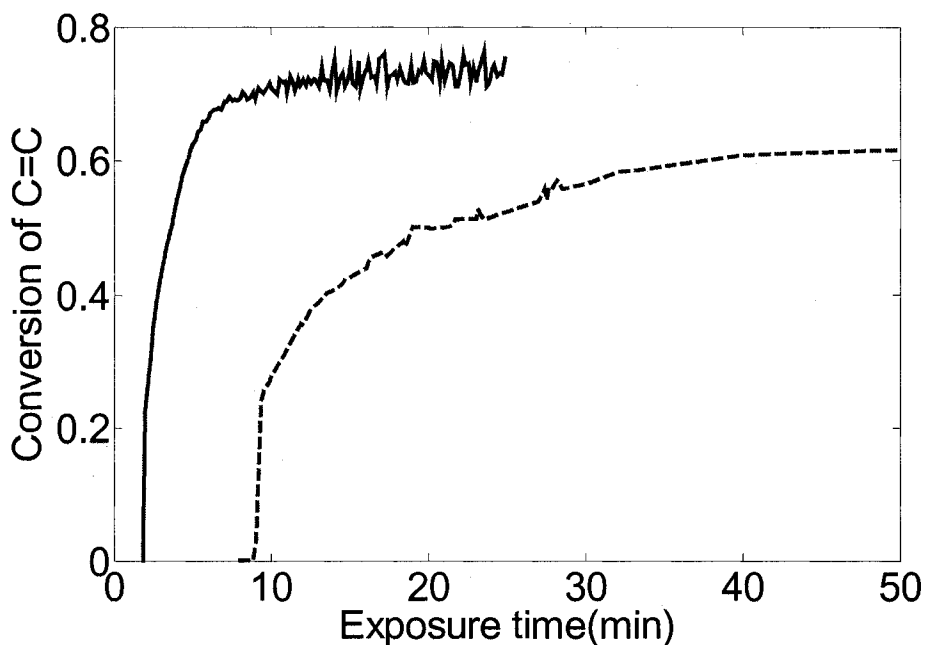


Figure 6.21 Dielectric converted values using Equation 5-3. Cure kinetics of CD540-Irgacure 819 at the depth of 4 mm under the incident radiation intensity of $130\ \mu w/cm^2$.

(———) [PI]=0.05wt%, (— — —) [PI]=0.2wt%.

Figure 6.21 shows that the cure rate at the 4 mm depth does not increase for the system with a higher initiator concentration under the same incident intensity. This result explains the curves in Figure 6.8 in which the bulk cure rate is slower for the system with a higher initiator concentration due to the decrease in intensity.

(4) Last, the cure kinetics measured by dielectric sensors will be compared with the theoretical prediction. Figures 6.22 to 6.30 show all the experimental data measured under different conditions and the corresponding predicted data together in the same plot. The results are analyzed in Table 6.3 following these figures.



Figure 6.22 Cure kinetics at the depth of 4 mm for the system CD540-0.05wt%IC819, Ii=130 $\mu w$/cm$^2$, f=0.1kHz. ($\blacklozenge$) Experimental data derived from FDEMS result, (————) calculated data.

Figure 6.23 Cure kinetics at the depth of 8 mm for the system CD540-0.05wt%IC819,

$I_i$=130 $\mu w$/cm$^2$, f=0.1kHz. (♦) Experimental data derived from FDEMS result, (———)
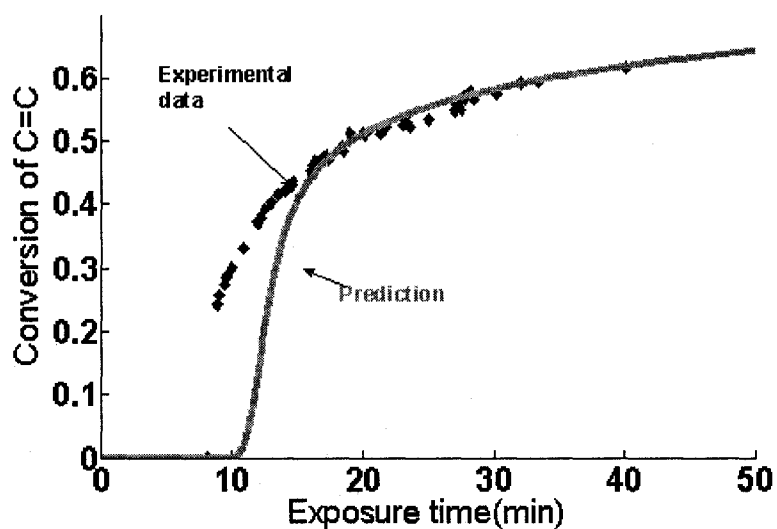
calculated data.



Figure 6.24 Cure kinetics at the depth of 4 mm for the system CD540-0.2wt%IC819,

Ii=130 $\mu w$/cm$^2$, f=0.1kHz. (♦) Experimental data derived from FDEMS result, (— — —)

calculated data using 4 mm (spacer thickness) as the thickness.
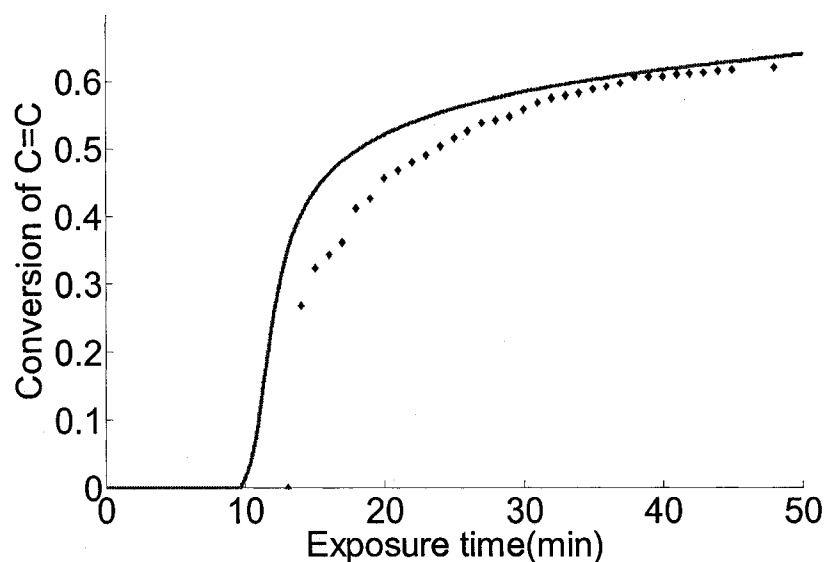
Figure 6.25 Cure kinetics at the depth of 2 mm for the system CD540-0.4wt%IC819,

Ii=65 $\mu w$/cm$^2$, f=0.1kHz. ($\blacklozenge$) Experimental data derived from FDEMS result, (———)

calculated data.



Figure 6.26 Cure kinetics at the assumed depth of 4 mm for the system CD540-

0.2wt%IC819, I$_i$=65 $\mu w$/cm$^2$, f=0.1kHz. (———) Experimental data derived from FDEMS

result, (— — — —) calculated data using 4 mm (spacer thickness) as the thickness.

Figure 6.27 Cure kinetics at the depth of 3 mm for the system CD540-0.4wt%IC819,

Ii=30 μw/cm², f=0.1kHz. (———) Experimental data derived from FDEMS result, (— —

—) calculated data using 3 mm (spacer thickness) as the thickness.
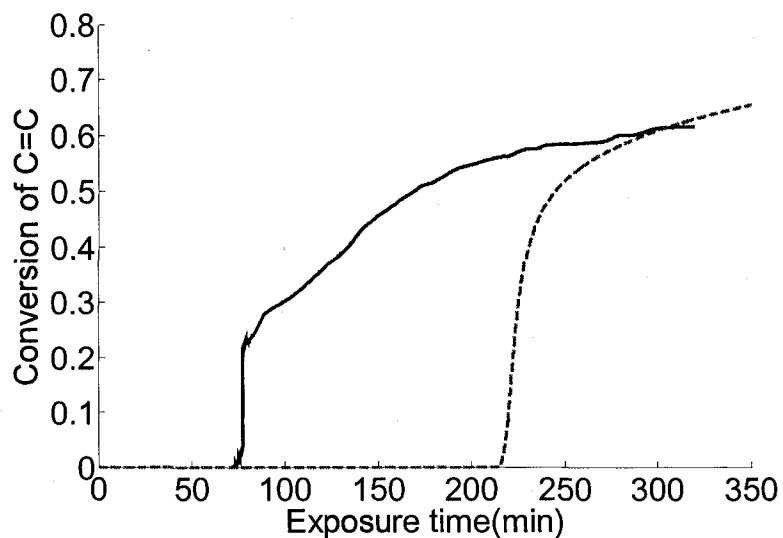


Figure 6.28 Cure kinetics at the depth of 4 mm for the system CD540-0.4wt%IC819,

Ii=65 μw/cm², f=0.1kHz. (———) Experimental data derived from FDEMS result, (— —

—) calculated data using 4 mm (spacer thickness) as the thickness.
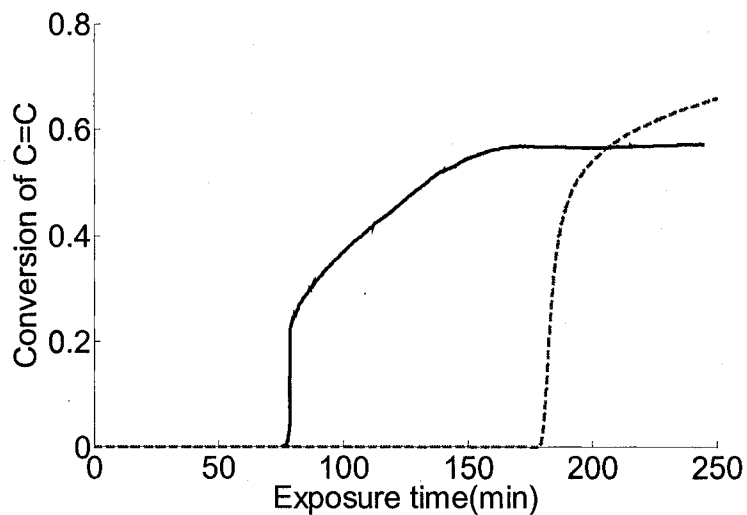
Figure 6.29 Cure kinetics at the depth of 8 mm for the system CD540-0.2wt%IC819,

Ii=130 μw /cm$^2$, f=0.1kHz. (——) Experimental data derived from FDEMS result, (— —

—) calculated data using 8 mm (spacer thickness) as the thickness.
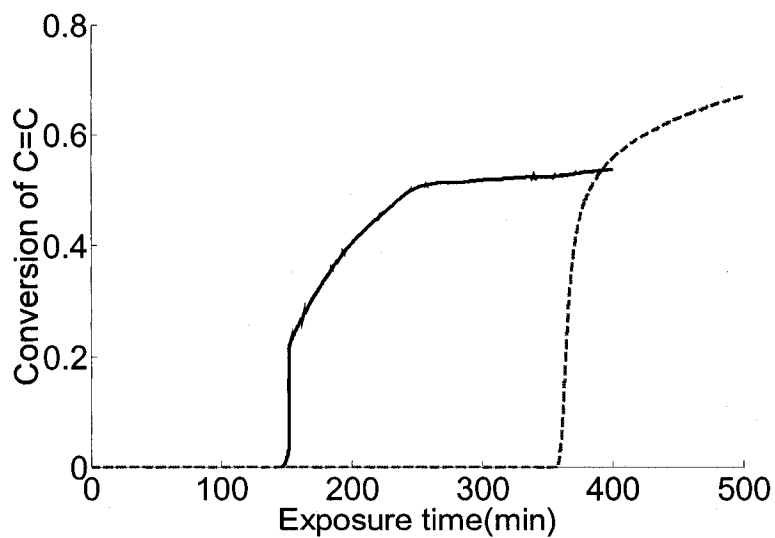


Figure 6.30 Cure kinetics at the depth of 8 mm for the system CD540-0.2wt%IC819,

Ii=65 μw /cm$^2$, f=0.1kHz. (——) Experimental data derived from FDEMS result, (— —

—) calculated data using 8 mm (spacer thickness) as the thickness.

The cure conditions and the relationship between the experimental data and the corresponding predicted data of the UV polymerization from Figure 6.22 to 6.30 are listed in Table 6.3. Figures in the table are arranged according to the length of the inhibition period.

Table 6.3 UV cure under different conditions: experimental data and theoretical calculation

| Figure | [PI] wt% | Incident intensity $\mu w/cm^2$ | Sample Thickness mm | Delay time (min) | | Final conversion Experiment data matches Predicted data |
|--------|----------|----------|----------|-----|---------|------|
| | | | | Exp. | Predict | |
| 6.22 | 0.05 | 130 | 4 | 2.8 | 2.5 | E>P |
| 6.23 | 0.05 | 130 | 8 | 8.6 | 7.5 | N/A |
| 6.24 | 0.2 | 130 | 4 | 8 | 10 | Good |
| 6.25 | 0.4 | 65 | 2 | 13 | 10 | Good |
| 6.26 | 0.2 | 65 | 4 | 14 | 21 | E>P |
| 6.27 | 0.4 | 30 | 3 | 72 | 120 | OK |
| 6.28 | 0.4 | 65 | 4 | 75 | 215 | E<P |
| 6.29 | 0.2 | 130 | 8 | 76 | 180 | E<P |
| 6.30 | 0.2 | 65 | 8 | 147 | 360 | E<P |

Note: E represents experimental values and P represents predicted values, "<" represents "less than", ">" represents "more than", "Good" means "matches very well", "Ok" means "matches but not quite well".

Table 6.3 shows that the predicted inhibition periods fit the experimental data well when the inhibition period of the cure at the bottom of a sample is less than 13 minutes. However, when the inhibition period is long, the experimental value of inhibition period is obviously shorter than the predicted value as shown in Figures 6.27 to 6.30. There are several reasons for the difference between the experimental data and the predicted data. The most **likely reason** is that the real transmitted intensity at the bottom of the sample is higher than the predicted values. This was also observed in Chapter 3 for thick samples with a very high absorption of light. A possible reason that was proposed in Chapter 3 is the error of using the thickness of the spacer as the exact sample thickness. When a smaller thickness value based on the measured intensity at the bottom is used, the predicted curves match the experimental curves better as shown in Figures 6.31 to 6.35.
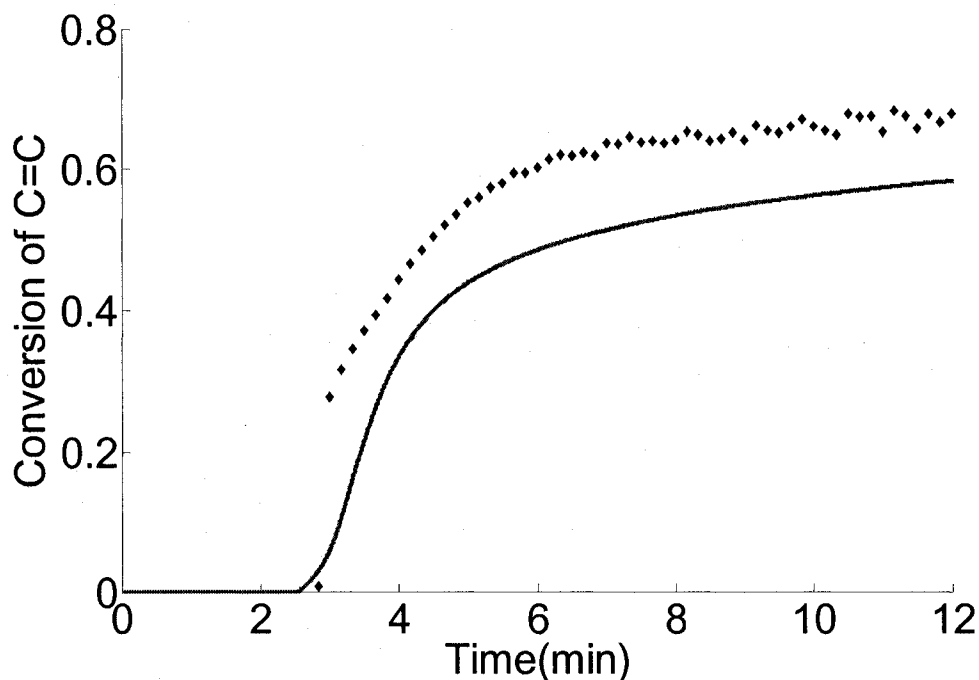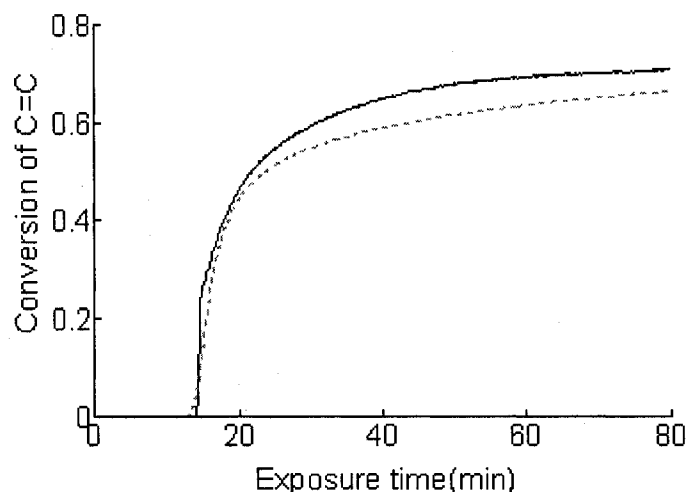


Figure 6.31 (see older Figure 6.26) Cure kinetics at the assumed depth of 4 mm for the system CD540-0.2wt%IC819, $I_i$=65 $\mu w$/cm$^2$, f=0.1kHz. (———) Experimen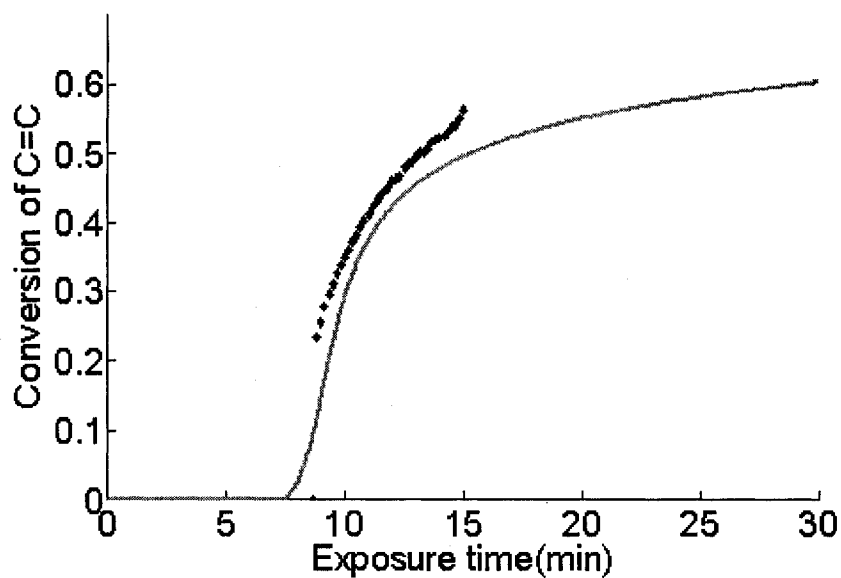tal data derived from FDEMS result, (------) calculated data using 3.5 mm (calculated using transmitted intensity) as the thickness.
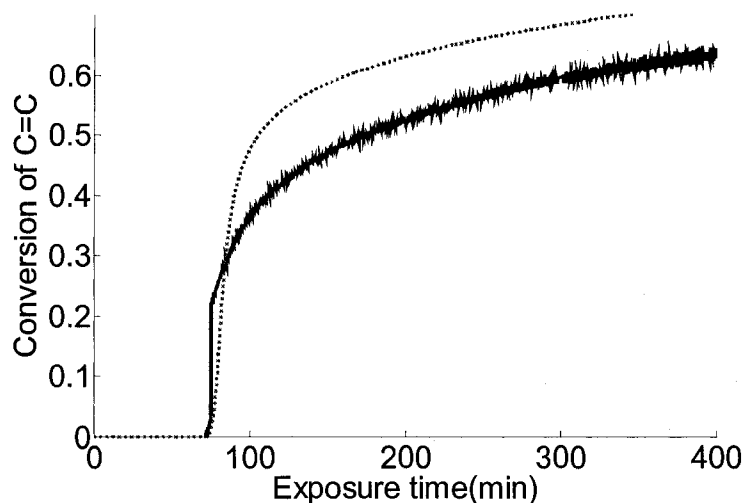
Figure 6.32 (see older Figure.6.27) Cure kinetics at the depth of 3 mm for the system

CD540-0.4wt%IC819, $I_i$=30 µw/cm$^2$, f=0.1kHz. (——) Experimental data derived from

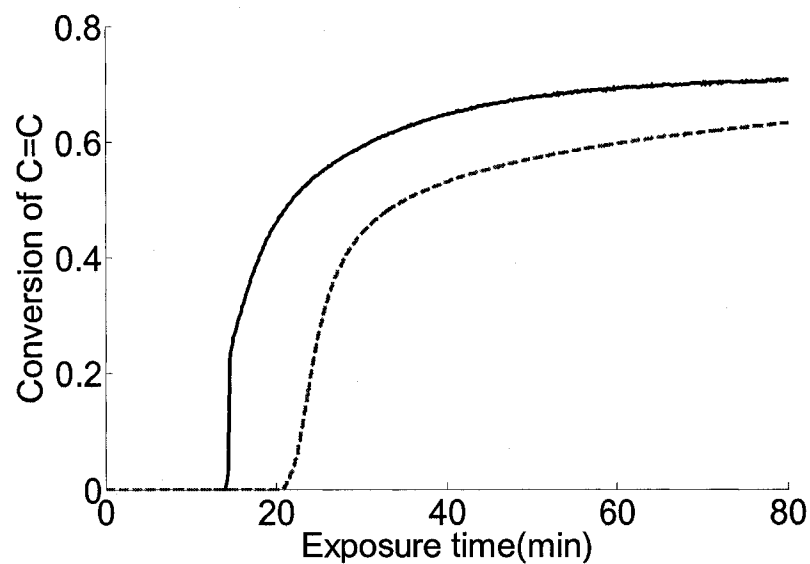FDEMS result, (------) calculated data using 2.7 mm (calculated using transmitted

intensity) as the thickness.
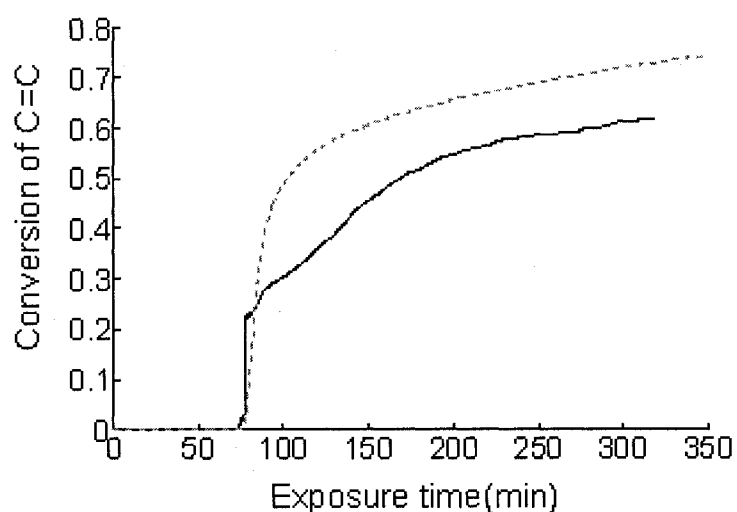


Figure 6.33 (see older Figure 6.28) Cure kinetics at the depth of 4 mm for the system

CD540-0.4wt%IC819, Ii=65 µw/cm$^2$, f=0.1kHz. (——) Experimental data derived from

FDEMS result, (------) calculated data using a best fit 3.2 mm as the thickness.

(transmitted light intensity was not measured here)

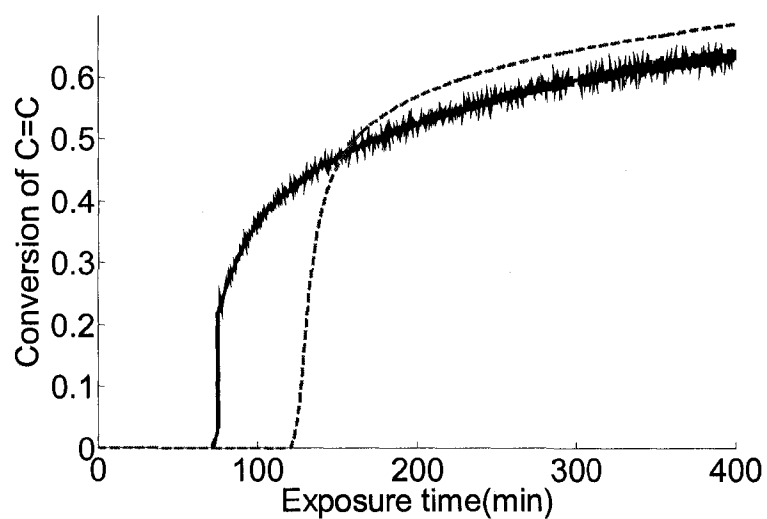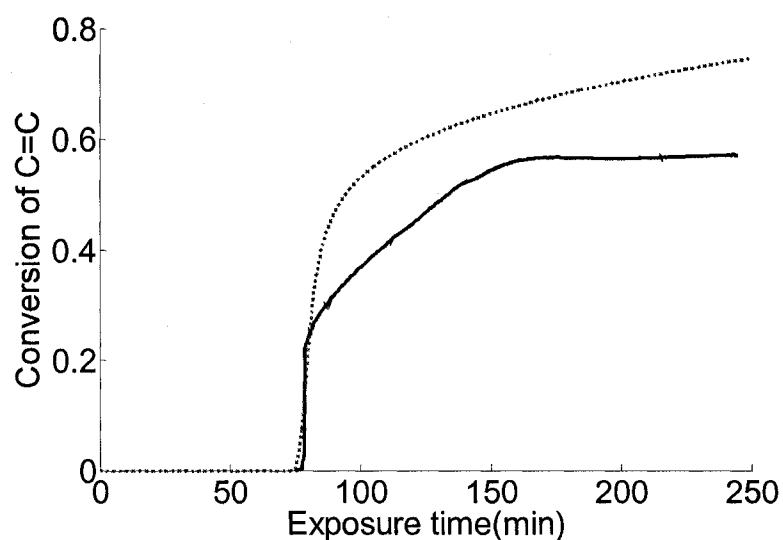Figure 6.34 (see older Figure 6.29) Cure kinetics at the depth of 8 mm for the system

CD540-0.2wt%IC819, Ii=130 $\mu w$/cm$^2$, f=0.1kHz. (———) Experimental data derived from

FDEMS result, (------) calculated data using a best fit 6.5 mm as the thickness. (light

intensity was not measured here)
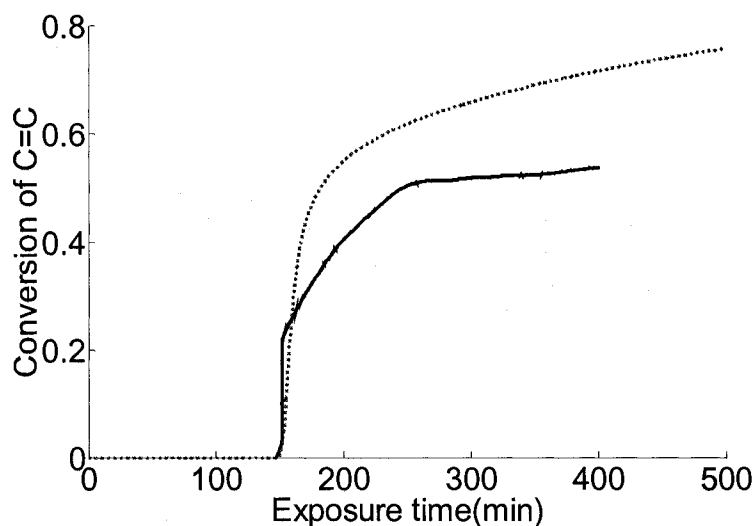


Figure 6.35 (see older Figure 6.30) Cure kinetics for the system CD540-0.2wt%IC819,

Ii=65 $\mu w$/cm$^2$, f=0.1kHz. (———) Experimental data derived from FDEMS result, (------)

calculated data using a best fit 6.5 mm as the thickness. (Light intensity was not

measured here)

Figures 6.31 and 6.32 shows that using the thickness calculated from transmitted intensity, the model predictions matches the experimental data well. The calculated thickness is less than the spacer thickness and their values are listed in Table 6.4. For some experiments that we did not measure the transmitted intensities, we use a thickness value (shown in Table 6.4) that makes the model predictions fits the experimental data best.

Table 6.4 Correction of thickness for the prediction

| Figure | Delay time (min) | [PI] wt% | Incident intensity $\mu w/cm^2$ | Sample Thickness (mm) | | |
|---|---|---|---|---|---|---|
| | | | | Based on space | Based on $I_t$ | Based on best fit |
| 6.22 | 2.8 | 0.05 | 130 | 4 | | |
| 6.23 | 8.6 | 0.05 | 130 | 8 | | |
| 6.24 | 8 | 0.2 | 130 | 4 | | |
| 6.25 | 13 | 0.4 | 65 | 2 | | |
| 6.26/6.31 | 14 | 0.2 | 65 | 4 | 3.5 | |
| 6.27/6.32 | 72 | 0.4 | 30 | 3 | 2.7 | |
| 6.28/6.33 | 75 | 0.4 | 65 | 4 | | 3.2 |
| 6.29/6.34 | 76 | 0.2 | 130 | 8 | | 6.7 |
| 6.30/6.35 | 147 | 0.2 | 65 | 8 | | 6.5 |

Table 6.4 shows that the calculated thickness using the transmitted intensity is 0.5 mm (0.3 mm) less than the spacer thickness and the error of using spacer thickness as the

sample thickness is less than 12.5%. For the experiments that we did not measure the transmitted intensity, the thickness for a best fit is 20% less than the spacer thickness. This result proves that the error of using the thickness of the spacer as the exact sample thickness is a likely reason for the difference between some model predictions and the experimental curves.

In addition, the diffusion of substances, such as oxygen, initiator, and free radicals between layers is another possible reason for a shorter inhibition period. And we believe the diffusion effect is more significant for the sample with more absorption of light and therefore a longer inhibition period. This will be studied in Chapter 7. Further, the experimental method itself has several additional sources of error. First, the correlation curve obtained in Chapter 5 shows about 10% error in prediction of conversion at high conversions. Second, when the conversion is less than 25%, a small change in $\log(\varepsilon''\omega)$ results in a large change in conversion as shown in Figure 5.9 at Chapter 5. This results in very few data points between 0 and 25% conversion and also results in a large error in the predicted conversion due to small error in $\log(\varepsilon''\omega)$. Third, the value of $\log(\varepsilon''\omega)$ is sensitive to the change of temperature. Thus for the curves that have been adjusted by the change of temperature, this adjustment involves some error. Fourth, an increase of temperature in the sample also results in an increase in the cure rate and the final conversion as shown in Figure 6.22, which is higher than those model predictions. The temperature effect on the cure will be studied in Sections 6.3.4 and 6.3.5.

Due to the complexities of the experimental method and optical properties of the system which has such a strong absorption of light, it is very hard to clarify which are the major reasons for the difference between the experimental data and the predicted data of

thick samples that have strong absorption. But when the absorption is not high and the inhibition period is shorter than 13 minutes, the predicted curves match well the experimental data.

### 6.3.4 Study of the temperature versus exposure time at different depths in thick samples

It has been discussed above that the increase of temperature in samples results in an increase in the reaction rate and the final conversion and hence a difference between the experimental and the predicted curves as shown in Figure 6.22 (6.13 and 6.14). Therefore, it is important to correct the model prediction for changing temperature inside thick samples to understand more about the cure kinetics.

Figures 6.36 to 6.43 show the experimental data of temperature versus exposure time at different positions inside samples of different thickness and under varying radiation intensities.
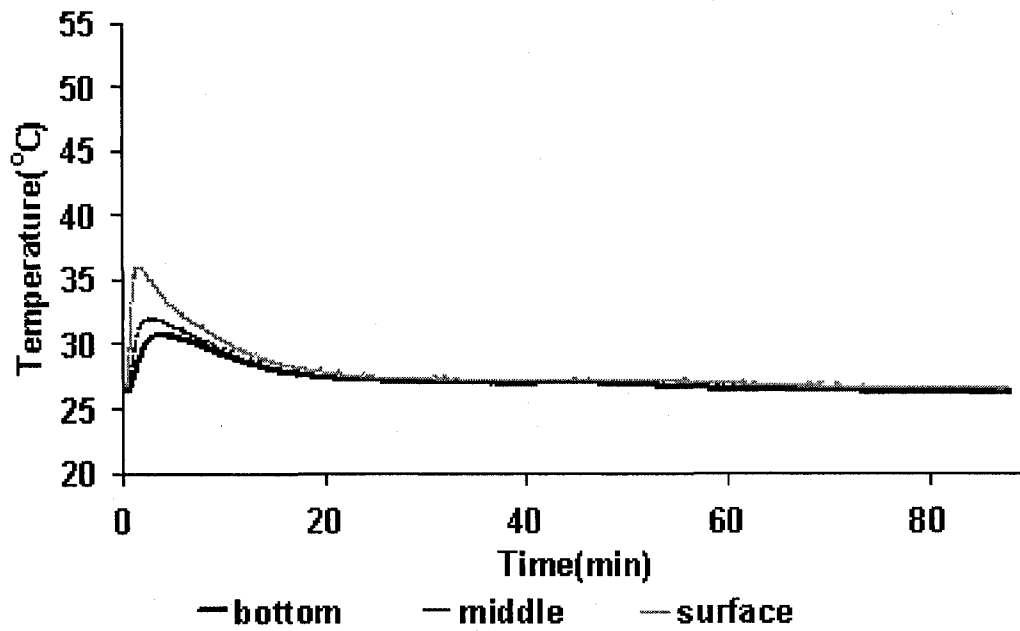
Figure 6.36 (see older Fig. 6.33) CD540-0.4%IC819, Ii=65 μ w/cm², thickness=4 mm.
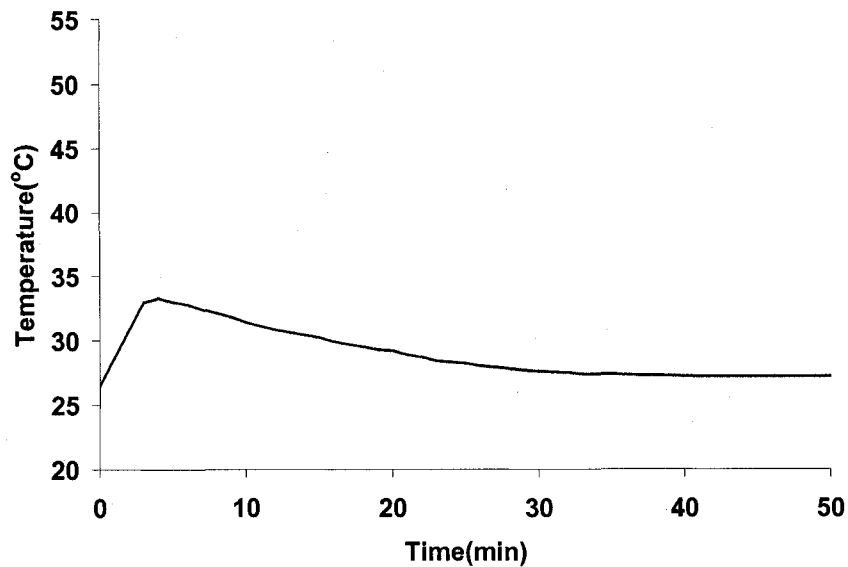


Figure 6.37 (see older Fig. 6.25) CD540-0.4%IC819, Ii=65 μ w/cm², thickness=2 mm.

The thermocouple wire is in the middle of the mold.
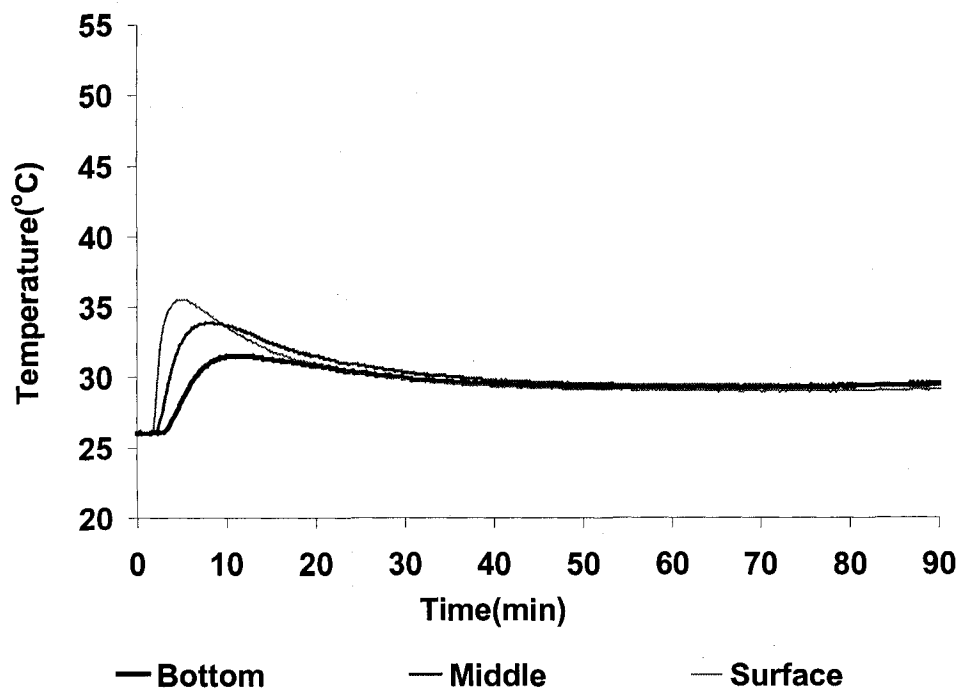
Figure 6.38 (see older Fig.6.35) CD540-0.2wt%IC819, I=65 μ w/cm², Thickness=8 mm

(6.5 mm based on the best fit)
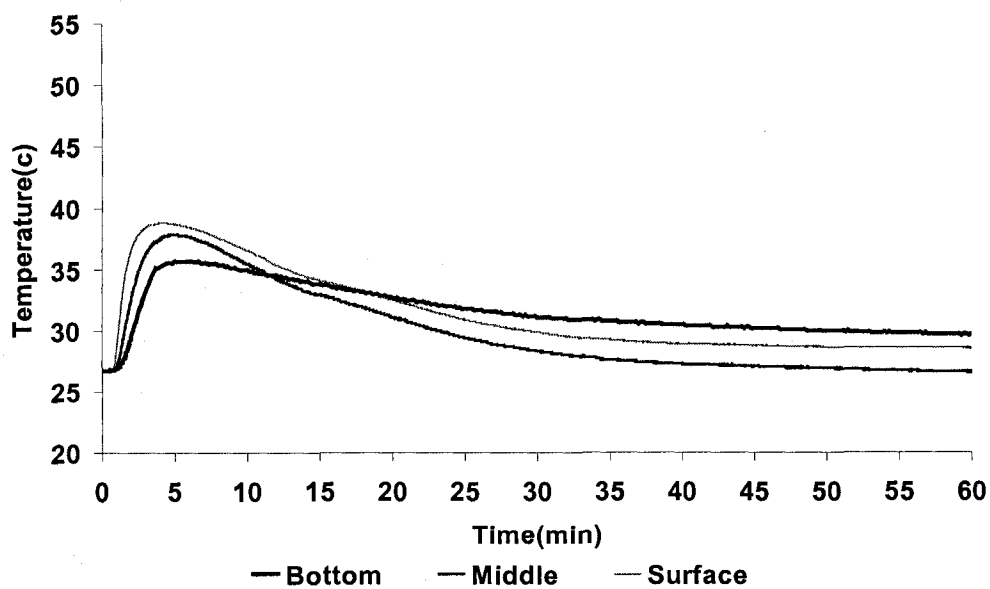


Figure 6.39 (see older Fig.6.31) CD540-0.2wt%IC819, I=65 μ w/cm², spacer thickness =

4 mm (3.5 mm based on transmitted intensity)
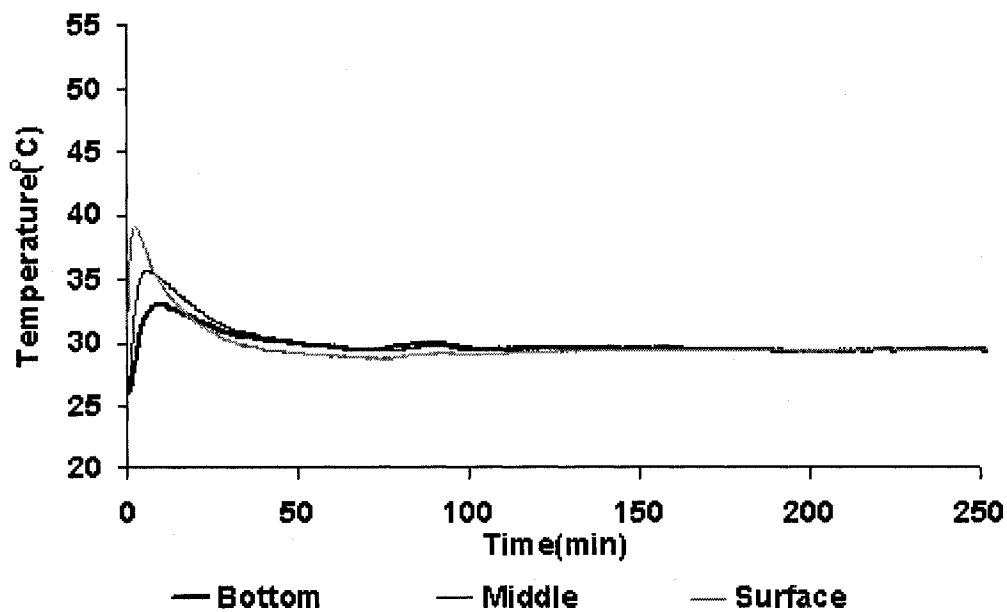
Figure 6.40 (see older Fig.6.29) CD540-0.2wt%IC819, I=130 μ w/cm$^2$, spacer thickness

= 8 mm (6.5 mm based on the best fit).
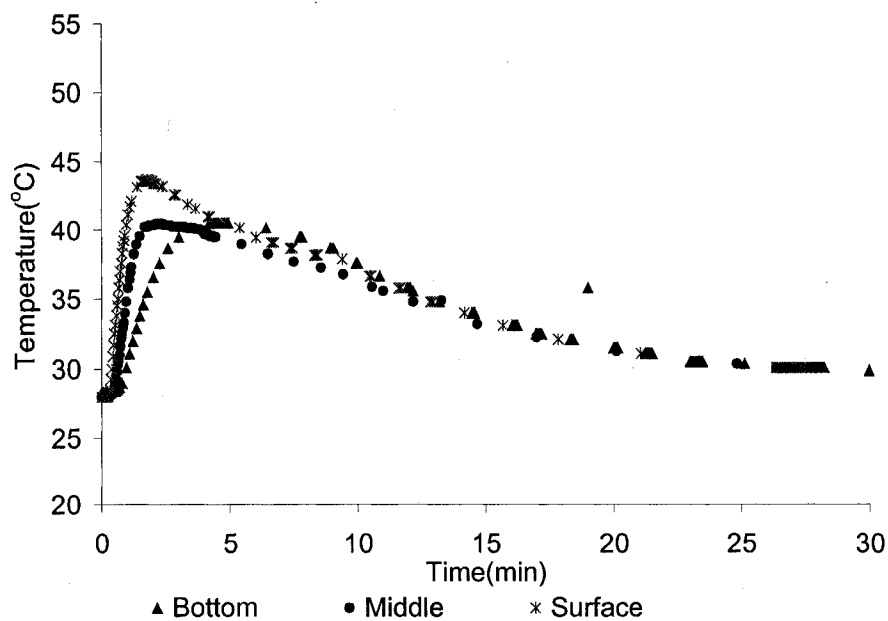


Figure 6.41 (see older Fig.6.24) CD540-0.2wt%IC819, I=130 μ w/cm$^2$, Thickness=4 mm.
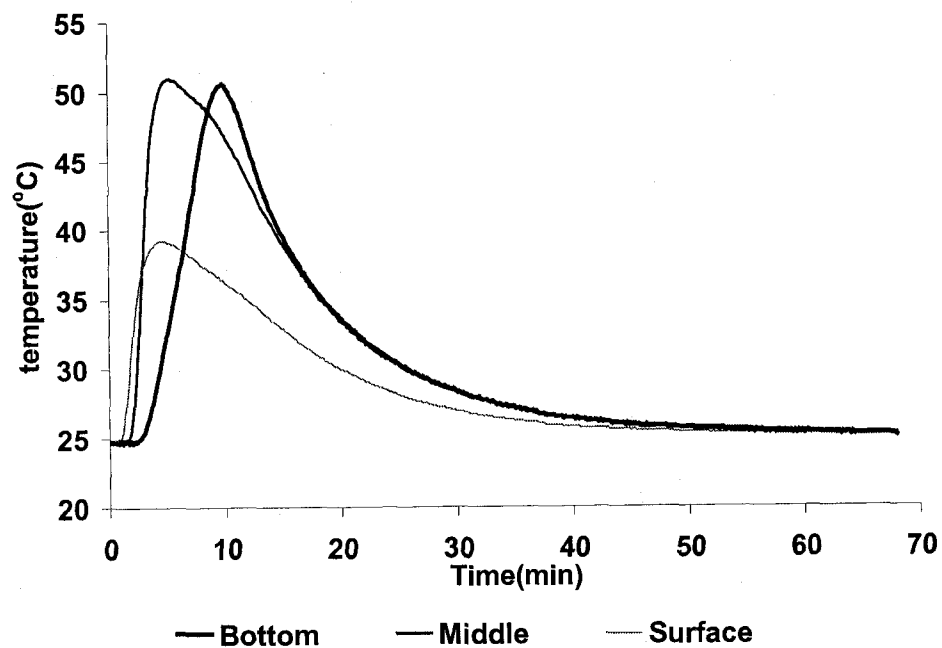
Figure 6.42 (see older Fig.6.23) CD540-0.05wt%IC819, I=130 $\mu$ w/cm$^2$, Thickness=8

mm.
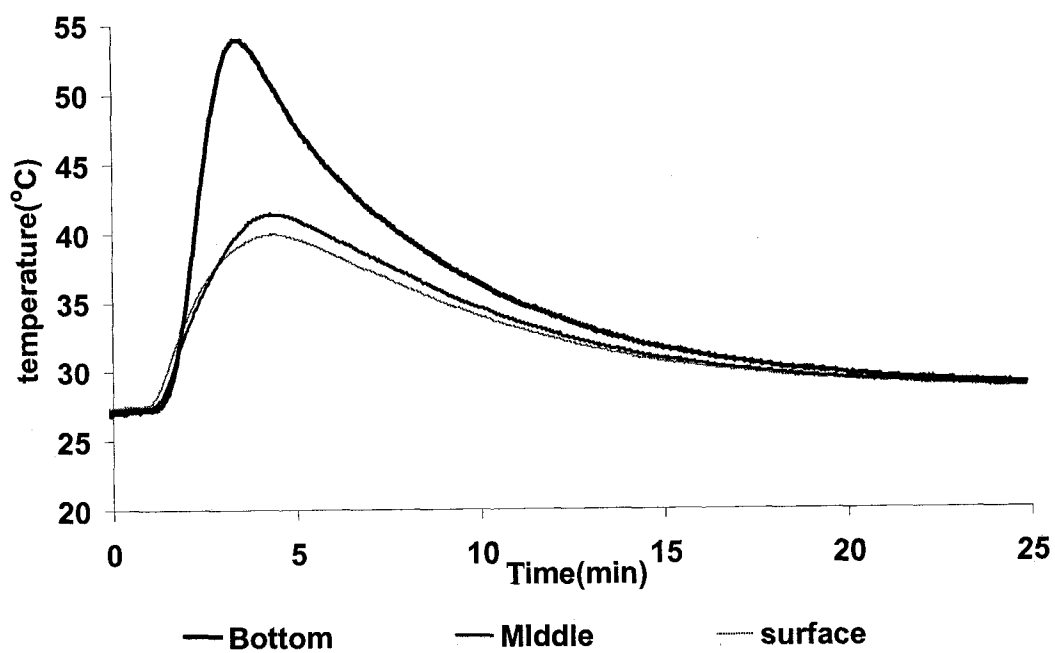


Figure 6.43 (see older Fig. 6.22) CD540-0.05wt%IC819, I=130 $\mu$ w/cm$^2$, thickness = 4

mm

These 8 figures show that the temperature increases first and then decreases with exposure time. The change of temperature is due to two effects. One is the heat released from the cure reaction and another is heat transmitted to the environment. The resulting increase in temperature is proportional to the net heat released from the reaction minus the heat transmitted to the environment at each point in time. It was also found that the temperature of samples at different depths was affected by the radiation intensity and initiator concentration. In order to study this more conveniently, the increase of the temperature at different depths in thick samples for the cure under different conditions are listed in Table 6.5.

Table 6.5 Increase of temperature in thick samples during the cure under different conditions

| Figure Number | [PI] wt% | Intensity $\mu w/cm^2$ | Sample Thickness | Maximum increase of Temperature ($^{o}$C) | | |
|---|---|---|---|---|---|---|
| | | | | Surface | Middle | Bottom |
| 6.36 | 0.4 | 65 | 4 | 9 | 5 | 4 |
| 6.37 | 0.4 | 65 | 2 | | 6 | |
| 6.38 | 0.2 | 65 | 8 | 10 | 8 | 6 |
| 6.39 | 0.2 | 65 | 4 | 12 | 11 | 9 |
| 6.40 | 0.2 | 130 | 8 | 13 | 10 | 7 |
| 6.41 | 0.2 | 130 | 4 | 16 | 13 | 12 |
| 6.42 | 0.05 | 130 | 8 | 14 | 26 | 25 |
| 6.43 | 0.05 | 130 | 4 | 12 | N/A | 27 |

Comparing Figures 5.33 with 5.35, and 5.34 with 5.36, it is found that increasing the radiation intensity can increase the peak value of the temperature at all three positions. This is reasonable since the net increase in temperature is proportional to the cure rate and hence the radiation intensity. Comparing 6.31 with 6.34, 6.35 with 6.37, and 6.36 with 6.38, it is found that the increase in temperature at the bottom of the sample is higher for the system with less photo initiator for the [PI] range studied here. This is because the intensity at the bottom of the sample is much lower for the system with high initiator concentration. The result also shows that the increase of the temperature at the bottom of the sample CD540-0.05wt%Irgacure 819 is more than $25^{\circ}C$. This explains why the predicted cure rate and conversion is lower than the experimental data in Figure 6.13, 6.14, and 6.22. However, the surface temperature does not increase much with initiator concentration as might be expected. One reason may be that the transfer of heat to the environment is much faster near the surface.

### 6.3.5 Prediction of cure kinetics in thick samples with temperature adjustment

From Sections 6.3.3 and 6.3.4, it is known that temperature is an important reason for the deviation of predicted curves from the experimental curves. In this section, the model prediction is corrected for the temperature effect for four experiments including 6.39(6.31), 6.41(6.24), 6.42(6.23), and 6.43(6.22). These experiments have an increase in the bottom temperature of higher than $9^{\circ}C$. We do not adjust the temperature effect for the other four experiments listed in Table 6.5. The first reason is the increase of their bottom temperature is less than $7\ ^{\circ}C$. The second reason is the delay time before the reaction initiation at the bottom for the other four experiments is much longer. Thus by the time the cure starts, the bottom temperatures are almost back to room temperature.

In order to calculate the cure kinetics corrected for the temperature effect, we first fit the measured temperature at a particular depth in a thick sample to polynomials as shown in Figure 6.44 for the cure of CD540-0.05wt%IC819 at the incident intensity of $130 \, \mu w/cm^2$.
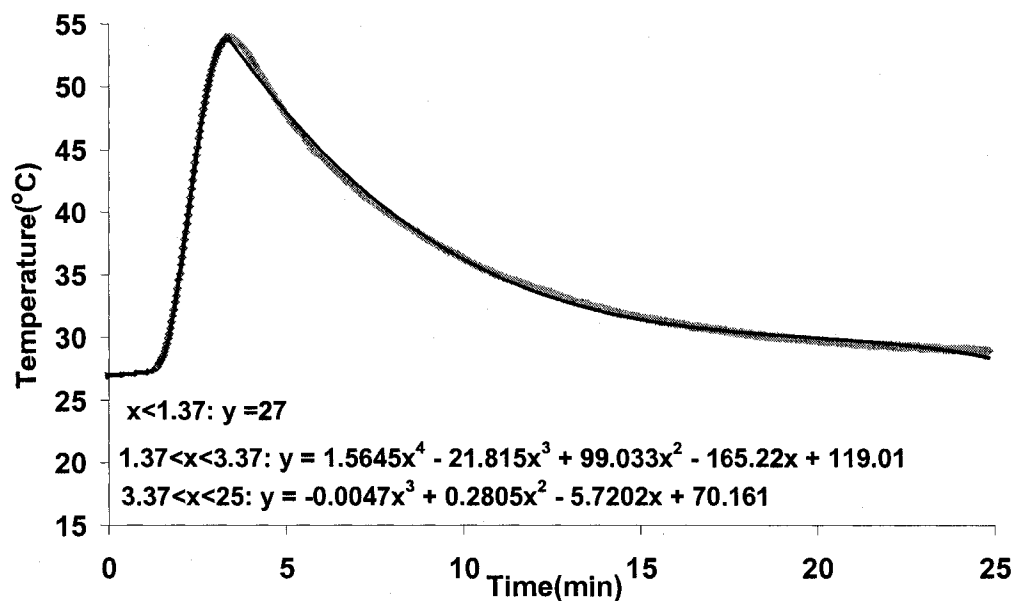


Figure 6.44 (see older Fig. 6.43) Temperature at the depth of 4 mm for the system CD540-0.05wt% IC819, $I_i$=130 $\mu w/cm^2$. ($\lozenge$) Measured temperature data, (—) fit to power series.

Next, the cure kinetics at varying temperatures are calculated by combining the prediction method for thick samples and the temperature effect on the cure kinetics parameters as described in section 4.34 (Chapter 4). The Matlab program for the calculation is shown in Appendix 6. The result is shown in Figure 6.45 compared with the experimental measured data and the predicted result without considering the temperature effect.
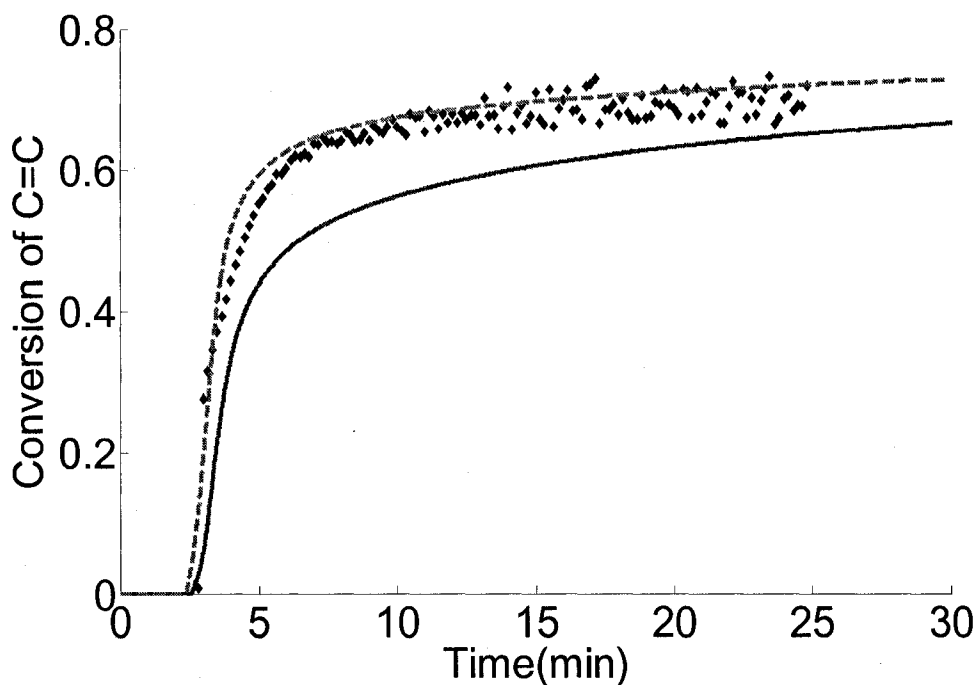
Figure 6.45 (see older Figure 6.22) Cure kinetics at the depth of 4 mm for the system

CD540-0.05wt%IC819, $I_i$=130 $\mu w$/cm$^2$, f=0.1kHz. (♦) Experimental data derived from

FDEMS result, (———) model prediction without considering temperature effect, (— — —)

model prediction after temperature adjustment.


Figure 6.45 shows that the predicted cure curve when considering the temperature

effect has a higher final conversion than the predicted result without considering the

temperature effect. In addition, the predicted result matches the experimental data well

with the temperature adjustment. Using the same method as described above, the

temperature at the bottom of the cure at three other conditions are fit to polynomials as

shown in Appendix 5. The cure curves after temperature adjustment are shown in Figures

6.46 to 6.48.
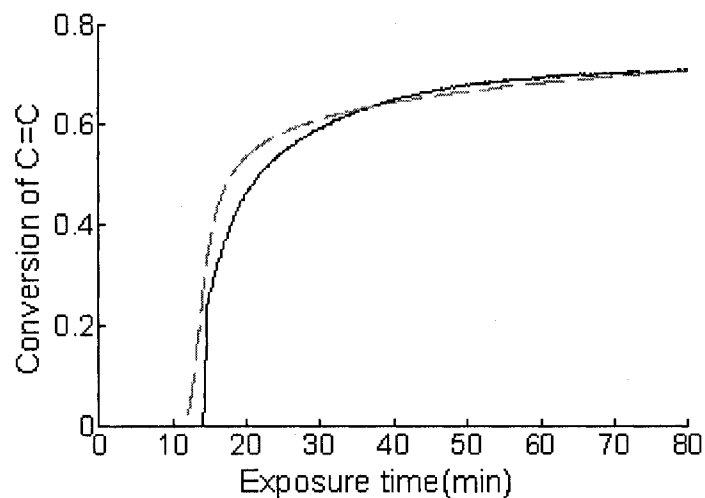
Figure 6.46 (Figure 6.31) Cure kinetics at the assumed depth of 4 mm for the system CD540-0.2wt%IC819, Ii=65 $\mu w$/cm$^2$, f=0.1kHz. (———) Experimental data derived from FDEMS result, (------) calculated data using 3.5 mm (calculated using transmitted intensity) as the thickness after temperature adjustment.
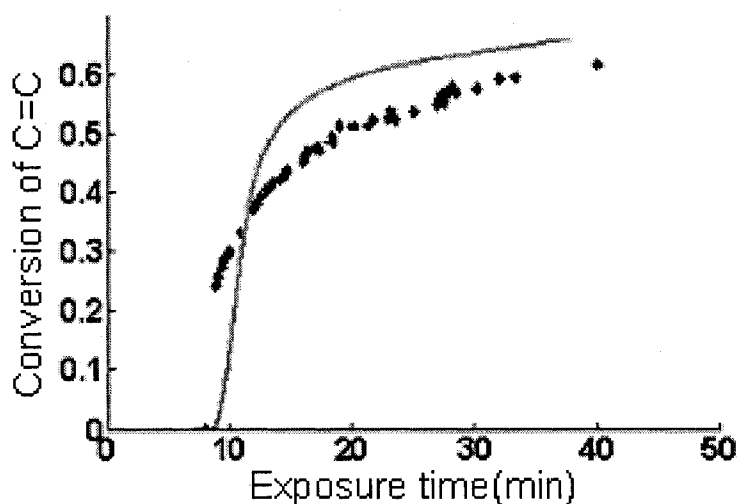


Figure 6.47 (Figure 6.24) Cure kinetics at the depth of 4 mm for the system CD540-0.2wt%IC819, I$_i$=130 $\mu w$/cm$^2$, f=0.1kHz. (♦) Experimental data derived from FDEMS result, (———) model prediction using 4 mm (spacer thickness) as the thickness after temperature adjustment.
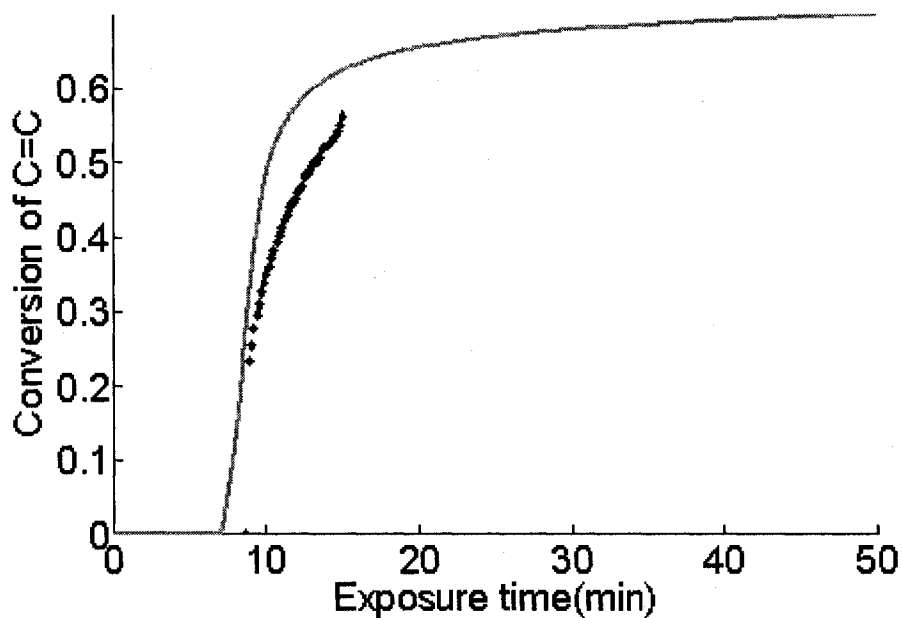
Figure 6.48 (Figure 6.23) Cure kinetics at the depth of 8 mm for the system CD540-

0.05wt%IC819, $I_i$=130 $\mu w$/cm$^2$, f=0.1kHz. (♦) Experimental data derived from FDEMS

result, (———) model prediction after temperature correction using spacer thickness as the

sample thickness.

Next, the model predictions of bulk cure kinetics (Figures 6.13 and 6.14) are

adjusted by temperature effect using the measured temperature in the middle of thick

samples. The results are shown in Figures 6.49 and 6.50.
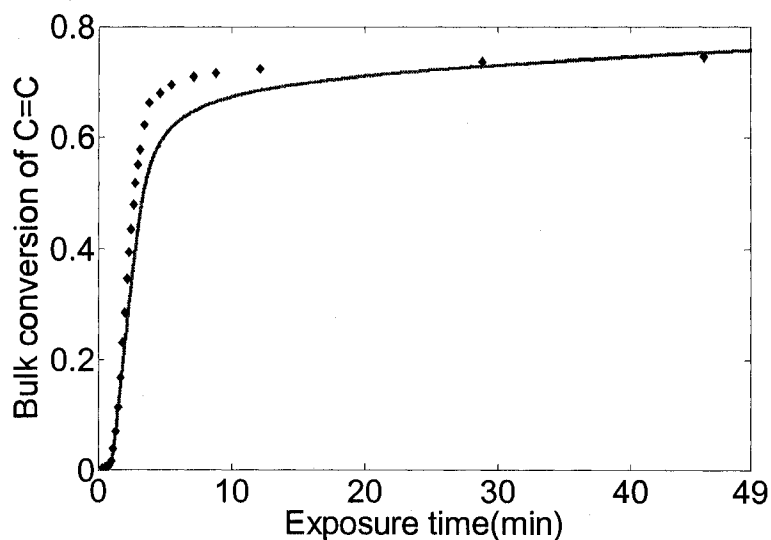
Figure 6.49 (see Figure 6.13) Bulk conversion versus time for the cure of 4 mm thick

system, CD540-0.05wt%Irgacure 819. $I_i = 130\mu w/cm^2$. (♦) FTIR measured data; (———)

Predicted cure curve after temperature correction.
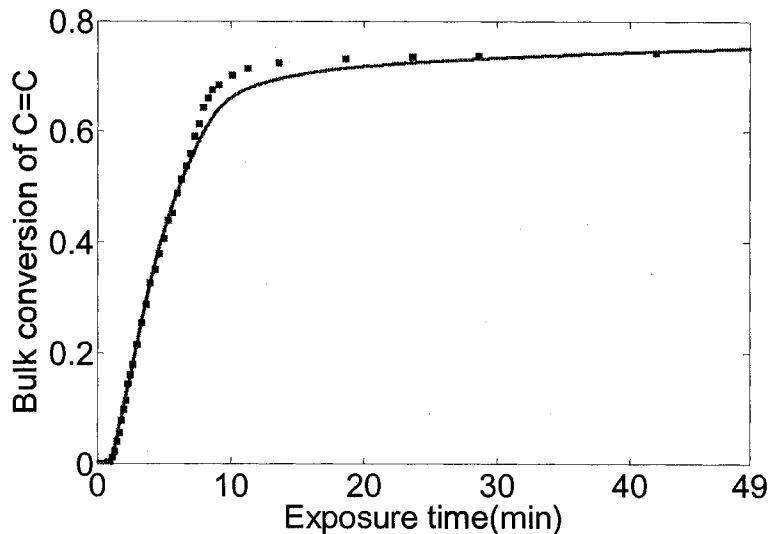


Figure 6.50 (see Figure 6.14) Bulk conversion versus time for the cure of 8 mm thick

system, CD540-0.05wt%Irgacure 819. $I_i = 130\mu w/cm^2$. (■) FTIR measured data; (———)

Predicted cure curve after temperature correction.

Compared with those predictions without considering temperature effect, Figures 6.45 to 6.50 shows that the prediction after temperature correction does fit experimental results better.

## 6.4 Conclusion

The study of thick samples shows that the UV cure kinetics are a function of depth, affected by radiation intensity, and also affected by initiator concentration. Increasing intensity will always increase the bulk cure rate, but increasing the initiator concentration can decrease the bulk cure rate as the sample thickness increases.

A Matlab program was written to calculate the cure kinetics at particular depths and the average cure kinetics through depth by dividing the thick samples into many thin layers (0.05 mm). The predicted result shows that the deeper the position, the slower the cure rate. It also shows that the increasing radiation intensity can always increase the bulk cure rate and shorten the inhibition period of the bulk cure of thick samples. However, increasing the photo initiator concentration, [PI], may decrease the cure rate. These results help explain how the radiation intensity and [PI] affect the cure as a function of depth in thick samples.

The bulk cure kinetics are monitored by transmitted real-time near FTIR and the result is compared to the corresponding predicted bulk UV cure curves. The results verified that the calculation model predicts well the bulk cure kinetics of thin samples at room temperature and can be used to predict the bulk cure of thick samples when the sample temperature does not increase more than 10°C without considering the temperature effect. If the temperature increases more, the calculated degree of cure versus

time had a smaller cure rate and a lower predicted final conversion than the experimental value. After the temperature correction, the model predictions fit the experimental data well.

The changing temperature in thick samples is monitored at different depths. The result shows that the peak value of temperature at the bottom of the sample increases with exposure intensity but decreases with initiator concentration.

Dielectric sensors were used to measure the cure kinetics of thick samples with different thickness at the bottom layer, thereby as a function of depth. The experimental data were transferred into C=C conversion data using a correlation curve generated from the thin sample data. The FDEMS converted value of C=C conversion matches the calculated outcome using the model when the temperature of the system did not increase more than 10 $^{\circ}$C and the inhibition period is shorter than 13 minutes. When the temperature is higher than 10 $^{\circ}$C, the prediction method needs to be adjusted by the temperature and the result after temperature adjustment matches the experimental data. However, for some samples that have a strong absorption of light due to a low incident intensity, a large thickness, or a high initiator concentration, and hence a slow reaction at the bottom, the FDEMS data shows a much shorter inhibition period compared to the model's predicted results based on the assumed spacer thickness. When the thickness is calculated using the transmitted intensity, the sample thickness is seen to be less than the value predicted by the spacer dimensions. Using this smaller thickness based on the decrease in transmitted light intensity, the agreement between the model predictions and the FDEMS experimental value of C=C versus time is good. Other reasons for

differences between the experimental data and model predictions include the diffusion between layers of oxygen and free radicals in the system.

# References

1. Schrof, W.;Beck, E.;Koniger, R.;Reich, W.; and Schwalm, R. *Progress in Organic Coatings* 1999, *35*, 197-204.

2. Desilles, N.;Lecamp, L.;Lebaudy, P.; and Bunel, C. *Polymer* 2003, *44*, 6159-6167.

3. Desilles, N.;Lecamp, L.;Lebaudy, P.; and Bunel, C. *Polymer* 2004, *45*, 1439-1446.

4. Lee, J. H.;Prudhomme, R. K.; and Aksay, I. A. *J. Mater. Res.* 2001, *16*, 3536-3544.

5. O'Bren, A. K.; and Bowman, C. N. *Macromolecules* 2003, *36*, 7777-7782.

6. Terrones, G.; and Pearlstein, A. J. *Macromolecules* 2004, *37*, 1565-1575.

7. Terrones, G.; and Pearlstein, A. J. *Macromolecules* 2001, *34*, 3195-3204.

8. Terrones, G.; and Pearlstein, A. J. *Macromolecules* 2001, *34*, 8894-8906.

9. Ivanov, V. V ; and Decker, C. *Polym Int* 2001, *50*, 113-118.

10. Cussler, E.L. *Diffusion-Mass transfer in fluid systems*; Cambridge University Press: New York, 1984.

**Appendix**

1.    Calculation of the cure at particular depths and the average cure through depth (Matlab)

clear all;

%Initial conditions:

II=65;                    %Incident intensity value at the surface( $\mu$ w/cm$^2$)

TH=0.4;                   %Total thickness (cm)

PI=0.4;

IC=PI*0.011087216/0.4;   %Initiator concentration in the system (mol/l)

e=760;                    %extinction coefficient

q=0.5;                    %quantum yield of initiator consumption

 %Space allocation: sample is divided into NL layers of thin sample

sL=0.005                  %thickness of layers(cm)

NL=TH/sL;                 %number of layer


%Time allocation, whole process is divided into nt time points

nt=10000;                 %Number of time point(minutes)

st=0.05;                  %step size of time

t=zeros(NL+1,nt+1);

for k1=1:nt+1

   t(1:NL+1,k1)=st*(k1-1); %Value of time points

end

%Calculation of initial intensity and initiator concentration at differnt depth before cure

I=zeros(NL+1,nt+1);  %I is Intensity( μ w/cm2);x is layer, y is time;

CI=zeros(NL+1,nt+1);  %C is the concentration of photo initiator

I(1,1:nt+1)=II;  %Intensity of light at the surface of the sample

CI(1:NL+1,1)=IC;  %Initial concentration of initiator

AC=zeros(1,nt+1);  %Average of initiator concentration through depths


%Calculate the initial intensity through depth before exposure starts

for k5=1:NL+1

 z=(k5-1)*sL;

 I(k5,1)=II/10^(e*z*IC+0.0778*sL*2.14832);

end


%Calculation of the change in intensity versus time at different depths

for k4=1:NL+1

 for k3=2:nt+1

  IE=(I(k4,k3-1)*3.05e-9/sL);  %Convert unit of I to Einstein/l-s

  CI(k4,k3)=CI(k4,k3-1)-q*st*60*IE*(1-10^(-e*sL*CI(k4,k3-1)));

  I(k4+1,k3)=I(k4,k3)/10^(e*sL*CI(k4,k3)+0.0778*sL*2.14832);

 end

 AC=AC+CI(k4,1:nt+1);

 %plot(t(k4,1:nt+1),CI(k4,1:nt+1))

 hold on

```
end

hold on

CI(NL+1,1:nt);

%plot(t(NL+1,1:nt+1),I(NL+1,1:nt+1))

%plot(t(NL,1:nt+1),AC(1,1:nt+1)/NL)

 hold on

%Calculation of delay time

TR=zeros(NL+1,nt);       %TR is the real time after adjusted by inhibition

Tdi=zeros(NL+1,nt);

Td=zeros(NL+1,nt);

Tdc=zeros(NL+1,nt);

td=zeros(NL+1,1);

N=zeros(NL+1,1);


for L=NL-1:NL+1

Err=1;

while Err>0

   N(L,1)=N(L,1)+1;

   Td(L,1)=Td(L,1)+5.542/(PI*I(L,N(L,1)));

   td(L,1)=Td(L,1)/N(L,1);

   Err=td(L,1)-st*N(L,1);

end

end
```

```
C=zeros(NL+1,nt);          %Conversion

MC=zeros(NL+1,nt);         %calculated concentration of C=C(mol/l)

S=zeros(NL+1,nt);          %-dlnM/dt

dC=zeros(NL+1,nt);

I1=32.5;


for k=NL-1:NL+1

    MC(k,N(k,1))=4.955;    %Initial concentration of C=C(mol/l)

for g=N(k,1):nt

    A=((I(k,g)/I1)^0.7)*((PI/0.2)^0.75); %(CI(k,g)*0.4/0.011087216)

    S(k,g)= A*1*((1/(1+exp(-30*(C(k,g)-0.05))))-(1/(1+exp(-13.7*(C(k,g)-0.36)))));

    if S(k,g)>0

        if MC(k,g)>0

        dC(k,g)=S(k,g)*st;

        MC(k,g+1)=exp(log(MC(k,g))-dC(k,g));

        C(k,g+1)=1-MC(k,g+1)/MC(k,N(k,1));

        end

    end

end

end

%plot(t(NL,1:nt),C(NL,1:nt),'k-')
```

```
for L=1:1:NL

%plot(t(L,1:nt),C(L,1:nt),'r:')

   hold on

end

plot(t(NL,1:nt),C(NL,1:nt),'r:')

 CA=zeros(1,nt+1);     %Average of concentration of different depths

 for L=1:NL

   CA(1,1:nt)=CA(1,1:nt)+C(L,1:nt);

end

CA=CA(1,1:nt)/(NL);

%plot(t(1,1:nt),CA,'b-')
```

## 2. Effect of time interval
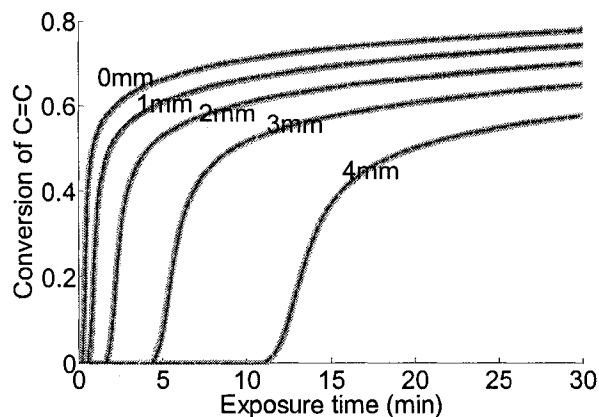


Figure 6.51 UV cure kinetics of CD540-0.2wt%Irgacure 819 at different depths. The depths are marked in the figure as 0 to 4 mm. $I_i = 130 \mu w / cm^2$. (••••••) Time interval is 0.1 minutes, (— — —) Time interval is 0.01 minutes, (———) Time interval is 0.001 minutes.

## 3. Effect of photo-initiator
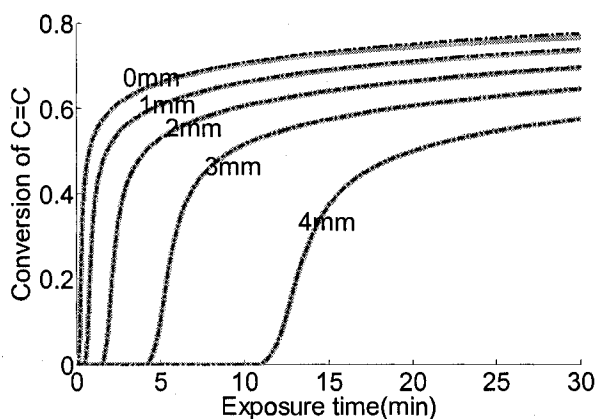


Figure 6.52 UV cure kinetics of CD540-0.2wt%Irgacure 819 at different depths. The depths are marked in the figure as 0 to 4 mm. $I_i = 130 \mu w / cm^2$. (—) Considering effect of the changing initiator concentration on the cure kinetics of the sample in the same layer, (– • –) not considering the effect of the changing initiator concentration.

4. Calculation of C=C Conversion according to its $\log(\varepsilon''\omega)$ data

clear all;

T=[ ];                    %exposure time(min)

y=[ ];                    %the value of $\log(\omega\varepsilon'')$

N=length(y);

x=zeros(N,1);             %the value of C=C conversion

for i=1:N

  ff=@(x) -12.658*x^6 - 31.852*x^5 + 81.614*x^4 - 59.146*x^3 +

      12.868*x^2 - 0.8397*x + 5.9-y(i);

  x(i)=fzero(ff,i*0.8/N );

end

plot(T,x,'k-')

xlabel('Time(min)')

ylabel('Conversion')

5. Fit the temperature at the bottom of a thick sample under different cure conditions
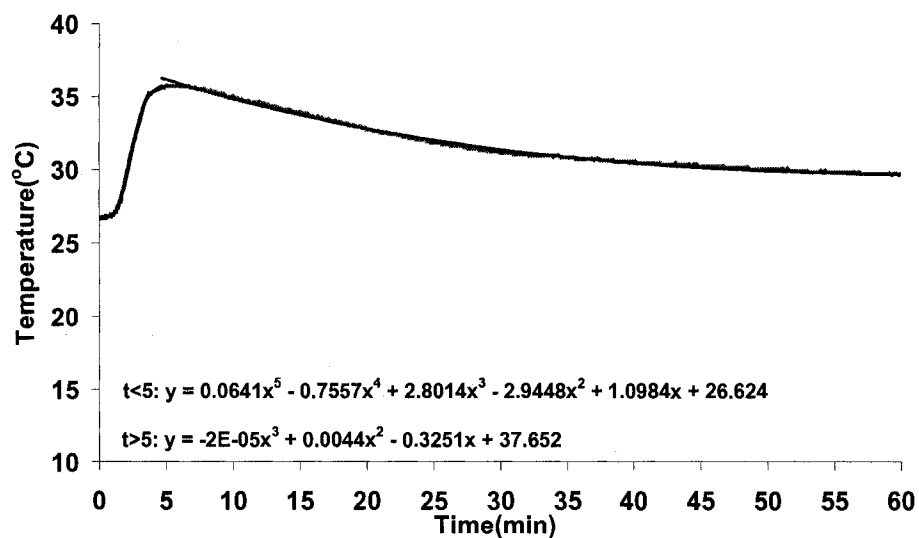
Figure 6.53 (see Figure 6.39, 6.46) Temperature versus exposure time at the bottom of a 3.5 mm (calculated using transmitted intensity) thick sample CD540-0.2wt%IC819, $I_i$=65 $\mu w$/cm$^2$.
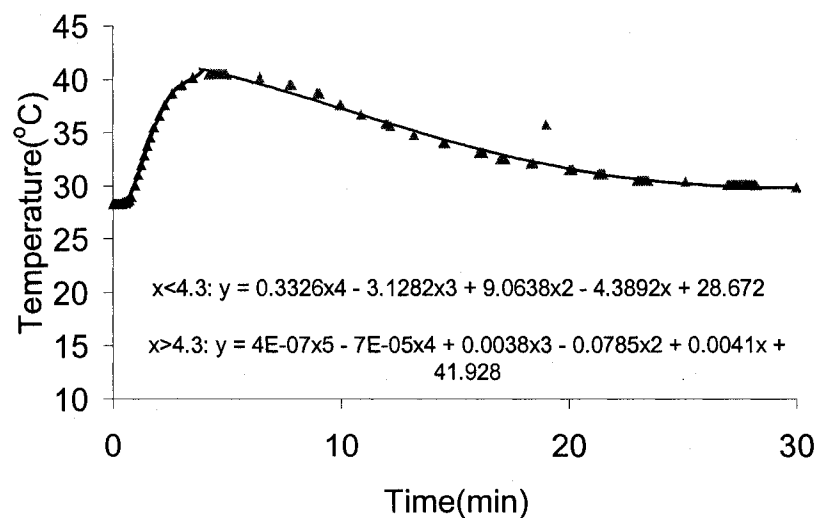


Figure 6.54 (see Figures 6.41 and 6.47) Temperature versus exposure time at the bottom of a 4 mm thick sample CD540-0.2wt%IC819, $I_i$=130 $\mu w$/cm$^2$. (▲) Experimental data derived from FDEMS result, (————) calculated data using 4 mm (spacer thickness) as the thickness after temperature adjustment.
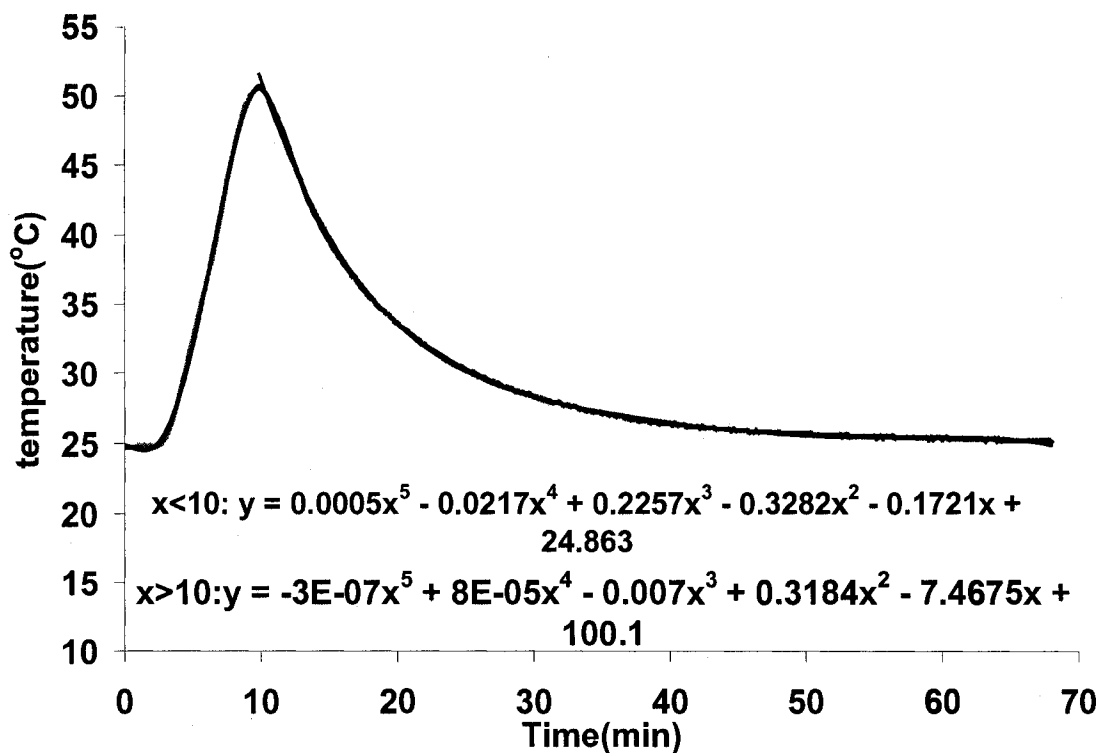
Figure 6.55 (see Figures 6.42 and 6.48) Temperature versus exposure time at the bottom

of an 8 mm thick sample CD540-0. 05wt%IC819, $I_i$=130 $\mu w$/cm$^2$.

6. Calculation of the cure at particular depths with temperature correction for the cure at

the bottom of 4 mm thick sample CD540-0.05wt%IC819 under 130 $\mu w$/cm$^2$ incident

intensity.

clear all;

%Initial conditions:

II=130;                          %Incident intensity value at the surface(uw/cm2)

TH=0.4;                          %Total thickness (cm)

PI=0.05;                         %Initiator concentration in the system (wt%)

IC=PI*0.011087216/0.4;           %Initiator concentration in the system (mol/l)

```
e=760;                    %extinction coefficient

q=0.5;                    %quantum yield of initiator consumption

%Space allocation: sample is divided into NL layers of thin sample

NL=50;                    %number of layer

sL=TH/NL;                 %thickness of layers(cm)

%Time allocation, whole process is divided into nt time points

nt=5000;                  %Number of time point(minutes)

st=0.01;                  %step size of time

t=zeros(NL+1,nt+1);

for k1=1:nt+1

   t(1:NL+1,k1)=st*(k1-1); %Value of time points

end

%Calculation of intensity at different depths during the cure process

I=zeros(NL+1,nt+1);              %I is Intensity(uw/cm2);x is layer, y is time;

CI=zeros(NL+1,nt+1);             %C is the concentration of photo initiator

I(1,1:nt+1)=II;                  %Intensity of light at the surface of the sample

CI(1:NL+1,1)=IC;                 %Initial concentration of initiator

AC=zeros(1,nt+1);

% initial intensity at different depths before cure

for k5=1:NL+1

   z=(k5-1)*sL;

   I(k5,1)=II/10^(e*z*IC+0.0778*sL*2.14832);

end
```

%Calculation of the change in intensity and initiator concentration versus time at different depths

```
for k4=1:NL+1

    for k3=2:nt+1

        IE=(I(k4,k3-1)*3.05e-9/sL);              %Convert unit of I to Einstein/l-s

        CI(k4,k3)=CI(k4,k3-1)-q*st*60*IE*(1-10^(-e*sL*CI(k4,k3-1)));

        I(k4+1,k3)=I(k4,k3)/10^(e*sL*CI(k4,k3)+0.0778*sL*2.14832);

    end

    AC=AC+CI(k4,1:nt+1);

end

It=I;

CI(NL+1,1:nt);

hold on

%fit bottom temperature versus conversion

TEMP=zeros(1,nt);

for N=1:nt

    if t(NL,N)<1.37

        TEMP(1,N)=27;

    else

        if t(NL,N)<3.37

        TEMP(1,N)=1.5645*t(NL,N)^4 - 21.815*t(NL,N)^3 + 99.033*t(NL,N)^2 -

                165.22*t(NL,N) + 119.01;

        else
```

```
TEMP(1,N)=-0.0047*t(NL,N)^3 + 0.2805*t(NL,N)^2 - 5.7202*t(NL,N) + 70.161;

     end

   end

end

%Calculation of delay time

TR=zeros(NL+1,nt);                    %TR is the real time after adjusted by inhibition

Td=zeros(NL+1,nt);

Tdc=zeros(NL+1,nt);

td=zeros(NL+1,1);

Tdc(1:(NL+1),1)=0.1745/PI;

N=zeros(NL+1,nt);

for L=NL:NL

   Err=12;

   while Err>0.1

      N(L,1)=N(L,1)+1;

      Td(L,1)=Td(L,1)+(32.5*Tdc(L,1)/It(L,N(L,1)))*(exp(587*(1/(273+TEMP(N(L,1)))-

          1/(273+25))));

      td(L,1)=Td(L,1)/N(L,1);

      Err=abs((td(L,1)-st*N(L,1)));

   end

end

%calculate conversion of C=C(mol/l) versus exposure time

C=zeros(NL+1,nt);                    %Conversion
```

```matlab
MC=zeros(NL+1,nt);                    %calculated concentration of C=C(mol/l)

S=zeros(NL+1,nt);                     %-dlnM/dt

dC=zeros(NL+1,nt);

I1=32.5;

 for k=NL:NL

   MC(k,N(k,1))=4.955;               %Initial concentration of C=C(mol/l)

   for g=N(k,1):nt

     A=((It(k,g)/I1)^0.7)*((PI/0.2)^0.75);

     f=1/(273+TEMP(g));

     f1=0.0007*exp(2164*f);

     f2=0.0003*exp(3394*f);

     f3=-219*f+1.1;

     S(k,g)=A*1*((1/(f1+exp(-f2*(C(k,g)-0.05))))-(1/(f1+exp(-13.7*(C(k,g)-f3)))));

     dC(k,g)=S(k,g)*st;

     MC(k,g+1)=exp(log(MC(k,g))-dC(k,g));

     C(k,g+1)=1-MC(k,g+1)/MC(k,N(k,1));

   end

end

plot(t(NL,1:nt),C(NL,1:nt),'k-')
```

# Chapter 7. Diffusion of oxygen and free radicals during free radical polymerization

## 7.1 Introduction

It was concluded in Chapter 6 that the diffusion of substrates, such as oxygen, free radicals, and photo initiator, may affect the cure kinetics as a function of depth in the system. In this Chapter, frequency dependent dielectric sensing (FDEMS) will be used to monitor the UV cure kinetics in the dark non-irradiation region under a mask to study the diffusion of free radicals from the exposure area to the dark area. Using FDEMS to monitor the cure of coating in industry has been reported in several papers.[1-11]

In addition, a free radical thermal cure of an acrylic resin will be examined to study the oxygen diffusion from the surface layer to deeper layers. This is done at the suggestion of Prof. Roberto William from Argentina.

## 7.2 Experimental

### 7.2.1 Materials

Two types of reactions are studied in this paper. The first type is **UV polymerization**. The second type of reaction is **thermal polymerization**. For UV polymerization, four systems are studied. The first system includes only CD540 (Akzo-Nobel) and Irgacure 819 (Ciba) as what was studied in Chapters 3 to 6. In the second

system, we added toluene to CD540 and Irgacure 819 to study the viscosity effect on the UV cure kinetics. The third system is composed of CD540, Irgacure 819, toluene, and 1-dodecanethiol (Aldrich), a chain transfer agent. The composition of the fourth system is based on a real application of making contact lenses. It is composed of CD540, Irgacure 819, styrene (Aldrich), and 1-dodecanethiol.

**The thermal polymerization system** is composed of Isobornyl methacrylate(IBoMA, Aldrich) and 2 phr of initiator Benzoyl peroxide(BPO, Akzo-Nobel). All products were used as received.

## 7.2.2 Equipment

### Dielectric Impedance Measurements

The dielectric impedance measurements for monitoring the **UV cure** are the same as what was described in Chapter 5. The sample setup is shown in Figure 7.1(a). To create a nonirradiated region, a mask is made using transparency film (3M) as shown in Figure 7.1(b). Several masks are made and used in this dissertation. They are described in the Appendix 1. The parameters of these masks are shown in Appendix 1. All of them have 50% dark area and 50% clear area, the only difference between these masks is the strip width (SW).
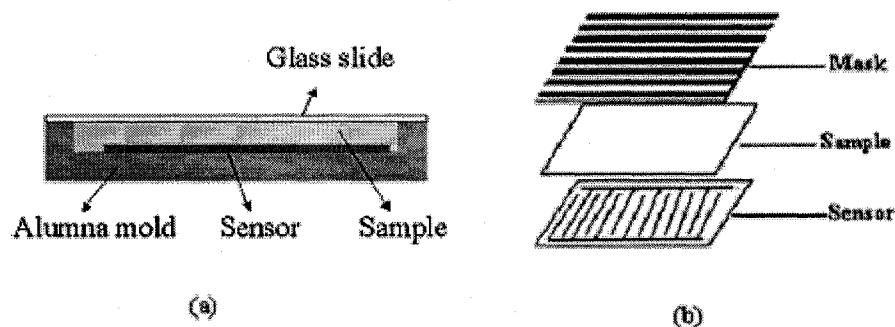
Figure 7.1 Experimental setup for UV cure.

For the **thermal cure** of IBOMA, a HP 4192A LF impedance analyzer is used to monitor the curing process. Both cures in the air and without air are studied to compare the air diffusion effect on the cure kinetics. For the thermal cure **without air**, the experimental setup is shown in Figure 7.1 (a) using a glass slide instead of a mask to cover (seal) the sample so that the oxygen from the air can not diffuse into the sample to affect the cure. For the thermal cure **in the air**, the experimental setup is shown in Figure 7.2. The sample is sealed in a space with air in it to prevent the evaporation of IBOMA at 80°C.
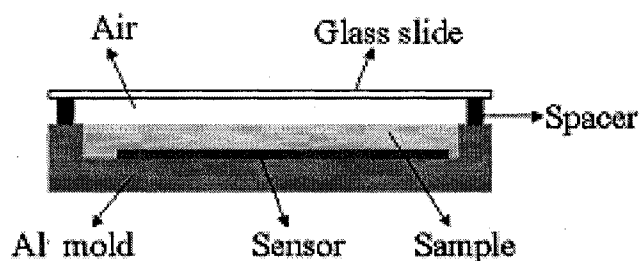


Figure 7.2 Sample setup of thermal cure of IBOMA in the air.

The theory of dielectric impedance measurements was elaborated in Chapter 5. Since the sensor is on the bottom of the mold, it is monitoring changes at the bottom of a

layer equal to the spacing between the sensor's inter-digitaled electrodes. The thickness of the sample is equal to the mold's depth minus the thickness of the sensor.

**DSC Measurements**

The thermal polymerization kinetics were also studied by DSC using a TA Instruments 2920 modulated DSC to compare and correlate these results with the dielectric data. The thermal analysis consisted of an isothermal DSC run to determine $\Delta H_1$ at each temperature. Then this was followed by a temperature ramp to a suitable high temperature to determine the residual heat ($\Delta H_2$) and thereby the total heat of the polymerization ($\Delta H_1 + \Delta H_2$). The cure extent at a given time was calculated from

$$\alpha(t) = \frac{\Delta H(t)}{\Delta H_1 + \Delta H_2}$$

Equation 7-1

Where $\alpha(t)$ is the cure extent and $\Delta H(t)$ is the heat produced by the reaction at time t.

**UV Radiation source**

The UV radiation source is the same as what was used in Chapter 4.

## 7.3 Results and Discussion

### 7.3.1 UV cure in the irradiated and nonirradiated regions when using a mask

In order to study the diffusion of free radicals in the system, mask experiments were designed and the cure under both the exposure area and the dark area is monitored by FDEMS. The typical result is shown in Figure 7.3.
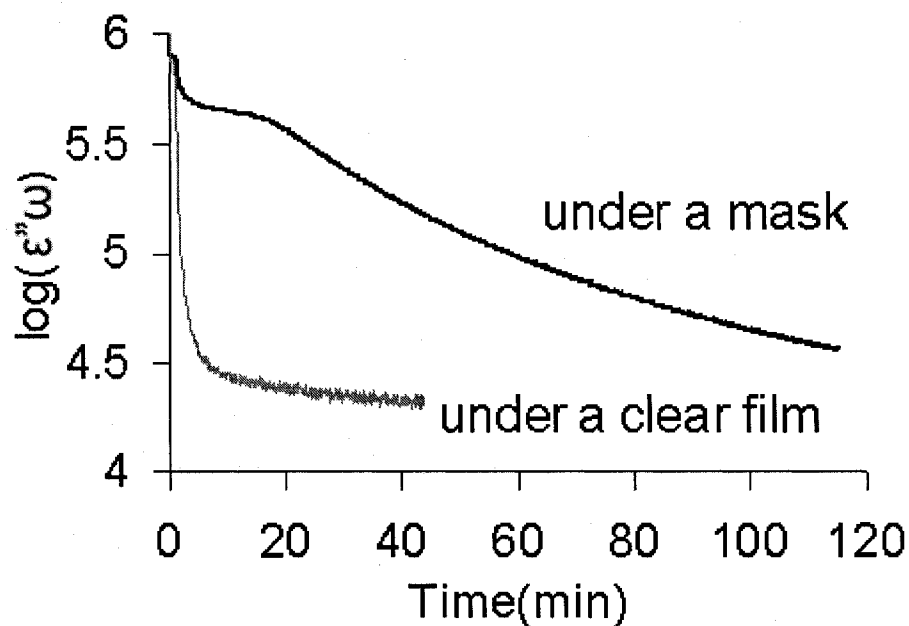
Figure 7.3 UV cure under a clear film and a mask (M₂) measured by FDEMS, CD540-0.2wt%IC819, clear strip width=dark strip width = 0.025inch, sample thickness=0.05mm, $I_i$=32.5 $\mu w/cm^2$.

Figure 7.3 shows a curve for the cure under the M₂ mask and another curve for the cure under a clear film. It is found that the cure under a clear film terminates in 5 minute. The cure under the mask can be divided into two periods. The first period is before the 5th minute, which we associate with the cure under the clear strips of the mask by comparing the cure under a mask to cure under a clear film. The second period is after the 5th minute which we believe is the cure under the dark strips. This can be seen even clearer in Figure 7.4 in a non-log scale.
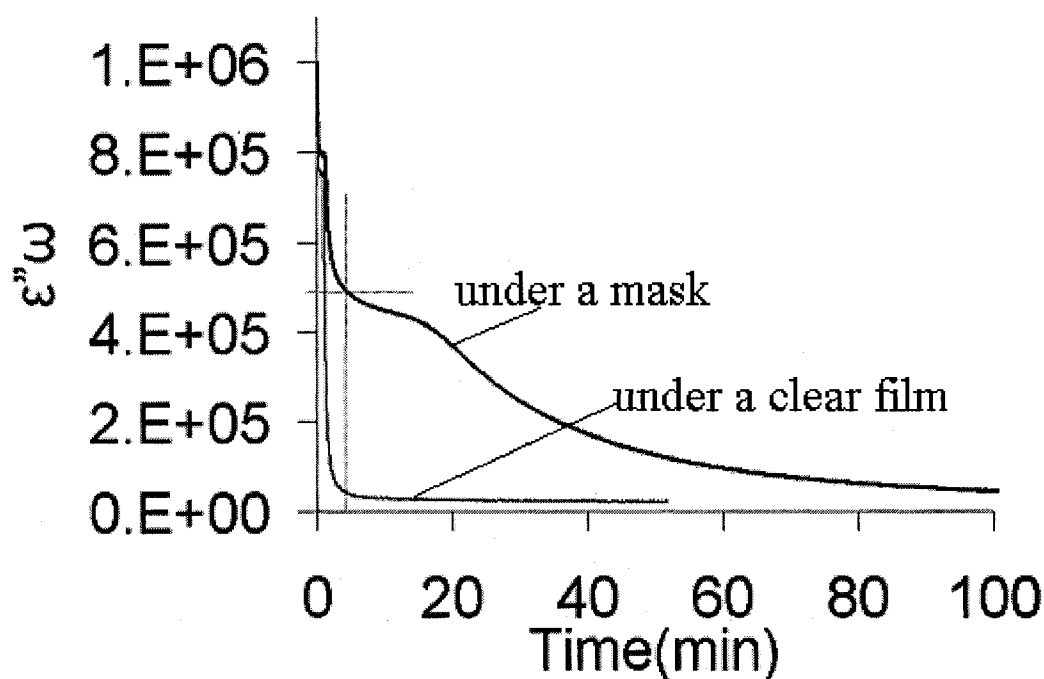
Figure 7.4 UV cure under a clear film and a mask (M$_2$) measured by FDEMS, CD540-0.2wt%IC819, clear strip width = dark strip width = 0.025inch, sample thickness=0.05mm, $I_i$=32.5 $\mu w/cm^2$.

Figure 7.4 shows that, by the time that the cure under the clear film terminates, the value of $\varepsilon''w$ for the cure under a mask reaches half of its total value before the cure starts. We know that the area of the dark strips is the same as the area of the clear strips. According to the theory of impedance, the conductivity that a capacitor measures is proportional to the area of the parallel plates of the capacitor that is fully filled by sample. Therefore, by the 5$^{th}$ minute, where the sample under the clear film is cured, the conductivity measured is contributed mainly by the conductivity of the uncured sample in the dark area as it is equal to half of the total area. Note 50% of this mask is dark and 50% is clear since the width of the line and spaces are equal. We know that at 0.1kHz, the

value of $\varepsilon''w$ measured by FDEMS is proportional to the conductivity of the material. Thus, the decrease of $\varepsilon''w$ after the 5$^{th}$ minute is due to the cure in the dark area.

What is the reason for the dark cure in the nonirradiated region? We believe the cure that occurs in the dark nonirradiated regions near the interface of the mask's non-irradiated dark area and the exposed area is due to the diffusion of free radicals across the boundary of the exposed area. In order to examine this, another plot is made based on the idea of no diffusion between the boundary. In this case, half of the area is filled with sample that has the same cure performance as the sample under the clear film. The other half of the area is filled with sample that did not react at all since it is not exposed to light. The conductivity versus exposure time, G(t), for this situation can be calculated using Equation 7-2.

$$G(t) = \frac{G_{clear}(t)}{2} + \frac{G_{bc}}{2}$$
Equation 7-2

$G_{clear}(t)$ is the conductivity as a function of exposure time for the sample cured under a clear film. $G_{bc}$ is the conductivity of the sample before it is cured. The reason that each conductivity is divided by two is that they both occupy 50% of the sensor area. The scaled curve is shown in Figure 7.5.
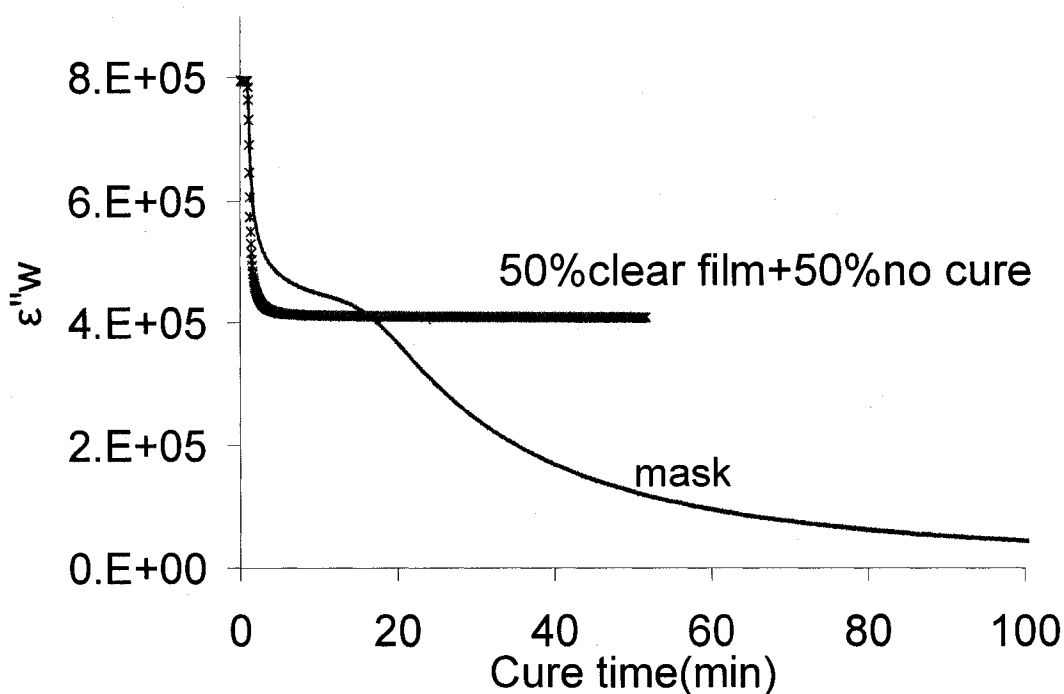
Figure 7.5 UV cure under a mask (M$_2$) measured by FDEMS compared with the situation that no diffusion between the boundary of exposure area and nonirradiated area. CD540-0.2wt%IC819, clear strip width = dark strip width = 0.025 inch, sample thickness=0.05 mm, $I_i$=32.5 $\mu w/cm^2$.

Comparing the two curves in Figure 7.5, we find the conductivity of the cure in the exposure area of a mask decreases slower than the cure under a clear film. Using the correlation curves as shown in Figure 5.6 in Chapter 5, the cure conversion of C=C under the clear film and in the exposure area under a mask (M$_2$) can be calculated for the intensity of 32.5 uw/cm$^2$. The result is shown in Figure 7.6.
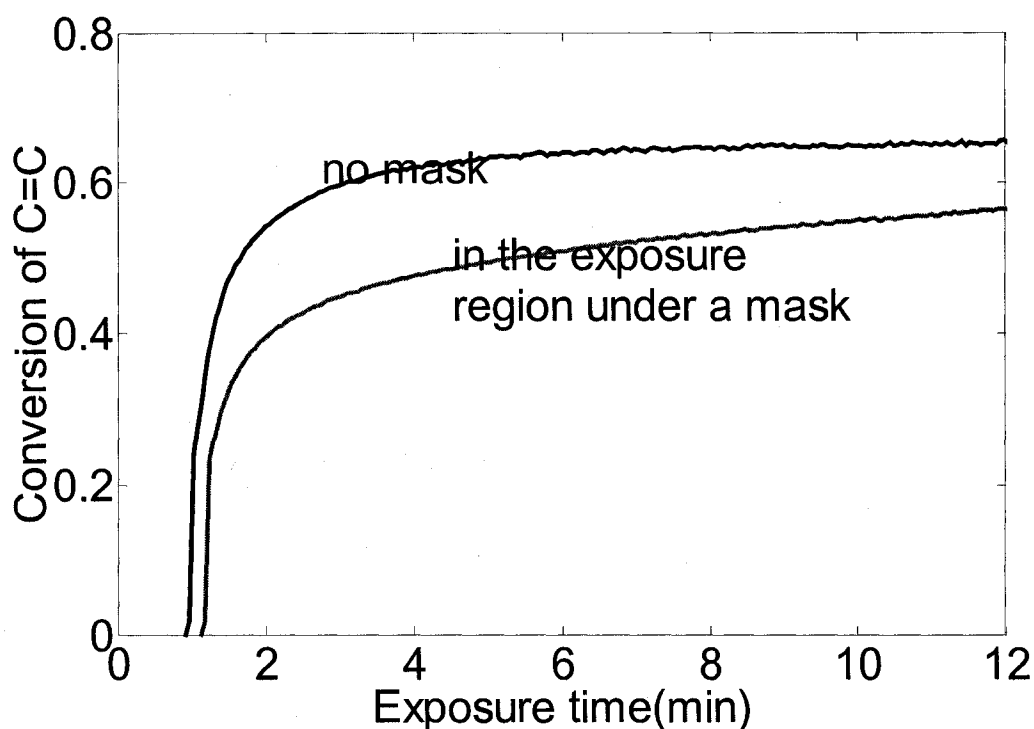
Figure 7.6 CD540-0.2wt%IC819, $I_i$=32.5 uw/cm$^2$, thickness=0.05 mm, frequency=0.1kHz.

Figure 7.6 shows that the cure under a clear film without a mask is faster and has a shorter inhibition period than the cure in the exposure region under a mask. We believe this is due to the diffusion of oxygen from the nonirradiated area to the exposure area since the cure and the consumption of oxygen in the clear area is much faster. Oxygen reacts with free radicals as studied in Chapter 4 hence the migration of oxygen from the dark area into the exposure area will slow down the cure rate in the exposure area under a mask.

In addition, it is also seen from Figure 7.5 hat after 16 minutes, the conductivity of the cure under the mask keeps decreasing while it is becomes a constant for cure in a

clear film. This also supports that diffusion of free radical from the exposure region to the nonirradiated region is causing the cure under the dark strips.

In order to study the diffusion of substances such as oxygen and free radicals through the boundary of the exposure region and the nonirradiated region, a series of mask experiments were designed. The first system we study is CD540-Irgacure 819. We measured the cure under a mask at varying intensities and initiator concentrations. We also studied the effect of viscosity and of a chain transfer agent on the cure by putting toluene and 1-dodecanethiol into the system. A fourth system we studied is based on examining a composition of a more applied formulation used for contact lenses. The system is composed of CD540, styrene, Irgacure 819, and 1-dodecanethiol. We measured the cure under a variety of masks by varying the strip width, the thickness of the sample, and the concentration of chain transfer agent in the system.

### 7.3.1.1 Intensity effect on the cure under a mask

The cure of CD540-0.2wt%IC819 under a mask (M$_2$, dark strip width = clear strip width=0.025 inch) at different intensities from 32.5 to 8 $\mu w/cm^2$ is monitored by FDEMS at the frequency of 0.1kHz. The result is shown in Figure 7.6.

Figure 7.7 UV cure of CD540 with 0.2% Irgacure 819 under a mask ($M_2$, dark strip width

= clear strip width=0.025inch) at different intensities from 32.5 to 8 $\mu w/cm^2$, f=0.1kHz,

thickness=0.05mm.

Figure 7.7 shows that the decrease of the value $\log(\varepsilon''w)$ is faster for both the

cure under the clear strips and dark strips when the light intensity are higher. For the cure

under the clear strips, it agrees with what was reported in Chapter 4. Figure 7.7 also

shows the cure under the dark area increase with light intensity too. We believe this is

due to Equation 7-3 (also see Equation 4-8b).

$$R_i = \frac{d[M\cdot]}{dt} = 9.2\varepsilon I_i b[Irgacure819] \qquad \text{Equation 7-3}$$

Equation 7-3 shows that increasing the radiation intensity increases the radical concentration, $[M\cdot]$, in the system, According to Fick's first law of diffusion,

$$j = -D\frac{dC}{dz}$$

Equation 7-4

j is the flux of the free radicals, D is the diffusion coefficient, z is the average distance between the free radicals in the exposure area and dark area.

According to Equation 7-4, the diffusion rate is proportional to the difference between the free radical concentration in the exposure and the dark area. At higher intensity, the concentration of free radicals in the exposure area is higher, so the diffusion into the dark area is faster and thereby the cure in the nonirradiated region is faster too.

Next, the diffusion of oxygen from dark area to exposure area for the cure at different intensities is studied in Figures 7.8 a to c.
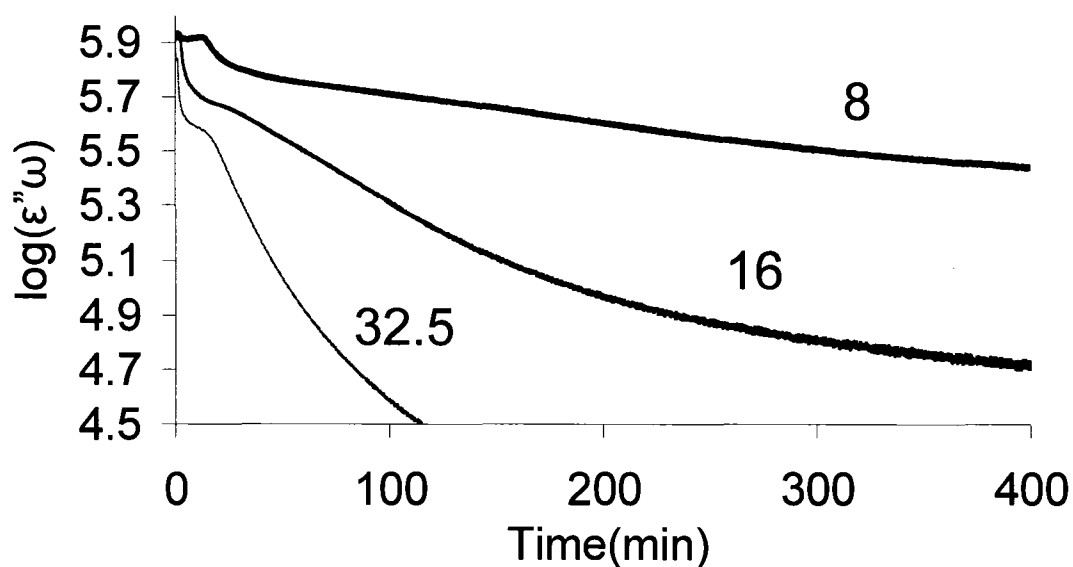
Figure 7.8 UV cure of CD540 with 0.2% Irgacure 819 under a mask ($M_2$, dark strip width

= clear strip width=0.025inch) compared with the cure without diffusion effect at

different intensities from 32.5 to 8 $\mu w/cm^2$ as marked in Figures a, b and c, f=0.1kHz,

thickness=0.05mm. m represents the measured cure curve under a mask, n represents the

calculated curves without considering the diffusion effect.

It is found from Figures 7.8a to c that at the lower the intensity, the difference is

larger between the cure under the clear strips of a mask and the cure under a clear film

without diffusion effect. Using the correlation curves as shown in Figure 5.6 in Chapter

5, the cure conversion of C=C under the clear film and in the exposure area under a mask

($M_2$) can be calculated for the intensity of 16 uw/cm$^2$. The result is shown in Figure 7.9.
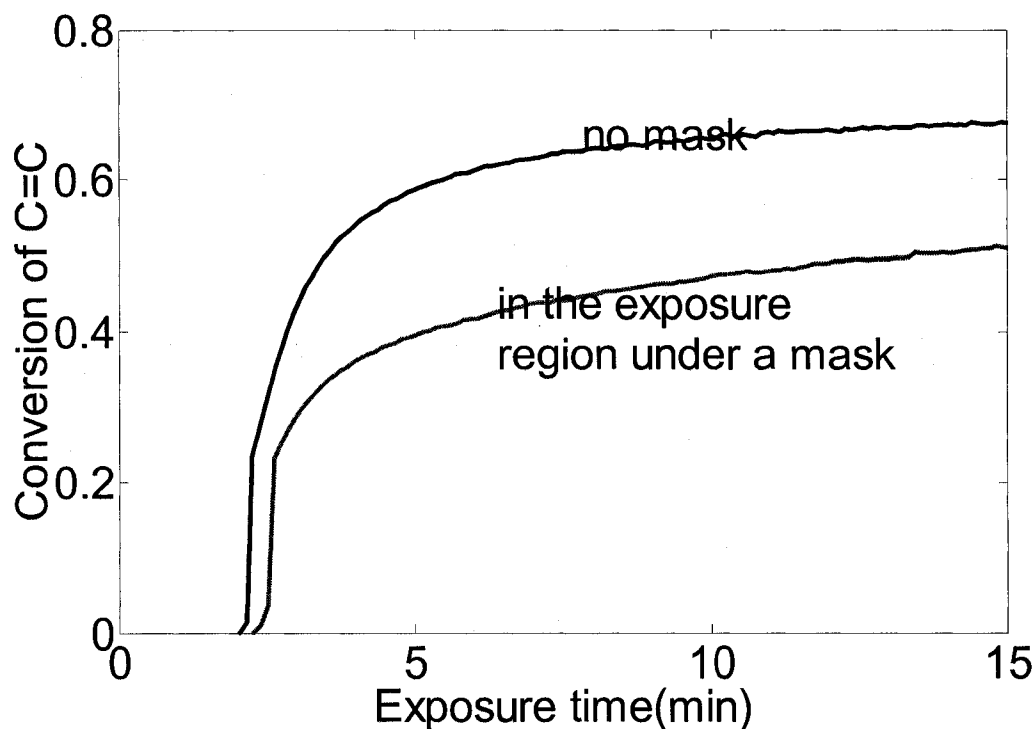


Figure 7.9 CD540-0.2wt%IC819, $I_i$=16 uw/cm$^2$, thickness=0.05 mm, frequency=0.1kHz.

Figure 7.9 is similar to Figure 7.6 that the cure under a clear film without a mask

is faster and has a shorter inhibition period than the cure in the exposure region under a

mask. The difference between the two curves here in Figure 7.9 for the cure at the

intensity of 16uw/cm$^2$ is more than the difference between the two curves in Figure 7.6 at

the intensity of 32uw/cm$^2$. This means the oxygen diffusion effect is larger for the slow

cure at low intensity. This is reasonable since the slow cure rate offers more time for the

oxygen to diffuse from the nonirradiated region into the exposure area.

## 7.3.1.2 Initiator concentration effect on the cure under a mask

The cure of 0.05 mm CD540-IC819 with varying initiator concentrations under a mask (dark strip width = clear strip width=0.025 inch) at the radiation intensity of 32.5 $\mu w/cm^2$ is monitored by FDEMS at the frequency of 0.1 kHz. The result is shown in Figure 7.10.
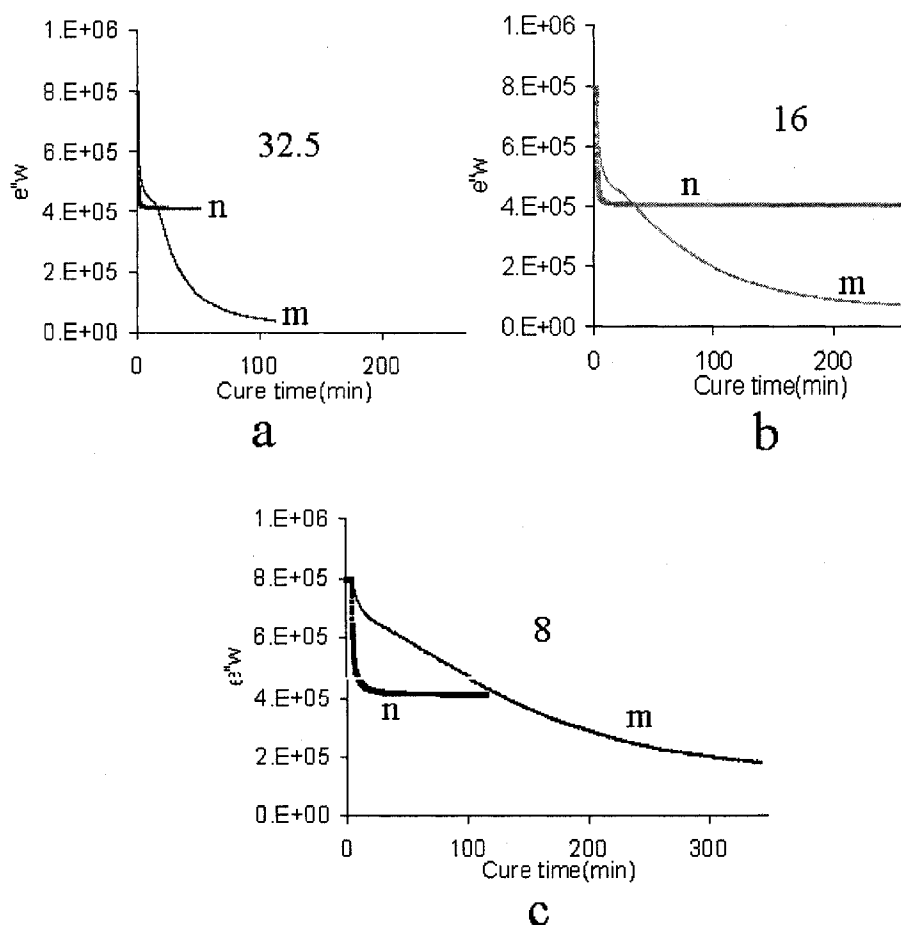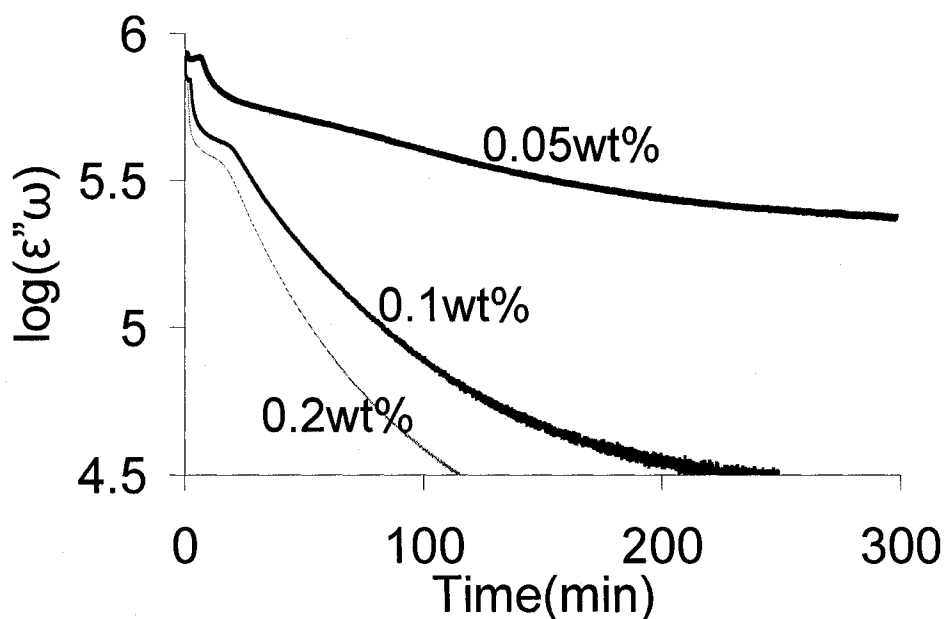


Figure 7.10 UV cure of CD540 with Irgacure 819 under a mask (M$_2$, dark strip width = clear strip width=0.025 inch) at the intensity of 32.5 $\mu w/cm^2$ with varying [PI] from 0.05 to 0.2wt%, f=0.1kHz, thickness=0.05 mm.

It is seen from Figure 7.10 that the cure under both the clear strips and black strips is faster for the system with more initiator concentration. The reason is due to Equation 7-2 that radical concentration, [$M\cdot$], is higher for the system with more initiator, so the diffusion of radicals from clear area to the dark area is larger and the cure in the dark area is faster.

Next, the diffusion of oxygen from dark area to exposure area for the cure at different intensities is studied in Figures 7.11 a to c.
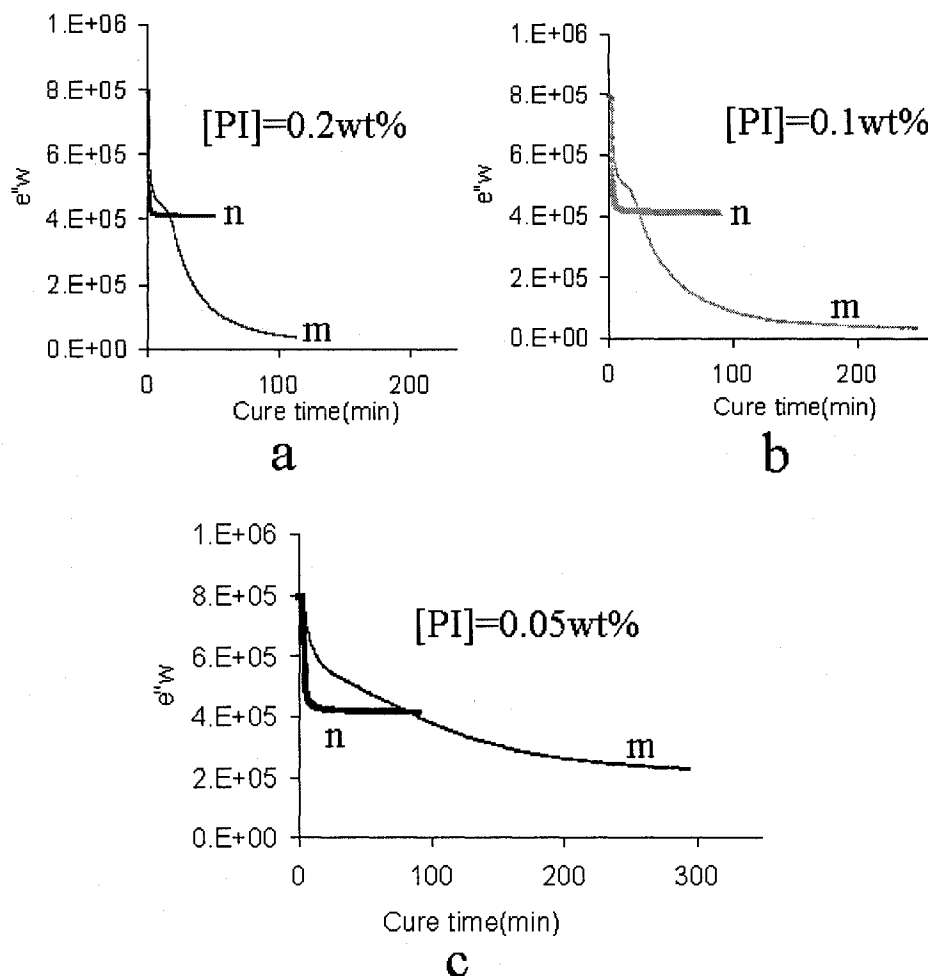


Figure 7.11 UV cure of CD540-Irgacure 819 under a mask ($M_2$, dark strip width = clear strip width=0.025inch) compared with the cure without diffusion effect with varying [PI] from 0.2 to0.05wt%, at the intensity of 32.5 $\mu w/cm^2$ as marked in Figures a, b and c, f=0.1kHz, thickness=0.05 mm. m represents the measured cure curve under a mask, n represents the calculated curves without considering the diffusion effect.

Figures 7.11 a to c show that for the system with less initiator concentration, the difference is larger between the cure under the clear strips of a mask and the cure under a

clear film. Using the correlation curves as shown in Figure 5.6 in Chapter 5, the cure conversion of C=C under the clear film initiator concentration of 0.1wt%. The result is shown in Figure 7.12.
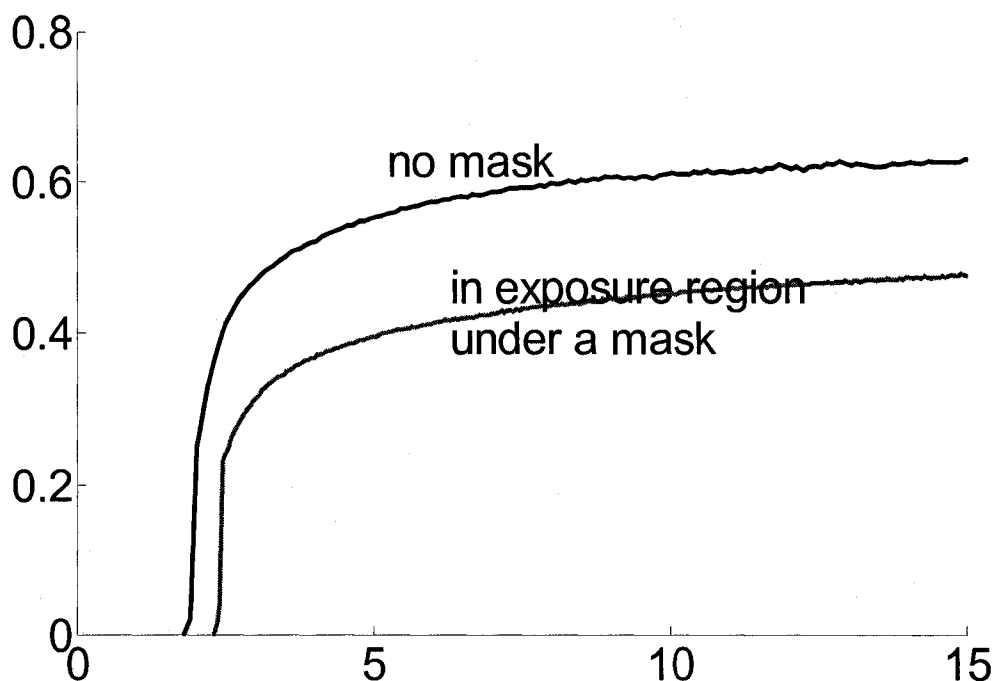


Figure 7.12 CD540-0.1wt%IC819, $I_i$=32.5uw/cm$^2$, thickness=0.05 mm, frequency = 0.1kHz

Figure 7.12 is similar to Figure 7.6 that the cure under a clear film without a mask is faster and has a shorter inhibition period than the cure in the exposure region under a mask. The difference between the two curves here in Figure 7.12 for the cure of the system with 0.1wt% initiator is more than the difference between the two curves in Figure 7.6 for the system with 0.2wt% initiator. This means the oxygen diffusion effect is stronger for the slow cure of the sample with less initiator concentration. This is similar to the intensity effect observed in Figures 7.8a to c.

**Study of system with various modifications**

### 7.3.1.3 Viscosity effect on the cure under a mask

In order to study the viscosity effect on the cure under a mask, we put 10% toluene into the system to reduce the viscosity. The curves of the system with and without toluene are listed together in Figure 7.13a and Figure 7.13b (in a larger scale).



Figure 7.13a UV cure of CD540-0.2wt%IC819 (with/without toluene) under a mask ($M_2$, dark strip width = clear strip width=0.025inch) at the intensity of 32.5 $\mu w/cm^2$, f=0.1kHz, thickness=0.05mm. Curves 1 and 2 are cures under $M_2$ mask, 3 and 4 are cure curves under clear film, 1 and 4 are cure curves of the sample with toluene, 2 and 3 are cure curves of the sample without toluene.

Figure 7.13b UV cure of CD540-0.2wt%IC819 (with/without 10wt% toluene) under a

mask (M₂, strip width = clear strip width=0.025 inch) at the intensity of 32.5 $\mu w/cm^2$,

f=0.1kHz, thickness=0.05 mm. Curves 1 and 2 are cures under the M₂ mask, 3 and 4 are

cure curves under clear film, 1 and 4 are cure curves of the sample with toluene, 2 and 3

are cure curves of the sample without toluene.


Figures 7.13 a and b show that the decrease of $\log(\varepsilon''w)$ for the system without

toluene is a little faster at both the exposure area and the dark area. The system with

toluene reaches a lower value of $\log(\varepsilon''w)$ that corresponds to a higher final conversion.

This is also observed by the real-time near FTIR measurement as shown in Figure 7.14.
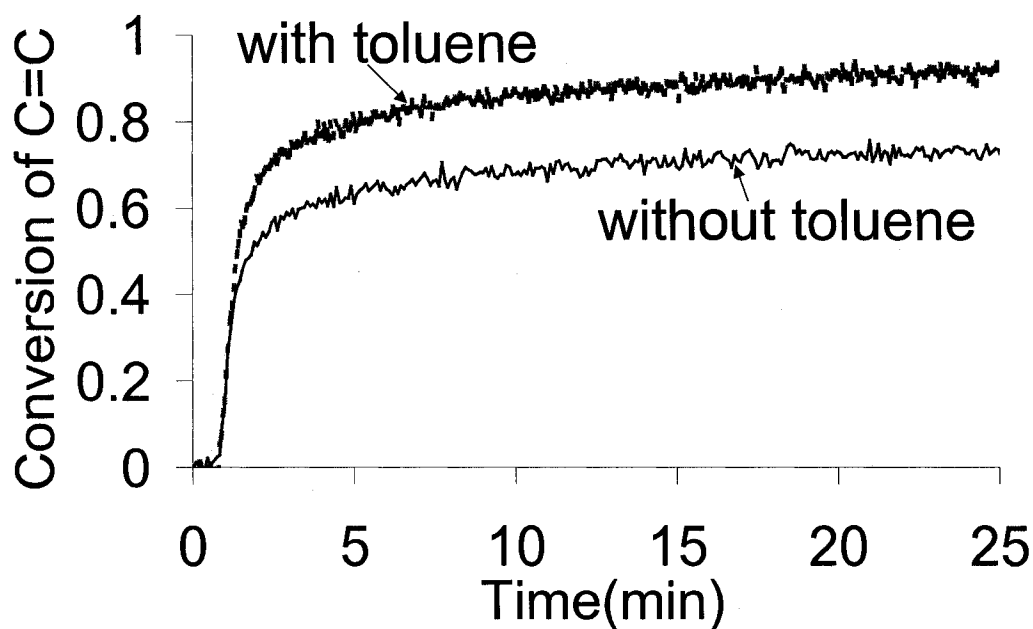
Figure 7.14 UV cure of CD540-0.2wt%IC819 (with/without 10wt%toluene) measured by FTIR at the intensity of 32.5 $\mu w/cm^2$, thickness=0.05 mm, no mask

Figure 7.14 shows that the system with toluene reaches a higher final conversion than the system without toluene. This agrees with what was observed in Figure 7.13. This is because toluene, as the solvent, decreases the viscosity of the system. So the system reaches its glassy state at a higher conversion. But there is no obvious difference of the cure rate between two systems until the final cure is approached.

Next, the diffusion of oxygen from dark area to exposure area for the cure at different intensities is studied in Figures 7.15 a and b.
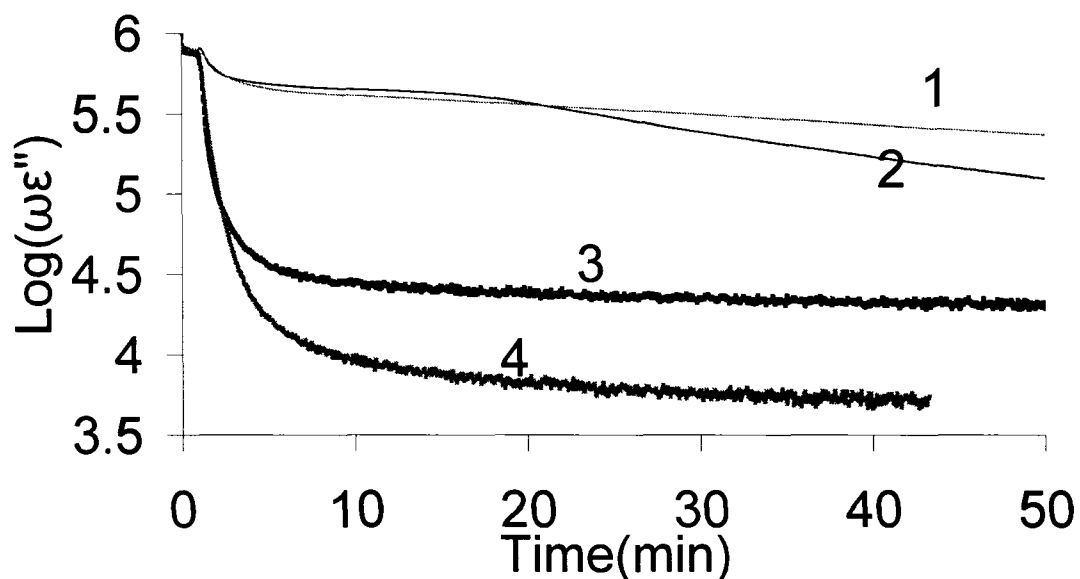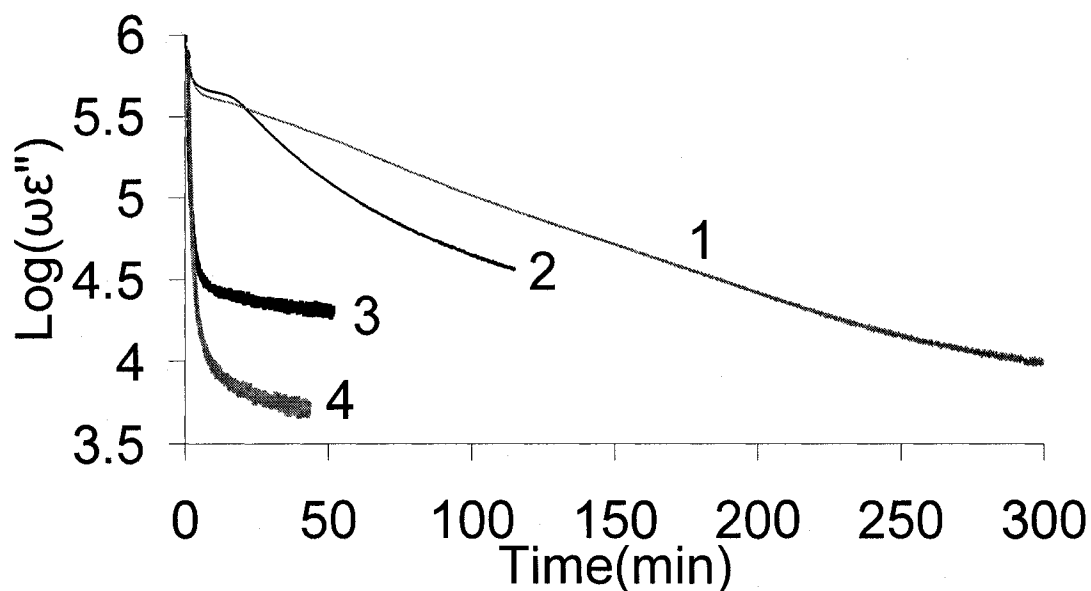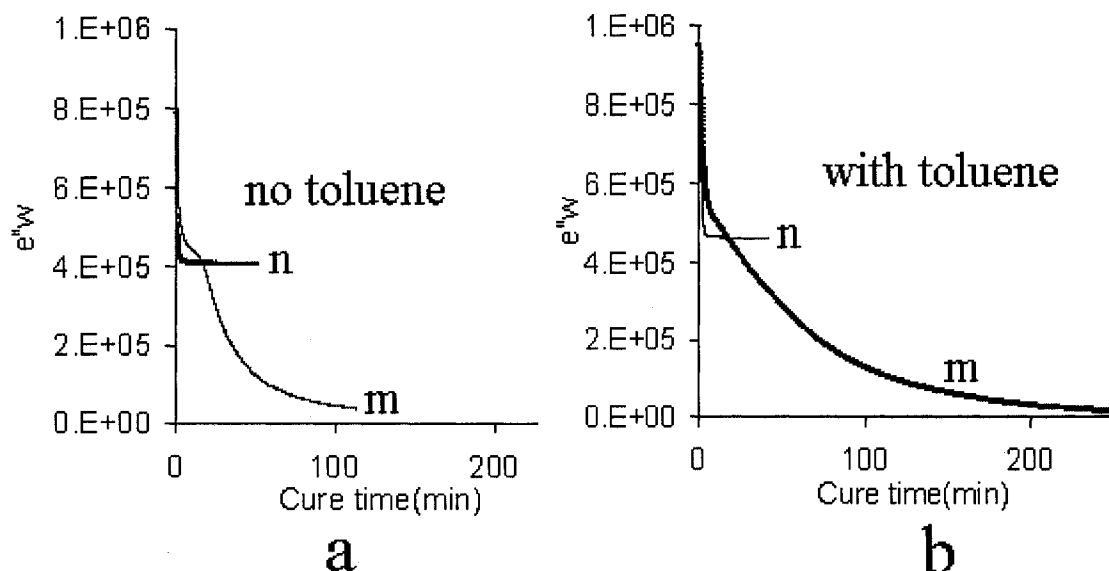
Figure 7.15 UV cure of CD540-0.2wt%IC819 (with/without toluene) under a mask ($M_2$, strip width = clear strip width=0.025inch) at the intensity of 32.5 $\mu w/cm^2$, f=0.1kHz, thickness=0.05 mm. a is the cure of the system without toluene and b is the cure of the system with toluene. m represents the measured cure curve under a mask, n represents the calculated curves without considering the diffusion effect.

Comparing Figures 7.15a and b, the difference between the curves n (cure under clear film without diffusion effect) and m (under a mask) are similar for Figures a and b. This means the oxygen diffusion effect on the cure of exposure region under a mask for the system with and without toluene is quite similar.

In addition, the cure in the nonirradiated region is a little faster for the system without toluene than the system with toluene. This is contrary with what we expected since the system with toluene has a lower viscosity that is helpful for the diffusion of free radicals. The reason for the contrary result is probably due to the decreased concentration

of initiator in the system with toluene and the more rapid cure in the exposed area which makes diffusion of the radicals more difficult.

### 7.3.1.4 The effect of chain transfer agent on the cure kinetics under a mask

Next, the effect of the chain transfer agent on the cure kinetics is studied in Figure 7.13 for the system, 90%CD540-0.2 phr IC819-10%Toluene (with/without 2 phr 1-dodecanethiol). (The reason that we put toluene in the system here is because it is hard to dissolve 1-dodecanethiol directly into CD540.) The cures of the system with and without 1-dodecanethiol are listed together in Figure 7.16a and 7.16b (in a larger scale).



Figure 7.16a UV cure of CD540-IC819-Toluene (with/without chain transfer agent (CT)) under a mask ($M_2$, dark strip width = clear strip width=0.025 inch) at the intensity of 32.5 $\mu w/cm^2$, f=0.1kHz, thickness=0.05mm. Curves 1 and 2 are cures under $M_2$, mask, 3 and 4 are cures under clear film, 1 and 4 are cures of the sample without chain transfer agent, 2 and 3 are cures of the sample with chain transfer agent.

Figure 7.16b UV cure of CD540-IC819-Toluene (with/without chain transfer agent(CT)) under a mask ($M_2$, dark strip width = clear strip width=0.025 inch) at the intensity of 32.5 $\mu w/cm^2$, f=0.1kHz, thickness=0.05 mm. Curves 1 and 2 are cures under $M_2$ mask, 3 and 4 are cures under clear film, 1 and 4 are cures of the sample without chain transfer agent, 2 and 3 are cures of the sample with chain transfer agent.

Figures 7.16 a and b show that the cures in both the exposure area and the dark area are faster for the system with chain transfer agent. This probably because the chain transfer agent, 1-dodecanethiol, has a higher reactivity than the monomer, CD540. Since 1-dodecanethiol has a smaller molecular weight and a higher mobility, it is easier for it to diffuse to dark area than the monomer radicals, $[M \cdot]$, and induce the cure there.

Next, the diffusion of oxygen from dark area to exposure area for the cure at different intensities is studied in Figures 7.17 a and b.
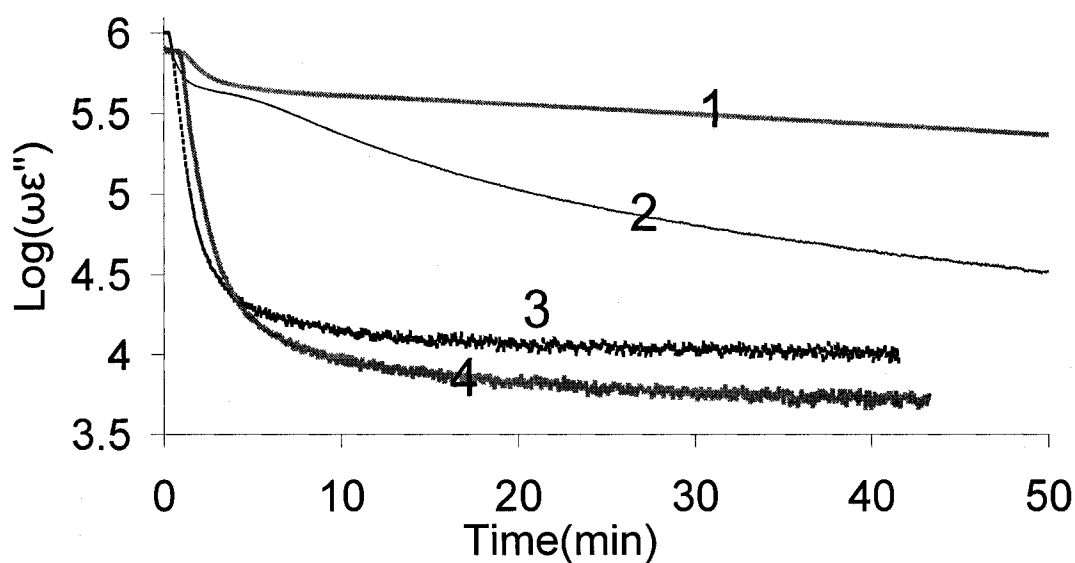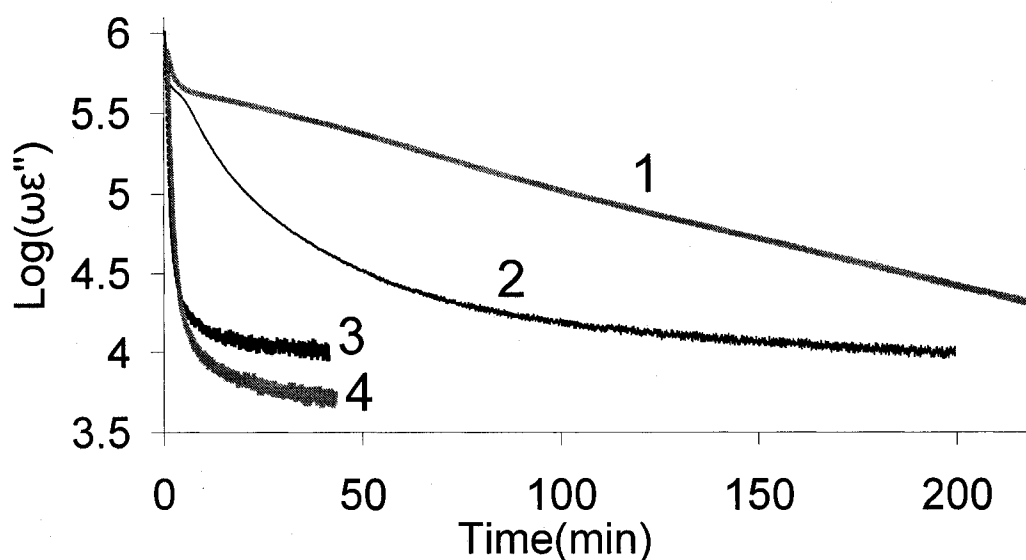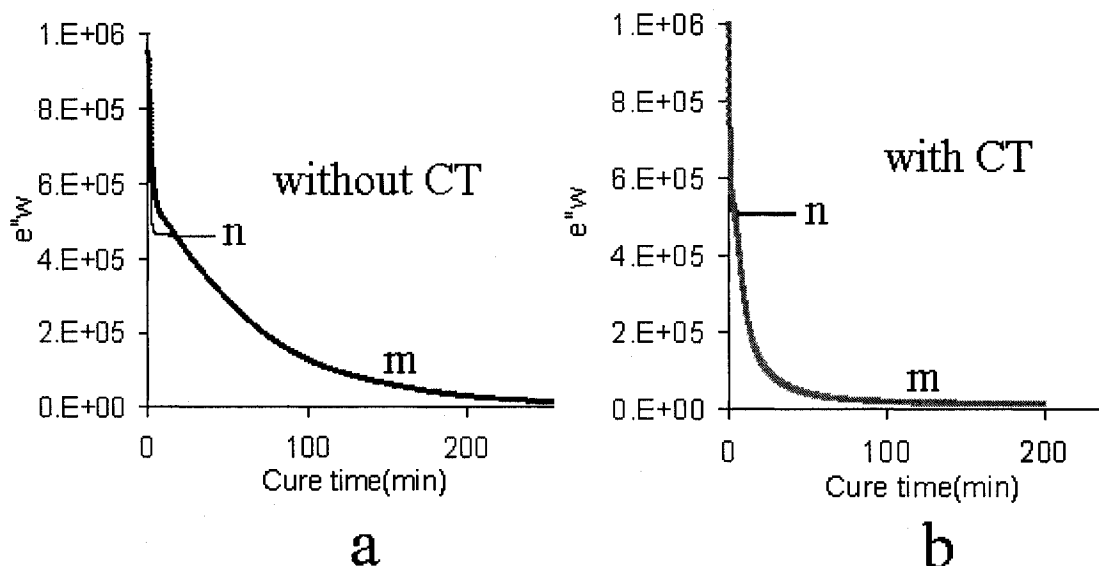
Figure 7.17 UV cure of CD540-IC819-Toluene (with/without chain transfer agent(CT)) under a mask (dark strip width = clear strip width=0.025 inch) at the intensity of 32.5 $\mu w/cm^2$, f=0.1kHz, thickness=0.05 mm. **a** is the system without CT and Figure **b** is the system with CT. m represents the measured cure curve under a mask, n represents the calculated curves without considering the diffusion effect.

Figure 7.14 shows that for the system with chain transfer agent in it, the difference between the curve, n (cure under clear film without diffusion effect) and m (under a mask) is small compared with the system without chain transfer agent. The reason is the rapid cure of the system with the chain transfer agent decreases the opportunity of oxygen to diffuse from the dark area into the exposed area under the mask.

### 7.3.1.5 The effect of styrene on the cure kinetics under a mask

Next, styrene was put into the system to replace Toluene. The cure of the system with toluene and the system with styrene under a mask and under a clear film are monitored and listed together in Figures 7.18a and b.
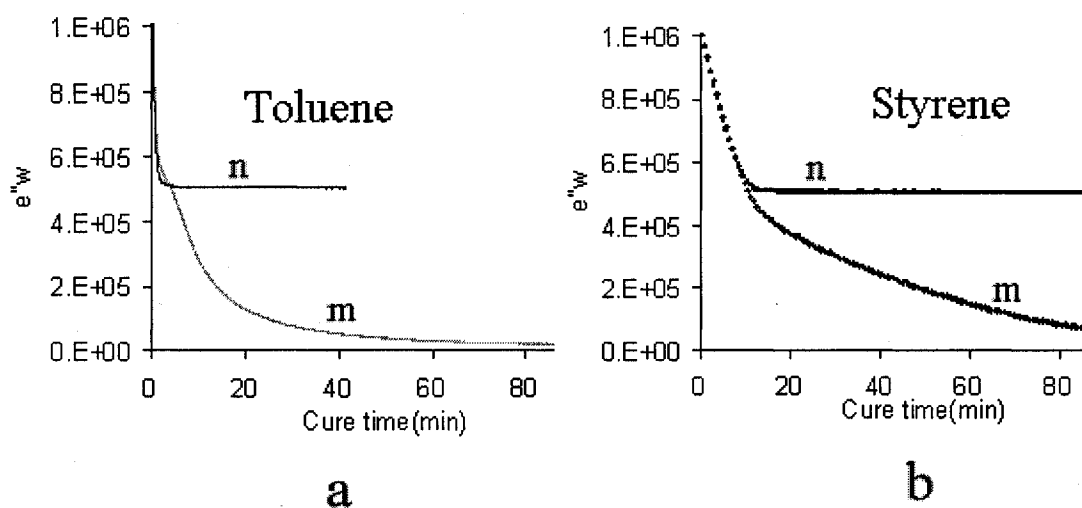


Figure 7.18 UV cure of two systems under the same mask $M_2$ (dark strip width = clear strip width=0.025 inch) and under a clear film, f=0.1kHz, thickness=0.05 mm. (a) the system of 90wt%CD540-10wt%toluene-2 phr Chain transfer agent-0.2phr IC819 at the intensity of 32.5 $uw/cm^2$; (b) is the system of 80wt%CD540-20wt%styrene-0.5phr Chain transfer agent-1phr IC819 at the Intensity of 8 $uw/cm^2$. m represents the measured cure curve under a mask, n represents the calculated curves without considering the diffusion effect.

Both Figure 7.18a and b show little effect of oxygen diffusion from the dark region to the exposure area. This is probably because the rapid cure rate for both experiments due to the low viscosity of the system and the high reactivity of styrene.

Therefore there is very little time for the diffusion of oxygen from the dark area to the exposed area under the mask.

### 7.3.1.6 Study of the diffusion of free radicals by varying the strip width of masks

Here in this section, the sample composition is 80wt% CD540, **20wt% styrene**, 0.5 phr of chain transfer agent and 1 phr of initiator Irgacure 819. The area of the sensor used here is half that of the sensor used in other parts of this dissertation. A series of masks that have **the same total clear area and dark area** but with **differing widths** are used in these experiments. Therefore the number of dark strips and the length of the boundary line between the unexposed and the exposed area varies. Examining the dielectric data of the mask experiment shown in Figure 7.19, the film forming process can be divided into two periods. The first period occurs from the beginning to the $10^{th}$ minute. The second period occurs after the $10^{th}$ minute continuing over a much longer time.

Figure 7.19 UV cure of the system (80wt%CD540-20wt%Styrene-1phr IC819-0.5phr

CT) under masks measured by FDEMS at the frequency of 0.1kHz at the depth of 0.05

mm. Three masks, $M_1$, $M_2$, and $M_3$ are used in these experiments with the strip width

from 0.0125 inch to 0.05 inch. All masks have 50% dark area and 50% clear area.

Incident intensity is 32.5 $\mu w$ /cm$^2$.

The curing during the first period follows the kinetics of the clear mask. They are

similar because the intensity of the light in the clear areas is the same for masks of

different strip widths. But in the second period, there are significant differences even

though the dark areas of the three masks are the same, 50% of the total area. These

differences are due to variation in the amount of diffusion of free radicals across the

boundary line between the dark and clear areas. The initiator radicals and activated

monomers after being excited by the light diffuse across this interface of the clear to the

dark area initiating reaction under the dark strips. In addition, the chains diffuse and grow

into the dark nonirradiated regions. Therefore, the curing under the dark strips is affected by the mobility of these activated species, the distance from the interface and the number or total length of the interface boundary. For the mask with narrower strips, the diffusion distance to reach all of the dark area is shorter and the length of the interface boundary is larger. Therefore, for the same condition, the narrower the strips, the faster the cure in the dark nonirradiated regions.

Another series of experiments, shown in Figure 7.20, which were carried out at a different depth showed a similar outcome.
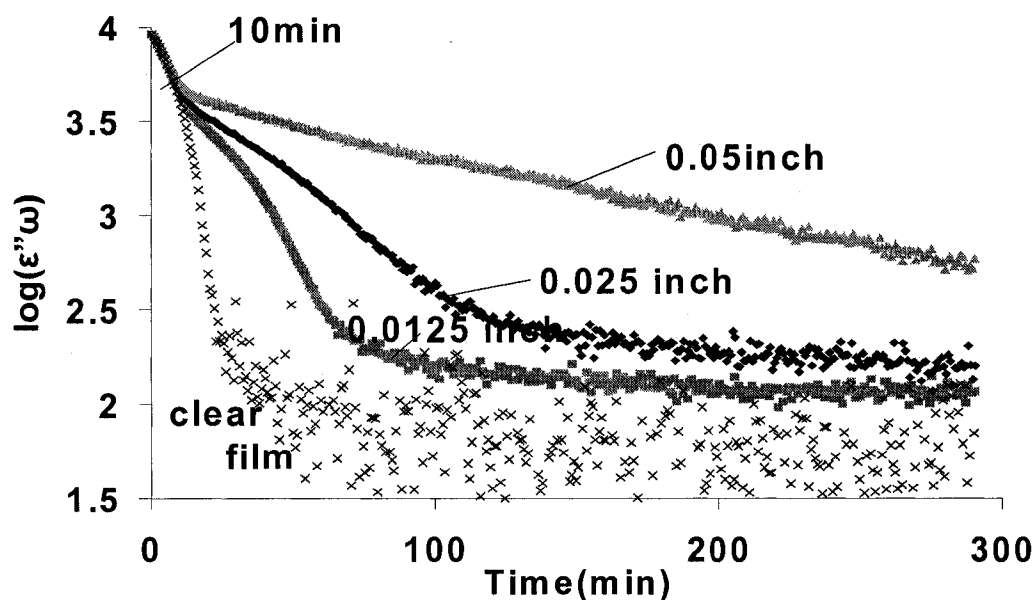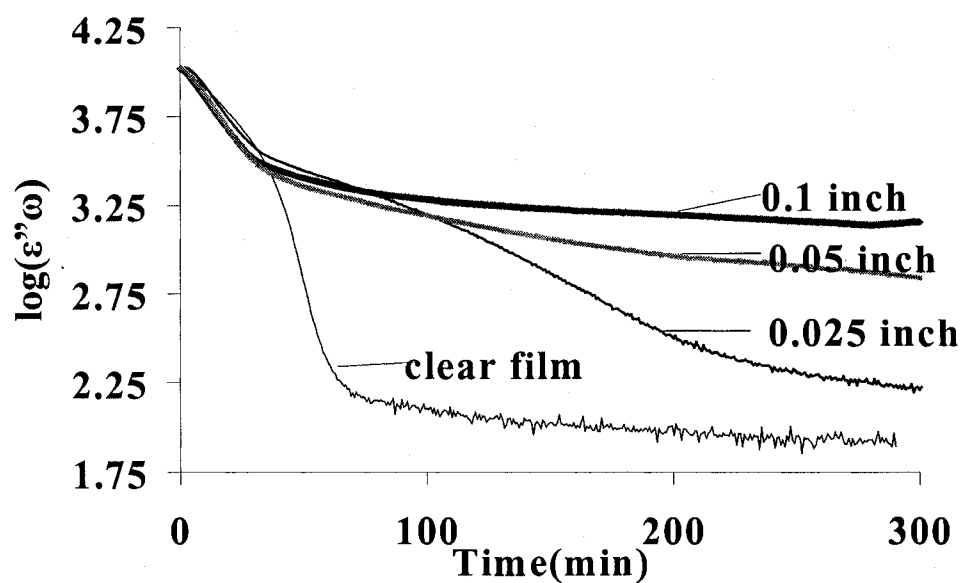


Figure 7.20 UV cure of the system, 80wt%CD540-20wt%Styrene-1phr IC819-0.5phr CT, under masks measured by FDEMS at the frequency of 0.1kHz at the depth of 0.5 mm. Three masks, $M_2$, $M_3$, and $M_4$ are used in these experiments with the strip width from 0.025 inch to 0.1 inch. All masks have 50% dark area and 50% clear area. Incident intensity is 32.5 $\mu w/cm^2$.

## 7.3.1.7 The cure at nonirradiated region at different depths

In order to study the thickness effect on the cure in the nonirradiated region, a series of mask experiments was conducted using masks with the same strip width under the same intensity of light but at different depths, due to the varying thickness of samples. The results are shown in Figure 7.21.
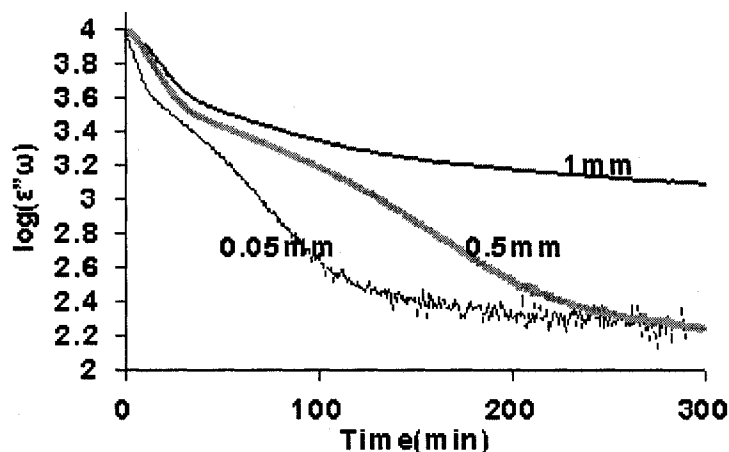


Figure 7.21 Mask experiments of the sample, 80wt%CD540-20wt%Styrene-1phr IC819-0.5phr CT, by FDEMS at the frequency of 0.1kHz, at the thickness of 0.05 mm, 0.5 mm and 1 mm, I=32.5 $\mu w/cm^2$, under the mask, $M_2$ (dark strip width = clear strip width=0.025 inch). All masks have 50% dark area and 50% clear area.

From Figure 7.21, the cure rate in both clear areas and dark areas decreases with the depth, at the bottom of the film. The dark cure is not only affected by the mobility of the activated molecules but also affected by the intensity of the light and therefore the depth at which the cure is occurring. Increased depth results in a decrease in intensity, a lower cure and a low concentration of radicals to diffuse into the dark area.

### 7.3.1.8 The effect of chain transfer agent on the cure in the irradiated and nonirradiated regions when using a mask

In order to study the chain transfer agent effect on the cure under a mask, the systems are prepared with varying CT concentration (from 0 to 2 phr). The system also includes 80wt%CD540, 20wt%Styrene, 1phr of initiator Irgacure 819 (Ciba). The curing process under a mask ($M_2$) monitored by FDEMS is shown in Figure 7.22.
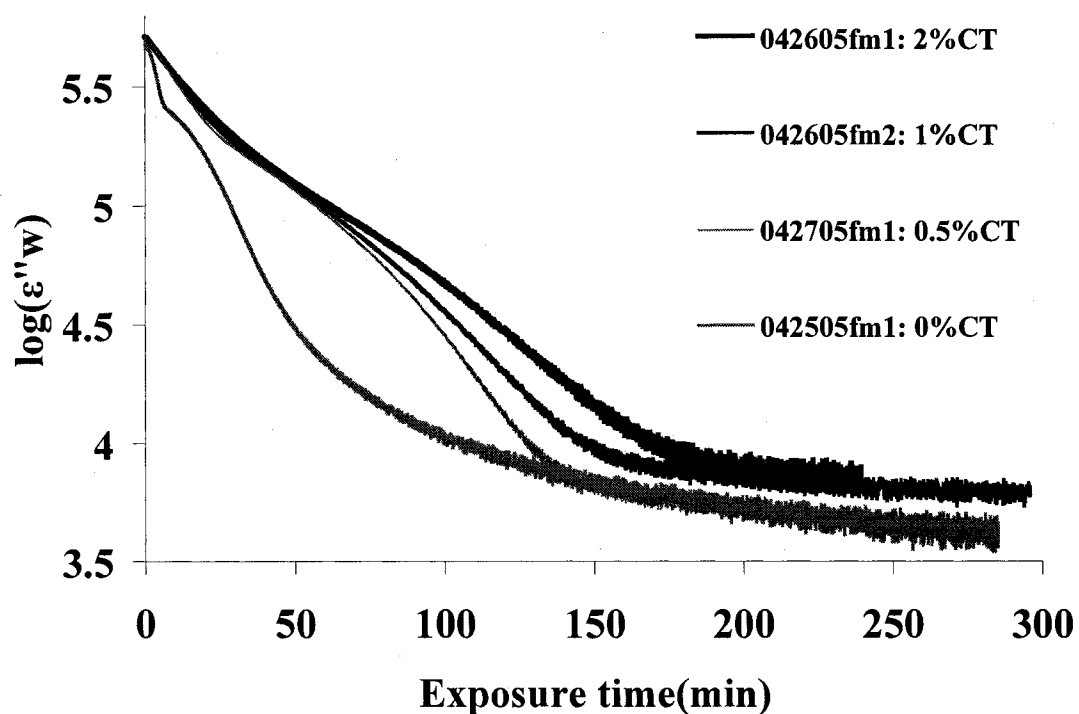


Figure 7.22 Chain transfer agent effect on the cure under a mask ($M_2$) for the system, 80wt%CD540-20wt%Styrene-1 phr IC819 with varying amount of chain transfer agent under the mask, $M_2$ (dark strip width = clear strip width=0.025 inch), I=32.5 $\mu w / cm^2$.

Figure 7.19 shows clearly that the cure rates in both the exposure regions and the nonirradiated regions decrease when the concentration of chain transfer agent in the system increases. This is contrary to what we observed for another system in Figure7.16. The sample used here has an important active content, 20% styrene, that is not included in the system studied in Figure 7.176 (Note that toluene used in Figure 7.16 is not active in the cure reaction, it worked only as a solvent). We know that styrene has a very high activity and mobility. So the addition of 1-dodecanethiol may decrease the total mobility and activity of the styrene free radicals in the system with styrene. So the cure under both clear strips and dark strips are slower for the system with more 1-dodecanethiol in it.

### 7.3.2 The effect of diffusion of oxygen on the free radical thermal cure

First, the effect of oxygen on the thermal polymerization kinetics of IBOMA with 2% BPO at 80 °C was studied by DSC. Plotting the cure rate ($\alpha$) versus time in Figure 7.23.
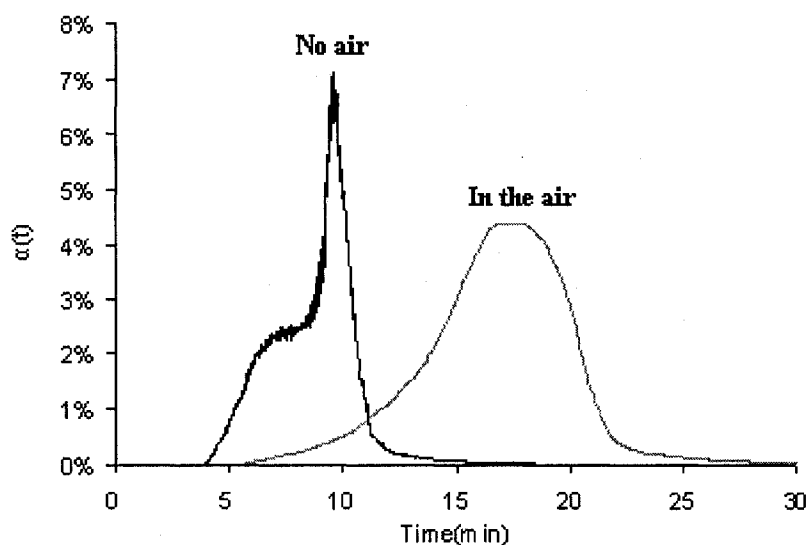
Figure 7.23 Using DSC to study the oxygen diffusion effect on the curing rate of IBoMA-2%BPO at 80°C.

It is seen that the polymerization without oxygen (air) reached the highest reaction rate much earlier than the polymerization under oxygen. This is because the oxygen that diffused from the environment reacts with the free radicals and inhibits the polymerization. Since the oxygen diffuses from the surface of the sample to the bottom, its effect is a function of depth. Therefore, the polymerization kinetics are also a function of depth. It was also observed that both reactions are inhibited at the beginning of the reaction. This is because there is some inhibitor and oxygen dissolved in the IBOMA system initially.
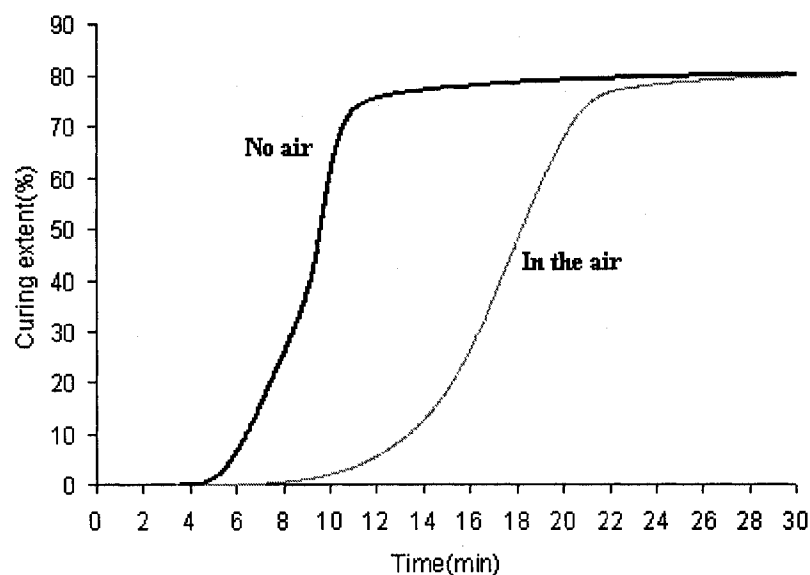
Figure 7.24 Using DSC to study the oxygen diffusion effect on the curing extent of IBoMA-2%BPO at 80°C.

Figure 7.24 shows both reactions reach the final cure extent of 80%, but the polymerization without oxygen is complete after 11 minutes which is much earlier than under oxygen where the completion occurs after 21 minutes.

Since the kinetics of the reaction are a function of depth, it is not as interesting to study the oxygen effect on the reaction by DSC because DSC measures an average of the reaction rate with depth instead of the reaction at a particular depth. In order to study the oxygen effect in greater detail, FDEMS experiments were conducted at the same thickness as in the DSC experiment. The polymerization without oxygen is shown in Figure 7.25.

Figure 7.25 Using FDEMS to study the oxygen diffusion effect on the curing extent of IBoMA-2%BPO at 80°C without oxygen.

Figure 7.25 shows that dipole relaxation peaks occur around the 10th to 11th minute. They reflect the buildup to the glass transition temperature. The $T_g$ peaks occur at the same time as the completion of the DSC reaction because the glass transition quenches the reaction and the reaction ceases when the cure temperature is lower than the glass transition temperature

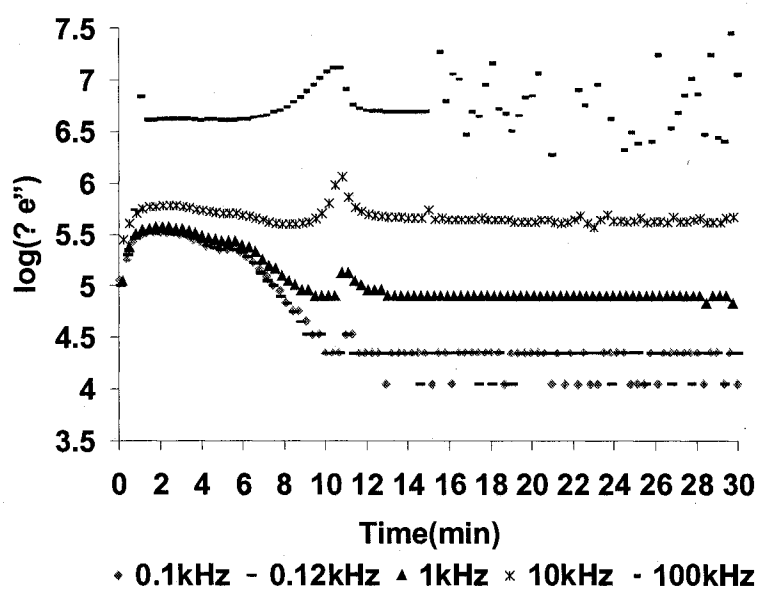For the experiment under oxygen (in the air), the FDEMS experimental data are shown in Figure 7.26.
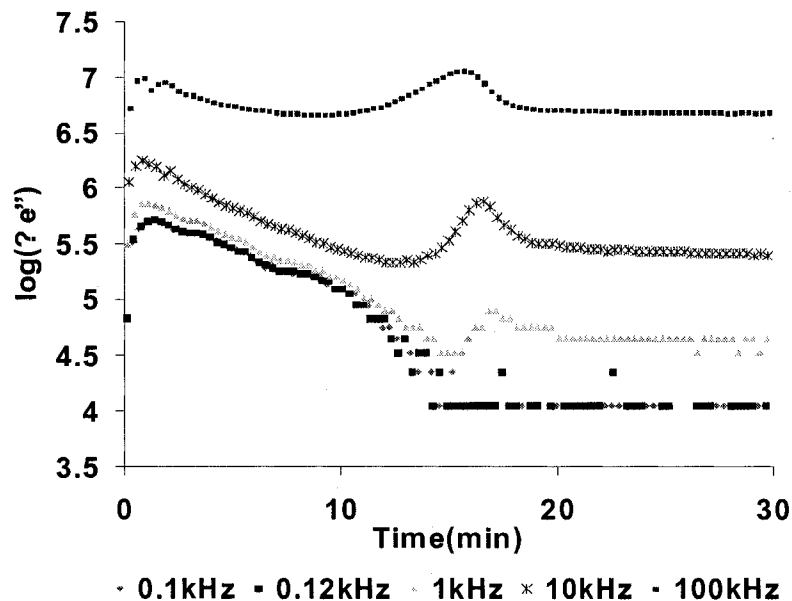
Figure 7.26 Using FDEMS to study the oxygen diffusion effect on the curing extent of

IBoMA-2%BPO at 80°C with exposure to air containing oxygen.

For the experiment under oxygen (in the air) shown in Figure 7.26, the dipole relaxation peak occurs around the 16$^{th}$ to 17$^{th}$ minute, which is much earlier than the end of the reaction that was measured by DSC at the 21$^{st}$ minute. This is because FDEMS measures the reaction process at the bottom of the film where there is much less diffusion of oxygen than has occurred at the surface. Therefore, the polymerization at the bottom is faster than the polymerization at the surface and the average rate for the bulk of the sample.

## 7.4 Conclusions

FDEMS can measure the polymerization rate of a film at a particular depth. The polymerization kinetics of a UV cure system are a function of depth because the light intensity decreases with depth. The cure rate at the top is faster than in the bottom layer and the conversion at the top, the air film surface, is larger than at the bottom of the film at the substrate interface.

Using FDEMS to monitor UV cure under a mask, it was observed that the cure under the mask's nonirradiated regions occurs due to the mobility of activated molecules. In addition, the dark cure occurs more slowly if the width of the mask's strips increases and with depth. The rate of dark cure was determined by not only the mobility of the radicals but also the length of the exposed-masked interface.

The cure under the exposed area of a mask was slower than under a clear film (without mask) due to oxygen diffusion from the unexposed area into the exposed area. When cure was very rapid there was little effect on the cure rate in the exposed area under the mask as the cure rate was much faster than oxygen diffusion.

The cure kinetics of IBoMA film under oxygen are a function of depth because of the diffusion of oxygen. The cure rate at the upper layer was less because the oxygen reacts with the radical initiator molecules.
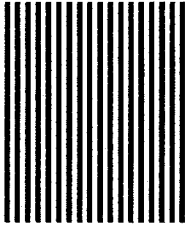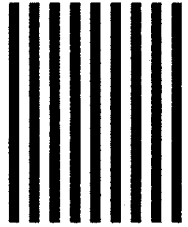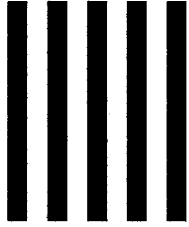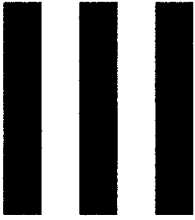
The FDEMS planar sensor measurements were shown to be a convenient and effective way to monitor cure in a film and in particular to monitor cure as a function of depth and film thickness.

## References

1       Kranbuehl, D. E. Dielectric Spectroscopy of Polymeric Materials 1997, 303-28.

2       Kranbuehl, D. E. Processing of Composites, 2000.

3       Kranbuehl, D. E. Journal of Coating Technology 2004, 48-55.

4       Kranbuehl, D. E.; Hood, D.; Kellam, C.; Yang, J. In ACS Symposium Series;

Provder, T., Ed., 1996, p 96-117.

5       Kranbuehl, D. E.; Hood, D.; McCullough, D.; L.Aandahl, H.; Haralampus, N.;

Newby, W.; Eriksen, M. Progress in Durability Analysis of Composite Systems,

Proceedings of the International Conference, Brussel, July, 16 1996, pp 53-59.

6       Kranbuehl, D. E.; Hood, D.; Rgozinski, J.; Meyer, A.; Powell, E.; Higgins, C.;

David, C.; Hoipkenmeier, L.; Ambler, C.; Elko, C.; Olukcu, N. 4th International

Conference on Durability Analysis of Composite Systems, Brussels, Belgium, July 11-14

1999, pp 413-20.

7       Kranbuehl, D. E.; Hood, D.; Rogozinski, J.; Meyer, A.; Neag, M. Progress in

Organic Coatings 1999, 35, 101-07.

8       Kranbuehl, D. E.; Rogozinski, J. Polymeric Materials Science and Engineering

1999, 81, 197-98.

9       Kranbuehl, D. E.; Rogozinski, J.; Meyer, A.; Hoipkemeier, L.; Nikolic, N. In

ACS Symposium Series, 2001, p 141-56.

10      Kranbuehl, D. E.; Rogozinski, J.; Meyer, A.; Neag, M. 24th International

Conference in Organic Coatings, July 6-10 1998, pp 197-211.

11      Kranbuehl, D. E.; Warner, J.; Knowles, R.; Best, P. 60th annual Technical

Conference, Soc. Plastic Engineers,, 2002, pp 3384-88.

**Appendix**

Table 7.1 Masks

| Mask number | Dark strip width (inch) | Clear strip width (inch) | Plot |
|---|---|---|---|
| $M_1$ | 0.0125 | 0.0125 | |
| $M_2$ | 0.025 | 0.025 | |
| $M_3$ | 0.05 | 0.05 | |
| $M_4$ | 0.1 | 0.1 | |

# Chapter 8. Summary and conclusions

This dissertation focuses on the UV cure kinetics of thin and thick dimethacrylate samples.

Increasing the <u>intensity and initiator concentration</u> versus depth and exposure time in UV curable samples was characterized and then calculated by using a Matlab program in Chapter 3. Then, in Chapter 4, we studied the UV cure kinetics of thin samples (0.05 mm) as a function of intensity, initiator concentration, and temperature. Combining the results of Chapter 3 and 4, the UV cure kinetics versus depth of thick samples were calculated and compared with experimental results in Chapter 5. Then the effect of oxygen and free radical diffusion on the polymerization rate was characterized in both a UV cure system and a thermal cure system by dielectric sensing in Chapter 7. The specific results of the UV cure kinetics of thin and thick samples are elaborated below.

The UV cure kinetics of thin samples show that the inhibition period of the free radical photo-polymerization is inversely proportional to the initiator concentration and the incident intensity. The rate of polymerization ($\frac{d(\ln[M(t)])}{dt}$) is found proportional to $I^{0.7}$ and $[PI]^{0.75}$ during the cure conversion from 10% to 40% at the same reaction temperature. The increase of the exponential value from the theoretical value of 0.5 in equation 4-20 has been proposed to be due to unimolecular termination of some of the

"trapped" radicals. Based on the trapped radical theory, two sigmoid equations have been used to fit the curve of $\dfrac{d(\ln[M(t)])}{dt}$ versus conversion at different temperatures. With these results, a Matlab program has been successfully developed to predict the cure kinetics of the system CD540 with Irgacure 819 at varying incident intensities, initiator concentrations, and cure temperatures.

The UV cure kinetics versus depth of thick samples are studied in Chapter 6. A Matlab program was written first based on the results from Chapter 3 and 4 to calculate the cure kinetics at particular depths and the average cure kinetics throughout the entire thick samples. The results match the experimental data measured by transmitted FTIR and dielectric sensing when the absorption of the light is not too high and the delay time is less than 13 minutes. These results verified that the model can be used to predict the bulk cure of thick samples. The research on thick sample cure kinetics shows that the deeper the position in the film, the slower the cure rate. It also shows that increasing the radiation intensity will increase the bulk cure rate and shorten the inhibition period of the bulk cure of thick samples. However, increasing the photoinitiator concentration, [PI], may decrease the cure rate. These results help explain how the radiation intensity and initiator concentration affect the cure as a function of depth in thick samples.

The dielectric planar sensor measurements were shown to be a convenient and effective way to monitor cure in a film and in particular to monitor cure as a function of depth and reaction conditions and the role of oxygen diffusion.

# VITA

Yuemei Zhang

Yuemei Zhang was born in Beijing, P. R. China, on January $1^{st}$, 1977. She received her B.S. at Tsinghua University in 1999 with a degree in Chemistry. In 2002, she received her M.S. degree in Polymer Science at Institute of Chemistry, Chinese Academy of Science. She received another M.S. degree in Chemistry at the College of William and Mary in 2004.

In August of 2004, the author became a Doctor of Philosophy candidate in the Applied Science Department, College of William and Mary. As of October 2006, she will embark on a career as an R&D Scientist at Sun Chemical Corporation in Carlstadt, New Jersey.